

The Influence of Salinity on the Mechanical Behavior of High Plasticity Soils

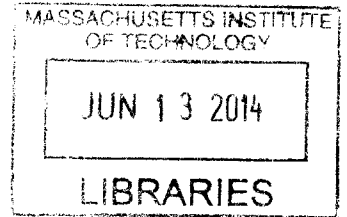
by

Brian Patrick Fahy

Bachelor of Engineering (Ord.) in Civil Engineering,
Limerick Institute of Technology, Limerick, Ireland (2005)

Bachelor of Engineering (Hon.) in Civil Engineering,
National University of Ireland Galway, Ireland (2007)

ARCHIVES



Submitted to the Department of Civil and Environmental Engineering in Partial Fulfillment of the requirements for the Degree of

Master of Science in Civil and Environmental Engineering

at the

MASSACHUSETTS INSTITUTE OF TECHNOLOGY

June 2014

© 2014 Massachusetts Institute of Technology. All rights reserved.

Signature of Author..... **Signature redacted**

Department of Civil and Environmental Engineering
May 9, 2014

Certified by..... **Signature redacted**

John T. Germaine
Senior Research Associate and Senior Lecturer of Civil and Environmental Engineering
Thesis Supervisor

Accepted by..... **Signature redacted**

Hedi Nepf
Chair, Departmental Committee for Graduate Students

The Influence of Salinity on the Mechanical Behavior of High Plasticity Soils

by

Brian Patrick Fahy

Submitted to the Department of Civil and Environmental Engineering on May 9, 2014 in Partial Fulfillment of the requirements for the Degree of Masters of Science in Civil and Environmental Engineering

ABSTRACT

This thesis investigates the influence of salinity on the mechanical behavior of smectitic rich high plasticity soils resedimented with pore fluid salinities ranging from 0 to 256 g/L.

An extensive laboratory testing program involving Constant Rate of Strain (CRS) and K_0 consolidated undrained shear in compression triaxial testing (CK_0UC) was undertaken. Specimens tested in the modified CRS device reached axial effective stresses between 30 and 40 MPa. Triaxial testing was performed over a very wide range of effective stresses from 0.125 to 10 MPa, with one test consolidated to 63 MPa. Behavior is examined at pore fluid salinities of 4, 64, and 256 g/L. The shear behavior of all specimens was obtained in the normally consolidated region.

Six different soils from the Gulf of Mexico region, ranging in liquid limit from 62 % to 90 %, were tested to determine the impact of varying salinity on one dimensional consolidation and permeability properties. The majority of testing was carried out on Gulf of Mexico – Eugene Island (GOM EI). This material was used to examine the behavior of a soil whose fabric has been changed by the removal of the natural salts via leaching. Both leached and natural GOM EI were tested to investigate the influence of salinity on strength properties.

CRS results show similar trends for each soil. Compressibility decreases and permeability increases significantly with increasing salinity. Increasing consolidation stresses to 40 MPa decreased the influence of salinity on compressibility to negligible levels while stress dependent permeability behavior varied amongst the soils tested.

Significant decreases in both normalized undrained shear strength and critical state friction angle of GOM EI with increasing stress level were observed, corresponding with an increase in the value of K_0 . An increase in shear strength and critical state friction angle was observed with increasing salinity at a consolidation stress of 0.4 MPa. No definitive trend was evident between the strength properties of leached and natural GOM EI. The strength behavior of GOM EI is consistent with that observed for other materials from a wide variety of geologic backgrounds and is in agreement with correlations between critical state friction angle and undrained strength to liquid limit.

Thesis Supervisor: John T. Germaine

Title: Senior Research Associate and Senior Lecturer of Civil and Environmental Engineering

ACKNOWLEDGEMENTS

Without question my greatest thanks must go to my research, thesis and academic adviser Dr. John Germaine. I would like to pay my sincere gratitude for his help, advice, and endless patience which he has shown to me during my time here. I greatly admire his attitude towards work, attention to detail, and knowledge of laboratory testing as well as engineering as a whole. It has been a pleasure and great honour to work with him.

I would like to thank Ward and Burke Construction Ltd. for sponsoring this research and making my time at MIT possible. I would particularly like to thank Robert Ward (MIT SM '89) who showed belief in my abilities. His work ethic is something to which I aspire to.

I would like to gratefully acknowledge my other teachers of geotechnical engineering; Professor Herbert H. Einstein, and Dr. Lucy Jen. They have instilled in me the academic skills and tools that I will use to further my career. I recognize that I have been educated by some of the best in the world.

My gratitude also extends to Sheila Fay, Kris Kipp, and the staff of the CEE department for their assistance and friendship during my time at MIT.

It is true that a person is influenced by those whom surround him. I am fortunate to have been surrounded by so many extremely talented and ambitious people while at MIT. It is not possible to mention them all but special mention to Brendan Casey, Amy Adams and Jana Marjanovic. I am grateful to them for both their help in the lab, particularly during the first few months, as well as all the welcome breaks from work they provided. Special thanks to Amer Deirieh. His unwavering optimism as well as great sense of humour has made sharing both an office and apartment for two years an absolute pleasure. Becoming friends with so many brilliant, hardworking people has inspired me to continuously better myself in all aspects of daily life.

I would also like to thank my family for their support and friends at home who have always kept me well grounded.

Finally, to Orlaith, a long distance relationship can be testing at the best of times but your endless patience, constant love and support during these last two years have been immeasurable. Our brief time together in Cambridge provided some of the best memories of my time at MIT.

To my parents, Gerard and Mary Fahy,
I dedicate this thesis to you.

TABLE OF CONTENTS

ABSTRACT	3
ACKNOWLEDGEMENTS	5
TABLE OF CONTENTS	9
List of Tables	13
List of Figures	15
List of Symbols	25
1 INTRODUCTION	29
1.1 RESEARCH STATEMENT.....	29
1.2 RESEARCH OBJECTIVES AND SCOPE.....	29
1.3 ORGANIZATION OF THESIS	31
2 BACKGROUND	33
2.1 INTRODUCTION	33
2.2 IMPACT OF SALT ON SOIL BEHAVIOR – PARTICLE LEVEL	33
2.2.1 Introduction.....	33
2.2.2 Specific Surface Area & Cation Exchange Capacity.....	35
2.2.3 Floc Formation.....	37
2.3 LITERATURE REVIEW	38
2.3.1 Introduction.....	38
2.3.2 Impact of Increasing Salinity on Mechanical Behavior.....	39
2.3.3 Leaching Salts from Soil.....	44
2.3.4 Testing Intact Soil with High Salinity	45
2.3.5 Evolution of pore fluid salinity with increasing confining stress	46
3 MATERIALS USED IN TESTING PROGRAM	55

3.1 INTRODUCTION	55
3.2 TEST MATERIALS	56
3.2.1 Gulf of Mexico – Eugene Island	56
3.2.2 Gulf of Mexico – Upper and Lower Interval	58
3.2.3 Gulf of Mexico – Specimens A and B	59
3.3 MATERIAL PROCESSING	61
3.3.1 Introduction	61
3.3.2 Processing of Leached Gulf of Mexico – Eugene Island	61
3.3.3 Processing of GOM Upper and GOM Lower	64
3.4 RESEDIMENTATION	67
3.4.1 Introduction	67
3.4.2 Resedimentation Procedure	69
3.4.3 Resedimenting Gulf of Mexico – Eugene Island	73
3.4.4 Resedimenting GOM Upper and GOM Lower	74
3.4.5 Resedimenting GOM A and GOM B	75
3.4.6 Consolidation behavior during resedimentation	75
3.4.7 Resedimentation Issues	76
4 EQUIPMENT AND TESTING PROCEDURES	109
4.1 INTRODUCTION	109
4.2 DATA ACQUISITION SYSTEM	109
4.2.1 Introduction	109
4.2.2 Measurement Instrumentation	110
4.2.3 Data Acquisition System	112
4.2.4 Computer Control System	113
4.3 TESTING EQUIPMENT	114

4.3.1 Introduction.....	114
4.3.2 Constant Rate of Strain (CRS) Testing Equipment	114
4.3.3 Triaxial Testing Equipment	119
4.4 TESTING PROCEDURES.....	122
4.4.1 Introduction.....	122
4.4.2 Index Testing	123
4.4.3 Constant Rate of Strain (CRS) Testing.....	124
4.4.4 Triaxial Testing.....	129
5 CRS TEST RESULTS	151
5.1 INTRODUCTION	151
5.2 ULTRA-LOW STRESS BEHAVIOR.....	152
5.3 DISCUSSION OF MECHANICAL BEHAVIOR	153
5.3.1 Introduction.....	153
5.3.2 Gulf of Mexico – Eugene Island.....	154
5.3.3 Gulf of Mexico – Upper and Lower Interval	159
5.3.4 Gulf of Mexico – Specimens A &B.....	160
5.3.5 Comparison of Different Soil Types.....	162
5.3.6 Evaluation of CRS Testing Program.....	163
5.4 SEM IMAGE ANALYSIS	165
5.4.1 Introduction.....	165
5.4.2 Hypothesis for Explaining Mechanical Behavior	165
5.5 CORRELATIONS WITH PLASTICITY	167
5.5.1 Introduction.....	167
5.5.2 Compressibility.....	167
5.5.3 Permeability	168

6 TRIAXIAL TEST RESULTS	197
6.1 INTRODUCTION	197
6.2 ONE DIMENSIONAL CONSOLIDATION BEHAVIOR	198
6.2.1 Introduction.....	198
6.2.2 Compression behavior during Consolidation.....	198
6.2.3 Consolidation Stress and Salinity Dependence of K_0	199
6.3 UNDRAINED SHEAR BEHAVIOR.....	201
6.3.1 Introduction.....	201
6.3.2 Shear Stress-Strain Behavior	202
6.3.3 Friction Angle	204
6.3.4 Effective Stress Behavior.....	205
6.3.5 Stiffness.....	207
6.4 STRENGTH CORRELATIONS WITH PLASTICITY	208
6.4.1 Introduction.....	208
6.4.2 Undrained Shear Strength Correlation.....	208
6.4.3 Friction Angle Correlation.....	209
7 CONCLUSIONS AND RECOMMENDATIONS	225
7.1 INTRODUCTION	225
7.2 ONE DIMENSIONAL CONSOLIDATION BEHAVIOR	226
7.3 STRENGTH BEHAVIOR.....	230
7.4 RECOMMENDATIONS FOR FUTURE WORK	232
REFERENCES.....	235
APPENDIX A	239
APPENDIX B	243
APPENDIX C	249

List of Tables

Table 3-1 Index properties of all soils associated with this research.....	79
Table 3-2 List of resedimentation batches produced as part of this research (1 of 2)	80
Table 3-3 List of resedimentation batches produced as part of this research (2 of 2)	81
Table 3-4 List of soils resedimented and the required mass of salt water required to create a stable slurry at the corresponding salt concentrations indicated.....	82
Table 4-1 Characteristics of instruments used in CRS TR4 apparatus. Note: Resolution and stability based on central data acquisition system, calculations based on specific dimensions .	133
Table 4-2 Characteristics of instruments used in triaxial MIT03 apparatus. Note: Resolution and stability based on central data acquisition system, calculations based on specific dimensions .	133
Table 4-3 Characteristics of instruments used in triaxial MIT04 apparatus. Note: Resolution and stability based on central data acquisition system, calculations based on specific dimensions .	134
Table 4-4 Characteristics of instruments used in triaxial MIT13 apparatus. Note: Resolution and stability based on central data acquisition system, calculations based on specific dimensions .	134
Table 5-1 List of Constant Rate of Strain tests performed (1 of 2).....	169
Table 5-2 List of Constant Rate of Strain tests performed (2 of 2).....	170
Table 6-1 List of CK0UC triaxial tests performed on RGOM EI and Leached RGOM EI in this testing program	211

List of Figures

Figure 2.1 Average values of relative sizes, thicknesses and specific surface area of the mostcommon clay minerals (Yong & Warkentin, 1975).....	47
Figure 2.2 Sodium montmorillonite at different pore fluid salinities. Saltwater content L-R: 1, 4,16, 64, 128 & 256 g/l NaCl. (1 g of soil used in each tube) (Horan, 2012).....	47
Figure 2.3 Modes of particle association in clay suspensions and terminology (a) dispersed and deflocculated (b) aggregated but deflocculated (c) edge to face flocculated but dispersed (d) edge to edge flocculated but dispersed (e) edge to face flocculated and aggregated (f) edge to edge flocculated and aggregated (g) edge to face and edge to edge flocculated and aggregated (Van Olphen, 1977)	48
Figure 2.4 Salinity of formation waters from the St. Genevieve Limestone formation, Illinois (Engelhardt & Gaida, 1963).....	49
Figure 2.5 Compression curves of the Bisaccia clay (30% smectite) resedimented with different types of pore fluids. Void ratio and compressibility increase with decreasing salinity (Calvello et al., 2005)	49
Figure 2.6 Hydraulic conductivity of the Bisaccia clay (30% smectite) resedimented with different pore fluids (Calvello et al., 2005).....	50
Figure 2.7 Coefficients of consolidation of the Bisaccia clay resedimented with different fluids relative to an increment of axial stress from 40 to 80 kPa (Calvello et al., 2005).....	50
Figure 2.8 Residual shear strength of smectitic clays resedimented with varying pore fluids. (a) soil with 30% smectite, (b) 100% smectite soils namely; Ponza Bentonite and Commercial Bentonite (Calvello et al., 2005).....	51
Figure 2.9 Comparison of the undrained shear strength of salt, leached and fresh-water clays (Bjerrum & Rosenqvist, 1956).....	52
Figure 2.10 Soil profiles from the Caspian Sea: Atterberg limits on the left and measured	53
Figure 2.11 Oedometer test results from Caspian Sea recovered from two different depths run at different cell fluid salinities (van Paassen. et al., 2004)	53
Figure 2.12 Concentration change of NaCl pore solution in compressed montmorillonite clay. Stress ranged from 3 to 320MPa (Engelhardt & Gaida, 1963).....	54

Figure 2.13 Concentration change of NaCl pore solutions in consolidated montmorillonite. From 80 to 320MPa NaCl concentration increases (Engelhardt & Gaida, 1963)	54
Figure 3.1 Location map showing the Eugene Island Block of the coast of Louisiana. GOM EI is a blended mixture of core extracted from A-12 in Block 316 and A-20ST2 in Block 330 (Stump & Flemings, 2002)	83
Figure 3.2 Sections of the two wells drilled with shaded area indicating section of core extracted for laboratory testing (Stump & Flemings, 2002).....	83
Figure 3.3 Section through part of Core A-20 from Block 330 (Betts, 2014).....	84
Figure 3.4 Finely ground GOM EI ready for laboratory testing	84
Figure 3.5 Results of grain size analysis for GOM EI (tested by Taylor Nordquist)	85
Figure 3.6 Mineralogy of Gulf of Mexico Eugene Island clay – bulk sample on left, < 2 micron on right.....	85
Figure 3.7 Plasticity chart showing data for GOM EI, GOM Lower, GOM Upper, GOM A, and GOM B.....	86
Figure 3.8 Condition of GOM Upper Interval prior to cleaning. The soil cuttings are coated in drilling fluid.	86
Figure 3.9 Size and color of GOM Upper Interval drill cuttings after removal of drilling fluid. 87	
Figure 3.10 Size and color of GOM Lower Interval drill cuttings after removal of drilling fluid	87
Figure 3.11 Finely ground GOM Lower Interval stored in 10 gallon sealed plastic containers..	88
Figure 3.12 Results of grain size analysis for GOM Upper and Lower (tested by Taylor Nordquist & Chunwei Ge).....	88
Figure 3.13 Mineralogy of Gulf of Mexico Upper Interval – bulk sample on left, < 2 micron on right.....	89
Figure 3.14 Mineralogy of Gulf of Mexico Lower Interval – bulk sample on left, < 2 micron on right.....	89
Figure 3.15 Ball Mill Grinder, Top: Rotating hexagonal steel drum powered by electric motor, Bottom: View inside drum of soil and steel ball mixture (Jones, 2010).....	90
Figure 3.16 Results of grain size analysis for GOM A and GOM B (tested by Amy Adams)....	91
Figure 3.17 Mineralogy of GOM A – bulk sample on left, < 2 micron on right	91
Figure 3.18 Mineralogy of GOM B – bulk sample on left, < 2 micron on right	92

Figure 3.19 Equipment required for leaching the salts from soil using dialysis tubing 92

Figure 3.20 Schematic of how dialysis tubing work (<http://ehumanbiofield.wikispaces.com/>).. 93

Figure 3.21 Leaching process underway with dialysis tubing filled with soil slurry placed in a bath of distilled water..... 93

Figure 3.22 Conductivity Meter and associated probe used to measure the salinity of the bath water..... 94

Figure 3.23 Evolution of soil salinity with time by measuring the salinity of the bath water at each water change (every ~12 hours) 95

Figure 3.24 Condition of GOM Lower with each chunk of soil coated in drilling fluid prior to cleaning..... 95

Figure 3.25 Removal of drilling fluid from GOM Lower. Top: First addition of Toluene to soil chunks, Middle: Sieving off toluene/drilling fluid mixture using #20 sieve, Bottom: adding toluene mixture back to soil chunks for secondary cleaning with drilling fluid at base of bowl removed..... 96

Figure 3.26 Removal of drilling fluid from GOM Lower. Top: Gently stirring the soil chunks in the toluene to prevent possible breakup of each chunk, Middle: final sieving of soil chunks, Bottom: cleaned soil placed on absorbent towel to allow any residual toluene to evaporate..... 97

Figure 3.27 Cleaned GOM Upper placed in trays for oven drying to reduce moisture content to a level suitable for grinding in the GPX Disk Grinder 98

Figure 3.28 Trays of soil chunks placed in oven set at a temperature of 60° Celsius..... 98

Figure 3.29 GPX Disc Grinder used in processing both GOM Upper and GOM Lower..... 99

Figure 3.30 GOM Lower - Final product ready for resedimentation after cleaning and grinding to a fine powder 100

Figure 3.31 Consolidometers used in this research. Left: 1.4” diameter triaxial testing consolidometer, Middle: 1.75” diameter consolidometers for CRS testing, Right: consolidometer used for CRS testing when small quantities of soil were required for resedimentation 100

Figure 3.32 Kitchen aid mixer used to mechanically agitate soil/water mixture into a slurry .. 101

Figure 3.33 Equipment used to deair the soil slurry. The ceramic bowl with soil is placed inside the cylindrical chamber and the vacuum pump beneath it creates the necessary vacuum 101

Figure 3.34 Pouring de-aired slurry into consolidometer with funnel and flexible tube. Note the end of the tube is maintained at the soil surface to prevent air pockets becoming trapped as the soil is placed (Horan, 2012).....	102
Figure 3.35 Consolidometer clamped in place with water bath filled midway on the porous stone ready to receive de-aired slurry (Horan, 2012).....	103
Figure 3.36 Resedimentation set-up for stresses up to 0.5MPa with weights applied via hanger. LVDT measuring strain connected to data acquisition channel at top of image	103
Figure 3.37 GOM EI placed in an Oedometer load frame (2000 lb capacity) for resedimenting to stresses ranging from 0.5MPa to 10MPa	104
Figure 3.38 Hydraulic cylinder used to extrude a resedimented specimen from the consolidometer. This device is used when the resedimentation stress exceeds 0.5MPa	105
Figure 3.39 Resedimented triaxial specimen being extruded from consolidometer.....	105
Figure 3.40 GOM EI resedimented to 64 g/L. Stress level at end of primary is 25 kPa. Top: Root time method for determining time to reach end of primary consolidation. Bottom: Log time method to determine end of primary consolidation for same data.....	106
Figure 3.41 Data for GOM EI resedimented at salinities ranging from 10 to 128 g/L. The stress increment (25 kPa at EOP) is the same for all salinities.....	107
Figure 3.42 Issue of salt precipitating out of solution when resedimenting with high pore fluid salinities (soil shown is GOM EI resedimenting with a pore fluid salinity of 256g/L).....	108
Figure 4.1 Electronic Transducers used during the testing program. Top Left: Trans-Tek LVDT's, Top Right: 0 – 200 psi capacity Pressure Transducer, Middle: 500 lb Load Cell, Bottom: Close-up of pressure transducer and section through one showing internal components (Horan, 2012).....	135
Figure 4.2 Pressure Volume Actuators (PVA's) used to control cell (left) and pore (right) pressures during triaxial testing in addition to cell pressure during CRS testing.	136
Figure 4.3 Schematic diagram of a central data acquisition system (Germaine & Germaine, 2009).....	137
Figure 4.4 Schematic diagram of the control system hardware components.....	137
Figure 4.5 CRS trimming rings, Left: Standard Trimming Ring, Right: Trimming ring used in this research (Horan, 2012).....	138
Figure 4.6 Schematic diagram of Trautwein CRS cell (TR4) (Horan, 2012).....	138

Figure 4.7 Components of CRS device and stages of set-up, Top: Device disassembled to individual components for cleaning, Middle: Device and porous stones prepared for testing, Bottom: Trimming ring with prepared specimen in test position with square ring seal..... 139

Figure 4.8 Trautwein CRS cell showing overflow hole which allows any water passing the piston seal to exit the device prior to contacting the roller bearings positioned higher in the piston column..... 140

Figure 4.9 A very slow leak at the piston seal throughout a test results in a build-up of salts on the outside of the overflow hole..... 140

Figure 4.10 CRS set-up showing insulated timber temperature enclosure and Wykeham Farrance load frame 141

Figure 4.11 CRS Cell TR4 under test conditions. Temperature is maintained at a constant 25.3° C within the enclosure 141

Figure 4.12 CRS equipment developed for testing to 100 MPa (axial effective stress) complete with 50 kip capacity load frame, 887 kN capacity hydraulic cylinder, modified CRS cell and temperature enclosure 142

Figure 4.13 Ancillary equipment for CRS testing to 100 MPa, Top Left: Air regulated PVA used for controlling cell pressure, Top Right: Electric motor driven PVA used to control the axial load hydraulic cylinder, Bottom: Sentran PG3 50,000 lb capacity low profile load cell 143

Figure 4.14 M150 Ultra-Miniature String Pot connected to CRS cell and piston for measuring axial displacement of specimen 144

Figure 4.15 Modified CRS base for 100 MPa CRS Cell. Elevated base with recess to accommodate pore pressure O-ring seal..... 144

Figure 4.16 Schematic of the standard automated triaxial testing system used in the MIT 145

Figure 4.17 Low stress triaxial base pedestal and top cap O-ring sealing arrangement with 2 rubber membranes. O-ring spacing exaggerated for clarity (Horan, 2012)..... 145

Figure 4.18 Low Stress Triaxial Set-up - MIT03 triaxial cell mounted on a 9.8 kN Wykeham Farrance screw driven load frame with electric motor controlled gears..... 146

Figure 4.19 Schematic of low stress triaxial cell (Santagata, 1998)..... 146

Figure 4.20 Medium Stress Triaxial Device, Top Left: MIT13 triaxial cell, Top Right: Schematic of medium stress triaxial device (from Casey, 2014), Bottom: Test specimen mounted

on base pedestal complete with double membrane, O-rings, and coiled copper top drainage line	147
Figure 4.21 High stress triaxial device, Top: MIT 09 high stress cell, Bottom: Schematic of high stress triaxial cell (Casey, 2014).....	148
Figure 4.22 Trimming device with CRS trimming ring placed upside down concentrically on resedimented sample ensuring equal amount of soil for trimming around perimeter	149
Figure 4.23 Trimming GOM EI sample into small diameter CRS ring, Top: Removing excess along the ring taper, Bottom Left: Positioning soil with plastic recess tool, Bottom Right: Final trimming with razor blade to ensure a level surface.....	150
Figure 5.1 Sedimentation test performed on natural BBC Series IV powder. Salinities from LR: 1, 4, 16, 64, 128 & 256 g/l NaCl. 5 grams of soil used in each tube (Horan, 2012).....	171
Figure 5.2 Sedimentation test performed on leached BBC powder. Salinities from L-R: 0	171
Figure 5.3 Sedimentation test performed on GOM EI powder. Salinities from L-R: 1, 4, 16, 64, 128, 256 g/l. 5g of soil in each tube.....	172
Figure 5.4 Sedimentation test performed on GOM EI powder. Salinities from L-R: 1, 4, 16, 64, 128, 256 g/l. 5g of soil in each tube.....	172
Figure 5.5 Compression behavior in $e - \log \sigma'_{ac}$ space for RGOM EI at various pore fluid salinities	173
Figure 5.6 Compression behavior in $\varepsilon_a - \log \sigma'_{ac}$ space for RGOM EI at various pore fluid salinities	174
Figure 5.7 Permeability in porosity space for RGOM EI at various pore fluid salinities.....	175
Figure 5.8 Coefficient of consolidation in $\log \sigma'_{ac}$ space for RGOM EI at various pore fluid salinities	175
Figure 5.9 Compression behavior in $e - \log \sigma'_{ac}$ space for Leached RGOM EI at various pore fluid salinities.....	176
Figure 5.10 Compression behavior in $\varepsilon_a - \log \sigma'_{ac}$ space for Leached RGOM EI at various pore fluid salinities.....	177
Figure 5.11 Permeability in porosity space for Leached RGOM EI at various pore fluid salinities	178
Figure 5.12 Coefficient of consolidation in $\log \sigma'_{ac}$ space for Leached RGOM EI at various pore fluid salinities.....	178

Figure 5.13 Compression behavior comparison for RGOM EI and Leached RGOM EI (in $e - \log\sigma'_{ac}$ space)	179
Figure 5.14 Compression Index versus salinity comparison between RGOM EI and Leached RGOM EI over three stress ranges	179
Figure 5.15 Permeability behavior comparison for RGOM EI and Leached RGOM EI (in porosity space)	180
Figure 5.16 Compression behavior in $e - \log\sigma'_{ac}$ space for RGOM Upper and Lower at various pore fluid salinities.....	181
Figure 5.17 Compression behavior in $\epsilon_a - \log\sigma'_{ac}$ space for RGOM Upper and Lower at various pore fluid salinities.....	182
Figure 5.18 Permeability in porosity space for RGOM Upper and Lower at various pore fluid salinities	183
Figure 5.19 Coefficient of consolidation in $\log\sigma'_{ac}$ space for RGOM Upper and Lower at various pore fluid salinities.....	183
Figure 5.20 Compression behavior in $e - \log\sigma'_{ac}$ space for RGOM A and B at various pore fluid salinities	184
Figure 5.21 Compression behavior in $\epsilon_a - \log\sigma'_{ac}$ space for RGOM A and B at various pore fluid salinities	185
Figure 5.22 Permeability in porosity space for RGOM A and B at various pore fluid salinities	186
Figure 5.23 Coefficient of consolidation in $\log\sigma'_{ac}$ space for RGOM A and B at various pore fluid salinities.....	186
Figure 5.24 Compression behavior synthesis plot in $e - \log\sigma'_{ac}$ space for all soils in testing program	187
Figure 5.25 Compression Index versus salinity for all soils in test program averaged over a stress range from 0.1 to 1.0 MPa	188
Figure 5.26 Compression Index versus salinity for all soils in test program averaged over three stress ranges (0.1 to 1 MPa data is the same as that shown in Figure 5.25)	188
Figure 5.27 Permeability in porosity space synthesis plot for all soils in testing program	189
Figure 5.28 Coefficient of consolidation synthesis plot in $\log\sigma'_{ac}$ space for all soils in testing program	189

Figure 5.29 Relationship between pore fluid salinity and dry density for all soils in test program after consolidation to 0.1 MPa	190
Figure 5.30 Relationship between pore fluid salinity and wet density for all soils in test program after consolidation to 0.1 MPa	190
Figure 5.31 Relationship between pore fluid salinity and initial water content for all soils in test program after consolidation to 0.1 MPa	191
Figure 5.32 Cryo SEM images of GOM EI in a slurry state. Top: pore fluid salinity of 7 g/L, Bottom: pore fluid salinity of 64 g/L	192
Figure 5.33 Cryo SEM image of Leached GOM EI hydrated with distilled water in a slurry state	193
Figure 5.34 Cryo SEM image of Leached GOM EI in a slurry state. Pore fluid salinity is 64 g/L	193
Figure 5.35 Cryo SEM image of GOM EI in a slurry state. Pore fluid salinity is 64 g/L	194
Figure 5.36 Void ratio as a function of pore fluid salinity for RGOM EI at 0.1 MPa, 1 MPa, and 10 MPa axial effective stress	195
Figure 5.37 Correlation between the parameter C and liquid limit. The value of C generally decreases with liquid limit, indicating that compressibility sensitivity to salinity increases with liquid limit.....	195
Figure 5.38 Permeability as a function of pore fluid salinity for RGOM EI at porosities of 0.5, 0.4, and 0.3	196
Figure 5.39 Correlation between the parameter D and liquid limit. The value of D generally increases with liquid limit, indicating that permeability sensitivity to salinity increases with liquid limit.....	196
Figure 6.1 1-D compression behavior in e - $\log \sigma'_{ac}$ space for RGOM EI at 64 g/L from triaxial tests	212
Figure 6.2 Pre-shear void ratio versus axial consolidation stress for RGOM EI and Leached RGOM EI at three salinities from CK_0UC triaxial tests	212
Figure 6.3 The variation in K_0 with stress level as measured during the consolidation stage of triaxial tests for RGOM EI at 64 g/L	213
Figure 6.4 Lateral stress ratio at the end of virgin consolidation versus stress level for RGOM EI and Leached RGOM EI at three salinities from NC CK_0UC triaxial tests	213

Figure 6.5 Stress-strain curves for RGOM EI at 64g/L salinity	214
Figure 6.6 Normalized stress-strain curves for RGOM EI at 64g/L salinity	214
Figure 6.7 Normalized stress-strain curves (small strains) for RGOM EI at 64g/L salinity	215
Figure 6.8 Strain at failure versus stress level for RGOM EI & Leached RGOM EI at three salinities	215
Figure 6.9 Normalized undrained shear strength versus stress level for RGOM EI & Leached RGOM EI at three salinities.....	216
Figure 6.10 Undrained shear strength versus stress level for RGOM EI & Leached RGOM EI at three salinities	216
Figure 6.11 Normalized undrained shear strength versus lateral stress ratio for RGOM EI & Leached RGOM EI at three salinities	217
Figure 6.12 Brittleness versus stress level for RGOM EI & Leached RGOM EI at three salinities	217
Figure 6.13 Friction angle versus axial strain for RGOM EI at 64 g/L	218
Figure 6.14 Friction angle at maximum obliquity versus stress level for RGOM EI & Leached RGOM EI at three salinities.....	218
Figure 6.15 Normalized excess pore pressure versus axial strain for RGOM EI at 64 g/L salinity	219
Figure 6.16 Normalized shear induced pore pressure versus axial strain for RGOM EI at 64 g/L salinity.....	219
Figure 6.17 Normalized effective stress paths for RGOM EI at 64 g/L salinity	220
Figure 6.18 Skempton A parameter at peak versus stress level for RGOM EI & Leached RGOM EI at three salinities.....	220
Figure 6.19 Normalized undrained secant modulus versus axial strain for RGOM EI at 64 g/L salinity.....	221
Figure 6.20 Correlation between undrained strength ratio and liquid limit. Top Left: Correlation between S_1 parameter and liquid limit, Top Right: Correlation between T parameter and liquid limit (updated from Casey, 2013)	222
Figure 6.21 Correlation between friction angle and liquid limit. Top Left: Correlation between parameter A and liquid limit, Top Right: Correlation between parameter B and liquid limit (updated from Casey, 2013).....	223

List of Symbols

AC	Alternating Current
A/D	Analog-to-Digital Converter
BBC	Boston Blue Clay
CF	Clay Fraction
CK ₀ UC	K ₀ -Consolidated Undrained Compression Test
CH	High Plasticity Clay
CRS	Constant Rate of Strain
D	Dielectric Constant
D/A	Digital-to-Analog Converter
DC	Direct Current
DCDT	Direct Current Displacement Transducer
DSS	Direct Simple Shear
ESP	Effective Stress Path
GOM	Gulf of Mexico
LVDT	Linear Variable Differential Transformer
MIT	Massachusetts Institute of Technology
NaCl	Sodium Chloride
NC	Normally Consolidated
NSP	Normalized Soil Parameter
OC	Overconsolidated
OCR	Overconsolidation Ratio
PVC	Pressure-Volume Controller
QBASIC	Quick Beginners All-purpose Symbolic Instruction Code
RBBC	Resedimented Boston Blue Clay
RGOM A	Resedimented Gulf of Mexico Specimen A
RGOM B	Resedimented Gulf of Mexico Specimen B
RGOM EI	Resedimented Gulf of Mexico – Eugene Island
RGOM Lower	Resedimented Gulf of Mexico – Lower Interval
RGOM Upper	Resedimented Gulf of Mexico – Upper Interval

TX	Triaxial
SHANSEP	Stress History and Normalized Soil Engineering Properties
USCS	Unified Soil Classification System
VCL	Virgin Compression Line
A (A_f)	Skempton's pore pressure parameter (at failure)
c_c	Compression index
c_v	Coefficient of consolidation in the vertical direction
E_u	Undrained secant Young's modulus
E_u (MAX)	Undrained secant Young's modulus (maximum)
e	Void ratio
e_0	Initial void ratio
G_s	Specific gravity
I_p	Plasticity index
K_0	Coefficient of lateral earth pressure at rest
K_{0NC}	Coefficient of lateral earth pressure at rest for NC soil
k_v	Vertical permeability
p, p'	Average effective stress, $(\sigma_1 + \sigma_3) / 2, (\sigma'_1 + \sigma'_3) / 2$
q	Shear stress, $(\sigma_1 - \sigma_3) / 2$
s_u	Undrained shear strength
t	Time
t_p	Time to end of primary
$u, \Delta u$	Pore pressure, change in pore pressure
u_e	Excess pore pressure
u_s	Shear induced pore pressure
$V, \Delta V$	Current volume, change in volume
w_c	Water content
w_L	Liquid limit
w_P	Plastic limit
ϵ	Strain
ϵ_a	Axial strain

ε_{af}	Strain at peak shear stress
ϕ, ϕ'	Friction angle, effective friction angle
ϕ'_p	Effective friction angle at peak
ϕ'_{mo}, ϕ'_{cs}	Effective friction angle at maximum obliquity
γ_w	Unit weight of water
ρ	Density
σ_v, σ'_v	Vertical stress, vertical effective stress
σ'_p	Preconsolidation pressure
σ'_{ac}	Axial consolidation effective stress
σ'_{vc}	Vertical consolidation effective stress
$\sigma_1, \sigma_2, \sigma_3$	Principal stresses

1 INTRODUCTION

1.1 RESEARCH STATEMENT

Geotechnical engineering projects where an understanding of the impact changes in salinity has on the mechanical behavior of a high plasticity soil is relevant include oil and gas wellbore stability problems, engineered clay barriers for waste confinement, dam construction, and deep nuclear waste storage. During the design of such projects, it is of primary importance to assess how one dimensional consolidation, permeability, and strength properties are affected by changes in the pore fluid salinity concentration.

In recent years an increasing desire to gain a deeper understanding of the mechanical behavior of fine-grained high plasticity soils over an effective stress range from 0.15 up to 40 MPa has been driven primarily by the petroleum industry for applications in shallow hydrocarbon reservoir development. Such reservoirs, at depths less than 1000m are frequently located in unlithified or weakly lithified fine-grained sediments.

In the Gulf of Mexico area, a marine sediment deposited in a saltwater environment (~35 g/L), can undergo significant changes in salinity concentration with increased burial. Sediments with pore fluid salinities of up to 250 g/L are known to exist around salt domes (structures), which form beneath the sea bed in the Gulf region. Areas of interest for hydrocarbon exploration have been identified close to these salt domes, in soil strata with a high smectite composition. Therefore, there is now a need to investigate what impact, if any, varying pore fluid salinities have on smectite rich high plasticity soils.

1.2 RESEARCH OBJECTIVES AND SCOPE

In order to investigate the influence of salinity on the mechanical behavior of smectite rich high plasticity soils, the research is divided into two main testing programs. Constant Rate of Strain (CRS) testing was used to determine the impact of salinity on the one dimensional compression and permeability properties, while K_0 consolidated undrained shear in compression triaxial tests (CK_0UC) were conducted to determine both the salinity and stress dependent behavior.

The main focus of the research was on material from the Gulf of Mexico – Eugene Island. Test specimens were provided by carrying out an extensive resedimentation program in which samples were prepared with pore fluid salinities ranging from distilled water to 256 g/L. An additional research objective was to investigate the impact of salinity on a high plasticity soil which had its natural salts removed via leaching. Once this leaching process was complete, the leached soil was resedimented with a similar range of salt contents and then CRS tested, allowing for comparisons to be made between the behaviors of both soils. An axial effective stress of 40 MPa was set as a target limit test stress for all CRS testing. This requirement is due to the recent need, particularly by the hydrocarbon exploration industry, to understand the mechanical behavior of soils under this high stress condition as well as to determine what impact, if any, pore fluid has at such stresses.

To confirm the observed influence of salinity on GOM EI and leached GOM EI, four additional high plasticity soils were investigated under the same stresses conditions and with a similar range of pore fluid salinity. The testing of all six soils, ranging in plasticity, with liquid limits between 62 % and 90 %, enabled the author to confirm trends in the mechanical behavior to salinity with increasing plasticity.

A further objective of this research was to investigate the ultra-low stress behavior of high plasticity soils with differing salinities. GOM EI and Leached GOM EI were investigated. This was done using two very different methods. Firstly, by carrying out simple sedimentation tests to determine how increasing salinity impacts the height at which a soil with sediment to. Secondly, scanning electron microscope (SEM) images were taken of the soil cryogenically frozen in a concentrated slurry state to investigate the influence of salinity on floc development.

A systematic study was conducted on GOM EI and Leached GOM EI to investigate the salinity and stress dependent shear behavior of a high plasticity soil. Three widely varying salinities of 4, 64, and 256 g/L were used when resedimenting the test specimens. In order to determine the stress dependent behavior, GOM EI with a pore fluid salinity of 64 g/L was consolidated to axial effective stresses ranging from 0.125 MPa to 10 MPa prior to undrained shear in compression. The influence of varying pore fluid salinity on strength properties was investigated at lower and higher salinities of 4 and 256 g/L. Comparisons in behavior were made

between the three salinities at a low consolidation stress of 0.4 MPa and a higher consolidation stress of 10 MPa. The final research objective with respect to strength behavior was to conduct strength testing on leached GOM EI at the same three salinities and two stress levels. This allowed for a comparison to be made between the behavior of a natural high plasticity soil, and that of one that had its salts removed, thereby changing the flocculated structure and then adding salts back in varying quantities.

1.3 ORGANIZATION OF THESIS

This thesis is organized into seven chapters, each of which has a separate and distinct function, as given below.

Chapter 2 presents the important background information relevant to the research, divided into two main topics. Firstly, on how altering the pore fluid salinity affects the behavior of soil at the particle level as well as the macro level. Secondly, on the previous research carried out the impact of salinity on low plasticity illitic soils and high plasticity soils with smectite as the dominant clay mineral.

Chapter 3 describes in detail the six different soils from the Gulf of Mexico region used in this research, including index properties. Two material processes used during this research, namely, leaching natural salts from GOM EI, and cleaning GOM Upper and Lower to a state ready for resedimentation, are also outlined. The resedimentation procedure used to produce samples for tests, as well as trends observed with salinity during resedimentation is also presented.

Chapter 4 identifies the equipment and procedures used throughout the research. An overview is provided of the measurement instrumentation, data acquisition, and automation systems used. A detailed description of the Constant Rate of Strain (CRS) device, low, medium, and high stress triaxial devices is presented. The development of a new CRS device with capacity of 100 MPa is described. Procedures for conducting CRS and triaxial testing are also outlined.

Chapter 5 presents the mechanical behavior obtained from one dimensional consolidation CRS tests on six different high plasticity smectitic soils. Results are presented which include one dimensional compression, permeability, and coefficient of consolidation data. A comparison is made between the behaviors of GOM EI to leached GOM EI. The behavior of each soil tested at a similar salinity is also compared. A qualitative analysis of SEM images of GOM EI in a slurry state is presented to provide an explanation for and assist in the understanding of the observed mechanical behavior with salinity. Correlations between the sensitivity of a soils compressibility and permeability with changes in pore fluid salinity to liquid limit are proposed.

Chapter 6 presents the results from K_0 consolidated undrained shear compression tests on GOM EI and leached GOM EI. Results of the stress dependent strength behavior at 64 g/L pore fluid salinity is presented over a consolidation stress range from 0.15 to 10 MPa (with one test to 63 MPa). The salinity dependent strength behavior is presented from tests on 4 and 256 g/L. Correlations between undrained shear strength properties and liquid limit are also discussed.

Chapter 7 presents the main conclusions which can be drawn from the research. Finally, recommendations for future work are presented.

Appendix A and B outlines the procedures involved in conducting a CRS test and K_0 consolidated sheared undrained in compression triaxial test respectively. Appendix C describes the leaching procedure for the removal of in-situ salts from soils using dialysis tubing.

2 BACKGROUND

2.1 INTRODUCTION

This chapter provides background information on two main topics. Firstly, on how altering the pore fluid salinity affects the behavior of soil at the particle level as well as the macro level. Secondly, on the previous research carried out the impact of salinity on low plasticity illitic soils and high plasticity soils with smectite as the dominant clay mineral. Throughout this thesis the terms smectite and montmorillonite will be used to describe the same mineral.

Section 2.2 describes the various factors that influence how the individual particles interact and in turn impact the formation of flocs. The addition or removal of salts from the pore fluid impacts the behavior of soil particles. The observed behavior change will vary depending on the type of minerals present in the soil. In the vast majority of cases, natural soils consist of a mixture of minerals in differing proportions. This complexity creates the uncertainty as to the impact of salt in a soil-water system. Therefore, the change in behavior may be different for a natural soil with a mixed composition as compared to pure mineral composition.

Section 2.3 outlines the previous research which has been conducted in this area. This research is divided into four areas, namely: the addition of salts to soils, the removal or leaching of salts from soils, research on intact soil samples with high pore fluid salinities, and lastly, the evolution of pore fluid salinity with increasing confining stress.

2.2 IMPACT OF SALT ON SOIL BEHAVIOR – PARTICLE LEVEL¹

2.2.1 Introduction

The discrete particles or clay minerals that make up a fine grained soil are composed of small plate-like particles (applies to clay minerals only) ranging in diameter from a few hundredths of a micron to several microns. Each such platelet consists of one or more unit layers, stacked like a deck of cards; the crystal structure of the unit layers consists of sheets of silica in a

¹ The following section is inspired by the work of Aiden Horan, SM, 2012.

tetrahedral shape in combination with sheets of either alumina or magnesia in an octahedral shape. A discrete montmorillonite particle has three layers consisting of a sheet of octahedral alumina or magnesia between two sheets of tetrahedral silica (Allen & Matijevic, 1974).

The way in which the pore fluid salinity affects soil behavior will be described for a homogeneous soil mass. The discrete particles that make up soil are not strongly bonded together and hence are relatively free to move with respect to one another. The deformation of a soil mass under an applied stress is controlled by interactions between the individual particles, in particular by the sliding motion of two particles in contact. Because sliding is a nonlinear and irreversible deformation, the stress-strain behavior of the soil is strongly nonlinear and irreversible. This process describes the mechanical contact between particles (Lambe & Whitman, 1969).

The space between soil particles is called pore spaces and they are filled with air and/or water. The nature of the pore fluid will influence the magnitude of the shear resistance existing between two particles by introducing chemical matter to the surface of contact. In the case of very small soil particles, the pore fluid may intrude between the particles meaning there is no mechanical contact and that physio-chemical forces dominate the behavior of the soil mass. The spacing of these particles will increase or decrease as the transmitted compressive forces decreases or increases. Therefore soil is an inherently multiphase system consisting of a mineral phase called the mineral skeleton and a fluid phase called the pore fluid. The constituents of the pore phase will influence the nature of the mineral surfaces and hence affect the process of force transmission at the particle contacts. This interaction between the phases is called chemical interaction (Lambe & Whitman, 1969).

The influence of pore fluid salinity on a soil is dependent on its mineralogy and composition. Differences in particle size and shape are mainly due to differences in the types and arrangements of elements in the crystalline structure which in effect defines the mineralogy of a soil. A clay particle is a colloid, which is a term used to describe a particle whose behavior is controlled by surface derived forces rather than mass derived forces. The size range of colloids has been more or less arbitrarily set as $1 \mu\text{m}$ to 1μ ($10^{-9} - 10^{-6}$ m), (Lambe & Whitman, 1969).

2.2.2 Specific Surface Area & Cation Exchange Capacity

The smaller the particle size, the larger its specific surface. The specific surface area (SSA) is the ratio of the surface area of a material to either its mass or its volume.

It is a common fact that larger particles, regardless of shape, have smaller surface areas per unit of mass and therefore smaller specific surfaces than small particles. Specific surface is inversely proportional to the grain size of a soil. A soil mass made up of many small particles will have, a larger specific surface than the same mass made up of larger particles. From the concept of specific surface, a larger moisture content should be expected from a fine-grained soil than a coarse grained soil at a given stress. Figure 2.1 shows the average values of relative sizes, thicknesses and specific surface areas for four of the most common clay minerals. It can be seen from this Figure that montmorillonite is the smallest clay mineral that is encountered and it is also the most sensitive to water. Kaolinite on the other hand, is one of the larger and less sensitive minerals to water encountered in clay (Holtz & Kovacs, 1981).

For a typical sodium soil, a montmorillonite particle would carry 1.4×10^4 ions while the kaolinite has 4×10^6 ions. If the individual clay particles are now dropped into water, both the mineral surfaces and the exchangeable ions pick up water i.e. hydrate. Upon hydration, the sodium ion grows about sevenfold. These hydrated ions are too large to fit into a monoionic layer on a mineral particle even if they wanted to, and the exchangeable ions with their shells of water move away from the mineral surface to positions of equilibrium. The ions are attracted to the mineral surface to satisfy the negative charge existing on the surface but they also desire to move away from each other because of their thermal energies. In actual fact, the position which they occupy is a compromise between these two types of forces. Therefore when the particles are dropped into water, the ions move away from the surface to form what is termed the double layer (Lambe & Whitman, 1969). Within this double layer the cation concentration falls from the particle surface in the direction of the surrounding solution. The concentration of anions consequently will be very low next to the particle surface and rise towards the free water – free water being the pore water not held in the double layer. It is at this juncture it should be noted that development of the double layer on a clay particle will be controlled by the salinity of the pore fluid. Because an increase in ionic concentration is noted with an increase in salinity, double layer growth will be hindered with an increase in pore fluid ionic concentration (salinity).

The maximum distance to which the double layer of a given soil will develop beyond the soil particle will only be realized in distilled water. In saltwater, the double layer of a given soil will extend away from the particle until the concentration of sodium ions in the double layer is equal to that of the pore water. It is therefore stated that at some salinity there will be no double layer growth as the ionic concentration of the pore fluid will be able to satisfy the ionic demand of the particle at the particle surface. The double layer length is therefore the distance from the surface of a soil particle over which there is an electric potential.

This is best demonstrated in Figure 2.2 where a simple sedimentation test is performed on hydrated sodium montmorillonite. Each tube contains the same quantity of soil (1 g), but the pore fluid salinity increases from 1 g/l on the left to 256 g/l on the right. It can be seen that the ionic demand of the double layer for this soil is satisfied in between salinities of 16 & 64 g/l as after 64 g/l there is no change in sedimentation height with an increase in salinity. The Figure also shows that between the 1 & 16 g/l pore fluid contents, when an increase in salinity is observed there is a corresponding decrease in double layer growth – this is evident by the lower sedimentation height. The behavior of the montmorillonite in the sedimentation tubes has been described by Witteveen et al. (2013) as *chemical consolidation* whereby the increase in cations in the higher salinities decreases the double layer and in turn the repulsive forces between each particle. This double layer reduction leads to a decrease in the overall volume occupied by the 5g of soil particles. This behavior is also described in the literature as *osmotic consolidation*.

The cation exchange capacity (CEC) of various clay minerals differs greatly. As the particle size increases the CEC decreases. The composition of the mineral also has an effect on CEC. Kaolinite has a value of 5meq/100g (millie-equivalent per 100 grams) whereas montmorillonite has a CEC value of 100meq/100g (Lambe & Whitman, 1969). It is well known that with an increase in CEC there is a corresponding increase in the sensitivity of the mineral to changes in the electrolyte content or salt concentration of the pore fluid. Therefore a soil with a majority of smectitic minerals will exhibit greater behavioral changes with changes in pore fluid salinity than a soil with majority kaolinite.

2.2.3 Floc Formation

A typical clay particle has charges on its surface. The narrow edges of the particle are predominantly positively charged, whereas the large face areas are predominantly negatively charged. As the face areas are greater than the edge areas, the clay particle has a net negative charge.

There exist both attractive and repulsive forces between each individual clay particle. When two fully hydrated clay particles which exist in water are brought closer together, they will reach an inter-particle spacing at which they begin to exert forces on each other. Because each particle carries a net negative charge, they tend to repel each other. Since this negative charge on clay particles is balanced by the cations in the double layer, the two particles begin to repel each other when their double layers overlap one another. This represents the repulsive force which exists between soil particles and it is directly related to the thickness of the double layer (Lambe & Whitman, 1969). By changing the pore water chemistry of a soil-water system, double layer development will be either increase or decrease. Generally, as the pore fluid salinity increases, the size of the double layer decreases.

The attractive force that exists between two particles is known as the van der Waals' force, or secondary bonding force which acts between all adjacent pieces of matter and it is independent of the characteristics of the fluid between the particles. If the net force between two clay particles is attractive then the two particles will move towards each other and become attached – this is known as flocculation. If the net force between the two particles is repulsive then they will move away or disperse. When a suspension of clay particles flocculates, three different modes of particle association may occur: face-to-face, edge-to-face and edge-to-edge. Face-to-face association leads to thicker and possibly larger flakes whereas edge-to-face and edge-to-edge associations will lead to three dimensional voluminous card house structures (Van Olphen, 1977). The various modes of particle association are shown in Figure 2.3.

The structure of a soil once formed consists of inter-particle forces and the fabric. The inter-particle forces describe how the shear and normal stresses are transmitted between soil particles, while the fabric of a soil is defined by the orientation and distribution of particles. The clay mineral montmorillonite is distinguished from illite first by the large size difference but also

by the presence of interlayer swelling in the presence of water. Montmorillonite, with 10 times the SSA, is also far more active than illite and therefore will be more susceptible to changes in pore fluid salinity than illite. Horan (2012) confirmed by carrying out an extensive testing program on an illitic soil such as resedimented Boston Blue Clay that varying the salinity of the pore fluid had negligible impact on its mechanical behavior. It is anticipated that based on the values of SSA and CEC, changes in pore fluid salinity will have a distinct effect on the mechanical behavior of smectitic soils.

2.3 LITERATURE REVIEW

2.3.1 Introduction

The research presented in this thesis involves both the addition and removal of salts from high plasticity smectitic soils. Although the effect salt has on the behavior of various types of soil have been previously studied, the results from this research will now be described in the following Sections.

Firstly, the addition of salts to the fabric after the soil has been deposited and its impact on mechanical behavior. This scenario exists in regions where the marine deposit has undergone further or prolonged burial and now exists in regions/elevations where the salinity of the pore water is higher than when the soil was deposited. This addition of salt to the soil fabric can occur under two scenarios. Figure 2.4 shows how the pore fluid salinity of a limestone formation in Illinois naturally increases with increasing burial (Engelhardt & Gaida, 1963). A marine clay beneath the Caspian Sea shows a similar trend in salinity with depth (Van Paassen & Gareau, 2004). Secondly, as a marine sediment undergoes burial a percentage of the pore solution is driven out under the increasing overburden stresses and will flow upwards through the whole section. Where this upward flow is interrupted by less permeable clay formations, these formations act as barriers resulting in the accumulation of dissolved salts and an overall increase in the pore fluid salinity (Engelhardt & Gaida, 1963). The Gulf of Mexico is one such region where this occurs and soils at depths below the sea bed in this location commonly encounter salinities much higher than those that existed when the soil was first deposited. Pore fluid salinities of 80 g/L are common but salinity can reach levels of up to 250 g/L (reference).

The second Section of the literature review covers what happens to a soil when salts are removed or leached out of a soil fabric. This research focuses on what happens when the salts are removed thereby reducing the electrolyte content of the pore fluid. Extensive research has been performed in this area as it is a more common issue which confronts Geotechnical Engineers. The issue arises in areas where a marine soil has been uplifted and either has or is currently undergoing the leaching process described.

The third Section looks at in-situ soil which is naturally high in salinity. Laboratory testing which was performed on recovered specimens will be examined and information which is relevant to this research will be discussed.

The fourth Section covers the previous research carried out in relation to the evolution of pore fluid salinity with increasing confining stress.

2.3.2 Impact of Increasing Salinity on Mechanical Behavior

2.3.2.1 One Dimensional Consolidation Behavior

In 2005, Calvello et al. carried out tests on three different resedimented smectitic clays whereby they varied the pore fluid composition and salinity. Two soils were pure smectite with the third consisting of 30% smectite. The dielectric constant (D) of the pore fluid was used as a reference to compare the behavior of each soil tested. The D of the pore fluid ranged from 1 (air) to 110 (formamide). Distilled water has a D value of 80 and a decrease in the D of a pore fluid is similar to an increase in the salinity or electrolyte content of that same fluid. Compressibility was evaluated by means of oedometer tests and

Figure 2.5 shows that for all three soils, the compression index increased with increasing D. Similar research by Bolt (1956), Mesri and Olsen (1971), van Paassen & Gareau (2004), Ajmera & Tiwari (2012), and Nguyen et al. (2013) on smectitic soils/high plasticity soils reached similar conclusions with compressibility decreasing with increasing pore fluid salinity.

In 2012 at MIT, Aiden Horan conducted extensive testing on several types of natural soils such Boston Blue Clay (BBC), London Clay, a clay from the Gulf of Mexico, and a pure sodium montmorillonite. As part of the testing program BBC Series IV was resedimented with

pore fluid salinities ranging from 4-256 g/l and then consolidated to an axial effective stress of 10MPa (Void ratio ranging from 1.3 – 0.5). The research showed that the pore fluid salinity was not a factor when it comes to the one dimensional consolidation behavior of this illitic clay. Similar strains for a given axial effective stress were required and very comparable void ratios were also produced for a given axial effective stress for all the salinities tested. The hydraulic conductivity of this illitic clay was also found to be independent of pore fluid salinity over this stress range.

Bolt (1956) found that the influence of electrolytes on the void ratio of compressed montmorillonite clays disappears or becomes negligible once consolidation stresses exceed 10atm or 1MPa. This indicates that for smectitic soils, once a certain stress is applied, the compression behavior becomes stress dependent and independent of pore fluid concentration.

2.3.2.2 Permeability and Coefficient of Consolidation

Calvello et al. (2005) found that for a soil consisting of 30% smectite, the permeability of the soil increases with increasing salinity. The results of which are shown in Figure 2.6. More recent work conducted by Nguyen et al. (2013) on a high plasticity soil ($w_L = 136\%$ and $w_P = 36\%$) with a 57% clay fraction consisting of 85% smectite and illite/smectite found a clear trend of increasing permeability with increasing pore fluid salinity.

Clay samples with differing pore solutions consolidate to the same void ratio at high stress but have different permeability's therefore the flocculated structure must be different. Clays with very low salt concentrations will consist of small flocs or individual primary particles. Greater orientation of particles occurs with pore solutions containing less electrolyte concentration. With less electrolyte concentration, the double layer thickness increases with less particle to particle contact preventing rotation due to friction. The clay with better orientation of particles leads to narrower flow channels and this results in lower permeability (Engelhardt & Gaida, 1963).

Mesri & Olsen (1971) offered a different hypothesis for the observed increased permeability with increasing pore fluid salinity in active clays such as montmorillonite. Their hypothesis was based on the belief that as salinity increases there is a further contraction of flocs

of clay particles, consequently decreasing the volume of the pores within the flocs (intra-aggregate or micro voids) and increasing the volume of voids between the flocs (inter-aggregate or macro voids). The increase in the macro voids becoming the key mechanism for the increase in permeability with salinity. This is in agreement with observations made by Nguyen et al. (2013) whereby analyzing SEM images of a smectite rich high plasticity soil with varying pore fluid salinities identified larger flow channels with increasing salinity.

The coefficient of consolidation, c_v , represents the rate at which a clay undergoes one-dimensional consolidation when subjected to an increase in stress. The c_v of the three smectitic soils tested by Calvello et al. (2005) was found to increase with increasing salinity. The c_v of the Bisaccia clay with respect to the pore fluid can be seen in Figure 2.7. Other researchers such as Engelhardt & Gaida (1963) found a similar trend in c_v with increasing electrolyte concentration and the effect being more pronounced with montmorillonite than kaolinite. This is in agreement with research conducted by Nguyen et al. (2013) on two high plasticity soils with varying clay fraction and smectite content. Results show an increase in the effect of salinity on c_v and hydraulic conductivity with increasing smectite content.

One-dimensional consolidation tests conducted by Robinson and Allam (1998) on three soils consisting of pure kaolinite, pure illite, and pure montmorillonite to investigate the c_v behavior with increasing stress up to 1MPa. They found that the c_v for both kaolinite and illite increased with increasing stress. Kaolinite showed the greatest increase with respect to stress. The opposite was observed for the montmorillonite as c_v was found to decrease with increasing stress. It is their belief that the observed increase or decrease in c_v up to a stress of 1MPa for a given soil depends on whether the consolidation behavior is governed by mechanical or physio-chemical factors. The compressibility and c_v of kaolinite and illite is governed by mechanical factors, whereas montmorillonite is governed by physio-chemical.

2.3.2.3 Strength Characteristics

Several researchers have investigated the influence of salinity on the strength properties of soils with kaolinite, illite, and smectite as the dominant clay mineral. In 1961 at MIT, Anwar Wissa performed research on the influence of salinity on the stress-strain properties of kaolinite. He ran a series of triaxial compression tests on resedimented sodium kaolinite. Also in 1961 at

MIT, William Bailey conducted research into the effects of salt on the shear strength of Boston Blue Clay (a glacio-marine illitic clay). He ran isotropically consolidated undrained triaxial tests on resedimented Boston Blue Clay (BBC) ranging in pore fluid salinity from 3 – 35 g/l. As part of his research, he also leached some Boston Blue Clay and strength tested this soil. Horan (2012) conducted similar strength testing on BBC resedimented with pore fluid salinities of 4 g/l and 256 g/l with a series of K_0 consolidated undrained shear in compression triaxial tests. Calvello et al. (2005) carried out shear strength testing of three smectitic soils by means of direct shear and ring shear tests. Similar research to that of Calvello et al. was also conducted by van Paassen & Gareau (2004) and Man & Graham (2010) on high plasticity smectite-rich soils. Pineda et al. (2013) carried out Direct Simple Shear (DSS) tests on Ballina Clay, a high plasticity estuarine clay from Richmond River Valley, NSW, Australia, with a natural pore fluid salinity of approximately 25 g/L. Intact specimens were tested using two different external pore fluid salinities – 0 g/l and 35 g/l NaCl. The pore fluids used refer to the salinity of the water surrounding the specimen in the DSS device. The findings of each researcher are outlined in the following sections.

In the case of kaolinite, the research by Wissa showed that with an increase in salinity, a corresponding reduction in undrained strength is observed. He links this change in behavior with an increase in salinity to the fact that the positive and negative charge on the clay particle will be reduced meaning that the degree of flocculation decreases as the pore fluid salinity increases. In fact, Wissa found that kaolinite soils resedimented with distilled water as the pore fluid were stronger than those resedimented with salt water as the pore fluid.

In contrast to the behavior of kaolinite soils, Bailey found that BBC containing more salt (35 g/l as opposed to 3 g/l) had a higher effective stress envelope at maximum principle stress difference, and that leaching the salt from a normally consolidated soil sample decreased the shear strength and the strain to failure. He also found a 6.5° reduction in the effective stress envelope at maximum principle stress difference for the leached soil. The results by Horan on similar BBC are in contrast to the behavior observed by Bailey. Horan observed that increasing the pore fluid salinity increased the strain to failure and actually decreased the shear stress producing failure. No definitive trend in friction angle was observed with respect to salinity for BBC.

The results of the research by Calvello et al. into the influence of salinity on smectitic soils can be seen in Figure 2.8. The results indicate an increase in residual shear strength of each soil with an increase in pore fluid salinity. The research by van Paassen & Gareau (2004) and Man & Graham (2010) reached similar conclusions with shear strength increasing with increasing pore fluid salinity for high plasticity smectitic soils. Pineda et al. found that for a high plasticity marine clay, varying the salinity of the fluid external to the test specimen showed that strength parameters have a clear dependence on the pore fluid. They found that shear strength increased with increasing salinity at normal stresses of 25kPa and 97kPa. Movement of fluid into the specimen to balance the salinity between the pore fluid and surrounding water occurred during testing, resulting in the change in strength properties.

This is an important finding as the strength testing carried out in this thesis involves a large range of pore fluid salinities. It is therefore essential to ascertaining the correct strength behavior that the salinity of the fluid in the strength testing device match that of the specimen. To neglect this criterion may result in water flow either in or out of the specimen undergoing consolidation via a concentration gradient generated between the external pore fluid and the pore water of the specimen.

Casey & Germaine (2013) investigated the undrained strength properties of a wide variety of soils over a range of effective stresses from 0.1 to 10 MPa. The majority of results are derived from K_0 consolidated undrained shear in compression triaxial tests. Plasticity ranged between 7.5 and 43.3 %, with liquid limits between 25.8 and 73.8 %. The findings showed that normalized shear stress-strain responses, undrained strength ratios, and critical state friction angles vary considerably amongst the soils tested and consistently over this large effective stress range. For the higher plasticity soils tested ($w_L > 40$ %), undrained strength and friction angle decreased with increasing effective stress. The research also showed that the previous concept of soil exhibiting constant normalized properties is only valid if behavior is viewed over a narrow stress range. Correlations developed by Casey & Germaine allow the undrained strength properties to be estimated from liquid limit. They described the variations in undrained strength ratio and friction angle with increasing consolidation stress using a power law function containing two parameters. These parameters were then correlated effectively to liquid limit. For both the undrained strength ratio and friction angle, the rate at which this property decreased

with increasing consolidation stress was found to increase with increasing liquid limit, for all soils with a liquid limit above 40 %.

2.3.3 Leaching Salts from Soil

The effect of salt on a soil mass has been well studied and researched. This involves removing (leaching) the existing salt from a marine soil to determine how the soil behavior changes. One example is a marine clay which has been laid down in a marine environment with a typical salinity of 35 g/l or less. Marine deposits frequently undergo uplift so that they rise above the level of the sea. The result of fresh groundwater percolating through the clay serves to gradually remove this natural salt from the clay. This process occurs over many thousands of years. The pore fluid at which a soil exists today can be much different from that at the time of deposition. This process also happens when artesian pressure is present in the groundwater such as is the case in areas of Boston. This reduction in the electrolyte content of the water around the soil particles can reduce the net attraction between them – in other words, leaching of the salt from the pore fluid can cause a reduction in shear strength (Lambe & Whitman, 1969). Laboratory experiments such as those described in Lambe & Whitman (1969) had previously been performed by Bjerrum & Rosenqvist (1956) on artificially sedimented clays. Their experiments proved that if a soil is sedimented in salt water and the soil is then later subjected to a hydraulic gradient resulting in the leaching of salt, the undrained shear strength will be reduced and its sensitivity increased. They also found that if the same clay is deposited in a fresh water, the shear strength is two to three times as high as the one sedimented in the salt water. The clay used in this research was an Asrum clay in which the salt had been leached from the soil naturally in-situ. The soil is of very low plasticity with a clay fraction consisting of 60% illite with the remainder composed of quartz and feldspar. Some of the results from this research can be seen in Figure 2.9. Their work shows that in the case of an illitic clay, the addition of salt increases the undrained shear strength whereby at a given stress, an increase in the shear strength is observed for an increase in salt content.

Horan (2012) carried out one-dimensional consolidation tests on BBC that had the natural salts leached from it. Specimens of leached BBC were resedimented with varying pore fluid salinities. Results showed an increase in the void ratio at low stress for a given salinity compared

to the natural soil. The leaching process increased the sensitivity of the majority illitic BBC clay to the presence of salts. The leaching process did not however have any impact on the permeability of the soil as both the natural and the leached BBC showed similar permeability's over the wide range of pore fluid salinities used. Strength testing was also carried out on the natural and leached BBC to determine the behavior with salinity. A salinity of 1 g and 256 g was used as the pore fluid for the leached. No trend in shear strength was noted for the leached BBC. However, the leached soil did show a more pronounced increase in friction angle with increasing salinity compared to the behavior observed in the natural BBC. Both salinities tested and both soils showed similar strains to failure indicating that the leaching process did not change the ductility of the soil.

Tiwari et al. (2005) also showed that the leaching of natural salts from a high plasticity soil with smectite as the dominant clay mineral resulted in lower shear strengths and a reduction in the soils friction angle by up to 30%.

2.3.4 Testing Intact Soil with High Salinity

Van Paassen and Gareau (2004) conducted one dimensional compression testing on intact marine clay recovered at depths of up to 180 m below the Caspian Sea. The soil was described as high to extremely high plasticity clay with salinity of the pore fluid at the recovery depths to be approximately 250 g/l. They found the pre-consolidation pressures of the soil to be less than the calculated overburden stress meaning that the soil is not normally consolidated, but is in fact under-consolidated. Their results can be seen in Figure 2.10 and show clearly that the measured pre-consolidation pressure is much lower than the calculated overburden stress. These low pre-consolidation pressures were attributed to using fresh water as the surrounding fluid in the oedometer cell. They believe that this in effect caused leaching of the salt from the soil during the test due to an osmotic potential between the pore fluid and the external fluid. To prove this theory, several more oedometer tests were run on recovered material with different cell fluid salinities and the results show that when the cell fluid salinity closely matches the pore fluid salinity, a higher pre-consolidation pressure is recorded than when fresh water is used. The results of these tests are shown in Figure 2.11.

This is an extremely important finding in relation to the research performed in this thesis as all one-dimensional compression testing will be performed on soils with a large range of pore fluid salinities. It is therefore essential to use cell fluid in the testing device which matches the pore fluid salinity of the soil being tested in order to ascertain the correct compression behavior.

2.3.5 Evolution of pore fluid salinity with increasing confining stress

Little research has been carried out on the evolution of the electrolyte content (salinity) of the pore solutions during consolidation. Engelhardt & Gaida (1963) consolidated specimens of kaolinite and montmorillonite to stresses ranging from 3MPa to 80MPa to investigate the aforementioned behavior.

No concentration change was evident in the pore fluid of kaolinites but for the case of pure montmorillonites, as the soil was consolidated to a porosity of 0.33 (stress ~ 80MPa) there was a removal of salt by the filtrates and a continuous decrease of the NaCl concentration in the pore solution. As the stress increased, the electrolyte rich free water was expelled and the electrolyte poor water of the double layer was left behind. Because of this, the mean salinity of the pore fluid decreased. This reduction in salinity is shown in Figure 2.12. At this porosity, the pore fluid salinity reduced to 15% of the original concentration. As the montmorillonite consolidates to a porosity below 0.3, the experiments showed that rather than the pore fluid transitioning to one with zero salt concentration there is actually an increase in the pore fluid salinity of the soil, shown in Figure 2.13. Stresses of 80MPa were required to reach these low porosities. They believe that this increase in salinity is due to flow channels becoming blocked off resulting in small pockets of salt solution becoming trapped and surrounded by clay particles with interpenetrating double layers. As consolidation continues, more water is expelled; the trapped solution will also lose water but retain the majority of the dissolved salt, with the result being an overall increase in the pore fluid salinity.


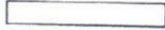

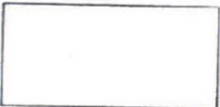
Edge View	Typical Thickness (nm)	Typical Diameter (nm)	Specific Surface (km ² /kg)
 Montmorillonite	3	100-1000	0.8
 Illite	30	10 000	0.08
 Chlorite	30	10 000	0.08
 Kaolinite	50-2000	300-4000	0.015

Figure 2.1 Average values of relative sizes, thicknesses and specific surface area of the mostcommon clay minerals (Yong & Warkentin, 1975)

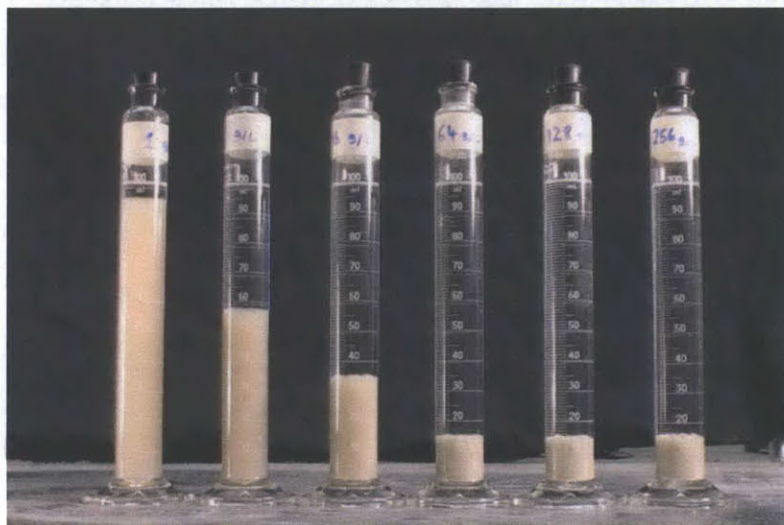


Figure 2.2 Sodium montmorillonite at different pore fluid salinities. Saltwater content L-R: 1, 4,16, 64, 128 & 256 g/l NaCl. (1 g of soil used in each tube) (Horan, 2012)

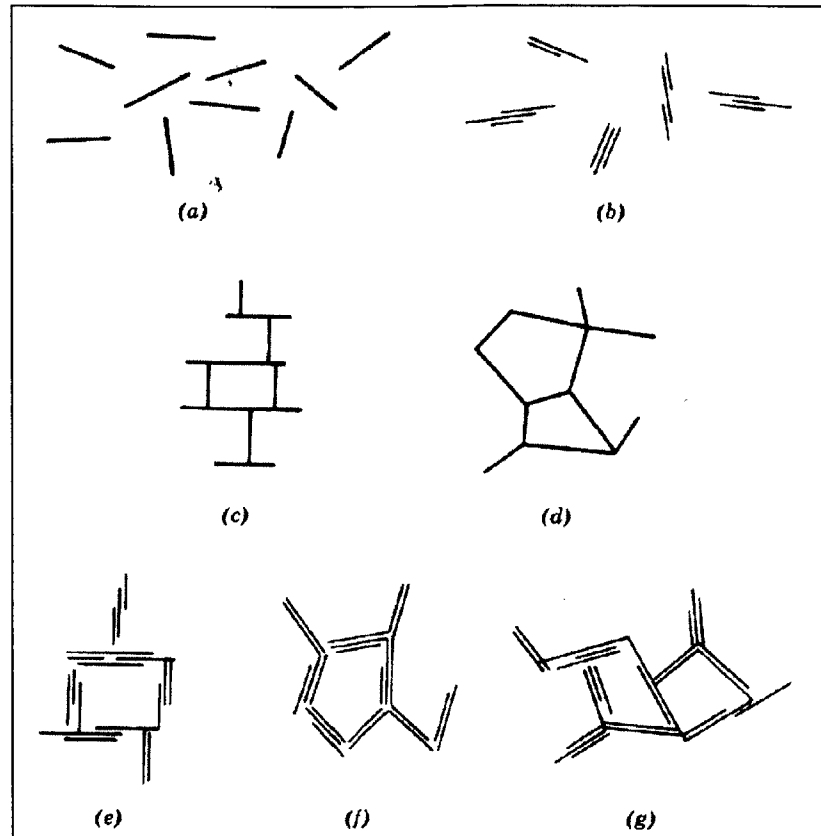


Figure 2.3 Modes of particle association in clay suspensions and terminology (a) dispersed and deflocculated (b) aggregated but deflocculated (c) edge to face flocculated but dispersed (d) edge to edge flocculated but dispersed (e) edge to face flocculated and aggregated (f) edge to edge flocculated and aggregated (g) edge to face and edge to edge flocculated and aggregated (Van Olphen, 1977)

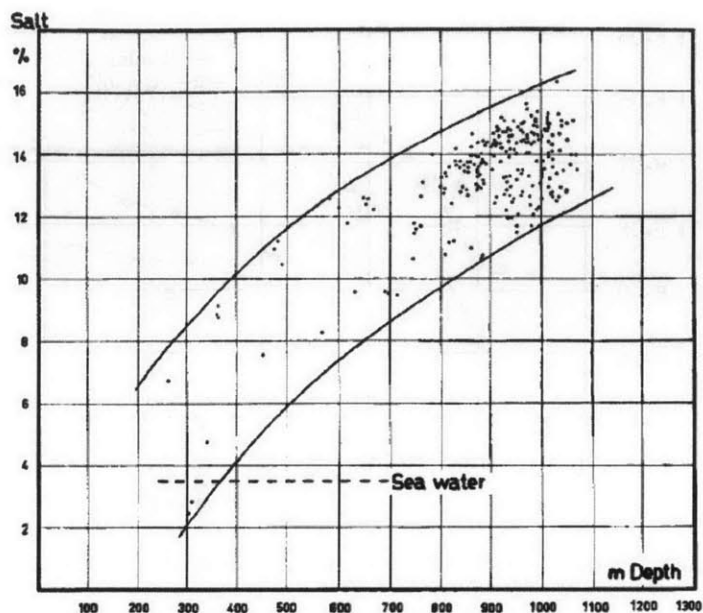


Figure 2.4 Salinity of formation waters from the St. Genevieve Limestone formation, Illinois (Engelhardt & Gaida, 1963)

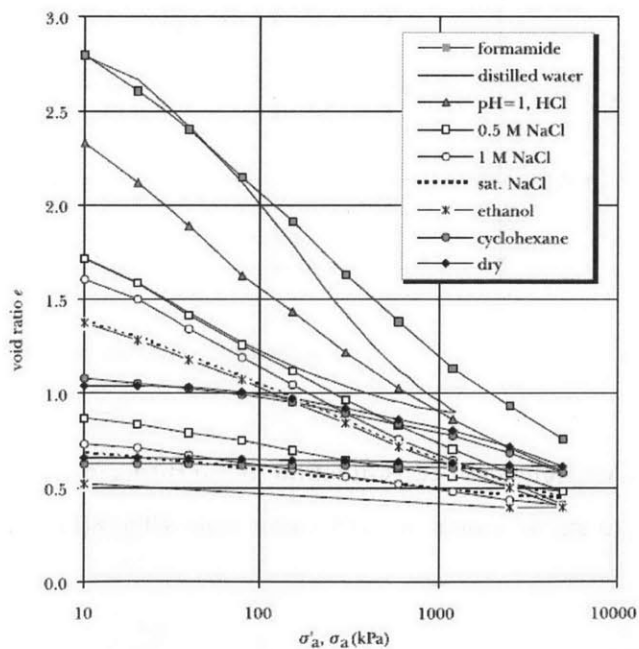


Figure 2.5 Compression curves of the Bisaccia clay (30% smectite) resedimented with different types of pore fluids. Void ratio and compressibility increase with decreasing salinity (Calvello et al., 2005)

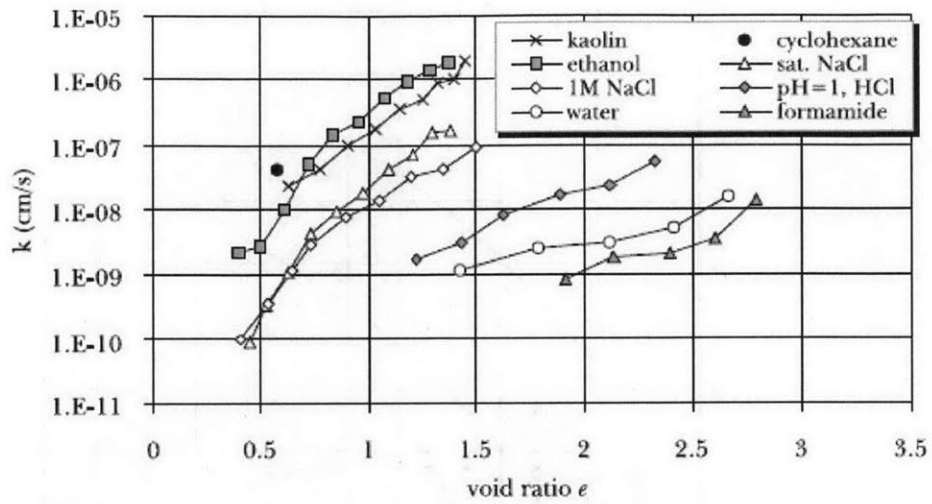


Figure 2.6 Hydraulic conductivity of the Bisaccia clay (30% smectite) resedimented with different pore fluids (Calvello et al., 2005)

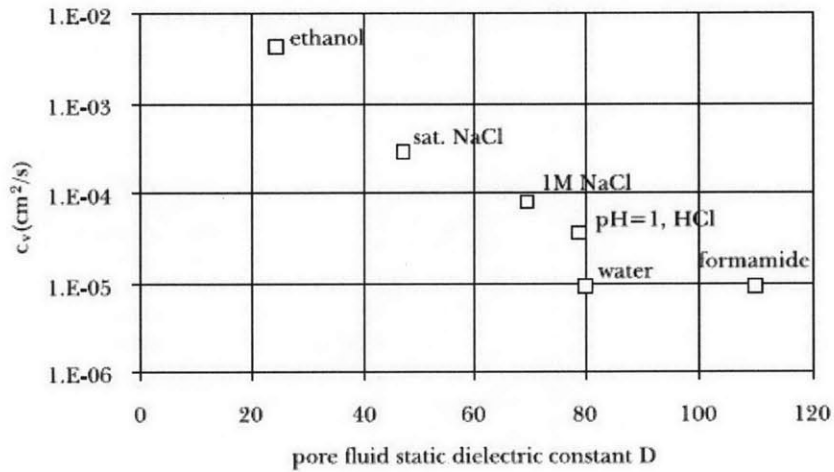
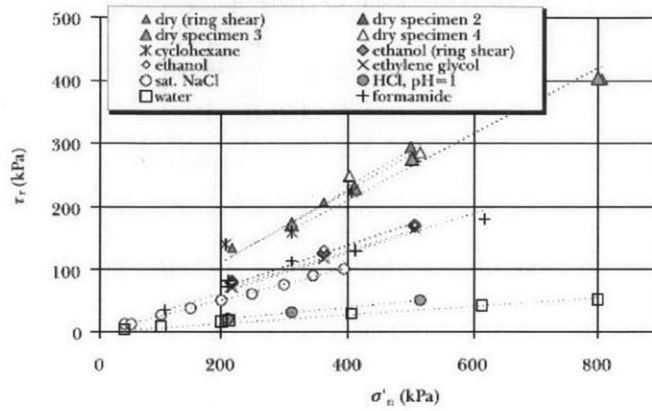
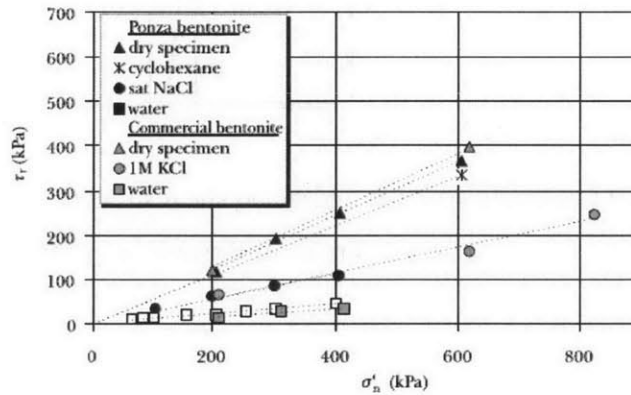


Figure 2.7 Coefficients of consolidation of the Bisaccia clay resedimented with different fluids relative to an increment of axial stress from 40 to 80 kPa (Calvello et al., 2005)



(a)



(b)

Figure 2.8 Residual shear strength of smectitic clays resedimented with varying pore fluids. (a) soil with 30% smectite, (b) 100% smectite soils namely; Ponza Bentonite and Commercial Bentonite (Calvello et al., 2005)

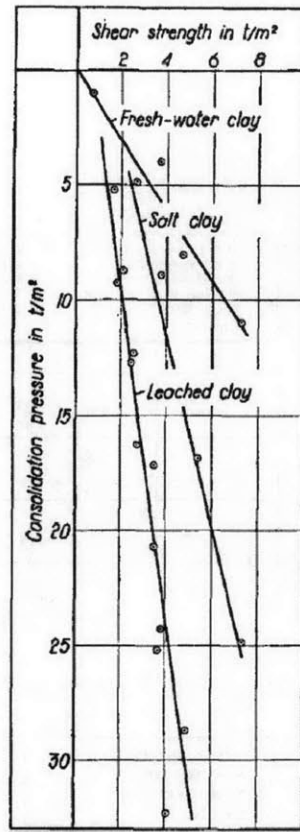


Figure 2.9 Comparison of the undrained shear strength of salt, leached and fresh-water clays (Bjerrum & Rosenqvist, 1956)

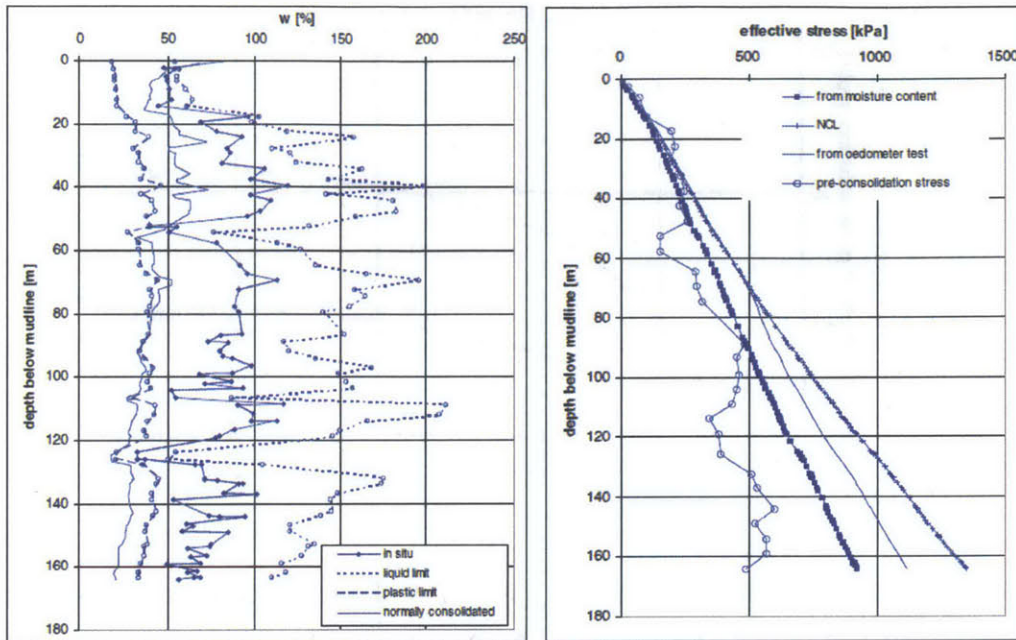


Figure 2.10 Soil profiles from the Caspian Sea: Atterberg limits on the left and measured preconsolidation pressures on the right (van Paassen. et. al., 2004)

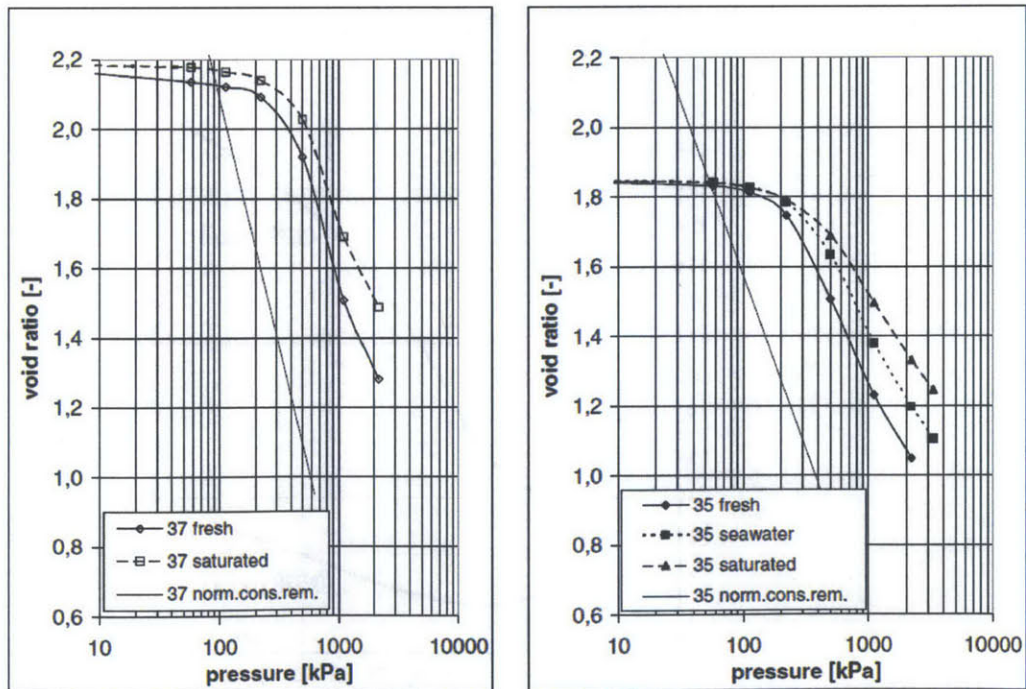


Figure 2.11 Oedometer test results from Caspian Sea recovered from two different depths run at different cell fluid salinities (van Paassen. et. al., 2004)

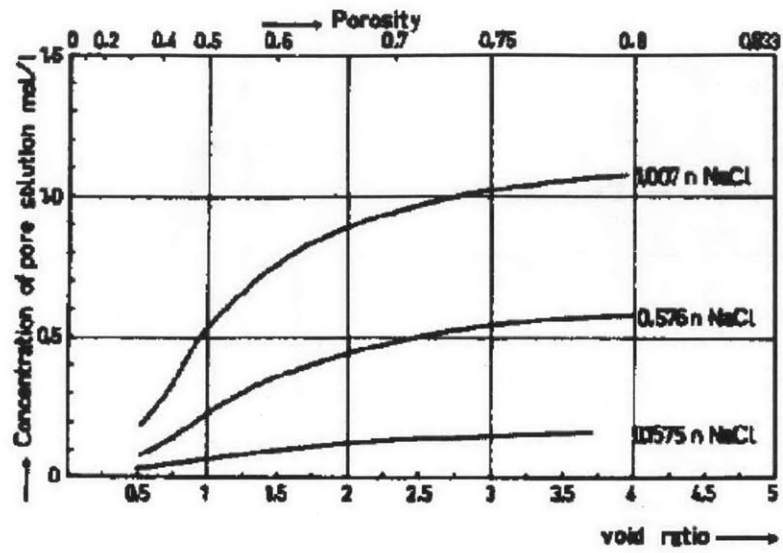


Figure 2.12 Concentration change of NaCl pore solution in compressed montmorillonite clay. Stress ranged from 3 to 320MPa (Engelhardt & Gaida, 1963)

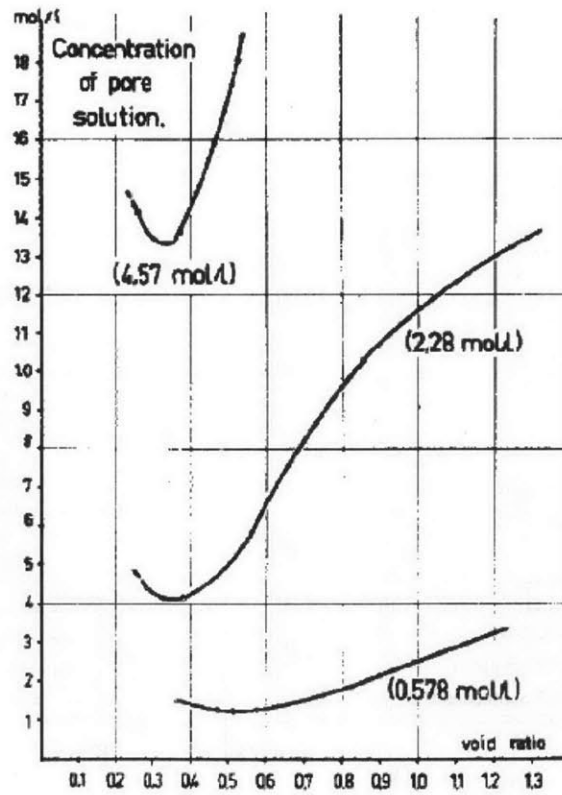


Figure 2.13 Concentration change of NaCl pore solutions in consolidated montmorillonite. From 80 to 320MPa NaCl concentration increases (Engelhardt & Gaida, 1963)

3 MATERIALS USED IN TESTING PROGRAM

3.1 INTRODUCTION

This chapter describes in detail the various soils used for the research, the material processing required for preparing soils for testing and lastly, details of the resedimentation technique used to prepare the samples of each soil for testing.

Section 3.2 describes the various soils tested during the course of this research into smectitic clay behavior. Each of these high plasticity soils that were prepared and tested originated from the Gulf of Mexico region. These include Gulf of Mexico – Eugene Island (GOM EI) obtained from cores obtained from Well A-12 in Block 331 and Well A-20 ST2 in Block 330. Gulf of Mexico – Upper Interval (GOM Upper) and Lower Interval (GOM Lower) whose cuttings were provided by a sponsor from confidential site, and two additional soils from the Gulf region, namely GOM A and GOM B whose core was provided by a sponsor from confidential site. The majority of testing was carried out on GOM EI. This soil was used to examine the behavior of a soil when the fabric has been changed by the removal of the natural salts via leaching. This leached derivative of GOM EI is termed LGOM EI and is treated as a different soil. Table 3.1 summarizes the index properties of all the soils in this research.

Section 3.3 describes the methods used for conducting two distinctly different material processes. The first part describes the process used to obtain leached GOM EI. In order to conduct research into behavioral changes due to changes in the soils fabric, the natural salts were removed from natural GOM EI. Due to the quantities of soil required for the testing program, a new method of salts removal from the soil using dialysis tubing and distilled water was developed. The second major material process was employed on the GOM Upper and GOM Lower soils. Both soils arrived at the MIT Geotechnical Laboratory as drill cuttings extracted from a borehole. The cuttings were saturated in drilling fluid. Before any experimental work could be conducted, this drilling fluid had to be completely removed from the soil, without causing any adverse effect to the soil. The chosen method was to wash the cuttings in Toluene, sieve off the fluids, and then repeat the washing for four repetitions in order to fully remove the drilling fluid from the soil surface.

Section 3.4 covers in detail the resedimentation technique used to prepare each soil for testing. A sub-section discusses the varying consolidation behavior observed for each soil and salinity during the resedimentation. A point is made about the trends observed during resedimentation with respect to time to reach end of primary consolidation and axial deformation of the resedimented column. The extensive resedimentation program was not without its issues and particular attention is given to these, with some mitigating measures proposed.

3.2 TEST MATERIALS

3.2.1 Gulf of Mexico – Eugene Island

Gulf of Mexico – Eugene Island (RGOM EI) is soil recovered from the Eugene Island block located approximately 160km off the coast of Louisiana at a water depth of ~ 77m. In this area, the basin consists of over 4 km of Pliocene and Pleistocene sedimentary fill deposited over a salt-weld. The soil was extracted from two cores drilled in July 1997, namely; A-20 in Block 330 and A-12 in Block 316. The soil existed at an elevation below seabed between 6690' (2039m) and 7550' (2301m). A location map of the cores is shown in Figure 3.1 with the sections of each boring extracted for laboratory testing shown in Figure 3.2. The soil deposit was found to have an in-situ vertical effective stress ranging between 7.1 and 7.4 MPa, an in-situ porosity of 0.23. In-situ measurements of the lateral stress ratio made during leak-off tests indicate a $K_0 = 0.84 - 0.91$. K_0 , the lateral stress ratio, is the ratio of the horizontal effective stress over the vertical effective stress (Stump and Flemings, 2002). A total of 485' (148m) of 4" diameter core was extracted from both wells. The soil was later extracted from the cores, air-dried, then roller ground to a fine powder with 100% passing the #100 sieve (<0.15mm), and finally homogenized. This processing was conducted at the University of Texas at Austin. Figure 3.3 shows a section through part of an extracted core prior to being dried and ground. In dried powder form, the soil has a light brown color as shown in Figure 3.4.

3.2.1.1 Series Data

Once a soil has been reduced to a dry powder and homogenized it is referred to as a series. Prior to any extensive laboratory testing can be done, it is necessary to perform several index and engineering tests to classify the soil in question.

Figure 3.5 shows the grain size distribution, determined in accordance with ASTM D422-63, for GOM EI powder obtained from the hydrometer test conducted by Taylor Nordquist at the MIT Geotechnical Laboratory in 2014. The clay fraction was determined to be approximately 63%.

In order to determine the mineralogy of both the bulk sample as well as the clay fraction of the soil, representative samples were sent to MacCaulay Scientific Consulting Ltd. for analysis. The mineralogy of the less than two micron clay fraction was determined using X-ray powder diffraction (XRPD) technique. The results showed that GOM EI is predominantly smectitic. 87% of the clay fraction consists of a mixed layer of illite-smectite with 85% expandability. The remainder of this fraction is made up of 8% illite, 4% kaolinite and 1% chlorite. Details of the mineralogy of the whole soil and the fraction of particles less than two microns in size are shown in Figure 3.6.

The Atterberg limits were determined by both the author and Brendan Casey in the MIT Geotechnical Laboratory. The limits were also determined by William Betts in the Geotechnical Laboratory at University of Texas. The liquid limit was determined using the Casagrande Cup with the plastic limit determined in accordance with ASTM D4318. The Atterberg limits were determined using distilled water. The liquid limit (w_L) was found to be 87% while the plastic limit (w_p) is 24%. This gives a plasticity index (I_p) of 63%. The soil is classed as a high plasticity clay (CH) using the Unified Soil Classification System (USCS). The location where this soil plots on the plasticity chart can be seen in Figure 3.7.

The specific gravity, G_s , of the soil was determined in accordance with ASTM D854 by Amy Adams (2014) at the MIT Geotechnical Laboratory. The average value was found to be 2.775 and this value is used in the phased relation calculations for all the research presented here.

The natural salt content, again determined by Amy Adams (2014) was found to be 8g of salt (NaCl) per kg of soil. Based on the in situ water content this equated to approximately 80g of salt per liter of pore fluid. This property was determined using electrical conductivity measurements of the supernatant after the soil was ran in the centrifuge (Germaine and Germaine, 2009).

3.2.2 Gulf of Mexico – Upper and Lower Interval

Gulf of Mexico – Upper and Lower Interval are two soils from the Gulf of Mexico region and will be termed GOM Upper and GOM Lower throughout this document. Site specific information such as location of wells, date drilled, and depth from seabed at which the soil was extracted from has not been made available to the MIT Geotechnical Engineering Laboratory. Both soils arrived at MIT coated in drilling fluid. The condition of the Upper Interval cuttings is shown in Figure 3.8. A specific cleaning process was implemented whereby the drilling fluid was removed from the soil cuttings. Figure 3.9 and Figure 3.10 show the condition of both soils after the cleaning process. The Upper Interval consists of dark grey chips, 1 – 2 cm in size and were easy to break with finger pressure. The Lower Interval cuttings have a similar dark grey color with a smaller chip size ranging from 0.5 – 1 cm. These chunks of soil were easier to break with applied finger pressure indicating a lower plasticity soil compared to the Upper Interval. For each interval, the cuttings were then air dried, hand blended to randomize and create a uniform source batch and lastly, ground into a fine powder passing the #100 sieve ($< 0.15\text{mm}$). Figure 3.11 shows the final powder product for the Lower Interval soil. This cleaning and grinding process is discussed in detail in Section 3.5.3.

3.2.2.1 Series Data

Figure 3.12 shows the grain size distribution for both GOM Upper and GOM Lower powder obtained from the hydrometer test conducted by Taylor Nordquist and Chunwei Ge at the MIT Geotechnical Laboratory in 2013. The clay fraction for GOM Upper and GOM Lower was determined to be 70% and 54% respectively.

Representative samples were sent to MacCaulay Scientific Consulting Ltd. in order to determine the mineralogy of both the bulk sample as well as the clay fraction of the two soils. The mineralogy of the less than two micron clay fraction was determined using X-ray powder diffraction (XRPD) technique. The results showed that the mineralogy of both soils was very similar. Both soils were found to be predominantly smectitic with very little difference in the illite-smectite fractions (88% and 87% of the clay fraction). The remainder of this fraction is made up of 8% illite, 3% kaolinite and 1% chlorite for GOM Upper, and 6% illite, 6% kaolinite

and 3% chlorite for GOM Lower. The major difference between the two soils, in terms of mineralogy, is the expandability of the interlayered illite-smectite mineral. The percent expandability ranges between 70 – 80% GOM Upper whereas it is only 40 – 50% for GOM Lower. Details of the mineralogy of the whole soil and the fraction of particles less than two microns in size are shown in Figure 3.13 and Figure 3.14.

The Atterberg limits for both soils were determined by Brendan Casey, Chunwei Ge, and Taylor Nordquist in the MIT Geotechnical Laboratory. The liquid limit was determined using the fall cone in accordance with BS 1377-3. The plastic limit was determined in accordance with ASTM D4318. Distilled water was used to determine both limits. For GOM Upper, the liquid limit (w_L) was found to be 64.7% while the plastic limit (w_P) is 25.5%. This gives a plasticity index (I_P) of 39.2%. For GOM Lower, the liquid limit (w_L) was found to be 62.7% while the plastic limit (w_P) is 26.0%, giving a plasticity index (I_P) of 36.7%. Both soils are classed as a high plasticity clay (CH) based on the USCS. The location where these soils plot on the plasticity chart can be seen in Figure 3.7.

The specific gravity, G_s , of the soil was determined by Taylor Nordquist. The average value was found to be 2.806 for GOM Upper and 2.715 for GOM Lower. The natural salt content, determined by Amy Adams was found to be 29.4g of salt (NaCl) per kg of soil for GOM Upper and 7.5g of salt (NaCl) per kg of soil for GOM Lower. Assuming an in situ porosity of GOM Upper and GOM Lower this equated to approximately 180g and 100g of salt per liter of pore fluid respectively.

3.2.3 Gulf of Mexico – Specimens A and B

These are two soils originated from the Gulf of Mexico region and will be termed GOM A and GOM B throughout this document. Site specific information such as location of wells, date drilled, and depth from seabed at which the soil was extracted from has not been made available to the MIT Geotechnical Engineering Laboratory. The material was removed from the cores utilizing a hammer and chisel and then broken up into small segments to dry. A ball mill grinder was then used to grind the segments to a fine powder passing the #100 sieve ($< 0.15\text{mm}$). The ball mill grinder shown in Figure 3.15 is a two part device consisting of a drive system powered by a 120v electric motor and processing drum. The processing drum has a hexagonal

shape, rubber lined interior. The drum is filled with 250 different specification steel balls ranging in size from ¼” to ½”. The hexagonal shape of the drums interior ensures proper rotation of the material during the grinding process. Once the soil is placed in the drum along with the steel balls, the motor is engaged which rotates the drum at high speed (up to 3600 rpm) producing centripetal force which carry the steel balls to a height at which point they fall breaking the material down by both grinding and striking (Jones, 2010).

3.2.3.1 Series Data

Figure 3.16 shows the grain size distribution for both GOM A and GOM B powder obtained from the hydrometer test. The clay fraction for GOM A and GOM B was determined to be 52% and 59% respectively. The index testing on both soils was conducted by Amy Adams at the MIT Geotechnical Laboratory in 2009.

Representative samples were sent to MacCaulay Scientific Consulting Ltd. in order to determine the mineralogy of both the bulk sample as well as the clay fraction of the two soils using the same methodology as outlined previously. The results showed that the mineralogy of both soils was very similar. Both soils were found to be predominantly smectitic with very little difference in the illite-smectite fractions (84% and 86% of the clay fraction). The remainder of this fraction is made up of 13% illite, 1% kaolinite and 2% chlorite for GOM A, and 11% illite, 1% kaolinite and 2% chlorite for GOM B. The expandability of the interlayered illite-smectite mineral was found to range between 50 – 60% for both soils. Based on the results of the grain size distribution and mineralogy it is evident that the difference in clay fraction provides the main difference between both soils and therefore any differences in the mechanical behavior will be as a result of this. Details of the mineralogy of the whole soil and the fraction of particles less than two microns in size are shown in Figure 3.17 and Figure 3.18.

The Atterberg limits for both soils were determined in the MIT Geotechnical Laboratory. Both the liquid limit and plastic limit were determined in accordance with ASTM D4318. The Casagrande Cup method was used for the liquid limit. Distilled water was used to determine both limits. For GOM A, the liquid limit (w_L) was found to be 70.4% while the plastic limit (w_P) is 28.5%. This gives a plasticity index (I_P) of 41.9%. For GOM Lower, the liquid limit (w_L) was

found to be 90.6% while the plastic limit (w_p) is 30.3%, giving a plasticity index (I_p) of 60.3%. Both soils are classed as a high plasticity clay (CH) based on the USCS. The location where both soils plot on the plasticity chart can be seen in Figure 3.7.

The specific gravity, G_s , of the soil was determined to be 2.704 for GOM A and 2.760 for GOM B. The natural salt content was found to be 3.5g of salt (NaCl) per kg of soil for GOM A and 4.4g of salt (NaCl) per kg of soil for GOM B. The in-situ water content of both soils can be calculated by assuming an in-situ porosity of 0.2. From this, an estimation of the in-situ pore fluid salinity was determined to be approximately 38g of salt per liter (g/L) of pore fluid for GOM A and 48g/L for GOM B.

3.3 MATERIAL PROCESSING

3.3.1 Introduction

The following section describes the methods used to process GOM Upper and GOM Lower as well as the process of leaching the natural salts out of GOM EI. This Section only discusses the processing of these soils as all other soils used in the research were already in a processed powder state ready for resedimentation. The processing of GOM EI is described by Betts (2014) with the processing of GOM A and GOM B described by Jones (2010).

3.3.2 Processing of Leached Gulf of Mexico – Eugene Island

A large portion of the research conducted by the author was carried out on Leached GOM EI. The leaching process reduced the material to individual particles, and was undertaken in order to understand the mechanical behavior of a soil that starts off as a powder with negligible salts and then by resedimenting with varying pore fluid salinities one can assess how the observed behavior and micro-fabric changes with salinity. An additional and equally important purpose was to compare the behavior and fabric of this leached GOM EI (RLGOM EI) with the natural GOM EI (RGOM EI) at similar pore fluid salinities. In order to achieve the above aim, it was first necessary to remove all the natural salts from GOM EI. GOM EI contains approximately 8g of salt for every 1kg of dry soil powder.

The process of leaching salts from soil has been carried out at MIT before. Horan (2012) conducted similar research on Series IV BBC whereby he leached the natural salts out of the illitic soil. Horan leached approximately 3.5kg of soil by mixing the dry powder with distilled water and running it through a centrifuge. The process, similar to a salinity test, (described in Section 4.4.2.2) involves mixing 15g of soil with 30g of distilled water (200 % water content) in a test tube and letting the mixture hydrate for 24 hours. The centrifuge has a capacity to hold eight of these test tubes per run which means only 120g of soil could be processed per run. Each 120g of soil had to be extracted from the tubes, dried, ground back into a fine powder, then mixed with distilled water and ran through the centrifuge a second time. After the second run the soil is again dried and ground into a fine powder and at this point it the soil was regarded as being leached and therefore ready for resedimenting.

The above procedure proved very time consuming and did not provide very large quantities of leached material. The planned program of research into leached GOM EI required the leaching of 3.4kg of soil to satisfy the quantity required for CRS and Triaxial resedimentation. Due to the large quantities involved, a new more efficient and less labor intensive method for removing the salts was required.

The chosen method of leaching the salts from GOM EI was by employing dialysis tubing. This method requires more time but is more suited for larger quantities of soil as it is not labor intensive. Clay powder is mixed with distilled water to form a slurry of pourable consistency. Rolls of dialysis tubing purchased from Carolina Biological Supply measuring 50 foot in length and 1 5/16" diameter were cut into suitable lengths. This size tubing was selected as it was ideal for fitting over standard plastic laboratory funnels used to transfer the slurry into the tubes. Each length of tubing has one end sealed using bag clips. The tubing, clips, and other equipment required for the process are shown in Figure 3.19. The slurry is then poured into the tubes via the funnel until full, at which point the funnel is removed and the other end of the tube sealed with another clip. Pouring is a messy process and between 5 - 10% of the original material can be lost. The filled tubes or 'sausages' are arranged in a large plastic container filled with a quantity of distilled water. Fickian dispersion causes migration of the salt through the semi-permeable membrane as a function of salinity gradient and time. Figure 3.20 shows a schematic of this process. A peristaltic pump is employed as part of the process to apply a small degree of

agitation to the leaching bath and speed up the diffusion process. Figure 3.21 shows a set up with 14 'sausages', sealed at each end using clips, and submersed in a bath of distilled water. Plastic tubing connects the water bath to the peristaltic pump. Typically 14 - 16 sausages are processed at a time to yield ~ 1 to 1.2 kg of leached soil.

The water bath is changed at regular intervals, typically 12 or 24 hours. On the first batch of soil leached, the author investigated the rate at which the dispersion occurs. Readings were taken every hour for the first 5 hours and it was noted that the vast majority of dispersion that would occur in a 12 hour period actually occurs during the first 4 hours. Based on these findings the author changed the water every 4 hours during the first day of leaching to expedite the process. In order to observe a trend in the bath water salinity, the water was changed every 12 hours thereafter. The used water is removed from the tank via syphon and the salinity measured using the conductivity meter shown in Figure 3.22, and recorded on the data sheet. The tank is refilled with the same volume of distilled water and let sit again. The salinity of a solution of 1 g/L salt solution is also recorded as a control to account for the effects of varying temperature. Over time, the salinity of the bath water decreases, typically halving at each water change for the first few days. Every 6 or so days the tubes are rotated 180° to ensure that the part of the tube in contact with the bath is exposed to the distilled water. It has been found that leaching past ~ 15 days results in breakdown of the dialysis tubing; if the measurement has not leveled off by this point, the soil should be removed from the tubes and new tubes filled to continue the process. For GOM EI, after approximately 30 days the salinity measurement will become constant and leaching is complete. At this point, the pore fluid salinity of the soil has been reduced to below 0.1 g/L. Figure 3.23 shows the evolution of the bathwater salinity for the 30 day period of leaching.

The leached clay is removed from the dialysis tubes by removing the clip from one end, placing the open end over a bowl and extruding the soil from the tube with the use of an index and fore finger. It is important to minimize loss of valuable leached material while at the same time minimizing the need for addition of water which will need to be removed later. Through trial and error it was found that the most efficient way to thoroughly remove the soil from the tubes was to remove the majority first, and then by placing the tube tightly between index and fore finger, pull the tube through forcing the soil along the tube and out.

The ‘nuggets’ of wet soil are then allowed to dry with the aid of a desk fan. Once dry, the soil is broken down using a mortar and pestle until it is converted to a powder which passes the US#100 sieve. Realizing the energy required in breaking down these dried, hard nuggets of soil with the mortar and pestle, upon completion of the second batch of leached soil, the soil was spread out into a thin layer approximately 10mm thick on several large glass plates and allowed to air dry with the assistance of a desk fan. This resulted in dried platy particles, approximately 5mm thick that were easier to break down and grind into a powder ready for resedimentation.

3.3.3 Processing of GOM Upper and GOM Lower

Six 5-gallon sealed buckets of soil arrived at the MIT Geotechnical Laboratory in late 2012. All soil was collected from the return cuttings from a borehole drilled in the Gulf of Mexico. Two of the buckets were regarded as being from an Upper zone with the remaining four buckets from a Lower zone or interval. Each elevation in which the soil was extracted has already been described in section 3.2.2. The soil in all buckets consisted of drill cuttings, which are small chunks of soil ranging in size from 0.5 cm to 3cm. An example of the condition of the cuttings is shown in Figure 3.24. These chunks of soil were coated in the drilling fluid used to core the borehole and bring the soil to the surface. The drilling fluid was composed of viscosifiers, emulsifiers and other lubricating agents such as bentonite. Prior to any work being carried out on the soil, the drilling fluid had to be first thoroughly and completely removed from the cuttings. The following section outlines the process involved in cleaning the soil and details of this process can be seen in Figure 3.25 and Figure 3.26.

1. Toluene was selected as the most appropriate solvent to use to remove the drilling fluid from the cuttings without going into the pore spaces of the soil itself. One drawback of using this product is the need to carry out all operations with this product under a fume hood. All cleaning operations were conducted under a fume hood in the basement of the MIT Geotechnical Laboratory. Use of safety glasses and gloves were required throughout the process. The cleaning process was divided into two main stages, namely, the primary and secondary cleaning.

2. The primary cleaning involved transferring approximately 1/3 kg of cuttings into a medium sized evaporating dish using a plastic spoon, taking care not to break the chunks of soil with the spoon.
3. The cuttings are then covered in Toluene and then gently mixed with a stainless steel stirrer for about 30 seconds with a focus on avoiding particle breakage. The fume hood sash is to be kept as low as possible throughout the cleaning process, yet still allow easy of access for all operations.
4. The mixture is poured onto an 8" diameter US#20 sieve placed over a second evaporating dish. Once all material has been transferred onto the sieve, film of drilling fluid is removed from the first evaporating dish with paper towels.
5. The cuttings are transferred back into the first dish and the sieve tapped to remove any bound particles. Next decant the Toluene back over the cuttings, pouring the settled out drilling fluid with a slurry composition into a glass beaker and clean the dish with paper towels.
6. Return to step #3 and repeat the process for three cleaning cycles, adding new Toluene if necessary.
7. Once the three primary cleaning cycles are complete, transfer the cuttings onto paper towels on a tray to allow excess fluids to either drain away or evaporate.
8. Repeat from step #2 for a total of three 1/3kg batches of cuttings while reusing the same Toluene.
9. Next, perform a secondary cleaning cycle of each batch starting from step #3 using new Toluene, and carry out two as opposed to three cleaning cycles.

10. Once the secondary cleaning for each batch is complete, place the cleaned cuttings onto paper towels and spread as thinly as possible to facilitate the evaporation of the Toluene from each particle surface.
11. Allow the cleaned cuttings a minimum of 2 hours for evaporation but no longer than 4 hours to prevent the particles from dehydrating. During this time, ensure that the fume hood sash is closed with only a slight opening.
12. After 2 hours, transfer the cleaned cuttings to a sealable plastic bag and label correctly.
13. Store all used paper towels under the fume hood for a period of 24 hours to ensure complete evaporation, and after such time, discard to waste disposal.
14. Transfer all waste Toluene and drilling fluid sludge to a correctly labeled waste container for hazardous waste collection.

After the cleaning process was complete, the soil from each interval was hand blended to randomize and create the source batch for GOM Upper and Lower. The blended soil was then placed into sealed 5 gallon buckets. Two forced draft ovens were set up with the temperature set to 60° Celsius. The temperature was set at 60° Celsius as drying the soil under standard laboratory oven temperatures of 120° Celsius would damage the natural fabric of the soil and possibly even the individual soil particles due to the shrinkage of the soil matrix under such high temperatures. The cleaned cuttings were placed in aluminum trays suitably sized to fit in the oven shelves. Photos of the ovens and trays of soil can be seen in Figure 3.27 and Figure 3.28.

Through some trial and error a period of 12 hours was determined to be sufficient for the soil cuttings to be dry enough to pass through the grinder without causing the equipment to clog up. The grinder used to convert the soil chunks to a fine powder was a GPX Disk-Style Grinder, shown in Figure 3.29. This machine has the capacity to grind material so that 100% of the resultant powder will pass the US#100 sieve. Additionally, the machine has the capability to grind the soil to varying sizes via control of an adjusting screw which moves the discs either

closer together or further apart. Fortunately, the soil was able to be ground to a powder with one pass by setting the discs to the finest adjustment, eliminating the need to reduce the cuttings to a powder over a two or three step process. Tests conducted on a batch of cleaned and ground soil cuttings to determine the particle size distribution confirmed that both soils had no particles greater than 0.15mm or US#100 sieve. The five trays of soil dried at a time equated to approximately 7kg of soil. With a slow and steady feed of soil into the hopper, preventing any clogging up occurring, 20 minutes was sufficient to grind this 7kg of soil, equating to an output of 21 kg per hour. Once all the GOM Lower soil was reduced to a powder, it was essential that the equipment (particularly the discs) be thoroughly cleaned to avoid cross contamination. This was achieved by disassembling the front section, removing both discs and removing all soil with a combination of wire and soft brushes.

The cleaning and grinding process resulted in a total of 22kg of GOM Upper and 58 kg of GOM Lower in powder form. Each soil was stored in sealable 5 gallon buckets. No further blending was required as the soil had already been blended after the cleaning process. A picture of the finely ground soil being prepared for storage is shown in Figure 3.30.

3.4 RESEDIMENTATION

3.4.1 Introduction

Resedimentation involves consolidating a uniform, homogeneous workable slurry one dimensionally in a rigid walled cylindrical container called a consolidometer. With incremental loading over time, resedimentation produces a soil sample that can be cut into one or more specimens and trimmed to the desired size and shape for testing.

The resedimentation procedure, developed at MIT in the 1960's, has been refined throughout the years. The most significant improvements were made by Germaine (1982) who refined the resedimentation technique to produce fully saturated and uniform samples of resedimented BBC with a salt concentration of 16g/L. This process has since been successfully employed on various soils. Abdulhadi (2009) introduced a different approach by preparing individual batches for each test specimen, as opposed to producing large soil 'cakes' which were subsequently divided into smaller pieces as had been done in the past. The approach of preparing

individual batches for each test specimen dramatically reduces the load which must be applied to achieve a particular batch pre-consolidation pressure, a critical issue for samples which need to be batched to high stresses. As part of this research, a resedimentation plan was carried out in order to satisfy the proposed CRS and triaxial testing. In the case of CRS tests, a soil was resedimented with a particular salinity and to a particular stress and in most cases the resedimented sample was of sufficient dimensions to obtain three test specimens from it. Whereas in the case of triaxial testing, each resedimented sample provided for only one test specimen

In recent years, both Mazzei (2008) and Horan (2012) carried out testing at MIT on a Gulf of Mexico soil, namely, GOM Ursa. However, as this soil differs from the Gulf of Mexico soils in this research, it was necessary to determine the water contents at which each Gulf of Mexico soil should be resedimented to. This is mainly because the resedimentation which was performed for this research was done using a large range in pore fluid salinity. When resedimenting with high salinity saltwater, the mass of fluid added to a soil powder does not resemble the mass of water available to wet the soil particles. A large fraction of the mass of fluid now comprises sea salt (up to 25 %) and therefore the quantity of fluid required to form a stable and pourable slurry varies with salinity.

Several high plasticity smectitic soils were resedimented as part of the testing program. These include Gulf of Mexico – Eugene Island (RGOM EI), Gulf of Mexico Upper (RGOM Upper) and Lower Interval (RGOM Lower), Gulf of Mexico Specimen A (RGOM A) and Gulf of Mexico Specimen B (RGOM B). In addition to this, three specimens of Boston Blue Clay (BBC) and one specimen of Ugnu Clay (UC) were resedimented but the results obtained from tests on these two soils are not included in this research. The most commonly used soil in the testing program was RGOM EI. This was selected as there was an abundant source available for testing compared to the other soils in the test group. A list of all the samples prepared for testing via the resedimentation technique is shown in Table 3-2 and Table 3-3.

The various types of soil which have been successfully resedimented as part of this research are described in the following Sections. These Sections detail what areas of the resedimentation procedure have to be altered to suit each individual soil type.

3.4.2 Resedimentation Procedure

The tube in which the soil is resedimented in is called a consolidometer. These consolidometers retain the soil throughout all load increments from the time of pouring the flowable slurry into it, to when it has reached the desired resedimentation stress level. In this research, two main types of consolidometers were used – one for CRS samples and one for triaxial samples. Consolidometers for CRS testing produce samples with diameters that are larger than the diameter required for testing. The tube diameters used for resedimenting for CRS testing were 3.81 and 4.45 cm. This is done to facilitate trimming of the soil into a cutting ring. Both consolidometers are clear plexiglass tubes. In contrast to the CRS consolidometers, the triaxial consolidometer has an internal diameter equal to that which is required for a triaxial testing meaning that only the ends of the soil require trimming after extrusion. These consolidometers are also clear plexiglass tubes. A photo of these consolidometers can be seen in Figure 3.31. This Figure also shows smaller height consolidometers which were employed when only small quantities of soil were required to be resedimented for CRS testing.

The following section describes the resedimentation procedure for the all the soils used in the research.

1. Hydration

The desired quantity of dry soil powder is obtained from storage. This powder is then added to a predetermined quantity of saltwater and allowed to hydrate. The water content required varies greatly from soil to soil. To create a workable yet stable slurry with no free water present at the surface it has been found that a water content approximately twice the liquid limit of the soil is required. Depending on the soil type and mineralogy, hydration can take several days. Mechanically agitating the slurry alone may not guarantee full hydration prior to placement in the consolidometer. It was found that for the soils used in this research, complete hydration was achieved after a period of 24 hours.

2. Mechanical Agitation

Once the slurry has fully hydrated, the soil is then mechanically agitated to help ensure a uniform paste. This is done in the MIT Geotechnical Laboratory with a Kitchen Aid mixer which is shown in Figure 3.32. This mixer is fitted with a flat beater attachment. The slurry is mixed on low speed for approximately 10 minutes in this manner, the sides and very base of the mixing bowl are cleaned down using a flexible rubber spatula to ensure thorough mixing, and then the slurry is mechanically mixed for another 10 minutes.

3. Deairing Slurry

Once the slurry is adequately mixed, it is transferred into a medium sized ceramic bowl. The bowl is then placed inside a cylindrical chamber with a removable lid. The transparent plastic lid is fitted with the necessary plumbing, valves and pressure gauge to provide a connection to the vacuum pump as well as facilitate inspection of the soil as it is being deaired. A large O-ring recessed into the top of the chamber wall forms a seal once the pump is activated. A partial vacuum (approximately 25 inches of Mercury (in Hg)) is then applied to the chamber to remove any entrapped air from the slurry matrix. The setup for vacuuming is shown in Figure 3.33. The time required for vacuuming depends on the quantity of soil, mineralogy and Atterberg limits of the soil. For the small quantities of GOM soils (180g – 250g of powder) prepared for each resedimented sample, 30 minutes of vacuuming is adequate to remove the entrapped air. Allowing the soil to be left under vacuum conditions can be detrimental as water will evaporate from the slurry, thereby leading to a thickening of the slurry which will reduce the ease at which the slurry can be poured into the consolidometer.

This method of de-airing the slurry was favored over an alternative method used by previous researchers at the MIT Geotechnical Laboratory, namely, Horan (2012) and Casey (2011). The alternative method employed the use of a flask, whereby the slurry was drawn into the flask under vacuum and the entrapped air was extracted from the soil within the flask. The major advantage the author found by using the bowl and cylindrical chamber over the flask was that almost all the soil can be transferred from the bowl to the consolidometer, whereas additional soil is required when using the flask to account for the slurry that will coat the inside of the flask.

4. Pouring

Once the slurry has been de-aired, it is then poured into the consolidometer. The slurry is poured directly from the bowl, with the aid of a spatula, into a funnel with a long flexible tube which discharges into the consolidometer as shown in Figure 3.34. The tip of the funnel should be kept just above the top of the rising soil column to minimize the entrapment of air bubbles.

5. Consolidation

The slurry can be poured into any size consolidometer. Consolidometers consist of a basic structure involving a cylindrical acrylic open ended tube in which the clay consolidates between top and bottom porous stones. Nylon filter fabric is placed between the porous stones and the soil. A picture of a typical consolidometer setup ready to receive the slurry can be seen in Figure 3.35. The inside wall of the consolidometer is lubricated with a thin film of either silicon oil or high viscosity vacuum grease. This lubrication reduces side wall friction during consolidation and also aids in the extraction of the clay from the consolidometer. The porous stones transfer the applied stress to the soil and also provide a drainage path through which excess pore pressure can escape. The reservoir or bath is filled with the same saltwater concentration as that used in the slurry to a level above the base of the slurry column, and the same solution is poured into the top of the slurry column. The water in the reservoir is maintained by filling with distilled water on a daily basis to account for evaporation losses, maintaining a constant salt content. The slurry is loaded incrementally in a consolidometer, which has double drainage, using a load increment ratio $\Delta\sigma_v/\sigma_v = 1$. Each load increment is maintained at least until the end of primary consolidation as determined by the square root of time method. After the desired maximum axial stress, i.e. pre-consolidation pressure σ'_p , has been achieved, this maximum stress is held constant for one log cycle of secondary compression. The resedimented sample is then rebounded to an OCR of 4. At OCR = 4 the soil is close to hydrostatic effective stress conditions, i.e. $K_0 \sim 1$, and the shear strains due to sample extrusion from the consolidometer are minimized, as confirmed by the work of Santagata (1994).

The pre-determined maximum stress level is governed by the type of test to be performed on the batch. For CRS testing, all resedimented samples were loaded to an axial effective stress

(σ'_{ac}) of 0.1 MPa. The stress level for triaxial testing varied depending on the target maximum stress to be applied to the soil in the triaxial device. In general, samples were resedimented to a stress approximately half of the consolidation stress in the triaxial device. The triaxial testing program involved consolidating specimens in the triaxial device over a wide range of stresses from 0.15 MPa to 10 MPa and therefore each resedimented sample was taken to an axial effective stress suitable for that particular test.

The method of consolidating the sample depends on the stress level. For low consolidation stress (0.5 MPa) the loading increments are to be applied using dead weights. In the very low stress range (up to 10 kPa), weights can be placed directly on top of the consolidometer. In the higher stress range (up to 0.5 MPa), the weights are hung from a frame as shown in Figure 3.36. For stresses exceeding 0.5 MPa and up to 10 MPa the consolidometer is transferred to an Oedometer frame where the load is applied via a lever arm with a 100:1 ratio. An example of the Oedometer frame is shown in Figure 3.37.

Throughout each consolidation increment, the axial deformation of the slurry column is measured using an LVDT. Each load increment is maintained until the End of Primary (EOP) consolidation, which is the time taken for all excess pore pressures to dissipate and secondary compression to commence. By monitoring the axial deformation versus the square root of time or log time, we can estimate this time to EOP. The square root of time method allows faster loading because there no need for secondary compression to determine EOP, as is the case with the Casagrande log time method.

6. Extrusion

After consolidation is complete, the sample is removed and prepared for testing. For all samples resedimented to a relatively low stress (< 0.2 MPa), extrusion can be done by applying a downward force on the soil via a solid plastic spacer by hand. The downward force transfers through the spacer and porous stone forcing the soil column to move relative to the outer plexiglass tubing. For stresses greater than 0.2 MPa it is not possible to extrude the soil in this manner, therefore a hydraulic hand-jack is used to apply the necessary force. Figure 3.38 shows the hydraulic hand-jack extruding a resedimented sample with the final extruded sample shown

in Figure 3.39. Once the soil is extruded, it is trimmed to the required dimensions for testing. The trimming process is covered in the respective test method in Chapter 4, as the techniques used are specific to the test type.

3.4.3 Resedimenting Gulf of Mexico – Eugene Island

One of the first tasks when working with a new soil is to determine the water content required to produce a stable and workable slurry for resedimentation. GOM EI had not been resedimented at the MIT Geotechnical Laboratory prior to this research and as the research used a wide range of pore fluid salinity – from 0 g/L up to 256 g/L, it was essential to determine a suitable water content for each salinity level. This is achieved by placing known masses of soil in several clear test tubes and then adding varying water contents at a particular salinity.

When a stable slurry is produced in the lab for resedimentation, no free water appears on the surface of the slurry after being allowed to sit for a time. This is the essence of the test which is performed to determine the correct resedimenting water content. The test tubes with soil and varying water contents should be left to sit for at least 24 hours, and then examined. It is important that the test tubes are not shaken because visual examination of the surface is required. Tubes in which clear water is present on top of the soil may produce slurry which can potentially segregate during consolidation. It is necessary to find the highest water content that will not produce this free water on top of the soil. This water content should then be used for resedimenting.

In order to determine a range of water contents to test, it is helpful to perform Atterberg limit tests of the soil. Once the liquid limit is determined, a good estimate is double this value. Say for instance a soil has a liquid limit of 70 %, a good range of water contents to test initially would be from 130 to 150 % in increments of 5 %.

Throughout this research, GOM EI was resedimented to pore fluid salinities of 6, 7, 10, 22, 64, 128, 256 g/L. Ordinary sea salt (Morton's Sea Salt) was used in the preparation of the saltwater for all resedimented samples. The water contents required to create a stable slurry ranged from 140 % for 6 g/L to 112 % for 256 g/L. Details of all the salinities and the

corresponding water contents can be seen in Table 3-4. In this case, the water content is the mass of water divided by the mass of soil and salt combined.

3.4.3.1 Resedimenting Leached GOM EI

GOM EI which was leached as described in Section 3.3.2, was resedimented to pore fluid salinities of 0, 1, 4, 16, 64, 128, 256 g/L for CRS testing and to 4, 64, and 256 g/L for triaxial testing. Leaching out the natural salts from GOM EI increased the sensitivity of the soil with respect to the water contents required for the same salinity range. Two main differences were observed between the natural and the leached. Firstly, for the same salinity, the quantity of water required to form a stable slurry was less for the leached than that required for the natural. Secondly, the range of water contents required for slurry's with salinities between 0 and 256 g/L was greater for the leached (35 %) compared to the natural (28 %). The highest water content required for the leached was determined to be 120 % and lowest was 85%.

3.4.4 Resedimenting GOM Upper and GOM Lower

Resedimentation and CRS testing was performed on both of these soils which had undergone cleaning and grinding as described in Section 3.3.3. Given time constraints, salinities of 4, 70, 256 g/L were selected as a low, medium, and high salinity for the resedimentation samples, in an attempt to determine the effect of pore fluid salinity on each soils behavior. In contrast to GOM EI, pure sodium chloride (NaCl) was used in preparation of the saltwater for both these soils. Both soils were new to the MIT Geotechnical Laboratory, resedimentation water contents had to be determined for each of the three salinities. This was carried out using the same method outlined in Section 3.4.3. For GOM Upper, with salinities of 4, 70, and 256 g/L the water contents were determined to be 80, 100, 115% respectively. For GOM Lower, the water contents were determined to be 85, 100, 118% with decreasing order of salinity. As both soils have a similar liquid limit and similar mineralogy, it was anticipated that the water contents would be similar. Both soils show a similar trend to that of GOM EI with increasing pore fluid salinity there is a reduction in the amount of water required to create a stable slurry.

3.4.5 Resedimenting GOM A and GOM B

GOM A and GOM B were resedimented at the MIT Geotechnical Laboratory by Horan (2012) prior to this research. Four samples in total were resedimented, two for each soil, in order to carry out CRS testing to assess the influence of salinity. A pore fluid salinity of 100 and 200 g/L was selected for each soil, prepared using NaCl. Horan found that a water content of 138 % was adequate to create a stable slurry for both soils at a pore fluid salinity of 100 g/L, However, no data are available on the water contents required for both soils using a salinity of 200 g/L.

All four resedimented samples were tested as part of this research in order to establish a bank of results for this material as well as assisting in understanding any trends that occur in the various other soils tested with varying salinity.

3.4.6 Consolidation behavior during resedimentation

During each consolidation phase or loading increment, the axial deformation of the resedimenting column of soil is measured using an LVDT. Each load increment is maintained until the End of Primary (EOP) consolidation, which is the time taken for all excess pore pressures to dissipate and secondary compression to commence. By monitoring the axial deformation versus the square root of time, we can estimate this time to EOP. An additional method to determine EOP is by plotting axial deformation against log-time. A sample graph that is produced from a typical load increment can be seen in Figure 3.40.

The time required to reach the EOP for each load increment during the resedimentation process depends on the drainage height of the sample as well as on the coefficient of consolidation (c_v) of the soil. In general, several days to a week are required to reach EOP for the first few load increments, though this reduces significantly at higher stresses as the drainage height becomes shorter. As stated previously, GOM EI was resedimented using a wide range of pore fluid salinities. During the resedimentation process it was observed that as the pore fluid salinity increased, the time to reach EOP decreased. In addition to this, the amount of axial deformation undergone by the soil at EOP decreased with increasing salinity. Figure 3.41 shows this trend for GOM EI resedimented with four different pore fluid salinities – 10, 22, 64, 128 g/L, with each sample undergoing a stress increment to 25 kPa. The figure shows that the time to

reach EOP decreases from 92 hours for 10 g/L salinity to 11 hours in the case of 128 g/L, while the amount of axial deformation during this increment in stress also decreased from 12.3mm for 10 g/L to only 2.4mm for 128 g/L. It is important to note that the drainage height for each of the four samples was approximately equal. These two observed trends with salinity occurred during each load increment applied and similar behavior was noted for LGOM EI, GOM Upper and GOM Lower. These two simple observations early in the research, prior to any extensive CRS testing being conducted, indicated that for smectitic high plasticity soils, an increase in salinity results in both increasing c_v and hence permeability as well as decreasing compressibility.

3.4.7 Resedimentation Issues

The saturation point for salt (NaCl) in water is approximately 360 g/L at 20° C. When resedimenting with a high salinity such as 256 g/l, a film of salt gradually grows on the water bath and consolidometer a few days after the slurry has been poured. This salt originated from the saltwater bath, which is charged with keeping the slurry saturated at the correct salinity during resedimentation. As salt is being lost from this water, the water will no longer be at the required salinity. A photo of this occurring while resedimenting GOM EI to 256 g/L, is shown in Figure 3.42. The salt was observed to ‘climb’ the walls of the bath, extend over the top and continue to expand down the outside of the bath.

Due to the above issue of salts coming out of solution, the author investigated the actual pore fluid salinity of several resedimented samples prior to being tested in the CRS device. Each sample was resedimented to a maximum axial effective stress of 100 kPa. GOM EI was chosen as the test soil – with 22 g/L and 256 g/L resedimented samples trimmed for salinity measurements. LGOM EI was also investigated using sub-samples from 16, 64, and 256 g/L resedimented samples.

The salinity of each sample was determined by a salinity test, described in Section 4.4.2.4. In short, this test involves placing approximately 15g of resedimented soil into a centrifuge tube, adding 15 g of distilled water, shaking thoroughly and then leaving to hydrate for 24 hours. After which time the tube is placed into the centrifuge and run at 5000 rpm for 20-30 minutes. The supernatant is then decanted from the tube and the conductivity of this liquid is measured. The soil is completely remove from the tube, placed in a massed oven tare and placed

in oven in order to obtain the water content of the soil. Once the water content was determined, the salinity of the soil could be calculated. The measurements showed that for the low salinity soils, namely the GOM EI at 22 g/L and LGOM EI at 16 g/L, the measured salinity was 24.3 g/L and 18.5 g/L, which are similar to the expected salinity. The LGOM EI at 64g/L was found to have a salinity of 55.5 g/L which is less than what was expected. However, the results for the high salinity of 256g/L provided actual salinities far less than the expected. GOM EI at 256g/L was determined to have a measured salinity of only 122g/L with LGOM EI having a measured salinity of 168 g/L.

At the present time, additional research is required to determine whether the reduction in pore fluid salinity is due to:

- i. Removal of greater quantities of salt from the soil with expelled pore fluid as consolidation stress increases to 100 kPa, resulting in a lower salinity pore fluid
- ii. A systematic error in determining the salinity of the supernatant from running the soil through the centrifuge, or
- iii. In the case of high salinities such as 256 g/L, the bath water evaporates causing the salinity to reach saturation level and start to come out of solution. This results in grains of salt settling to the bottom of the bath as well as a buildup of salts on the bath wall and consolidometer, leading to a reduction in the bathwater salinity. Salts in the higher concentration pore fluid are then drawn out of the soil towards the bath water during resedimentation as the bath water evaporates.

A possible solution to this problem of salts coming out of solution when resedimenting with high salinity pore fluids is to place the consolidometer and bath in a sealed enclosure, of preferably timber. The purpose of this enclosure would be two-fold. Firstly, the enclosure would help to reduce or eliminate the evaporation of the bath water by cutting off the drying influence of the powerful air conditioning units in the laboratory. Secondly, a temperature controlled environment within the enclosure would eliminate the issue of varying daily temperatures. A resedimentation set-up exposed to direct sunlight may undergo evaporation of the bathwater during the day, and at night, if temperatures drop well below room temperature (e.g. a lab window left open) may result in the salt coming out of solution. This latter concern is based on

the fact that when preparing saltwater with 256 g/L salinity at 20° C, it was found that some of the salt settled out. It is standard practice in the MIT Geotechnical Laboratory when preparing high salinity salt water, to heat the fluid to temperatures in the range of 30 – 50° C ensuring all salt grains go into solution. The author recommends that a trial batch of high salinity soil be resedimented with the consolidometer and bath housed in a sealed enclosure with monitoring of the bath water level and salinity conducted on a daily basis to determine if the issue is either reduced to some extent or completely prevented.

Soil	Liquid Limit w _L (%)	Plastic Limit w _P (%)	Plasticity Index, I _p (%)	Clay Fraction (%)	USCS Classification	Specific Gravity, G _s	Natural Salts (g/kg of soil)	Natural Salts (g/L)
Gulf of Mexico - Eugene Island (GOM EI)	87 ^{CC}	24	55	63	CH	2.775	8	80
Leached Eugene Island (LGOM EI)	77 ^{CC}	-	-	63	CH	2.775	0	0
GOM Upper Interval (GOM U)	64.7 ^{CF}	25	39.7	70	CH	2.807	29.4	180
GOM Lower Interval (GOM L)	62.7 ^{CF}	24	38.7	54	CH	2.715	7.5	100
GOM A	70.4 ^{CF}	28.5	41.9	52	CH	2.704	3.5	38
GOM B	90.6 ^{CF}	30.3	60.3	58.5	CH	2.760	4.4	48

Notes:
 CC - Determined using Casagrande Cup Method
 CF - Determined using Fall Cone Method

Table 3-1 Index properties of all soils associated with this research

RESEDIMENTATION DATA						
#	Sample Number	Start Date (dd/mm/yyyy)	Source Material	Salinity (g/l)	Pore Fluid Content (%)	Tested via (test number)
1	RS251**	29/1/2012	GOM B	100	138	CRS (1352, 1353, 1354)
2	RS252**	24/1/2012	GOM A	100	138	CRS (1312**, 1350, 1351)
3	RS262**	24/3/2012	GOM A	200	-	CRS (1356, 1357)
4	RS266**	23/4/2012	GOM B	200	-	CRS (1358, 1359, 1360)
5	RS332	5/2/2013	GOM EI	6	140	CRS 1361
6	RS333	5/2/2013	GOM EI	7	135	CRS 1362
7	RS335	2/3/2013	GOM EI	64	119	CRS 1364
8	RS336	2/3/2013	GOM EI	256	112	CRS 1368
9	RS339	23/3/2013	GOM EI	10	130	CRS 1363
10	RS342	16/4/2013	GOM EI	22	125	CRS 1400
11	RS343	16/4/2013	GOM EI	128	117	CRS 1366
12	RS346	27/4/2013	Leached GOM EI	0	120	CRS 1373
13	RS348	4/5/2013	GOM EI	64	119	TX 1180
14	RS349	4/5/2013	GOM EI	256	112	TX 1183
15	RS407	5/5/2013	GOM EI	64	119	TX 1214
16	RS351	5/5/2013	GOM EI	64	119	TX 1179
17	RS352	18/5/2013	Leached GOM EI	64	98	CRS 1370
18	RS353	18/5/2013	Leached GOM EI	128	92	CRS 1367
19	RS354	20/5/2013	GOM EI	64	119	TX 1175
20	RS355	20/5/2013	GOM EI	64	119	TX 1178
21	RS361*	3/6/2013	Ugnu Clay	10	-	-
22	RS362	6/6/2013	Leached GOM EI	256	85	CRS 1369
23	RS363	12/6/2013	GOM EI	256	112	TX 1195
24	RS364	19/6/2013	Leached GOM EI	64	98	TX 1182
25	RS365	19/6/2013	Leached GOM EI	64	98	TX 1192
26	RS373	25/7/2013	Leached GOM EI	1	113	CRS 1374
27	RS374	25/7/2013	Leached GOM EI	16	105	CRS 1372
28	RS375	1/8/2013	Leached GOM EI	256	85	TX 1186
29	RS376	1/8/2013	Leached GOM EI	256	85	TX 1206
30	RS377	15/8/2013	Leached GOM EI	4	110	CRS 1375

Notes:
* indicates sample whose results are not included in this thesis
** indicates sample that was prepared/tested by others
1 - Eugene Island soils resedimented with Sea Salt
2 - All other GOM soils resedimented with pure NaCl.
3 - Right hand column shows tests conducted on specimens and associated test number in parenthesis
4 - All Triaxial tests are CK₀UC

Table 3-2 List of resedimentation batches produced as part of this research (1 of 2)

RESEDIMENTATION DATA						
#	Sample Number	Start Date (dd/mm/yyyy)	Source Material	Salinity (g/l)	Pore Fluid Content (%)	Tested via (test number)
31	RS378	15/8/2013	GOM EI	10	130	TX 1199
32	RS379	15/8/2013	GOM EI	10	130	TX 1209**
33	RS380	23/8/2013	GOM Lower	70	100	CRS 1377
34	RS381	23/8/2013	GOM Upper	70	100	CRS 1376
35	RS382	14/9/2013	Leached GOM EI	4	110	TX 1201
36	RS383	14/9/2013	Leached GOM EI	4	110	TX 1213
37	RS397*	8/12/2013	GOM Lower	70	100	TX 1215*
38	RS398*	8/12/2013	GOM Lower	70	100	-
39	RS399	8/12/2013	GOM Lower	256	85	CRS 1395
40	RS400	9/12/2013	GOM Upper	256	80	CRS 1396
41	RS401	11/12/2013	GOM Lower	4	118	CRS 1398
42	RS402	11/12/2013	GOM Upper	4	115	CRS 1397
43	RS405*	13/12/2013	GOM Upper	70	100	-
44	RS406*	13/12/2013	GOM Upper	70	100	-
45	RS409*	18/1/2014	GOM Lower	70	100	-
46	RS410*	18/1/2014	GOM Upper	70	100	-
47	RS412*	7/2/2014	GOM Lower	256	85	-
48	RS413*	8/2/2014	GOM Upper	256	80	-
49	RS414*	2/3/2014	GOM Upper	4	115	-
50	RS415*	2/3/2014	GOM Lower	4	118	-

Notes:

- * indicates sample whose results are not included in this thesis
- ** indicates sample that was prepared/tested by others
- 1 - Eugene Island soils resedimented with Sea Salt
- 2 - All other GOM soils resedimented with pure NaCl.
- 3 - Right hand column shows tests conducted on specimens and associated test number in parenthesis
- 4 - All Triaxial tests are CK₀UC

Table 3-3 List of resedimentation batches produced as part of this research (2 of 2)

Soil Type	Pore Fluid Salinity (g/l)	Water Content (%)	Comments
RGOM EI	6	140	Decrease in fluid content with increasing salinity. 28% range in values.
	7	135	
	10	130	
	22	125	
	64	119	
	128	117	
	256	112	
RLGOM EI	0	120	Similar trend to RGOM EI. 35% range in values. In general, less fluid required for a workable slurry
	1	113	
	4	110	
	16	105	
	64	98	
	128	92	
	256	85	
RGOM UPPER	4	115	Similar trend to Eugene Island
	70	100	
	256	80	
RGOM LOWER	4	118	
	70	100	
	256	85	
GOM A	100	138	Water content for 200g/l not available
	200	-	
GOM B	100	138	
	200	-	

Note:

1 - Eugene Island soils resedimented with Sea Salt

2 - All other GOM soils resedimented with pure NaCl.

Table 3-4 List of soils resedimented and the required mass of salt water required to create a stable slurry at the corresponding salt concentrations indicated

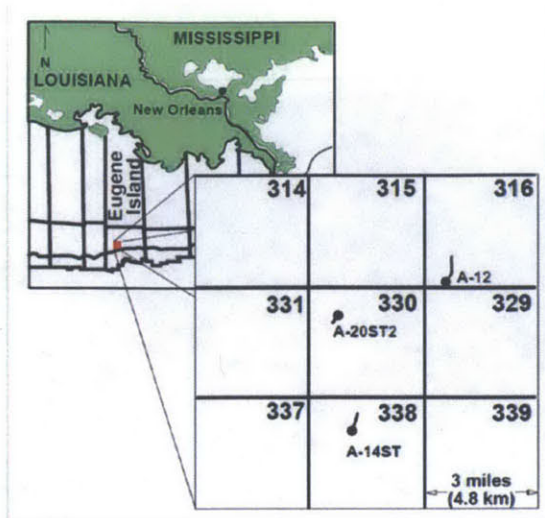


Figure 3.1 Location map showing the Eugene Island Block of the coast of Louisiana. GOM EI is a blended mixture of core extracted from A-12 in Block 316 and A-20ST2 in Block 330 (Stump & Flemings, 2002)

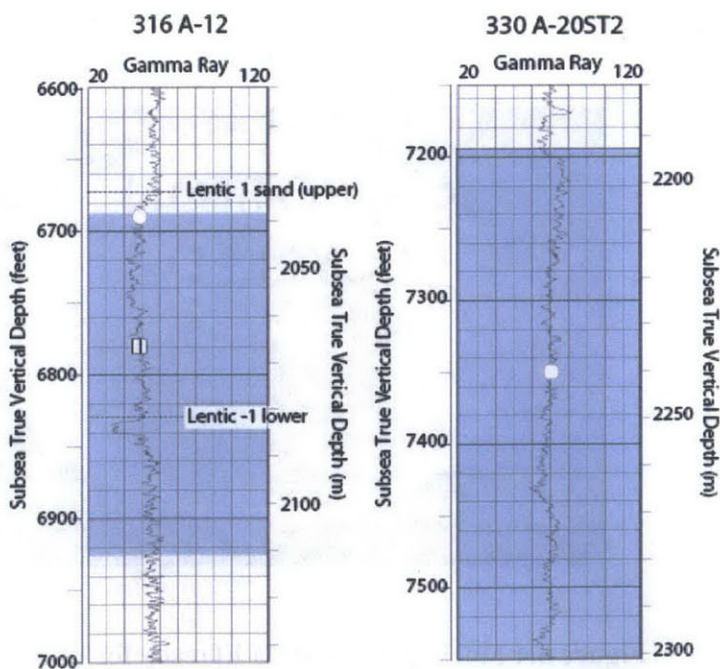


Figure 3.2 Sections of the two wells drilled with shaded area indicating section of core extracted for laboratory testing (Stump & Flemings, 2002)



Figure 3.3 Section through part of Core A-20 from Block 330 (Betts, 2014)



Figure 3.4 Finely ground GOM EI ready for laboratory testing

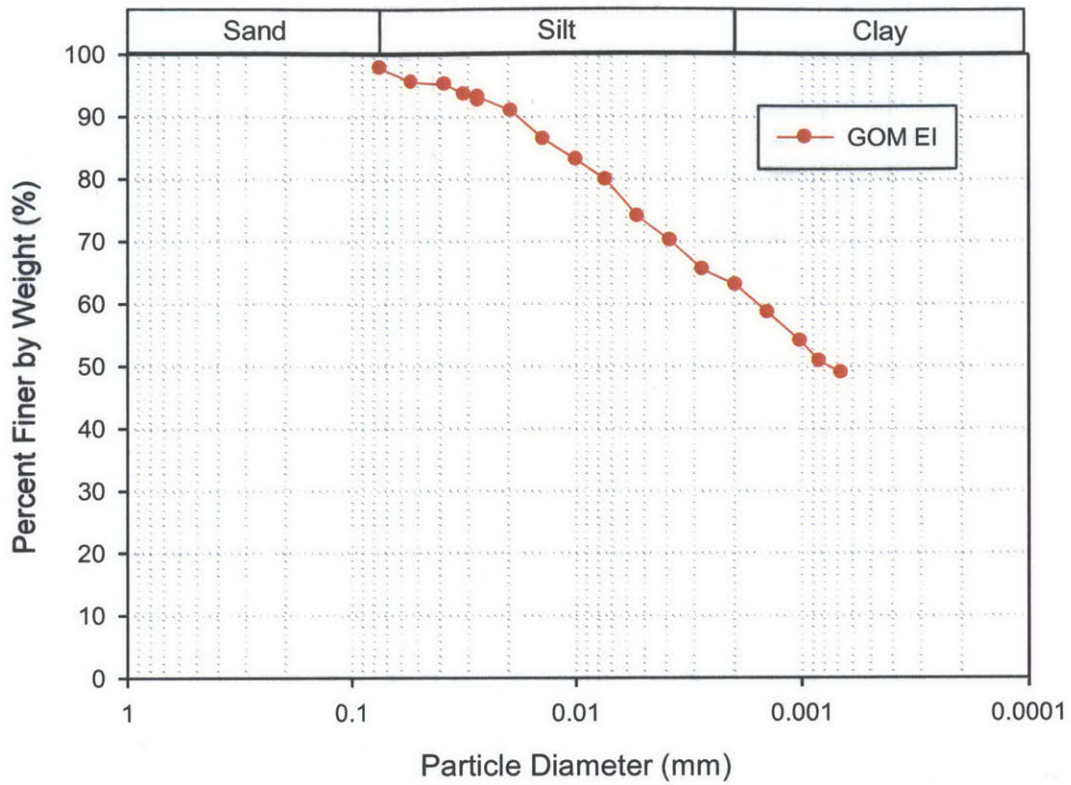


Figure 3.5 Results of grain size analysis for GOM EI (tested by Taylor Nordquist)

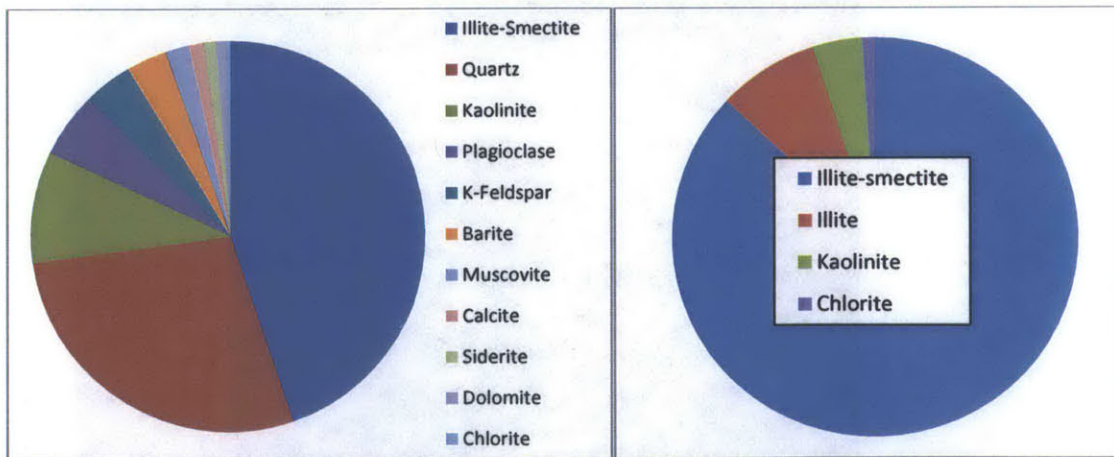


Figure 3.6 Mineralogy of Gulf of Mexico Eugene Island clay – bulk sample on left, < 2 micron on right

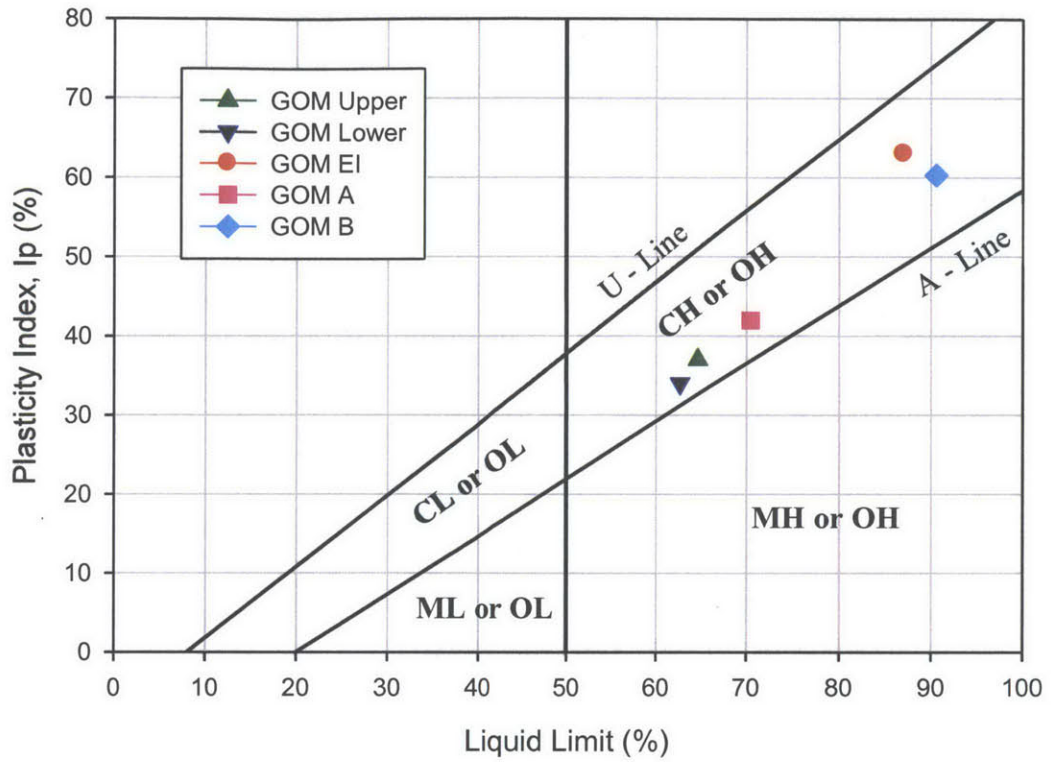


Figure 3.7 Plasticity chart showing data for GOM EI, GOM Lower, GOM Upper, GOM A, and GOM B

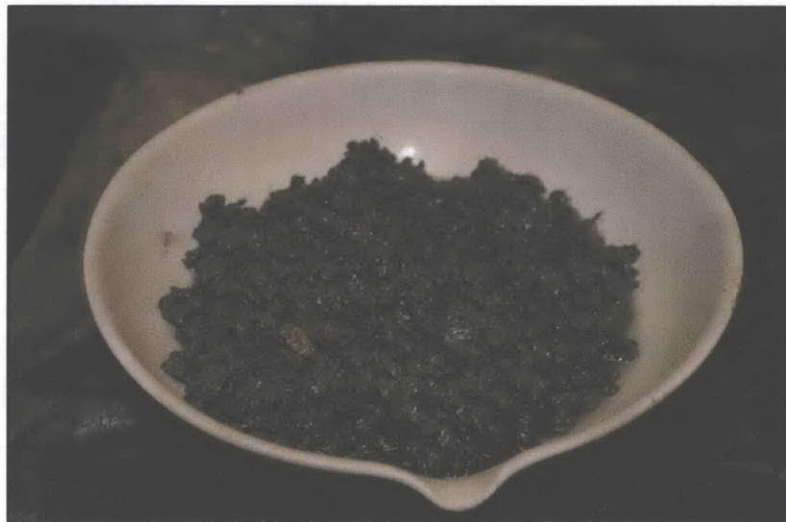


Figure 3.8 Condition of GOM Upper Interval prior to cleaning. The soil cuttings are coated in drilling fluid.



Figure 3.9 Size and color of GOM Upper Interval drill cuttings after removal of drilling fluid



Figure 3.10 Size and color of GOM Lower Interval drill cuttings after removal of drilling fluid

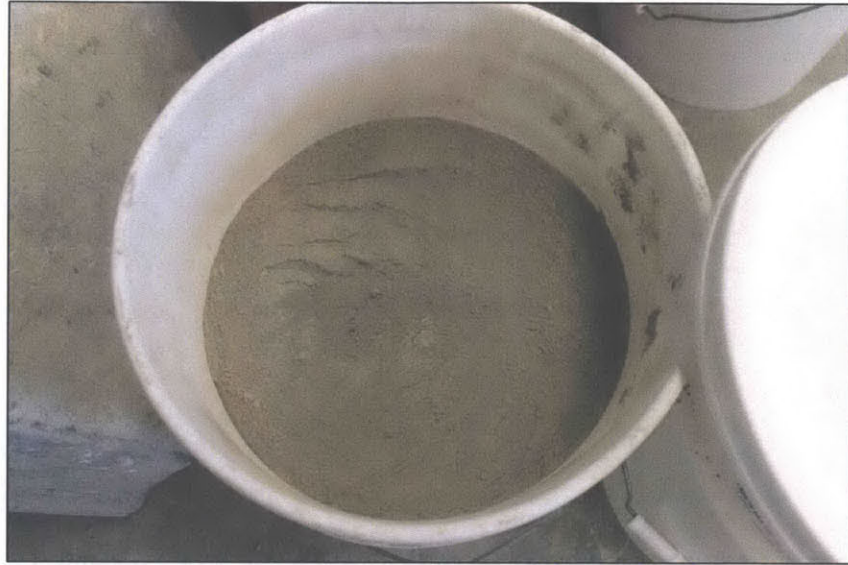


Figure 3.11 Finely ground GOM Lower Interval stored in 10 gallon sealed plastic containers

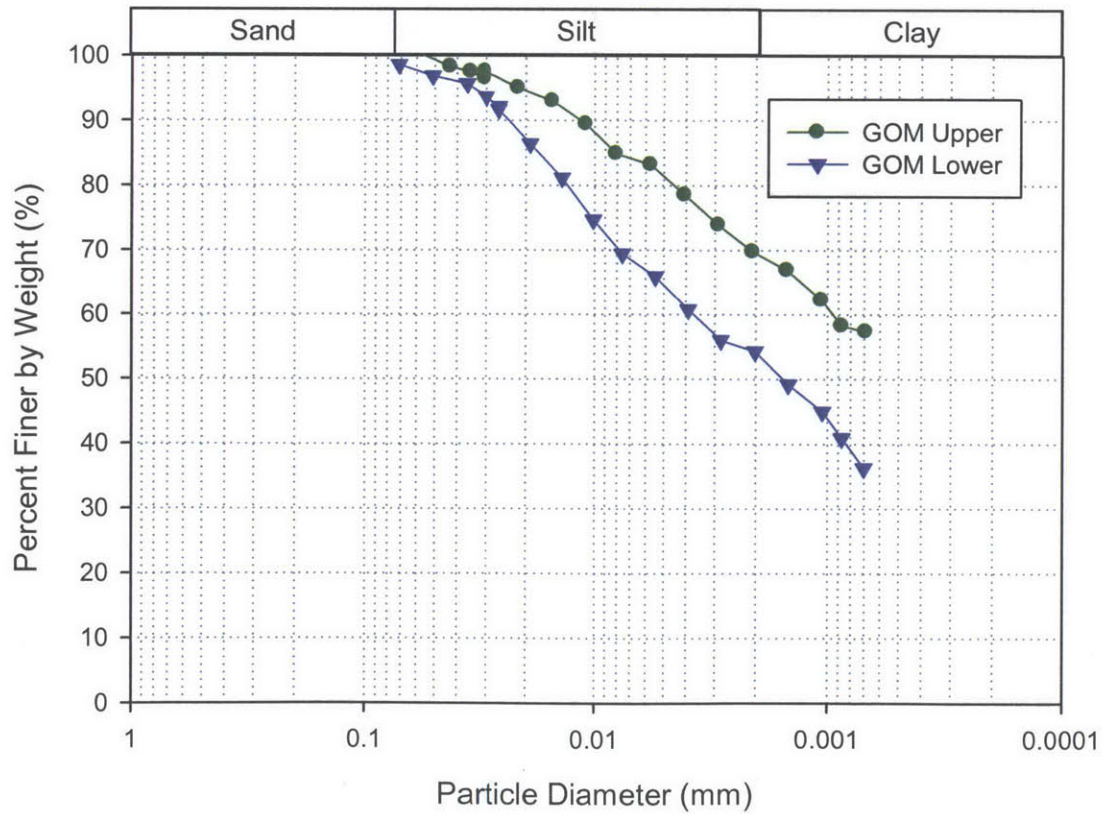


Figure 3.12 Results of grain size analysis for GOM Upper and Lower (tested by Taylor Nordquist & Chunwei Ge)

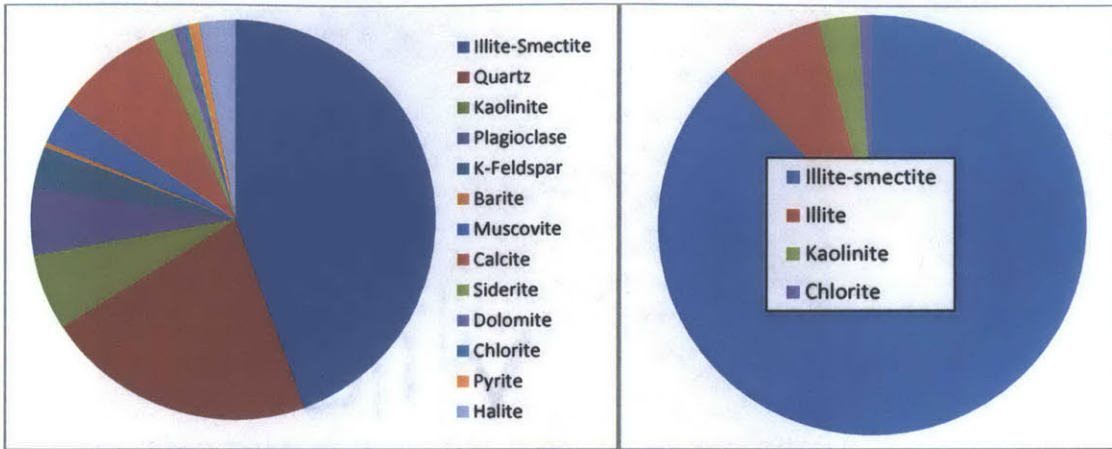


Figure 3.13 Mineralogy of Gulf of Mexico Upper Interval – bulk sample on left, < 2 micron on right

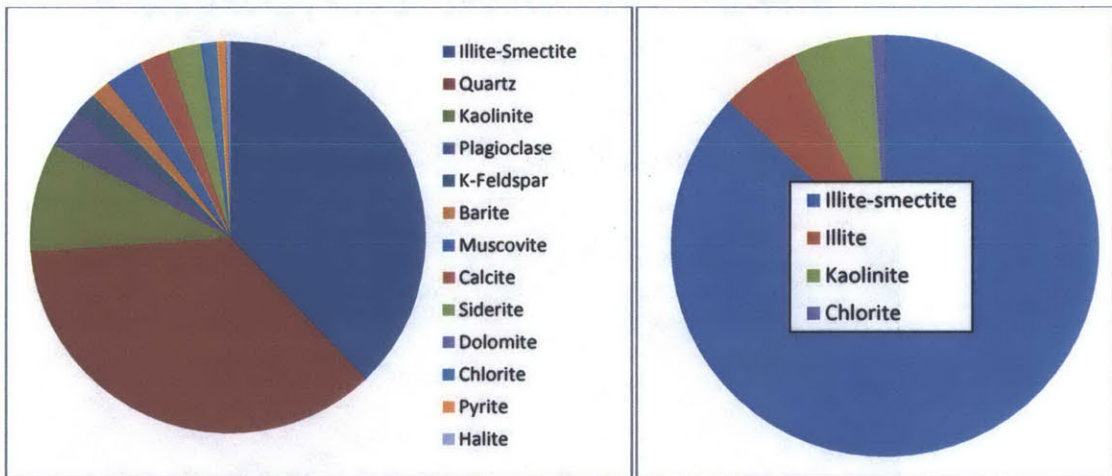


Figure 3.14 Mineralogy of Gulf of Mexico Lower Interval – bulk sample on left, < 2 micron on right



Figure 3.15 Ball Mill Grinder, Top: Rotating hexagonal steel drum powered by electric motor, Bottom: View inside drum of soil and steel ball mixture (Jones, 2010)

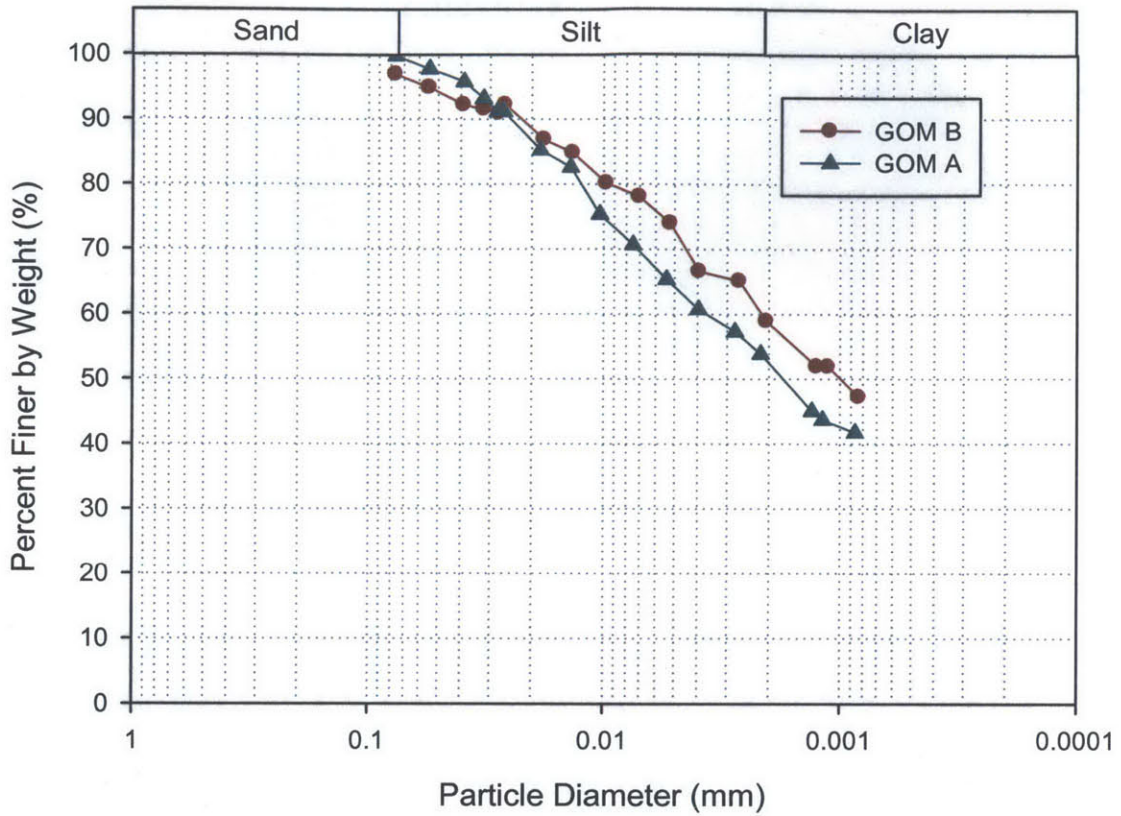


Figure 3.16 Results of grain size analysis for GOM A and GOM B (tested by Amy Adams)

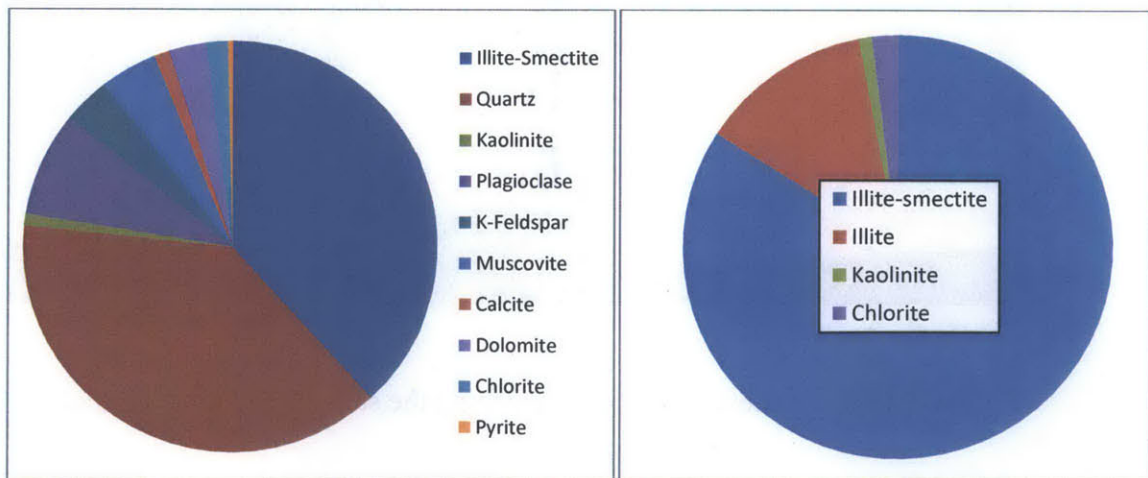


Figure 3.17 Mineralogy of GOM A – bulk sample on left, < 2 micron on right

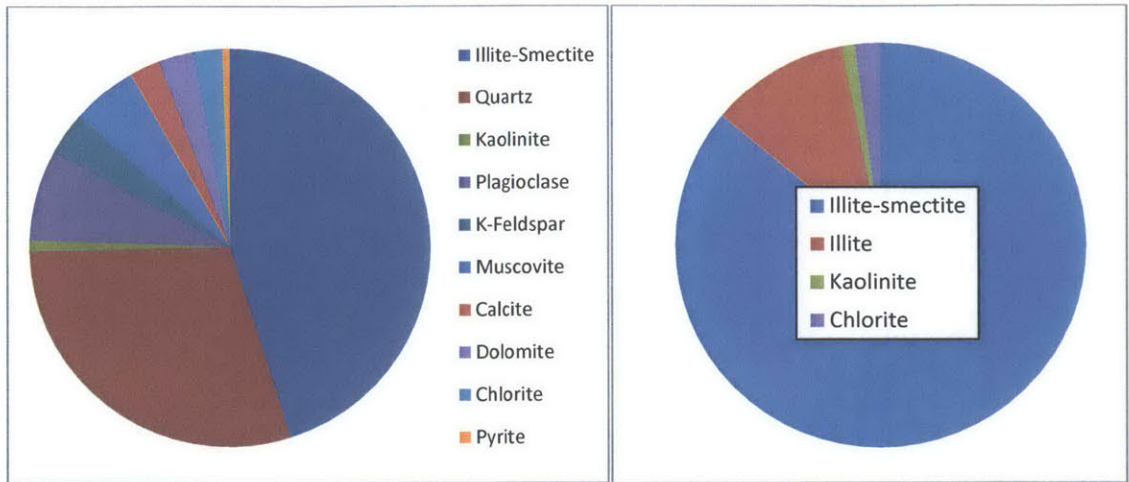


Figure 3.18 Mineralogy of GOM B – bulk sample on left, < 2 micron on right



Figure 3.19 Equipment required for leaching the salts from soil using dialysis tubing

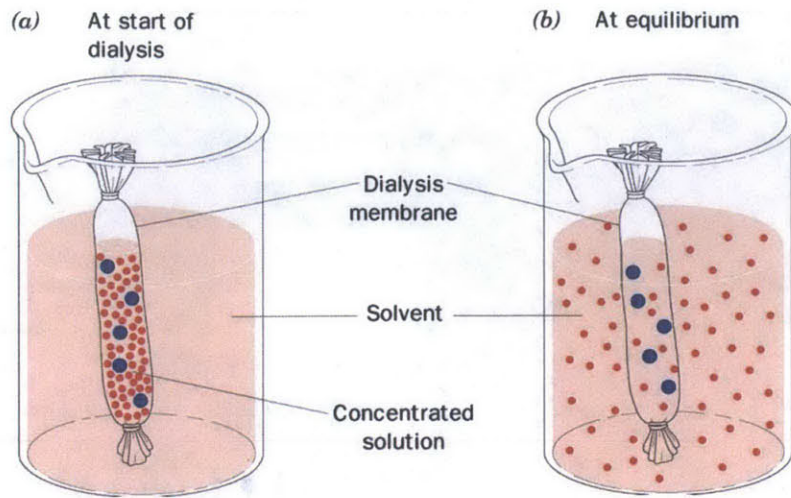


Figure 3.20 Schematic of how dialysis tubing work
(<http://ehumanbiofield.wikispaces.com/>)

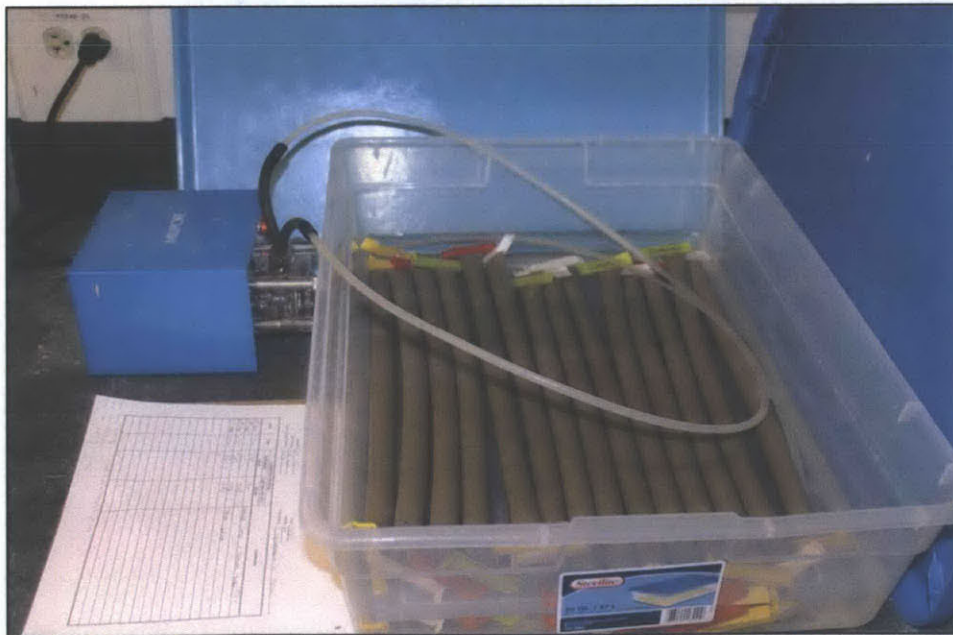


Figure 3.21 Leaching process underway with dialysis tubing filled with soil slurry placed in a bath of distilled water



Figure 3.22 Conductivity Meter and associated probe used to measure the salinity of the bath water

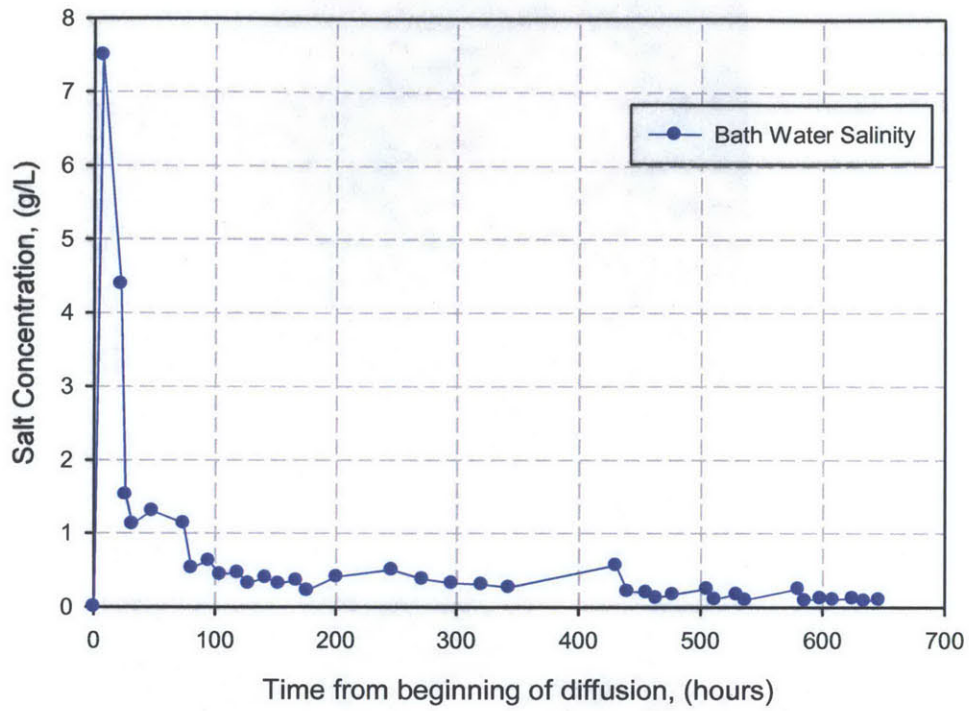


Figure 3.23 Evolution of soil salinity with time by measuring the salinity of the bath water at each water change (every ~12 hours)



Figure 3.24 Condition of GOM Lower with each chunk of soil coated in drilling fluid prior to cleaning

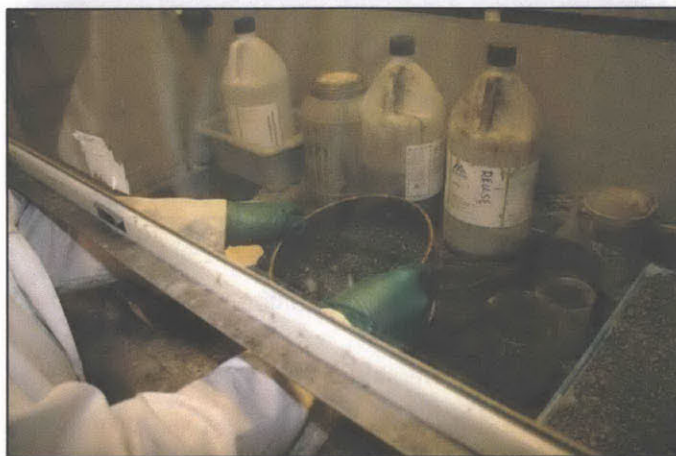
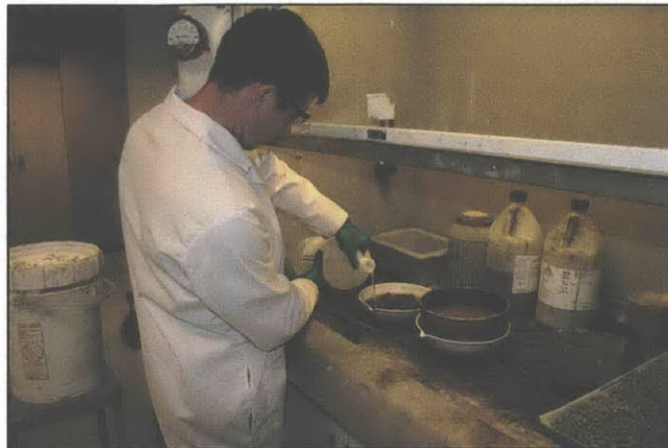


Figure 3.25 Removal of drilling fluid from GOM Lower. Top: First addition of Toluene to soil chunks, Middle: Sieving off toluene/drilling fluid mixture using #20 sieve, Bottom: adding toluene mixture back to soil chunks for secondary cleaning with drilling fluid at base of bowl removed

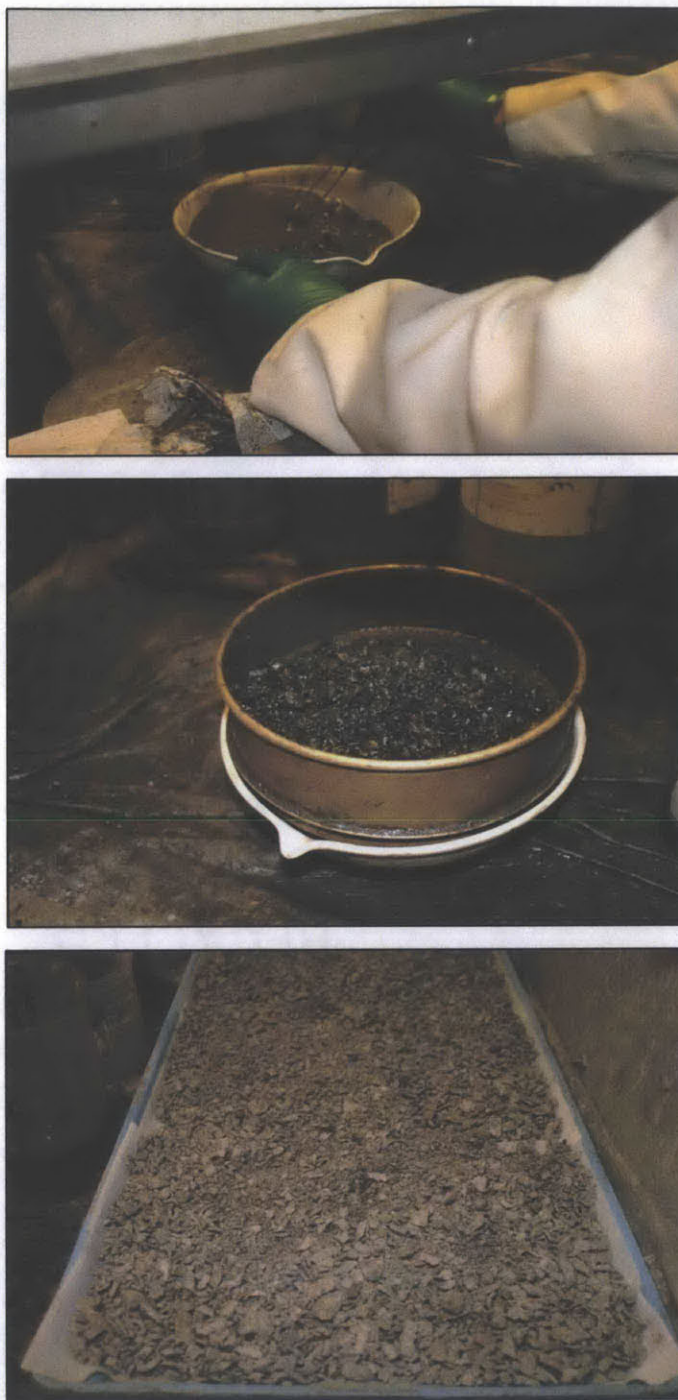


Figure 3.26 Removal of drilling fluid from GOM Lower. Top: Gently stirring the soil chunks in the toluene to prevent possible breakup of each chunk, Middle: final sieving of soil chunks, Bottom: cleaned soil placed on absorbent towel to allow any residual toluene to evaporate



Figure 3.27 Cleaned GOM Upper placed in trays for oven drying to reduce moisture content to a level suitable for grinding in the GPX Disk Grinder



Figure 3.28 Trays of soil chunks placed in oven set at a temperature of 60° Celsius



Figure 3.29 GPX Disc Grinder used in processing both GOM Upper and GOM Lower

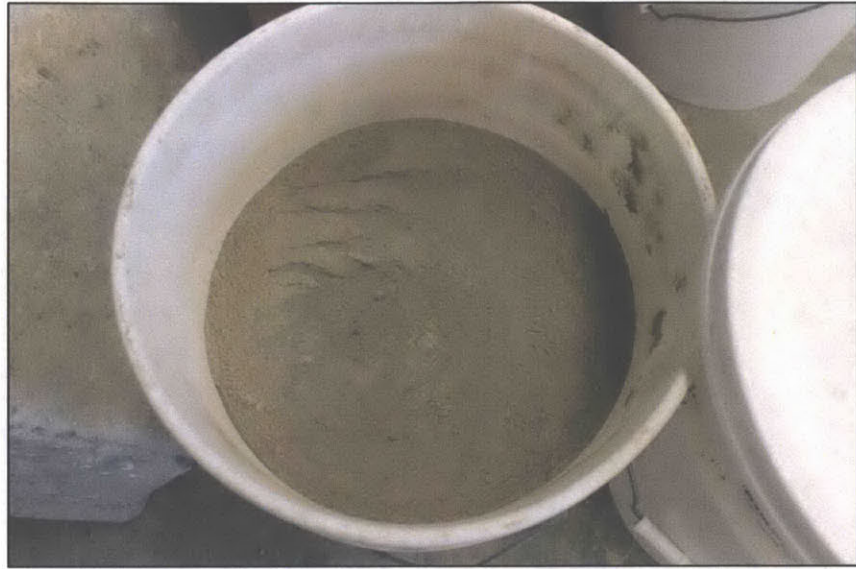


Figure 3.30 GOM Lower - Final product ready for resedimentation after cleaning and grinding to a fine powder

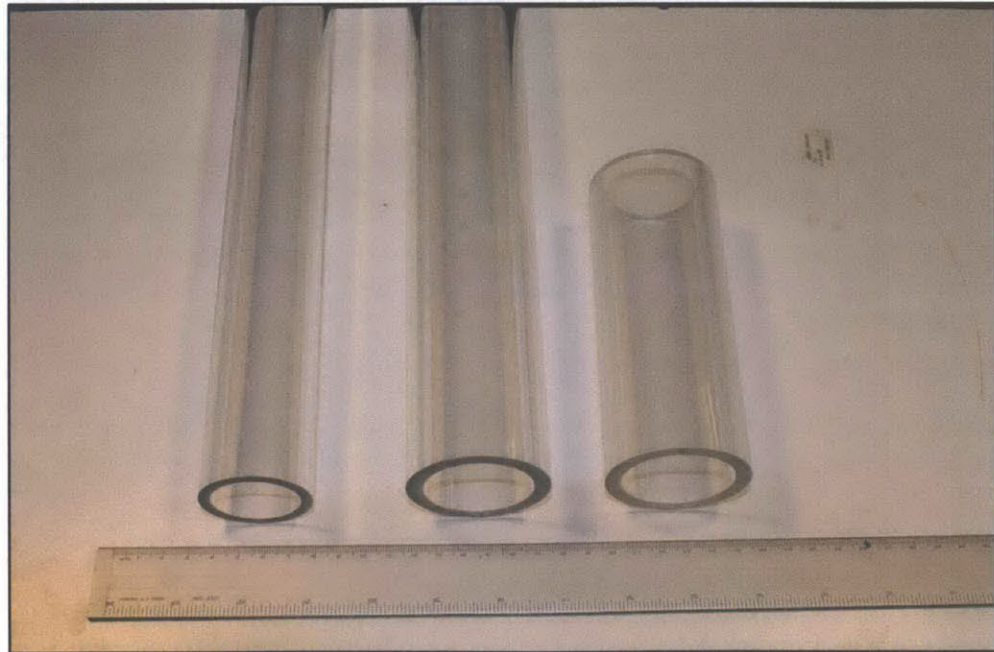


Figure 3.31 Consolidometers used in this research. Left: 1.4" diameter triaxial testing consolidometer, Middle: 1.75" diameter consolidometers for CRS testing, Right: consolidometer used for CRS testing when small quantities of soil were required for resedimentation



Figure 3.32 Kitchen aid mixer used to mechanically agitate soil/water mixture into a slurry

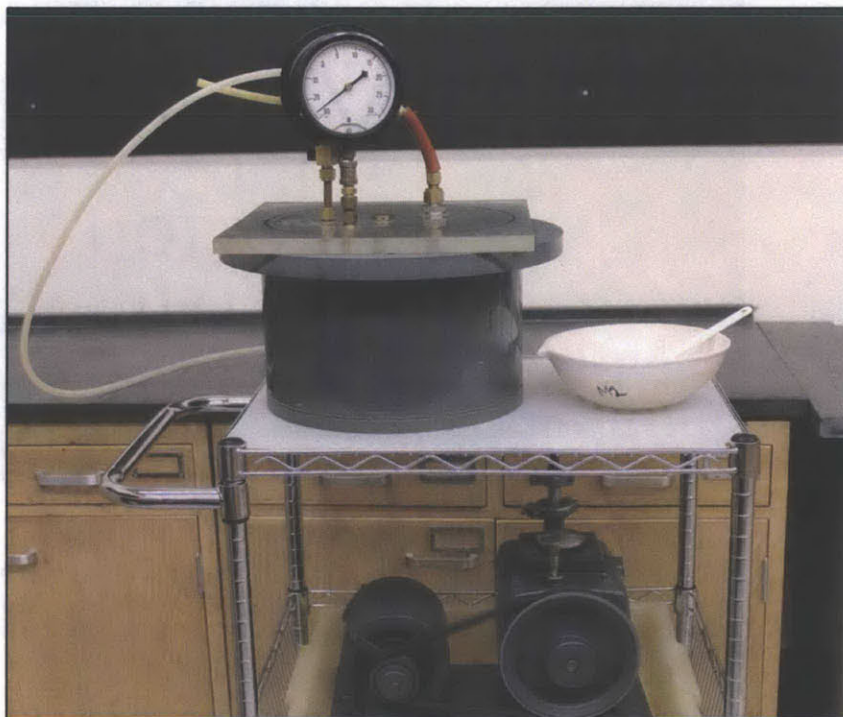


Figure 3.33 Equipment used to deair the soil slurry. The ceramic bowl with soil is placed inside the cylindrical chamber and the vacuum pump beneath it creates the necessary vacuum

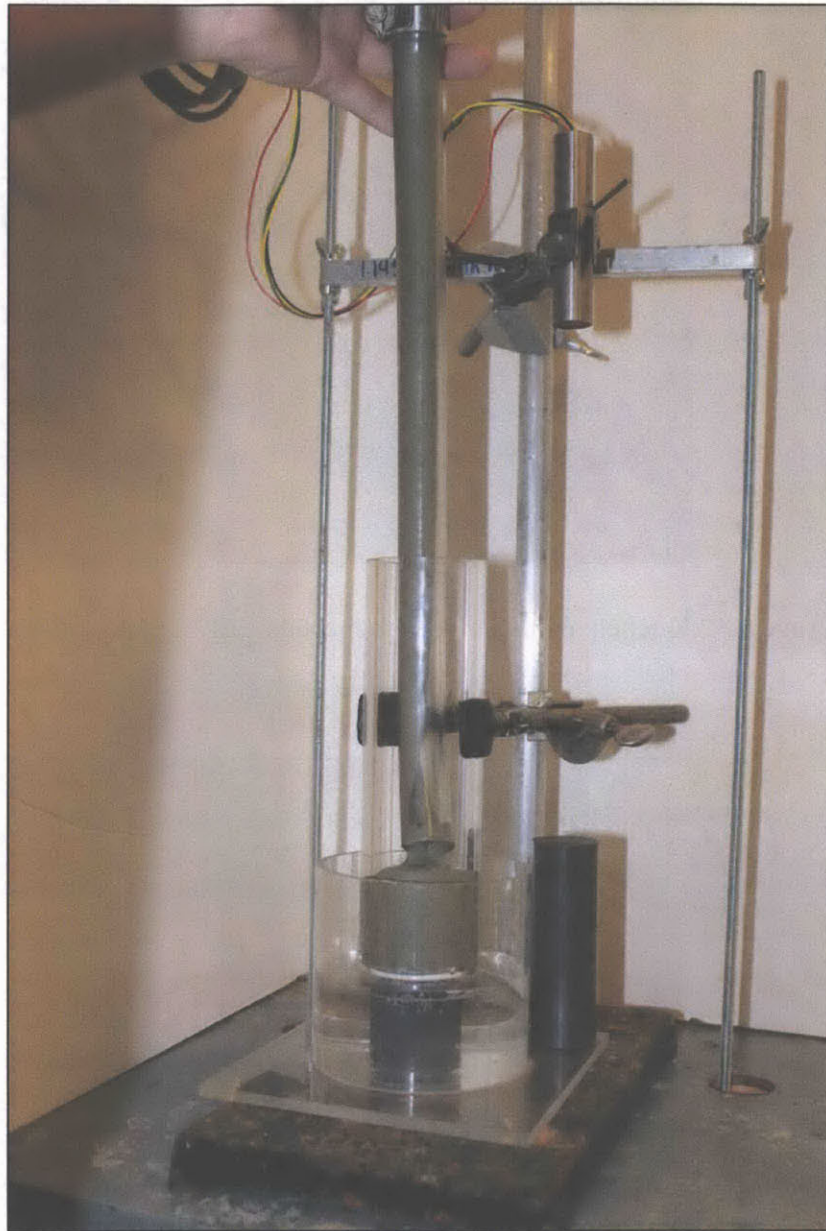


Figure 3.34 Pouring de-aired slurry into consolidometer with funnel and flexible tube. Note the end of the tube is maintained at the soil surface to prevent air pockets becoming trapped as the soil is placed (Horan, 2012)

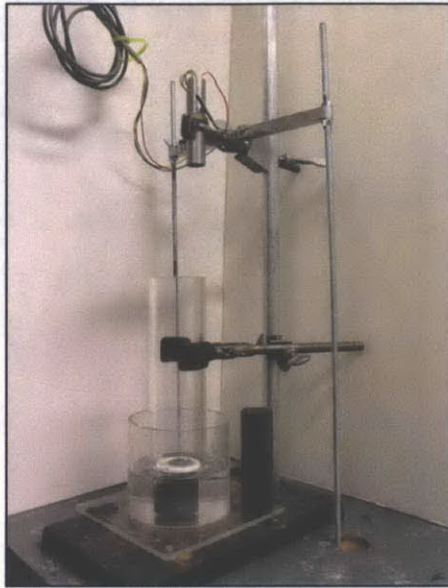


Figure 3.35 Consolidometer clamped in place with water bath filled midway on the porous stone ready to receive de-aired slurry (Horan, 2012)

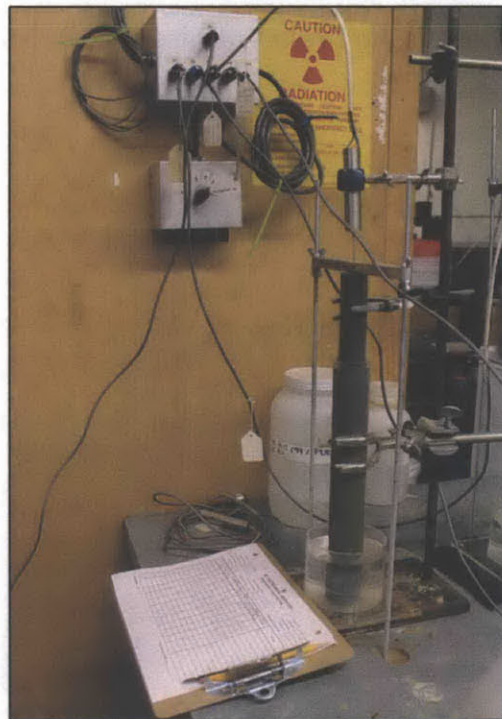


Figure 3.36 Resedimentation set-up for stresses up to 0.5MPa with weights applied via hanger. LVDT measuring strain connected to data acquisition channel at top of image

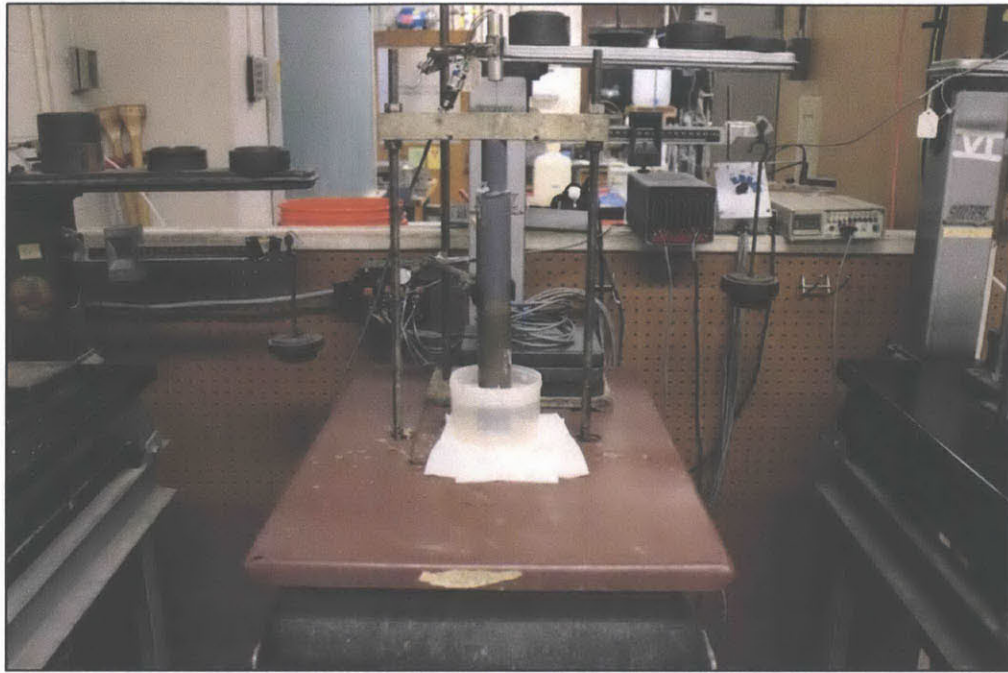


Figure 3.37 GOM EI placed in an Oedometer load frame (2000 lb capacity) for resedimenting to stresses ranging from 0.5MPa to 10MPa

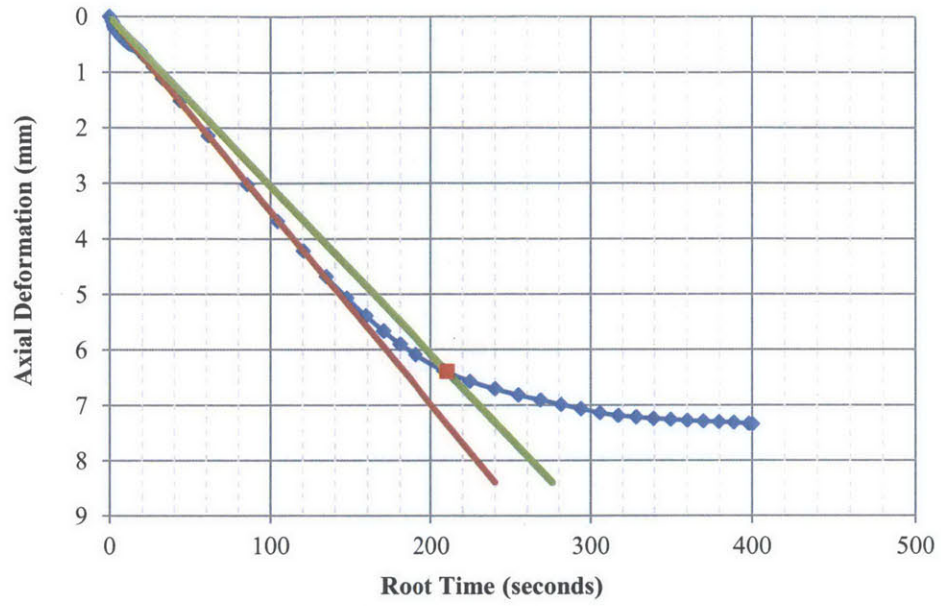


Figure 3.38 Hydraulic cylinder used to extrude a resedimented specimen from the consolidometer. This device is used when the resedimentation stress exceeds 0.5MPa



Figure 3.39 Resedimented triaxial specimen being extruded from consolidometer

Root Time Method



Log Time Method

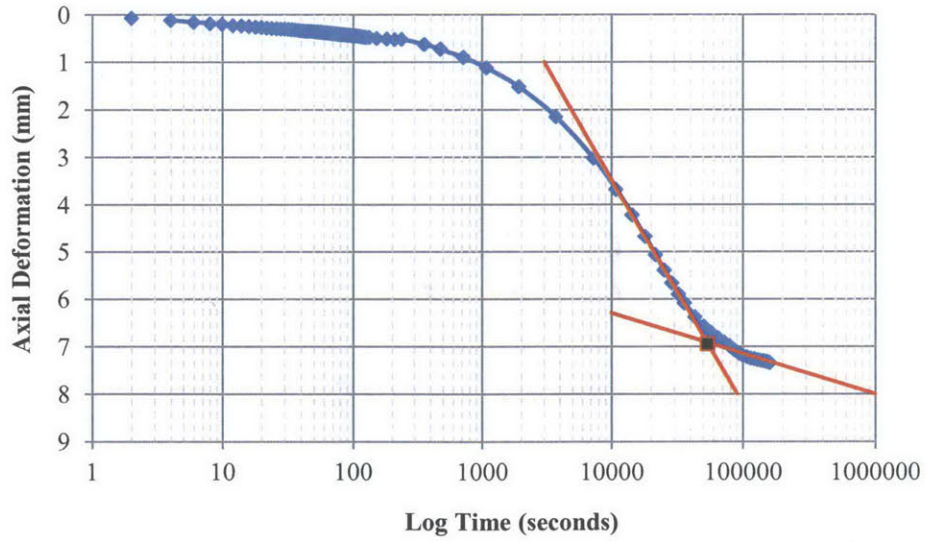


Figure 3.40 GOM EI resedimented to 64 g/L. Stress level at end of primary is 25 kPa.
Top: Root time method for determining time to reach end of primary consolidation. Bottom: Log time method to determine end of primary consolidation for same data

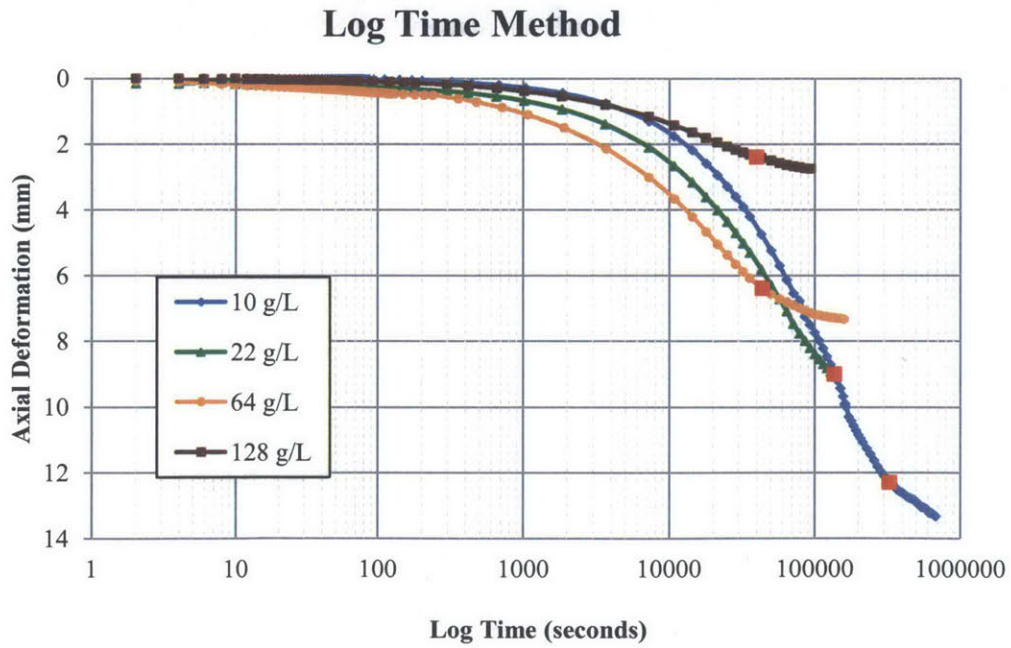
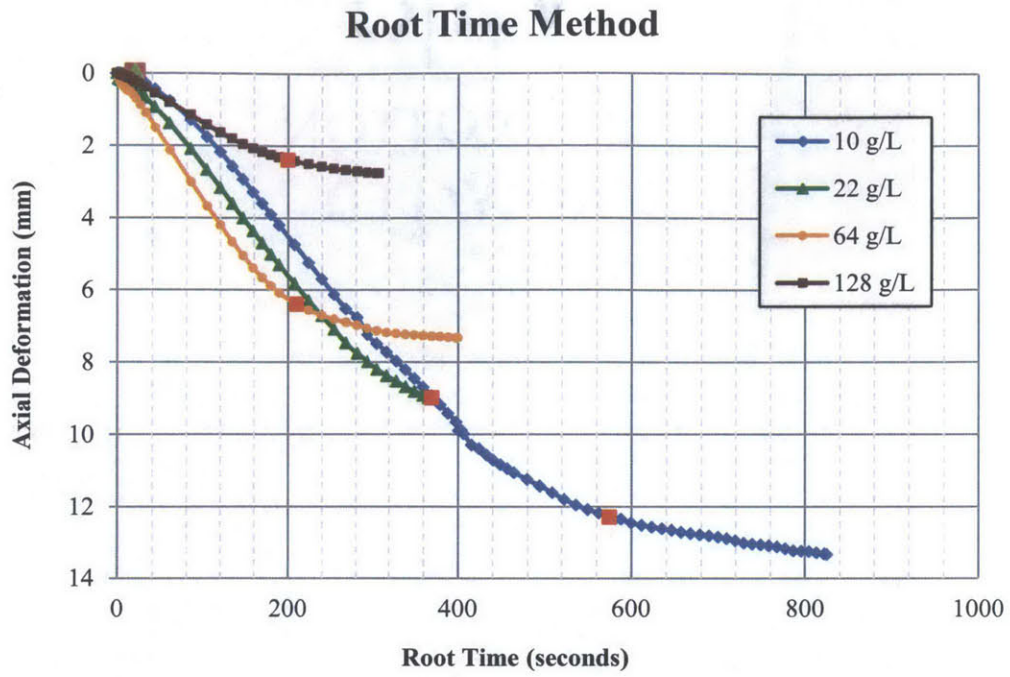


Figure 3.41 Data for GOM EI resedimented at salinities ranging from 10 to 128 g/L. The stress increment (25 kPa at EOP) is the same for all salinities.



Figure 3.42 Issue of salt precipitating out of solution when resedimenting with high pore fluid salinities (soil shown is GOM EI resedimenting with a pore fluid salinity of 256g/L)

4 EQUIPMENT AND TESTING PROCEDURES

4.1 INTRODUCTION

This chapter describes the equipment and procedures used for both the Constant Rate of Strain (CRS) and triaxial testing program performed in the course of the research.

Section 4.2 provides an overview of the data acquisition and automation systems used in the MIT Geotechnical Laboratory. This section provides all relevant transducer information for the various testing devices used in this study. Triaxial testing was performed using an MIT automated stress path triaxial cell. Computer control allows for higher quality results as well as for a dramatic reduction in labor. The control hardware and software which allows for automation of testing is already well described by previous researchers (e.g. Sheahan (1991), Abdulhadi (2009), Horan (2012)) and therefore a brief overview will be presented in this chapter.

Both the CRS and triaxial equipment used are described in Section 4.3. Due to the large stress range associated with the triaxial testing, three different triaxial cells were employed and the differences between the three will be briefly outlined. In addition, a description will be provided of the development of a completely new CRS cell and ancillary equipment capable of conducting CRS testing to an axial effective stress of 100MPa.

Lastly, Section 4.4 describes the various test procedures employed throughout the research for index testing, CRS testing and triaxial testing, as well as problems encountered and measures implemented to eliminate such problems.

4.2 DATA ACQUISITION SYSTEM

4.2.1 Introduction

The MIT Geotechnical Laboratory employs many devices to run laboratory tests, most of which are automated. This section describes the elements common to both CRS and triaxial testing, including measurement instrumentation devices, data acquisition and computer control programs.

4.2.2 Measurement Instrumentation

CRS and triaxial testing conducted throughout this study require accurate measurement of physical quantities that change throughout the test. Transducers can be used to measure these physical quantities. At MIT, a central data acquisition system (described in section 4.2.3) is used to collect and record transducer readings based on tasks that are set by the user for a particular test. The transducers that are used for this study can be subdivided into four categories: axial displacement transducers, pressure transducers, load cells, and volume change transducers. All transducers used in the MIT geotechnical laboratory require an input voltage of 5.5 volts of Direct Current (DC) and output a DC current. Each transducer is calibrated to obtain a calibration factor, and has a characteristic resolution and stability. Details of the transducers used for CRS and triaxial testing are given in Table 4-1, Table 4-2, Table 4-3, and Table 4-4. The following sections briefly describe each of the four categories of transducer type.

4.2.2.1 Axial Displacement Transducers

Axial deformation of a soil specimen during testing is measured using a Linear Variable Differential Transformer (LVDT) manufactured by Trans-Tek Inc. An LVDT consists of a free-to-move ferromagnetic core and primary and secondary coils that generate a magnetic field inside the LVDT tube. When the core displaces axially through the LVDT tube, an output voltage is produced which is directly proportional to the position of the core in the tube. This voltage can be related to the displacement using the calibration factor. An LVDT's linear range varies from as small as 0.1cm up to 10cm and therefore an appropriate transducer depends on the expected axial strain the soil will undergo during a test. The CRS device incorporated two LVDT's positioned at 180° to each other, with the average being taken as the true displacement, whereas all triaxial devices used required only one LVDT to measure axial movement. Figure 4.1 shows a typical LVDT with its associated core used in this research.

4.2.2.2 Pressure Transducers

Pressure transducers are used on both the CRS and triaxial devices. They are used to accurately measure applied cell pressures and specimen pore pressures. The pressure transducers used at the MIT Geotechnical Laboratory are manufactured by Data Instruments and are of type AB/HP or AB and measure the gauge pressure by means of deflection of a steel diaphragm instrumented with strain gauges. The CRS device uses two 200 psi (1.4 MPa) pressure transducers to measure the cell and pore pressure, whereas the transducers used with the triaxial device vary in capacity from 200 psi (1.4 MPa) to 2000 psi (14 MPa) depending on the stress capacity of each device. Figure 4.1 provides an example of a 200 psi (1.4 MPa) pressure transducer. This Figure also shows a section through a pressure transducer with its internal components.

4.2.2.3 Load Cells

The load cell used with the CRS device was manufactured by Toledo Transducers Inc. and has a 10,000 lb (44.5 kN) capacity. The low stress and medium stress triaxial devices used Data Instruments JP type shear beam load cells with a capacity of 500 lb (2.2 kN). All load cells consisted of an S-shaped steel section instrumented with strain gauges whose output voltage is related to the applied load using the calibration relationship. Load cells are mounted internally for triaxial testing and externally mounted for CRS testing during this research. An example of a typical load cell used for triaxial testing is shown in Figure 4.1.

4.2.2.4 Volume Change Transducers

Changes in volume of a specimen during a triaxial test are determined by measuring the displacement of a piston in a Pressure Volume Actuator (PVA), an example of which is shown in Figure 4.2. Volume change is computed by measuring the displacement of a piston within a PVA by means of an LVDT or string pot. The area of the piston is known and remains constant; therefore the volume change is a function of displacement only. String pots are similar to LVDT's in that they measure displacements; however they differ in that when axial movement occurs, the spooled cable extends, rotating an internal sensing device (precision potentiometer), producing an electric output signal proportional to the cable extension (Adams, 2011). For CRS

testing, a similar PVA has a more basic function of controlling the cell pressure at a constant value once the specimen has been back pressure saturated.

4.2.3 Data Acquisition System

The computer based data acquisition system in the MIT Geotechnical Laboratory provides a single location from where readings of multiple transducers can be taken simultaneously. The system allows for the operator to define a recording schedule that includes, but not limited to, the various transducers to be measured and the rate at which readings are taken. Once a set of readings are taken, they are written to a text file (.dat) and stored on a computer until the operator retrieves it. The system will continue to record data until either the number of prescribed readings specified by the operator has been reached, or the test is stopped. Abdulhadi (2009) and Horan (2012) describes the system in detail and therefore only a summary of the system components will be presented here.

Figure 4.3 is a schematic drawing of the central data acquisition system (Germaine and Germaine, 2009). The components of the system can be sub divided into the following categories:

- 1) The laboratory testing device, which includes the transducers, power supply, junction box, voltmeter and ground;
- 2) A switching mechanism which allows the data acquisition mechanism to connect to a particular transducer to make a measurement;
- 3) An Analogue to Digital (A/D) converter that converts the voltage output from each transducer and the power supply to a digital word which can be read by a computer. This device is critical to the precision of the final measurement; and
- 4) A computer which controls the process and components and performs the administrative and computational tasks associated with collecting and archiving the measurements

4.2.4 Computer Control System

The automation and computer control of tests conducted in the MIT Geotechnical Laboratory was first initiated in the early 1990's by Sheahan (1991). He developed an automated stress path triaxial cell for testing. The addition of new components to complete the system automation, increase flexibility and quality control has been continuous. The main advantages of automation are the huge reduction in man hours, reduced potential for human error, and increased accuracy.

Automation is controlled by drive systems using closed loop feedback control. This is achieved using the following steps:

- 1) The transducers make measurements of the actual stress-strain state of the specimen;
- 2) The voltage output from the transducer is sent to the computer via an A/D converter and converted to engineering units;
- 3) The software compares these engineering units with a prescheduled time history of the specimen state that is set by the user upon initiation of the test or test stage;
- 4) A control algorithm computes what action needs to be taken by the motors to maintain the prescribed stress-strain state schedule;
- 5) The signal is sent to the motors to carry out the computed action

Sheahan (1991) describes closed loop feedback control as direct measurements in an iterative system to maintain specific time histories of the parameters being measured.

Figure 4.4 shows the main hardware components required to carry out this process. The voltage output of the transducer is sent to an analog to digital (A/D) converter which converts the analog signal in volts to digital signal in bit counts. Multichannel A/D converter devices (MADC) are used as they provide a high precision with a 22 bit resolution. A computer processes the incoming signals and determines the new command signal to be sent to the testing device. The command signal generated is then converted back into an analog signal through a digital to analog (D/A) converter that is located within the computer. The D/A converter is a commercial board manufactured by Strawberry Tree Inc. with a 12 bit resolution and a ± 5 volt

range. The analog signals are sent via a motor driver from the D/A converter to the electric motor, which in turn operates at a rate that is proportional to the command signal. The electric motor then drives the associated component such as the piston of the PVA to adjust pressures (Horan, 2012).

Automated control is carried out using a control program written in the QBASIC programming language. The program allows the user to set up the system for testing and also allows for the control of the various stages of a test. The software was originally developed for automated triaxial testing but has been constantly updated. It is now task specific, allowing functions such as initial pressure up, saturation, consolidation and shear phases. CRS testing conducted during this research made use of a modified version (revision 2.01) of this program where computer control was implemented for the saturation phase and for the control of cell pressure during consolidation. Despite this local computer control, the central data acquisition is still used to record the data for all tests conducted throughout the laboratory.

4.3 TESTING EQUIPMENT

4.3.1 Introduction

The following section describes the CRS and triaxial equipment used during this research. Due to the large stress range associated with the triaxial testing, three different triaxial cells were employed and the differences between the three will be briefly outlined. In addition, a description will be provided of the development of a completely new CRS cell and ancillary equipment capable of conducting CRS testing to an axial effective stress of 100 MPa.

4.3.2 Constant Rate of Strain (CRS) Testing Equipment

4.3.2.1 Trautwein Cell

A modified Trautwein CRS cell (termed TR4 within the catalogue of MIT Geotechnical Laboratory testing devices) was used for all CRS tests performed. This cell has been modified from a standard CRS Trautwein cell for the purpose of previous research conducted at MIT. The modifications include:

- Use of a smaller specimen than standard
- Smaller diameter platten fitted that is more appropriate to the smaller specimen size
- Two LVDT's fitted, as opposed to one, providing an average reading of axial displacement and accounting for any piston rotation, and
- The drilling of a 3mm diameter hole in the piston column above the piston seal to allow any fluid that leaked past the piston seal (isolating the cell pressure from atmospheric pressure) to exit the device thereby preventing a build-up of fluid within the piston column that would cause damage to the piston roller bearings. The impact to the bearings can be more pronounced when the fluid has a high salinity.

A photo of the CRS ring used in this research is shown in Figure 4.5 alongside a standard CRS ring.

The cell consists of a clear plexiglass chamber which fixes onto a metal base. A recess in the metal base accommodates a large porous stone, which in turn provides access to a base drainage line from where excess pore pressures are measured during consolidation. The specimen is trimmed and encased between two filter screen - porous stone pairs in a rigid ring, which is then placed above the large porous stone. The specimen is incrementally back pressure saturated over a period of approximately 90 minutes and then loaded at a constant rate of strain via a piston while the excess pore pressure generated at the base of the specimen resultant from loading is measured. Only one-way drainage occurs along the top boundary during consolidation. A detailed schematic of the CRS cell with test specimen in place is shown in Figure 4.6. Only the cell pressure is required to be controlled during the test. Pressure control is achieved using a PVA that is equipped with motors connected to a computer allowing for computer control. Figure 4.2 provides an example of the PVA used with the CRS device, complete with fluid reservoirs on top to allow for refilling. The PVA is connected to the base of the cell by a combination of plastic and copper tubing.

Cell pressure and the excess pore pressure are measured using a pressure transducer. Axial deformation is measured using two LVDT's, with true axial deformation taken as the average of the two. The axial load is measured using an external load cell. Details of these

measurement instruments are provided in Section 4.2.2. Deformation of the soil specimen is corrected for apparatus compressibility. The apparatus compressibility was determined by running a test on a stainless steel block in place of the specimen.

Figure 4.7 shows the CRS cell used in this research at various stages during test set-up. The Figure shows both the cell disassembled into its individual components for cleaning and maintenance as well as in assembled form with test specimen in place.

4.3.2.2 Load Frame

All CRS testing was conducted using a Wykeham Farrance Model T-57, screw driven loading frame with a 10,000 lb (44.4 kN) axial capacity, shown in Figure 4.10. The loading frame has 6 gear positions with 5 gear ratios providing a total of 30 different displacement rates ranging from 0.0037 to 46 cm/hour. Previous research conducted on RBBC using this frame determined a suitable strain rate of 2 %/hour. However, due to the lower values of c_v for the soils tested in this research, a slower rate was required. Initially, the strain rate was set at 1.5%/hour at the beginning of the test, and then stepped down in increments of 0.3%/hour as the excess pore pressure increased. This was continued until the minimum strain rate of the frame, 0.3%/hour, was reached.

Although this loading frame is both robust and reliable in its operation, there are a number of drawbacks associated with it. Firstly, the frame is a purely mechanical device that is not computer controlled. It requires the operator to monitor the build-up of pore pressures and axial stress and turn off the frames motor in the event of either of those parameters exceeding a limiting value.

Secondly, due to the low c_v of the soils being tested, even when the frame is set to its slowest strain rate, the pore pressure in the specimen would increase to a point where it would exceed the capacity of the pressure transducer prior to the target axial consolidation stress being reached, usually 40 MPa. Due to this limitation, the frame would have to be turned off to allow the excess pore pressures to dissipate.

Thirdly, it was evident during the analysis of the test results that when the strain rate is changed during the test (this is achieved by turning off the frame, manually changing the gear

ratios and then turning the frame back on), the soil undergoes transient conditions where the data obtained is inaccurate and must be removed from the results. In order to avoid having several 'gaps' in the results, it was decided to conduct all further testing with a starting strain rate of 0.6%/hour, reducing to the minimum 0.3%/hour after a period of approximately 24 to 48 hours. At a strain rate of 0.6%/hour, 24 hours was sufficient for the soil to be stressed past its resedimented pre-consolidation pressure. From the results, it was also evident that once the frame is turned off to allow the excess pore pressures to dissipate, all data for permeability and c_v obtained beyond this point would be inaccurate.

4.3.2.3 Temperature Control

Over a 24 hour period, temperatures can fluctuate in the laboratory by several degrees above and below room temperature. Changes in temperature result in changes in the viscosity of the pore fluid within the specimen and test device, hence impacting the calculation of permeability and coefficient of consolidation measurement during the test. More importantly, changes in temperature causes differential expansion of materials resulting in abnormal variations in excess pore pressure. In order to eliminate this variation in temperature, an insulated timber enclosure was constructed so that the CRS cell could be placed within. Constant temperature is maintained within the enclosure by means of a light bulb which is turned off and on by a mercury contact switch. A small electric fan circulates the heat from the light bulb, ensuring a uniform temperature within the enclosure. Temperature was set at a constant value of 25.3° C for all testing conducted in this research, and this value was used to calculate the viscosity of the pore fluid in the permeability calculations. The enclosure itself, mounted on the Wykeham Farrance frame is shown in Figure 4.10 with a view of the CRS cell in operation inside the enclosure shown in Figure 4.11.

4.3.2.4 Development of CRS capability to 100 MPa

Current CRS capability in the MIT Geotechnical Laboratory is limited to an axial consolidation stress of 40 MPa. With advances in technology, the petroleum industry is now capable of drilling to greater depths in the exploration for new oil reserves. Recent wells drilled

in the Gulf of Mexico are located in deep sea water (1.5 km to seabed) with reservoir depths up to 9 km below the seabed. An axial consolidation stress of 40 MPa can be approximated to 3 km of overburden. In order to measure, analyze, and understand the mechanical behavior of soils at such depths it is necessary to develop laboratory equipment with the capacity to replicate the in-situ stresses.

A completely new CRS device was developed during this research capable of applying up to 100 MPa axial consolidation stress to a soil specimen. Details of the set-up are shown in Figure 4.12. The CRS cell is mounted in a load frame with a 222kN (50,000 lb) capacity consisting of a top and bottom 3" thick steel plate connected with 4 no. 1 ½" threaded steel rods. The plating provides both a flat even surface as well as the reaction platform for the test stresses, while the threaded rods act in tension during testing.

A low profile hydraulic cylinder, model RCS-1002 manufactured by Enerpac, with an 887kN (199,400 lb) capacity and a maximum stroke of 57mm, mounted on the frame provides the axial force. The hydraulic cylinder is operated by a computer controlled PVA, shown in Figure 4.13. Modification of the CRS control program written in QBASIC, allows for the rate of the PVA motor, and in turn the strain rate applied to the specimen via the hydraulic cylinder to be decreased gradually as the excess pore pressure increases. This gradual process of decreasing the strain rate will prevent any transient conditions occurring within the test specimen that has been associated with an abrupt rate change using the Wykeham Farrance frame. This system is capable of applying the very low strain rates (< 0.1%/hour) that will be necessary to prevent the excess pore pressure exceeding the capacity of the pressure transducer as the soil is consolidated to 100 MPa.

Similar to the CRS cell TR4, this new CRS cell is operated within a temperature controlled enclosure with the same components as that outlined in Section 4.3.2.4. The cell pressure is controlled using a PVA regulated using air pressure. Each increment of pressure during the back pressure saturation phase is applied manually and once the test cell pressure is reached, it is maintained using a regulated air supply. A Sentran PG3 222kN (50,000 lb) capacity low profile load cell with an output of 2.998mV/V is mounted to the underside of the top plate and concentric with the hydraulic cylinder. A spring supported three-arm plate holds a metal

spacer piece against the load cell, providing a smooth an even contact between the convex surface of the load cell and the flat surface of the top of the CRS piston. Details of the PVAs and load cell are shown in Figure 4.13.

Axial displacement is measured by two M150 ultra-miniature string pots mounted on top of the CRS cell, connected to the piston, and orientated at 180° to each other. These devices were favored over LVDT's due to their greater accuracy and compact size. Figure 4.14 shows the mounted position of each string pot.

The CRS cell itself required a new larger piston owing to the increased test stresses. The CRS trimming ring is maintained at the same small diameter size of 3.56 cm. A modified base was required due to expected larger excess pore pressures. Excess pore pressures, exceeding those developed when testing to 40 MPa, will be expected when reaching stresses of up to 100 MPa. With increased excess pore pressure, the square ring seal would be inadequate to isolate the pore pressure from both the cell and atmospheric pressure. A redesign of the base involved elevating the area of the cell base directly beneath the test specimen. A recess into which an O-ring is placed was machined along the vertical wall of the elevated section. This O-ring forms a seal against the inside of the CRS trimming ring, isolating the excess pore pressure. The square seal still functions as a barrier between the cell and atmospheric pressure. Details of the redesigned base are shown in Figure 4.15. The final modification was the replacement of the standard silicon carbide porous stones with a stronger ceramic based porous stone capable of withstanding the increased axial forces without fracturing or crushing.

The construction of the CRS cell, design and machining of components associated with the load cell and string pots as well as various other components were completed by Stephen Rudolph at the MIT Civil Engineering Department Machine Shop. The equipment was completed ready for testing towards the end of this research. No testing has been conducted with this device; however, trial testing is due to be carried out in the near future.

4.3.3 Triaxial Testing Equipment

Resedimented GOM EI and Leached GOM EI specimens were sheared undrained in a triaxial cell after being K_0 consolidated to stresses ranging from 0.15 MPa to 60 MPa. Due to this

large stress range, three different triaxial cells were employed. Figure 4.16 shows a general schematic of the standard automated triaxial testing system used in the MIT Geotechnical Engineering Laboratory. The system incorporates seven basic components: the triaxial cell itself; a load frame for axial load application; Pressure Volume Actuators (PVAs); a motor control box containing the drivers for the motors; a computer to run the control software; a power supply for the transducers and a data acquisition system. This system is the same for each of the three different triaxial cells, and each cell is housed in a temperature controlled enclosure. The differences between each cell, which were custom-designed and built within the MIT Geotechnical Engineering Laboratory, are outlined in the following section.

4.3.3.1 Low Stress Triaxial Cell

The majority of triaxial tests were conducted in a low stress triaxial cell capable of consolidation stresses of up to 2 MPa. The cell accommodates standard sized triaxial specimens of 3.55 cm diameter and a height of 8.1 cm. It has a plexiglass chamber which encloses the soil specimen, base pedestal, floating top cap, top and bottom drainage lines and a compact shear beam load cell of 2.2 kN (500 lb) capacity. Drainage is provided to the soil via ports in the base pedestal and top cap. The radial stress capacity of the plexiglass chamber is the limiting parameter for the maximum test stress achievable by this device.

The use of an internal load cell is essential as it eliminates the complication of having to account for piston seal friction, a major problem associated with the use of an external load cell. Axial load is applied to the specimen through a hardened steel piston which enters the top of the chamber. Axial deformation is measured by an externally mounted LVDT connected to the piston. The bottom of the load cell is connected with the floating top cap by means of an alignment device.

The soil specimen is isolated from the chamber pressure using two thin impermeable membranes; condoms being the chosen membranes for this device. These membranes are sealed to the base pedestal and top cap using 4 O-rings at each location. Details of this sealing arrangement are shown in Figure 4.17.

Cell pressure is applied to the triaxial specimen using low viscosity silicone oil (Dow-Corning '200 fluid', 20 centistokes). The oil is transparent, non-toxic, and does not degrade the seals or membranes used in testing. This oil has an added benefit of being non-conductive, thereby allowing electronic devices such as a load cell to be located inside the cell chamber.

The cell is mounted on a screw driven Wykeham Farrance load frame. The frame axially loads the specimen to a maximum achievable force of 9.8 kN. The frame has been modified to allow for computer control to direct the rate and direction of the frames axial movements via an electric motor. This computer control allows for the frame to be halted once a predetermined stress or strain state has been reached.

The triaxial testing system employs the use of 2 PVAs. The PVAs have a maximum pressure capacity of approximately 14 MPa, far exceeding that required for this cell. One PVA is used to apply cell pressure with the other being used to apply back-pressure to the soil specimen. Volume change of the specimen is monitored using an LVDT connected to the piston of the back-pressure PVA. Cell and back-pressures are measured using 1.4 MPa (200 psi) pressure transducers built into the base of the cell. Figure 4.18 shows a test set up in a low stress triaxial cell (MIT03). This figure also shows details of the loading frame and the two PVAs in the background. A schematic of the cell can be seen in Figure 4.19.

4.3.3.2 Medium Stress Triaxial Cell

The medium stress triaxial cell is suitable for consolidation stresses ranging from 2 to 10 MPa. All specimens tested in this cell were consolidated to 10 MPa prior to undrained shearing. Although the internal and external components of the cell are similar to that of the low stress, there are a number of distinct differences due to the increased stress capacity. These include:

- A steel chamber eliminating the benefits associated with the transparent chamber of the low stress cell
- Axial load is applied by a PVA that is connected directly to an 89 kN (20,000 lb) hydraulic load frame. The load frame uses the fluid pressure generated by the PVA to apply axial load to the specimen in the cell. The same silicone oil used to apply cell

pressure is also used for the hydraulic load frame in order to minimize problems associated with corrosion.

- A larger piston of 2.54cm diameter is required to apply the increased axial forces
- Two latex membranes (0.3 mm thick) are used in lieu of condoms. Abdulhadi (2009) found that leakage occurs if condoms are used at cell pressures greater than 3 MPa
- A coiled top drainage line to accommodate axial shortening which occurs during the consolidation and shearing phase of the test
- The stress capacity of the cell is limited by the PVA controlling the cell pressure compared to the limited factor being the cell chamber material in the low stress

Figure 4.20 shows both a photo and schematic of the cell with the main items identified. In addition, this Figure presents the condition of a test specimen with membranes and top drainage line installed prior to placing the cell chamber.

4.3.3.3 High Stress Triaxial Cell

During this research, additional triaxial testing was ongoing at the MIT Geotechnical Laboratory. Casey (2014) developed triaxial equipment capable of consolidating specimens to stresses up to 100 MPa and conducted tests on several different soils over a wide range of consolidation stresses from 20 to 100 MPa. One sample of GOM EI was resedimented by the author to 8 MPa and then tested by Brendan Casey in the high stress triaxial cell where it was K_0 consolidated to 63.5 MPa and then sheared undrained. Results of this test are included in this research. A photo of this high stress triaxial equipment as well as a schematic of the cell is shown in Figure 4.21. The development of this equipment and description of its various components are discussed in detail by Casey (2014).

4.4 TESTING PROCEDURES

4.4.1 Introduction

This section describes the various test procedures employed throughout the research for conducting index, CRS and triaxial testing. Also covered in this section are common problems encountered and simple checks or measures put in place to eliminate such problems.

4.4.2 Index Testing

This section describes the test procedures used to characterize the soils used in this research. Characterization of each soil was determined by several people within the research group at MIT.

4.4.2.1 Atterberg Limits

The Atterberg Limits refer to two states or water contents in which a soil can exist. The Plastic Limit (w_p) is the water content at which a soil transitions from a solid state to a plastic state. The Liquid Limit (w_L) refers to the water content of a soil transitioning from a plastic state to a liquid state. The Plasticity Index is then the range of water contents in which a soil exists in a plastic state, i.e. the Liquid Limit less the Plastic Limit.

The Plastic Limit test was performed in accordance with ASTM D4318. The Liquid Limit test was performed in accordance with BS 1377 – 2 which describes the Fall Cone Method. The Liquid Limit of GOM EI, GOM A, and GOM B were determined using the non-standardized Casagrande Cup method.

4.4.2.2 Specific Gravity

Specific gravity (G_s) is the ratio of the density of a substance to the density of distilled water at 20° C. Tests were performed in accordance with ASTM – D854.

4.4.2.3 Grain Size Analysis

All soils used in this research consisted of clay and silt size particles. Because of the small grain size, the Hydrometer test was used as the method to determine the grain size distribution of each soil. Hydrometer tests were conducted in accordance with ASTM – D422 Particle Size Analysis of Soils.

4.4.2.4 Salinity Testing

Almost all natural soils have a certain mass of salt included as solute in the pore fluid. The processing of each new soil at the MIT Geotechnical Laboratory removes the natural water by drying, leaving the natural salts behind as a solid in the soil. It is necessary to quantify this salt, which is then reported in grams per kilogram of soil or if the in situ water content of the soil is known, the soils salinity can be reported in units of grams per liter of pore fluid. The necessity of such a test can be explained by the following example. When a soil is resedimented its salinity is usually set to a particular value. The presence of salt in the natural powder must be accounted for when determining the quantity of salt to be added to the resedimented soil in order to obtain the target salinity. To ignore the natural salts leads to an underestimation of the actual pore fluid salinity.

There is no standard test method for measuring the salinity of a soil. The procedure used in the MIT Geotechnical Laboratory was adapted from Germaine and Germaine (2009) and is described in detail by Adams (2014).

4.4.3 Constant Rate of Strain (CRS) Testing

4.4.3.1 Introduction

The history and development of the CRS testing method is described in Gonzalez (2000). All CRS testing conducted during this research was in accordance with ASTM D4186 – 12. The CRS cell used was a modified Trautwein CRS apparatus. These modifications have been described in Section 4.3.2.1. The use of the small diameter CRS ring facilitated the efficient use of some Gulf of Mexico soils in the test program that were of limited availability.

4.4.3.2 Procedure

Although six different high plasticity soils were tested in the CRS device during this research, the test procedure is identical for all soils. The following is a description of the stages involved in conducting a CRS test using the equipment described in Section 4.3.2. Step-by-step

instructions on how to complete a test from apparatus preparation to disassembly is described in Appendix A. Extracts from the following procedure are obtained from Horan (2012).

APPARATUS PREPARATION

Commence by placing the CRS cell on a mobile trolley adjacent to the front of the load frame. The water in the pore pressure PVA is changed to match the pore fluid salinity of the test specimen. The line connecting the PVA to the cell chamber and base is then flushed with this water. Place the porous stones in the appropriate salinity water and put in ultrasound bath for 10 minutes. Clean the trimming ring and apply a thin film of silicon grease to the inside. Next, obtain the mass of two oven tares, the cleaned recess tool, and rigid ring with one filter screen.

SPECIMEN TRIMMING

At this stage the resedimented sample has been consolidated to a stress of 0.1 MPa and then unloaded to an OCR of 4. Extrude enough of soil for the test specimen from the consolidometer and square the ends using a squaring block.

Place the soil to be trimmed below the cutting ring concentrically ensuring an even amount of soil to be trimmed from the perimeter of the ring. This is shown in Figure 4.22. Carefully trim the specimen into the cutting ring using the trimming tool. The trimming process is shown in Figure 4.23. Continue trimming soil into the cutting ring until it contains enough soil to satisfy the requirements of the test (1.26 cm high in this study). Once this has been accomplished, remove the cutting ring from the trimming device. Trim the soil at the end of the ring initially using a wire saw, and then with a straight edge to remove any soil left behind due to the deflection of the wire. Apply a filter screen to the surface of the soil. The recess tool is then placed on top of the filter screen and pushed until the flanges of the recess tool make contact with the beveled edge of the trimming ring. At this point the required height of soil is in the trimming ring. The soil protruding from the opposite side of the ring must now also be trimmed to form a smooth surface in a similar fashion to the method already described. The before and after of this trimming is shown in Figure 4.23.

The mass of all ring, screen, soil, and recess tool is now recorded. The mass of the soil can then be found by subtracting the masses of the other components.

CELL ASSEMBLY

Allow water to flow from the PVA reservoir to the CRS base so that the base porous stone is saturated and surface dry. Apply a filter screen and porous stone to the underside of the trimming ring and then place the ring carefully on the CRS base. Next fit the square ring seal around the ring and ensure it is seated correctly. Remove the recess tool and add the top porous stone. Figure 4.7 shows the CRS ring and seal in position. Assemble the cell ensuring that the piston is fully retracted and locked in place. Once the cell is assembled, lower the piston so that it rests on the soil, apply a very small pressure to the piston to ensure the soil is seated on the base porous disc but be careful not to overstress the specimen. The piston is then locked in place and the cell placed into the load frame. Affix the bracket which holds both LVDT's to the load button and ensure the LVDT's will be in an acceptable voltage range for the duration of the test. Set the load frame to the correct strain rate for the soil being tested and then raise the cell so that the piston makes contact with the load cell. Before testing, allow all transducers at least 15 minutes to "warm up" before recording their zero values.

The cell can now be filled via a gravity feed from the PVA reservoir. The valve on the cell pressure line which accesses the base pressure is left open for the filling sequence so as to ensure saturation of all test lines. Once the water fills the pore pressure transducer housing, the transducer can be attached. The cell is filled once water starts coming out the vent port shown in Figure 4.6.

SPECIMEN SATURATION

Back pressure-saturate the specimen incrementally up to a pressure of 400 kPa. Depending on the plasticity and hydraulic conductivity of the soil, the time required between these increases in back pressure will change. Generally as the plasticity increases, so does the time between backpressure increments. Throughout this research, pressure increments of 50 kPa were applied at 20 minute intervals. It is important that the specimen be back pressure saturated from both the cell and the base at the same time.

CONSOLIDATION

Once the specimen is back pressure saturated, the specimen is almost ready to be tested. Three essential checks are required prior to activating the load frame and beginning the consolidation phase of the test. These checks are specific to TR4 and the Wykeham Farrance frame. They are:

1. The piston clamp must be released allowing the piston to move freely under axial load
2. The clutch on the frame must be engaged, otherwise the frames gears will be rotating but no axial strain is applied to the specimen, and
3. The ball valve on the line that connects the PVA to both the cell chamber and cell base must be closed. In the closed position, fluid from the computer controlled PVA can only enter the cell hence controlling only the cell pressure. Whereas, the open position allows fluid to flow to both the cell and the base, allowing the PVA to maintain both the cell pressure and base pore pressure at a similar and constant value. No permeability or c_v data would be obtained from a test conducted with the valve in the open position.

Once these steps are complete, loading of the specimen can commence at the selected strain rate. Once the maximum stress was realized, the load frame used was unable to perform secondary compression so the test was concluded by turning off the load frame and allowing the excess pore pressure to dissipate.

DISASSEMBLY AND DATA ANALYSIS

Once the test is completed, the cell pressure is reduced by opening the valve at the top of the PVA reservoir. Remove the CRS cell and extrude the soil from the confinement ring collecting any and all extruded soil that may be on the inside of the trimming ring or edge of the porous stones, or both. Place the extruded soil into an oven tare in order to obtain the dry mass. With the main test specimen, obtain the final wet mass and then place in an oven at 105° C for a period of 24 hours.

The raw test data are analyzed using a QBASIC computer program. The program converts the transducer voltages recorded by the central data acquisition system into engineering values of axial load and displacement, and cell and pore pressures, which are in turn used to

compute effective consolidation stresses, strains, permeability's and coefficients of consolidation.

4.4.3.3 Issues during testing

The CRS testing program involved testing soils with a wide range of pore fluid salinity – from 0 g/L up to 256 g/L. For each test, the CRS cell is filled with a fluid that matches the pore fluid salinity of the test specimen. When dealing with high salinities it is an essential requirement for successful testing as well as the longevity of the cell that the individual components be thoroughly cleaned every 2 to 3 tests. In order to do so, the cell must be disassembled into its various components, as shown in Figure 4.7, each component washed, and then reassembled. Particular attention must be given to the condition of the piston and its associated seal. As stated previously, the function of this seal is to isolate the cell pressure from atmospheric pressure. The seal is designed so that as the pressure in the cell increases, the pressure forces the seals U-shaped cross section to expand against the chamber wall and piston. Therefore the seal is at its weakest when under the least amount of cell pressure. This weak point occurs during the initial filling of the cell under by gravity feed from a reservoir placed approximately 1m above the cell. Water may flow from the cell, past the seal, through the 3mm diameter hole in the column, shown in Figure 4.8, if the piston is not completely free from solidified grains of salt or a build-up of rust caused from previous testing. If a leak is evident at this point, the apparatus must be disassembled, piston inspected and cleaned, and cell refilled without causing any adverse impact to the test specimen. However, throughout this research, with tests being conducted over a period of a week to 10 days, a very slow leak that is not evident during the initial filling of the cell, will materialize as a build-up of solidified salt on the outside of the cell. A similar build-up forms within the piston column. An example of this salt accumulation on the cell at the end of a test is shown in Figure 4.9.

Although this issue did not impact the operation of the test nor the results obtained, it serves to highlight that regardless of whether a leak is evident or not, it is essential that the piston be examined and cleaned thoroughly prior to each test. Left unchecked, salt will cause rust to

form on the piston creating additional friction that may impact the accuracy of the data obtained at low stress at the beginning of each test.

4.4.4 Triaxial Testing

4.4.4.1 Introduction

A series of K_0 consolidated undrained triaxial compression (CK_0UC) tests were conducted on GOM EI and Leached GOM EI as part of this research. Although testing was carried out using two different triaxial cells, the procedure is similar.

4.4.4.2 Procedure

The complete test procedure has been developed by Dr. John Germaine for the Graduate Laboratory course at MIT (course number 1.37) and it is this procedure that has been applied by the author during this research. Step-by-step instructions on how to complete a test from apparatus preparation to post-shearing disassembly in a low stress cell is described in Appendix B. The following is a description of the main stages involved in a triaxial test.

APPARATUS PREPARATION

The water in the pore pressure PVA is changed to match the pore fluid salinity of the test specimen. Top and bottom drainage lines are then flushed with this fluid and the pore pressure transducer is fitted. Both drainage valves are put in the closed position. The top cap and bottom pedestal are then cleaned and a film of vacuum grease applied to the cylindrical sides of each. Narrow membrane strips, approximately 1 cm wide, are placed over the pedestals. These pieces of membrane serve to prevent the rough porous stones from puncturing the membranes. 4 O-rings are coated in a film of vacuum grease and placed on each of two O-ring stretchers (8 O-rings in total). The first membrane is fitted on the base pedestal and sealed to the pedestal with two O-rings. The second membrane is then fitted over the first and also sealed to the pedestal with an additional two O-rings. Details of the O-ring positions are shown in Figure 4.17. The bottom porous stone and filter paper is then placed on the base pedestal.

SPECIMEN INSTALLATION

At this stage the sample is extruded from the consolidometer, trimmed, and prepared for placement in the triaxial cell. Once prepared, the test specimen is placed onto the bottom porous stone. The top porous stone is placed and then the top cap is lowered on the specimen. The first (inner) membrane is then rolled up the specimen and is sealed with two O-rings to the top cap. The process is repeated for the outer membrane. The internal load cell is connected and the cell chamber is placed over the specimen. The top plate of the cell and axial LVDT are then fitted and the chamber is filled with silicone oil. The cell oil is then pressurized to one quarter of the maximum stress applied to the specimen during resedimentation.

SPECIMEN SATURATION

The specimen is allowed to equilibrate overnight and the following day the sampling effective stress is recorded. In the event that the pore pressure is negative, the cell pressure should be increased, thereby increasing the effective stress, so that positive pore pressure is generated. The specimen is then back-pressure saturated while holding the sampling effective stress constant. A value of 0.3MPa is a typical value for the back pressure at the end of saturation. At the end of back-pressure saturation a B-value check is performed using a cell pressure increment of 50 kPa. A B-value greater than at least 0.95 is generally taken to indicate saturation of the drainage system. Occasionally, lower B-values may warrant an increased back-pressure.

CONSOLIDATION

K_0 consolidation is carried out to stresses at least twice that of the batch preconsolidation stress, resulting in consolidation strains $> 10\%$. The automated triaxial testing system ensures zero radial strain of the specimen occurs during this phase by continuously adjusting cell pressure to keep volume and axial strains equal. At the end of virgin consolidation, specimens are allowed at least 24 hours of [drained] secondary compression before being sheared undrained in compression mode of shear. A constant axial strain rate of 0.15 %/hr is used during virgin consolidation. This rate is sufficiently slow to prevent non-negligible excess pore pressures from developing in the specimen.

UNDRAINED SHEARING

Before undrained shearing, a leak check is performed by closing the drainage valves and monitoring the pore pressure for 30 minutes. During this 30 minute period the pore pressure should not change by more than plus or minus 0.005 MPa. Provided no internal or external leak is detected, the specimen is sheared undrained in compression using an axial strain rate of 0.5 %/hr. Shearing is carried out to axial strains $> 12\%$ (in addition to strains developed during consolidation), by which point a steady critical state friction angle had been reached.

DATA ANALYSIS

The raw test data are analyzed using revision 6 of a QBASIC computer program. The program converts the transducer voltages recorded by the central data acquisition system into engineering values of axial load and displacement, cell and pore pressures, and volume change, which are in turn used to compute effective stresses and strains.

4.4.4.3 Issues during testing

During a triaxial test, water flows both into the soil (during saturation) and out of the soil (during consolidation). Although the quantities of water that enter the specimen from the pore pressure PVA during the saturation phase is minimal, it is prudent to match the salinity of the water in the pore pressure PVA with that of the soil being tested. Previous studies by Pineda et al. (2013), outlined in Chapter 2, found that the shear strength of a soil with a pore fluid salinity of 25 g/L, tested in a DSS device, increased when the salinity of the water surrounding the specimen was greater (35 g/L) than that of the soil. Soils with salinities of 10g/L and 256 g/L were tested as part of this research, making the flushing out of the PVA with distilled water and filling with the correct salinity an essential task. For similar reasons, the porous stones should be placed in a jar of water with the same salinity as that of the test soil and then placed in an ultrasound bath for at least ten minutes.

Conducting triaxial testing on high salinity soils requires the highest standards of equipment cleanliness. Once a test is complete and the apparatus disassembled, all drainage lines

must be flushed with distilled water. The successful completion of a test can depend on many factors. While testing high salinity soils in the medium stress triaxial device, a test result indicated that a leak was present along the drainage lines external to the cell. The leak was not large enough to be identified as droplets of water on the drainage lines. Upon investigation it was determined that a grain of salt had solidified in the pore pressure transducer housing between tests. This grain then created a tiny gap between the O-ring and the housing resulting in water in the drainage lines to leak past the O-ring seal on the transducer. This leak resulted in the specimen being sheared partially undrained and therefore the shear strength data obtained was of no use. It is recommended by the author, that additional time be spent when preparing the cell for testing, on cleaning and inspection of the drainage lines. When compared to the several weeks or months required to prepare a soil for testing, 30 minutes allocated to cleaning the equipment meticulously is highly recommended and a small price to pay for a successful test.

Device	Data Acquisition Channel	Measurement	Device	Calibration Factor (per v/v)	Range	Resolution	Stability
TR4	126	Axial Deformation	External LVDT	- 2.535 cm	2.50 cm	±0.000248 % (0.1 mV)	±0.00248 % (1 mV)
	127	Cell Pressure	Pressure Transducer	- 69.5 MPa	1.4 MPa	0.004 kPa (0.001 mV)	0.004 kPa (0.01 mV)
	128	Axial Force	External Load Cell	14803.2 kN	44.48 kN	0.77 N (0.001 mV)	7.7 N (0.01 mV)
	130	Pore Pressure	Pressure Transducer	- 68.64 MPa	1.4 MPa	0.005 kPa (0.001 mV)	0.005 kPa (0.01 mV)
	131	Axial Deformation	External LVDT	- 2.57181 cm	2.50 cm	±0.000379 % (0.1 mV)	±0.00379 % (1 mV)
	132	Input Voltage	-	-	-	-	-

Table 4-1 Characteristics of instruments used in CRS TR4 apparatus. Note: Resolution and stability based on central data acquisition system, calculations based on specific dimensions

Device	Data Acquisition Channel	Measurement	Device	Calibration Factor (per v/v)	Range	Resolution	Stability
MIT03	102	Axial Deformation	External LVDT	1.9947 cm	2.50 cm		
	103	Cell Pressure	Pressure Transducer	68.67 MPa	1.4 MPa		
	104	Axial Force	Internal Load Cell	25.48 kN	2.22 kN		
	105	Pore Pressure	Pressure Transducer	68.72 MPa	1.4 MPa		
	106	Specimen Volume	Volume Strain LVDT	22.487 cm ³	45 cm ³		
	107	Input Voltage	-	-	-	-	-

Table 4-2 Characteristics of instruments used in triaxial MIT03 apparatus. Note: Resolution and stability based on central data acquisition system, calculations based on specific dimensions

Device	Data Acquisition Channel	Measurement	Device	Calibration Factor (per v/v)	Range	Resolution	Stability
MIT04	108	Axial Deformation	External LVDT	2.08 cm	2.50 cm		
	109	Cell Pressure	Pressure Transducer	69.1 MPa	1.4 MPa		
	110	Axial Force	Internal Load Cell	64.49 kN	2.22 kN		
	111	Pore Pressure	Pressure Transducer	68.68 MPa	1.4 MPa		
	112	Specimen Volume	Volume Strain LVDT	22.60 cm ³	45 cm ³		
	113	Input Voltage	-	-	-	-	-

Table 4-3 Characteristics of instruments used in triaxial MIT04 apparatus. Note: Resolution and stability based on central data acquisition system, calculations based on specific dimensions

Device	Data Acquisition Channel	Measurement	Device	Calibration Factor (per v/v)	Range	Resolution	Stability
MIT13	140	Axial Deformation	External LVDT	3.295 cm	3 cm	±0.00075% (0.1 mV)	±0.0075% (1 mV)
	141	Cell Pressure	Pressure Transducer	345.4 MPa	6.9 MPa	0.00628 kPa (0.001 mV)	0.0628 kPa (0.01 mV)
	142	Axial Force	Internal Load Cell	291.89 kN	8.9 kN	0.053 N (0.001 mV)	0.53 N (0.01 mV)
	143	Pore Pressure	Pressure Transducer	347.0 MPa	6.9 MPa	0.00631 kPa (0.001 mV)	0.0631 kPa (0.01 mV)
	144	Specimen Volume	Volume Strain LVDT	22.078 cm ³	45 cm ³	±0.00050% (0.1 mV)	±0.0050% (1 mV)
	145	Input Voltage	-	-	-	-	-

Table 4-4 Characteristics of instruments used in triaxial MIT13 apparatus. Note: Resolution and stability based on central data acquisition system, calculations based on specific dimensions



Figure 4.1 Electronic Transducers used during the testing program. Top Left: Trans-Tek LVDT's, Top Right: 0 – 200 psi capacity Pressure Transducer, Middle: 500 lb Load Cell, Bottom: Close-up of pressure transducer and section through one showing internal components (Horan, 2012)



Figure 4.2 Pressure Volume Actuators (PVA's) used to control cell (left) and pore (right) pressures during triaxial testing in addition to cell pressure during CRS testing.

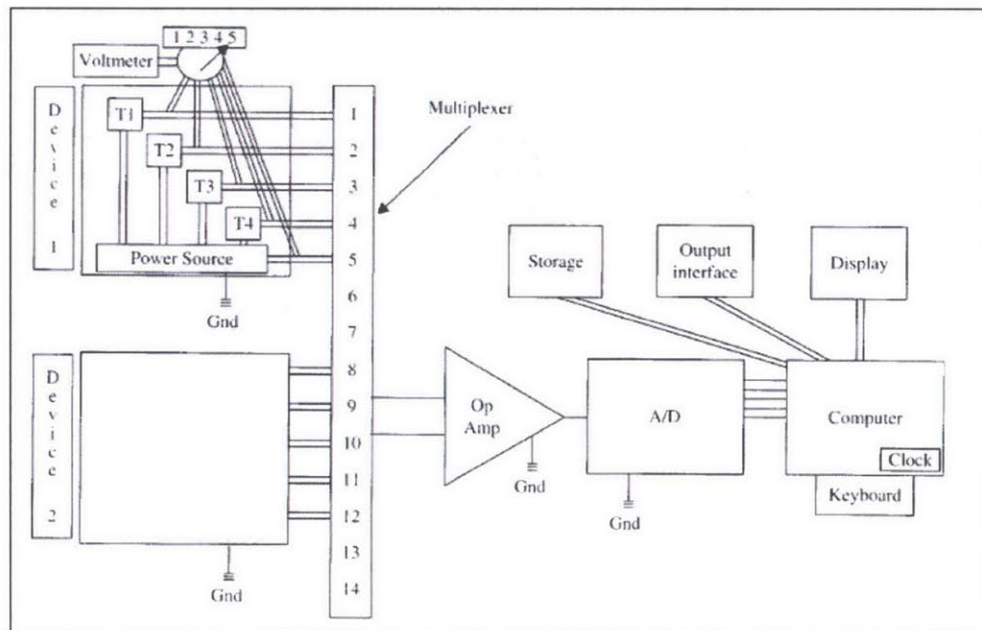


Figure 4.3 Schematic diagram of a central data acquisition system (Germaine & Germaine, 2009)

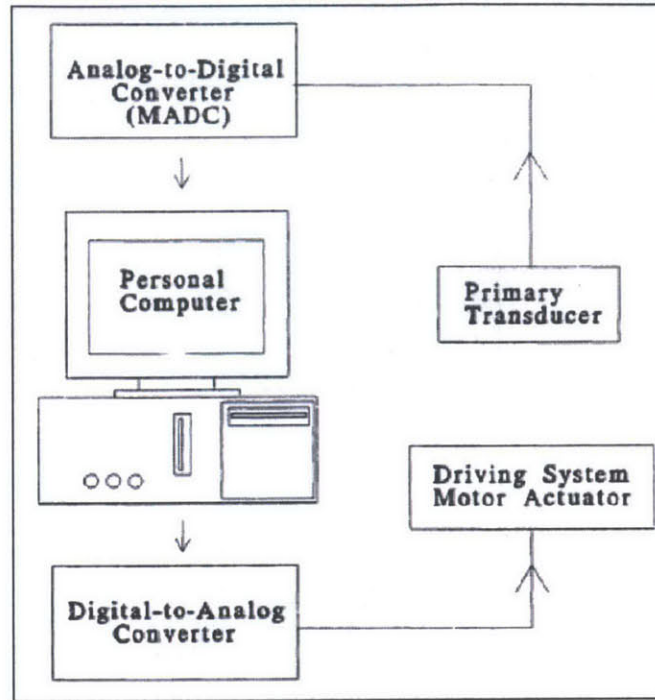


Figure 4.4 Schematic diagram of the control system hardware components



Figure 4.5 CRS trimming rings, Left: Standard Trimming Ring, Right: Trimming ring used in this research (Horan, 2012)

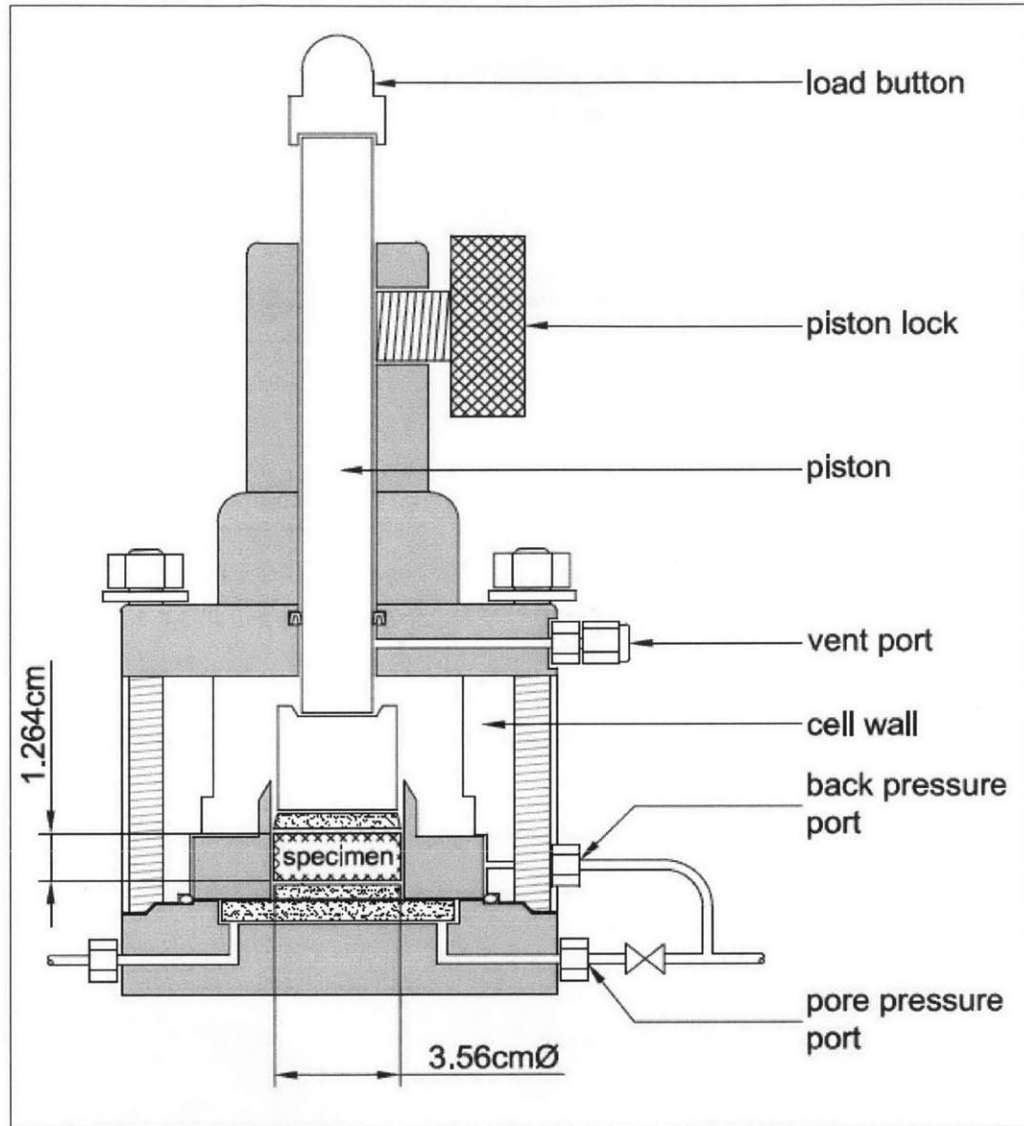


Figure 4.6 Schematic diagram of Trautwein CRS cell (TR4) (Horan, 2012)

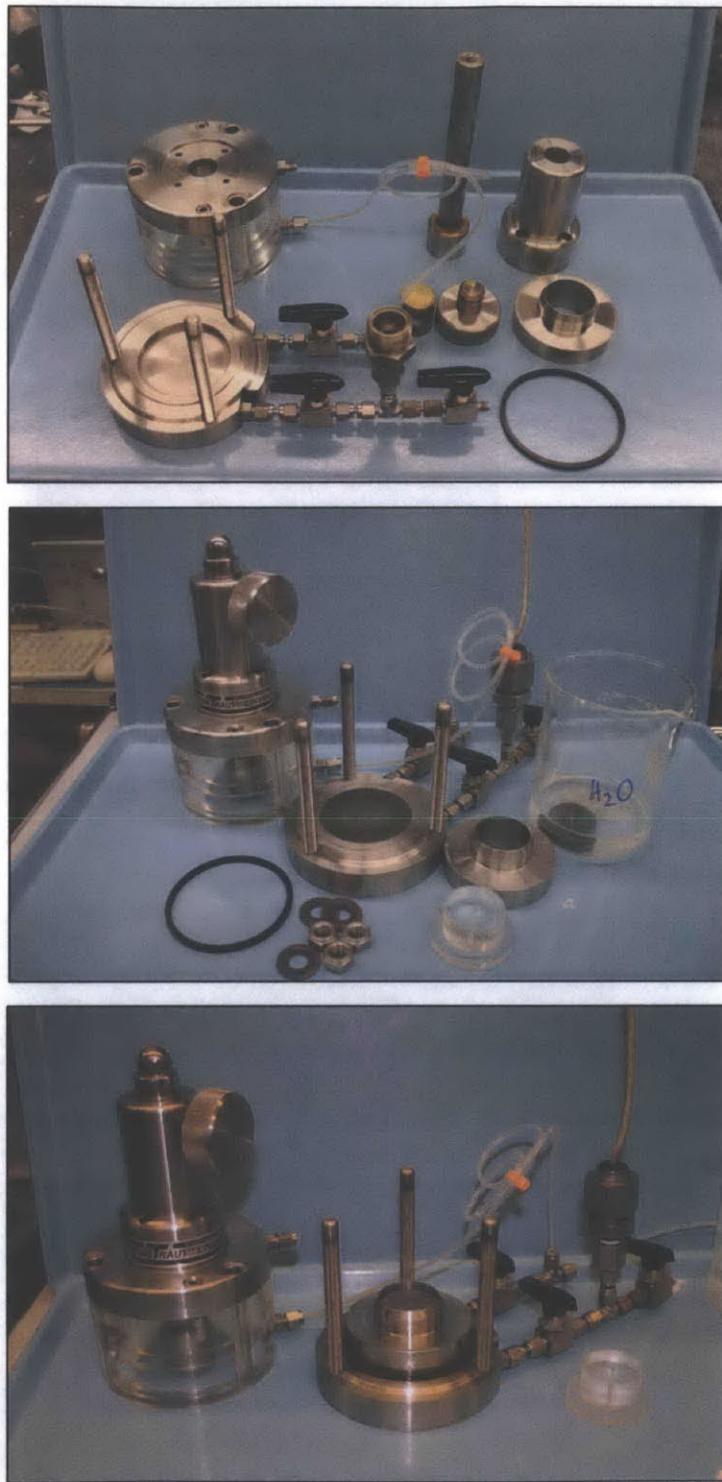


Figure 4.7 Components of CRS device and stages of set-up, Top: Device disassembled to individual components for cleaning, Middle: Device and porous stones prepared for testing, Bottom: Trimming ring with prepared specimen in test position with square ring seal



Figure 4.8 Trautwein CRS cell showing overflow hole which allows any water passing the piston seal to exit the device prior to contacting the roller bearings positioned higher in the piston column

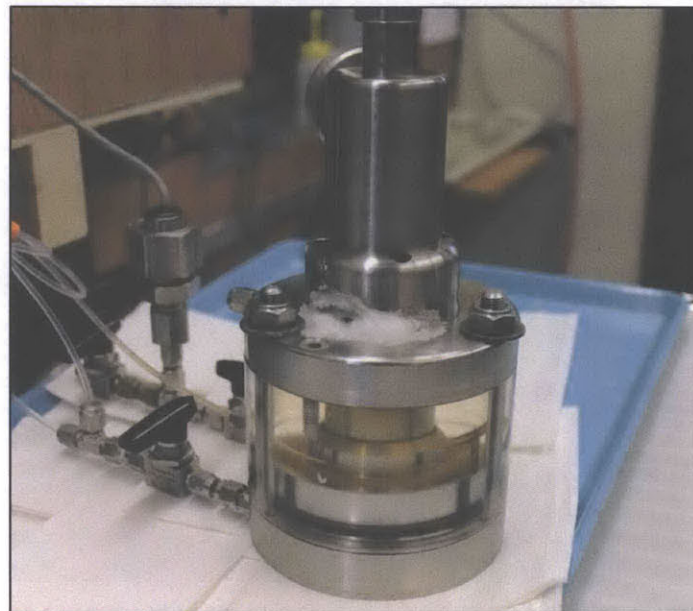


Figure 4.9 A very slow leak at the piston seal throughout a test results in a build-up of salts on the outside of the overflow hole

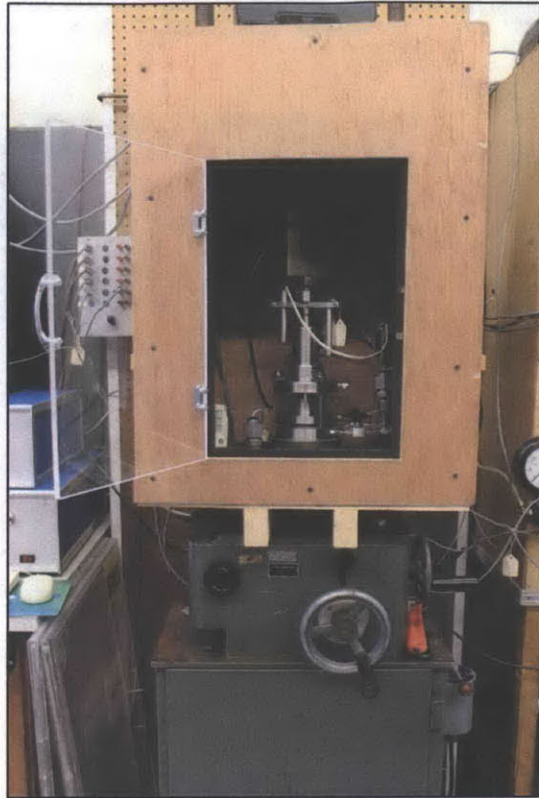


Figure 4.10 CRS set-up showing insulated timber temperature enclosure and Wykeham Farrance load frame



Figure 4.11 CRS Cell TR4 under test conditions. Temperature is maintained at a constant 25.3° C within the enclosure

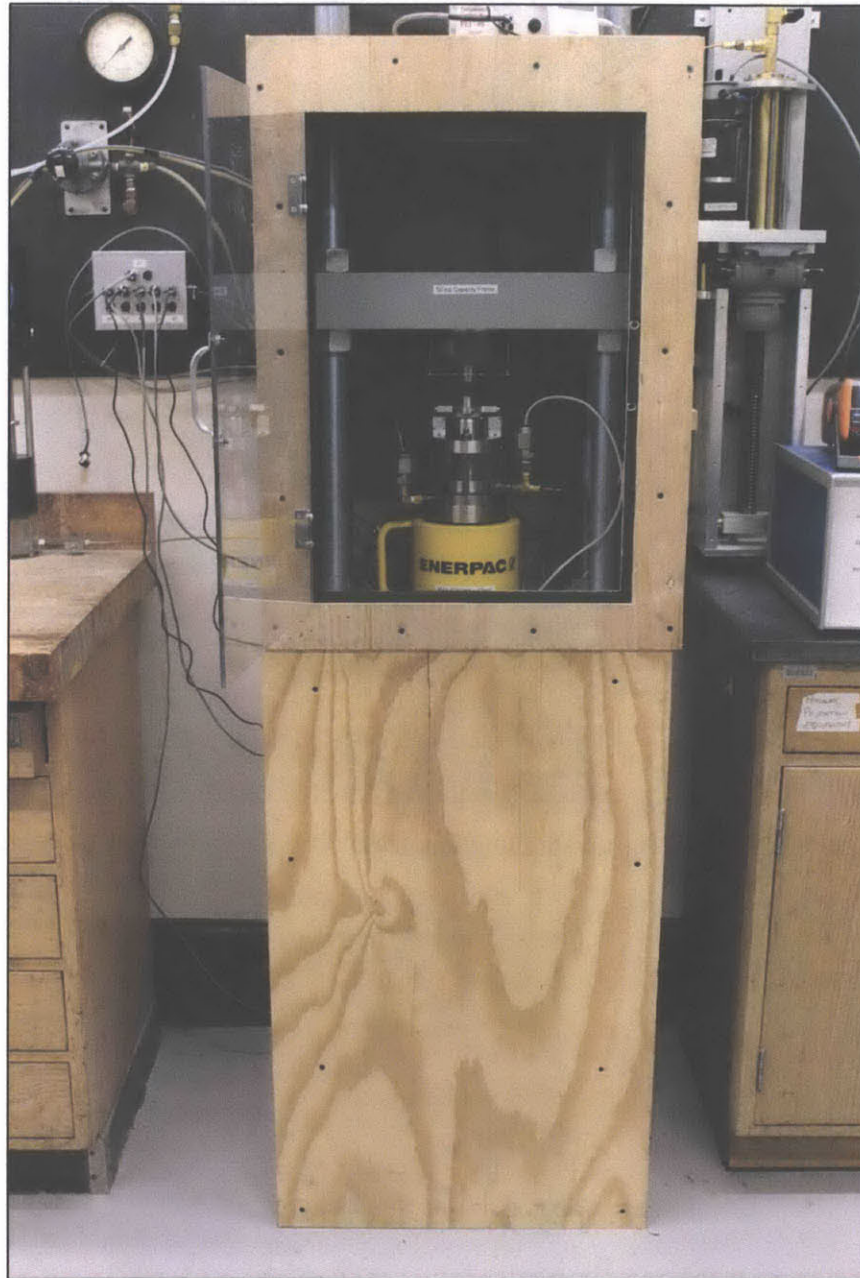


Figure 4.12 CRS equipment developed for testing to 100 MPa (axial effective stress) complete with 50 kip capacity load frame, 887 kN capacity hydraulic cylinder, modified CRS cell and temperature enclosure

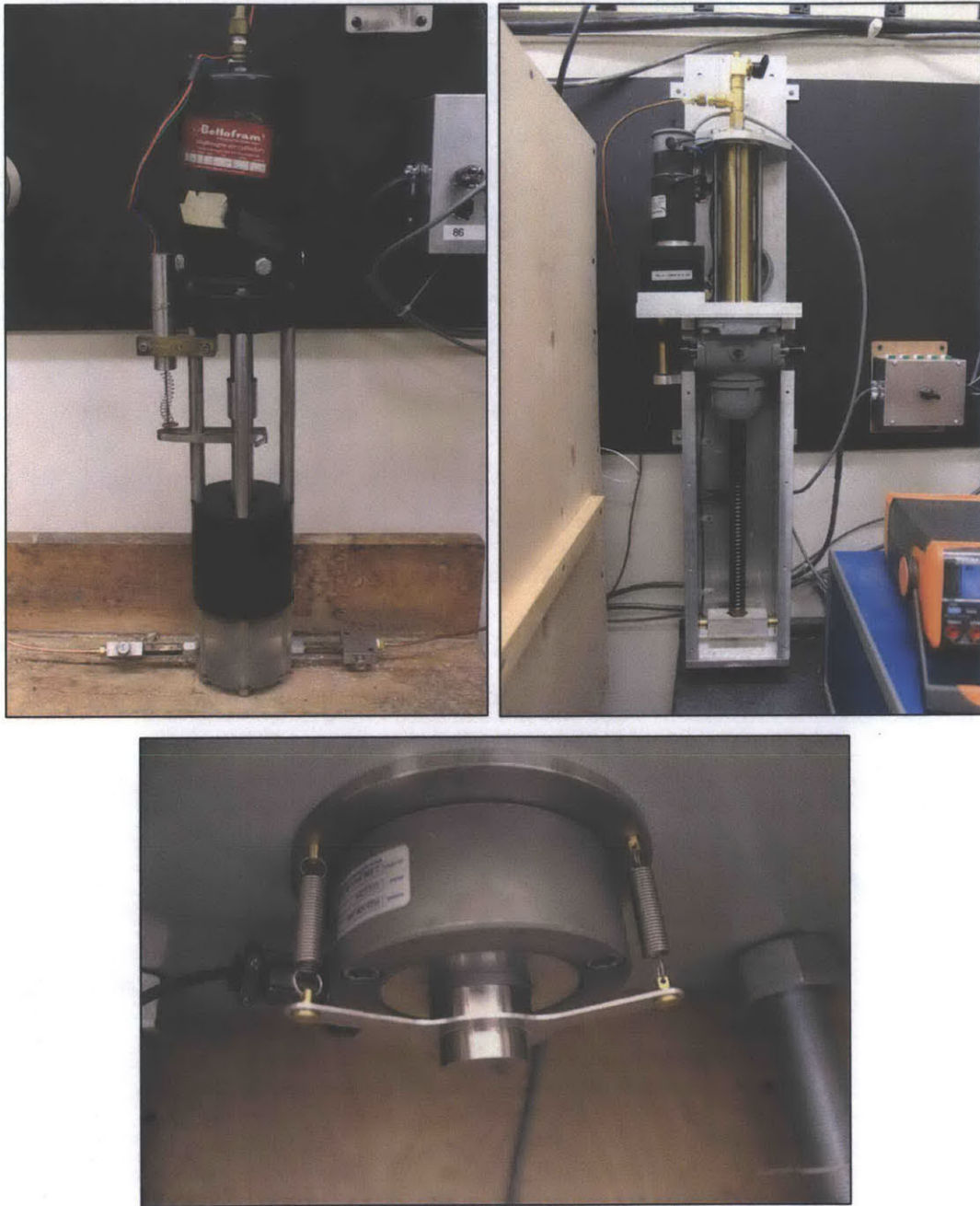


Figure 4.13 Ancillary equipment for CRS testing to 100 MPa, Top Left: Air regulated PVA used for controlling cell pressure, Top Right: Electric motor driven PVA used to control the axial load hydraulic cylinder, Bottom: Sentran PG3 50,000 lb capacity low profile load cell

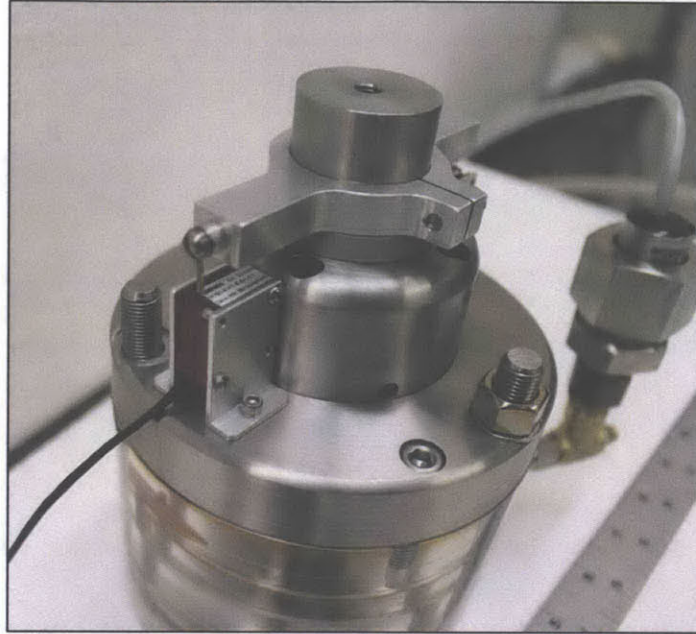


Figure 4.14 M150 Ultra-Miniature String Pot connected to CRS cell and piston for measuring axial displacement of specimen

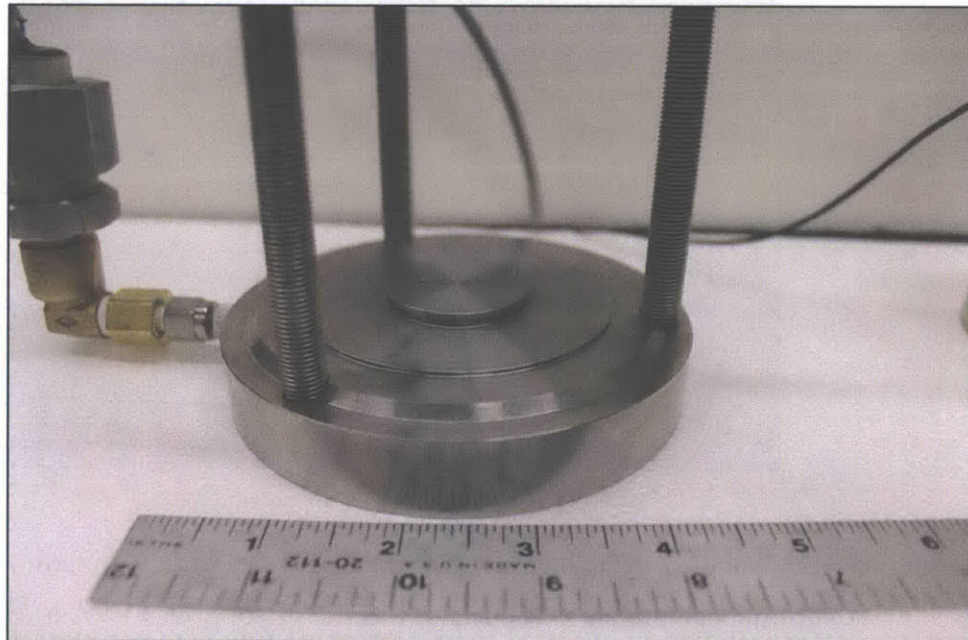
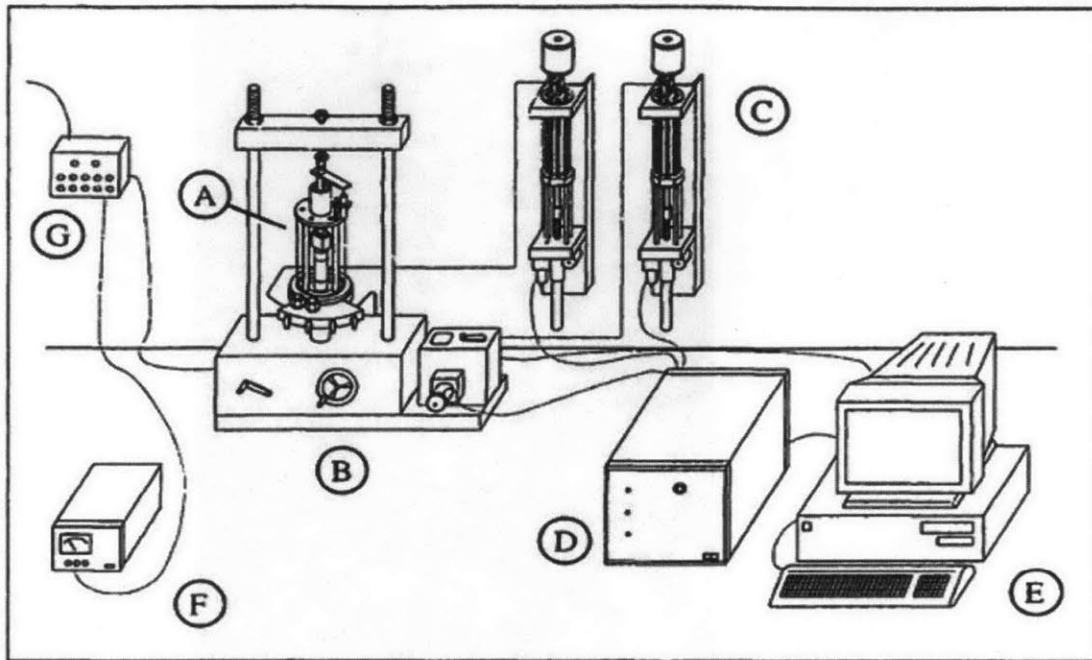


Figure 4.15 Modified CRS base for 100 MPa CRS Cell. Elevated base with recess to accommodate pore pressure O-ring seal



- | | |
|---------------------------------|-------------------------------|
| A - Triaxial Cell | E - Personal Computer |
| B - Load Frame | F - DC Power Supply |
| C - Pressure/Volume Controllers | G - Data Acquisition Channels |
| D - Motor Control Box | |

Figure 4.16 Schematic of the standard automated triaxial testing system used in the MIT Geotechnical Engineering Laboratory (Santagata, 1998)

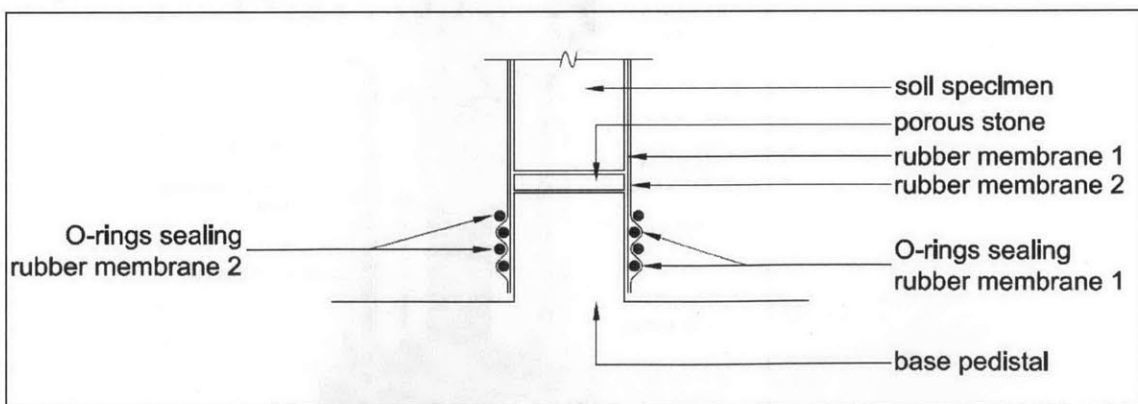


Figure 4.17 Low stress triaxial base pedestal and top cap O-ring sealing arrangement with 2 rubber membranes. O-ring spacing exaggerated for clarity (Horan, 2012)

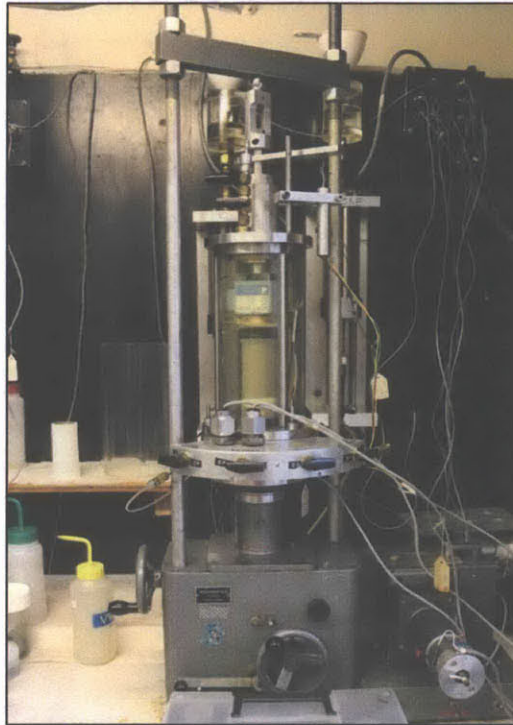


Figure 4.18 Low Stress Triaxial Set-up - MIT03 triaxial cell mounted on a 9.8 kN Wykeham Farrance screw driven load frame with electric motor controlled gears

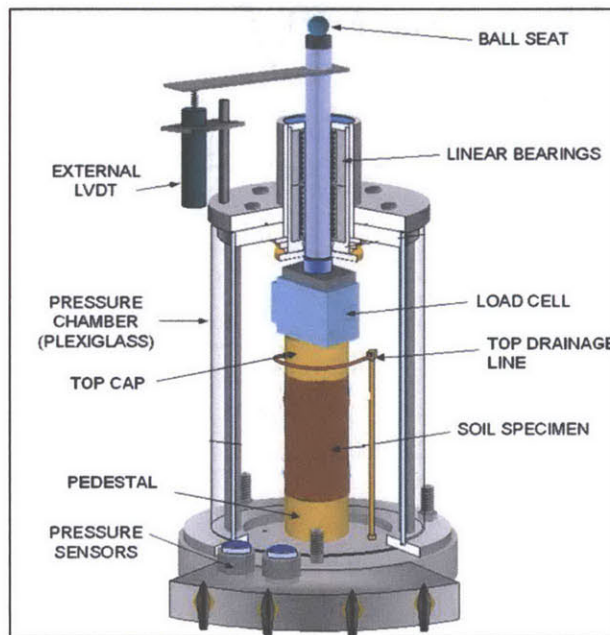


Figure 4.19 Schematic of low stress triaxial cell (Santagata, 1998)

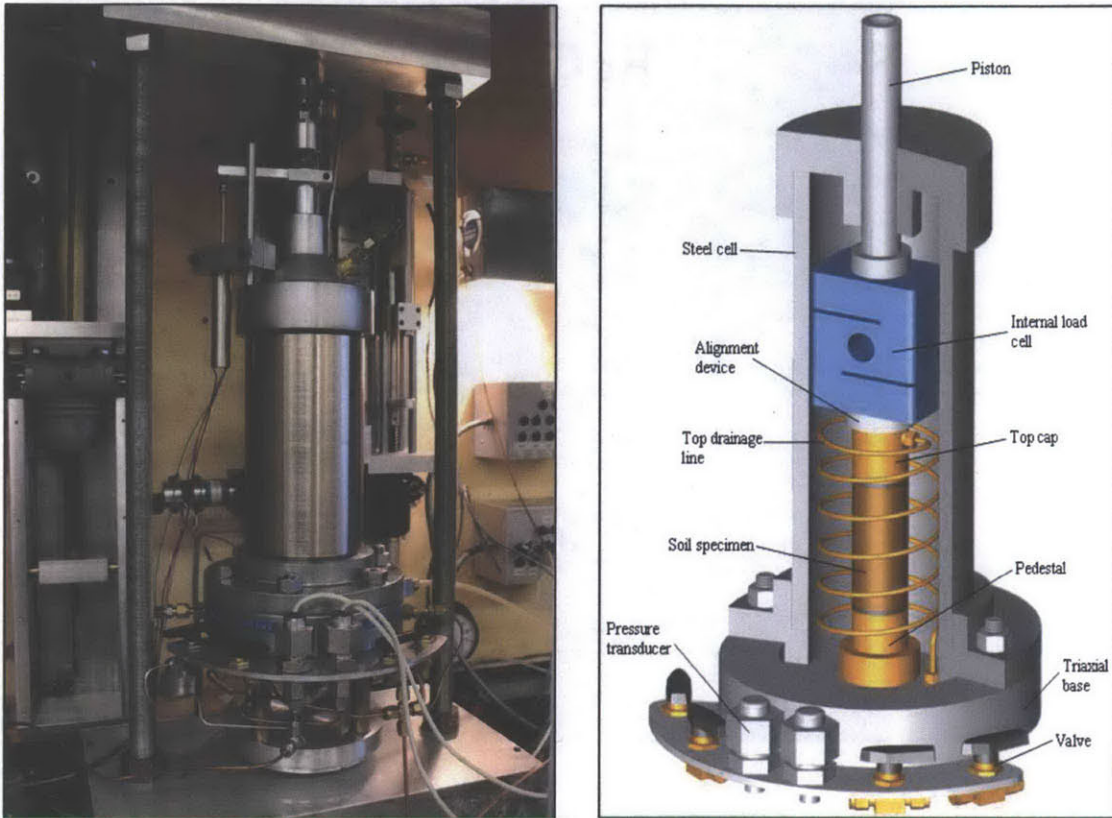


Figure 4.20 Medium Stress Triaxial Device, Top Left: MIT13 triaxial cell, Top Right: Schematic of medium stress triaxial device (from Casey, 2014), Bottom: Test specimen mounted on base pedestal complete with double membrane, O-rings, and coiled copper top drainage line

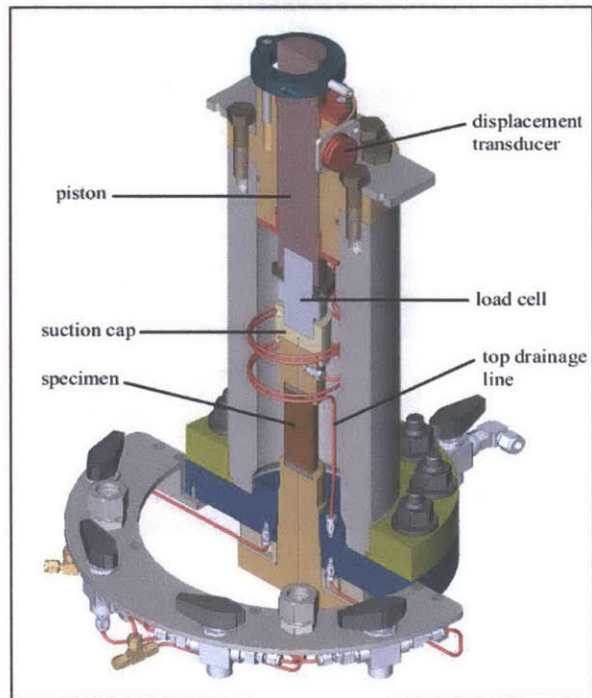


Figure 4.21 High stress triaxial device, Top: MIT 09 high stress cell, Bottom: Schematic of high stress triaxial cell (Casey, 2014)



Figure 4.22 Trimming device with CRS trimming ring placed upside down concentrically on resedimented sample ensuring equal amount of soil for trimming around perimeter



Figure 4.23 Trimming GOM EI sample into small diameter CRS ring, Top: Removing excess along the ring taper, Bottom Left: Positioning soil with plastic recess tool, Bottom Right: Final trimming with razor blade to ensure a level surface

5 CRS TEST RESULTS

5.1 INTRODUCTION

This chapter presents the mechanical behavior obtained from one dimensional consolidation constant rate of strain (CRS) tests on six different high plasticity smectitic soils.

Prior to conducting the extensive CRS testing program on GOM EI and Leached GOM EI, the author conducted a simple sedimentation test to assess what impact, if any, changes in salinity has on the soil at ultra-low stress. A discussion of the findings is presented in Section 5.2.

The CRS results for the various soils are presented and discussed in Section 5.3. One dimensional consolidation data as well as the permeability in the vertical direction are presented here. All resedimented soils tested were initially consolidated to a stress of 0.1 MPa, rebounded to an $OCR = 4$, and then CRS tested to 40 MPa. All CRS tests were run on soil specimens that are smaller than the standard ring. This was discussed earlier in Chapter 4. Comparisons of the mechanical behavior of all the soils tested are also presented in this section. A list of all tests performed is shown in Table 5-1 and Table 5-2.

In order to understand and explain the observed mechanical behavior determined from the CRS testing, scanning electron microscope (SEM) images of GOM EI and Leached GOM EI cryogenically frozen in a concentrated slurry form were taken by Amer Deirieh, a Ph.D. student at the Department of Civil Engineering at MIT. The observations, based on a qualitative analysis of the images, are described in Section 5.4

Section 5.5 presents proposed correlations between the observed compressibility and permeability sensitivity with changes in pore fluid salinity to the soils liquid limit. Data from the six soils tested as well as data from similar testing conducted on RBBC by Horan (2012) are included in the correlations for soils ranging in liquid limit from 46 % to 90 %.

5.2 ULTRA-LOW STRESS BEHAVIOR

In order to show the effect salt has on soil particles at ultra-low stress a simple sedimentation test was performed on GOM EI and Leached GOM EI whereby a specific quantity of soil was placed in a test tube with pore fluids of different salinities. The pore fluid salinities ranged from 1 g/L to 256 g/L, with a constant mass of 5g of soil placed in each tube. The purpose of this test is to determine how the soil behaves in different electrolyte concentrations and to give an indication as to where the greatest effects lay in terms of behavioral changes. Agitation of the soil in the tubes was carried out by placing the tubes in an ultrasonic bath. Horan (2012) found this to be the best method among several trialed.

Horan (2012) conducted the same test on RBBC Series IV and Leached RBBC Series IV, the results of which are shown in Figure 5.1 and Figure 5.2. The test shows that for a wide range of pore fluid salinities, natural BBC Series IV displays little if any visible change in behavior with the soil sedimenting to almost the same height for all salinities. The leached soil forms a sedimentation height roughly twice that which was observed for the natural BBC Series IV soil at any concentration. This increased height is due to disaggregation of the dense residual flocs by leaching. The test on the leached soil shows an additional tube containing 0 g/l (distilled water). An interesting observation is that a portion of the fine fraction in the distilled water tube has not settled out and continues to remain in suspension occupying all the free water space in the tube. The leaching process deflocculated the soil and without any electrolytes available to reduce the double layer and attract these very small particles to each other, the particles cannot form large enough flocs to settle in the tube. With the addition of just 1 g of salt (per liter) to the pore fluid, these particles form floccs and settle out. These two images show that at ultra-low stress, a low plasticity illitic marine soil is insensitive to changes in salinity with the only sensitivity to salts observed in the leached soil up to a salinity of just 1g/L. Note that in the case of the natural BBC, the sedimentation tube labelled 1 g/L is at a higher pore fluid salinity due to the presence of natural salts in the soil, which are approximately 2.65g of salt per kg of soil. The mechanical behavior of RBBC Series IV determined by Horan from CRS testing confirmed and agreed with the observations in the sedimentation test that the one dimensional consolidation and permeability behavior is independent of pore fluid salinity.

The results for the test on GOM EI and Leached GOM EI are presented in Figure 5.3 and Figure 5.4. GOM EI shows a clear reduction in sedimentation height with increasing salinity. The greatest change in sediment height occurs between 1 g/L and 64 g/L salinity. Increasing electrolyte concentration reduces the double layer around each particle resulting in an overall attraction between particles. The clay particles come together to form flocs with the number of particles forming each floc increasing with salinity. It is this interaction that creates a denser floc structure, reducing the sedimentation height, and thereby reducing the void ratio for the same mass of soil. Increasing the pore fluid salinity from 64 g/L up to 256 g/L has very little impact on the sedimentation height.

Although there is a similar trend of decreasing height with increasing salinity for the leached soil, the major difference in behavior is that this leached soil sediments to a height roughly twice that of the natural soil for every salinity. One explanation for the differing heights is natural GOM EI, even after the processing of the soil to a powder state, still consists of pre-existing dense flocs whereas the same soil that has been leached of its natural salts has had all the flocs dispersed. The dispersion of these clumps results in a looser soil structure which occupies more volume. The clumps of flocs found in the natural GOM EI will be discussed in Section 5.4.

5.3 DISCUSSION OF MECHANICAL BEHAVIOR

5.3.1 Introduction

The extensive CRS testing program undertaken in order to determine the one dimensional consolidation properties and permeability of the various soils incorporated a total of 32 tests. The same strain rates were used for each soil; the reason for this has been outlined in Section 4.3.2.2. All test specimens were stressed in the CRS device to an axial effective stress ranging between 30 MPa and 40 MPa. At the end of consolidation, it is not possible to obtain the secondary compression characteristics with the load frame used therefore the soil was removed from the test apparatus once the excess pore pressure had dissipated. The main trends in behavior associated with each graph presented for every soil will be discussed in detail for RGOM EI, and thereafter reference will be made to only the most important items for each soil dataset presented. The CRS test data were analyzed using standard linear theory (Wissa et al. 1971, ASTM D4186).

5.3.2 Gulf of Mexico – Eugene Island

5.3.2.1 Introduction

GOM EI powder was resedimented with pore fluids ranging from distilled water to 256 g/L salinity. Due to the natural salts present in the soil, the addition of distilled water to the soil results in a pore fluid salinity not of 0 g/L but of 6 g/L. The range of salt water concentrations used in the resedimented specimens were 0, 1, 4, 16, 64, 128 and 256 g/L resulting in pore fluid salinities of 6, 7, 10, 22, 64, 128 and 256 g/L respectively. At the higher salt water concentrations of 64 g/L and above, the natural salts create a negligible change to the overall pore fluid salinity and therefore the soil is regarded as having a pore fluid salinity matching that of the salt water added. Leached RGOM EI powder was resedimented with the same salt water concentrations, and with the natural salts removed, the concentration of the salt water used matched the pore fluid salinity of the specimens. CRS tests were conducted on RGOM EI and Leached RGOM EI with each of the above mentioned salinities.

5.3.2.2 Gulf of Mexico – Eugene Island

Figure 5.5 shows the compression curves in e - $\log \sigma'_{ac}$ space for RGOM EI. The shape of the compression curve is characterized by a well-defined break corresponding to a value below the target batch preconsolidation pressure. There is a clear trend in the initial void ratio at low stress versus the salt content, with void ratios decreasing from 1.86 for the low salinity soil to 1.46 in the case of the soil with 256 g/L salinity. Once the preconsolidation pressure is passed for all specimens, the compression behavior in the normally consolidated range gradually converges as stress increases. Significant curvature is observed in the normally consolidated region with the compression index, c_c value varying with stress. This will be discussed in detail in Section 5.3.2.4. At the final axial test stress between 30 MPa and 40 MPa the void ratios reduce to between 0.2 and 0.34. There is no clear trend in this value with salinity at this stress level, although the compression curve for the 6 g/L and 22 g/L represent outliers in the data compared to the behavior of the other five salinities. The compression curves for the same seven tests are shown in axial strain space in Figure 5.6. Up to an axial strain value of approximately 2 - 4 %,

the soil behaves as an overconsolidated soil. Beyond this level of axial strain, the soil is in the normally consolidated range. With increasing stress in the normally consolidated region (with the exception of CRS1400 at 22 g/L), the soil undergoes increasing amounts of axial strain for a given stress with decreasing salinity. The axial strain undergone by the specimens at an axial consolidation stress of 40 MPa ranges between 48 and 58 %. This trend in salinity is in agreement with the observations in void ratio space. Taking an arbitrary stress level of 10 MPa, the 6 g/L soil undergoes greater axial strain compared to the 256 g/L due to the fact that the lower salinity soil existed at a higher void ratio at the beginning of the test.

The preconsolidation pressure observed from the CRS results is consistently less than the target batch preconsolidation pressure. The reason for this is due to side-wall friction which exists between the soil and the consolidometer during resedimentation. As the diameter of the consolidometers employed was relatively small (~ 4.5 cm on average), the friction can be relatively substantial. The preconsolidation pressure for the tests shown in Figure 5.5 falls between 70 and 90 kPa which represents 70 – 90 % efficiency in terms of stress application during resedimentation. Even though lubrication is used internally on the consolidometer tubes prior to the placement of the slurry, the friction effect is still profound. The same effect is seen in all soil types resedimented throughout this research.

Figure 5.7 plots the bedding perpendicular permeability-porosity relationships for the range of pore fluid salinities tested. It can be seen that with increasing salinity permeability increases significantly for a given porosity. At a porosity of 0.5, the permeability of the 256g/L is over an order of magnitude greater than that of the 6 g/L. For each salinity, the permeability-porosity relationship is essentially log-linear over the porosity range 0.2 – 0.6. As stress increases and porosity decreases, the permeability of the higher salinities gradually convergences with the lower salinities resulting in the permeability for all salinities at a porosity of 0.2 becoming very similar. This indicates that with increasing stress, the permeability sensitivity to salts decreases to the point where the permeability is stress controlled rather than salinity controlled. An explanation for this observed behavior with salinity is provided in Section 5.4.2. Taking 256 g/L salinity as an example, the permeability ranges from a value of $9.75 \times 10^{-17} \text{ m}^2$ at a porosity of 0.55, to $5.25 \times 10^{-21} \text{ m}^2$ at a porosity of 0.2, over four orders of magnitude. Note that all test results were corrected for the differences in viscosity of the water due to the salinity. The

fluid density varied between 0.997 g/cm^3 for distilled water up to 1.162 g/cm^3 for 256 g/L salt water. This was done because the hydraulic conductivity obtained in the CRS test is calculated from the base excess pore pressure, which in turn is a function of the rate at which fluid can escape through the specimen. Different viscosities will allow water to dissipate at different rates. This calculated hydraulic conductivity is then converted to permeability.

The coefficient of consolidation in the vertical direction (c_v) lumps the permeability in the vertical direction (k_v) and the coefficient of compressibility in the vertical direction (m_v) into one parameter. Figure 5.8 presents coefficient of consolidation data obtained for the same seven tests. Data obtained before the preconsolidation pressure produced highly erratic data points and are not shown in the plot. In general, c_v increases with increasing salinity, which is to be expected based on the permeability behavior. At a low stress of 0.3 MPa , the coefficient ranges from $4 \times 10^{-5} \text{ cm}^2/\text{sec}$ (6 g/L) to $9 \times 10^{-4} \text{ cm}^2/\text{sec}$ (256 g/L). Two distinctly different behaviors occur with stress. The c_v of the high salinity specimens gradually decreases with increasing stress whereas the c_v of the low salinity specimens, namely the 6 g/L and 10 g/L remain fairly constant over the wide stress range. The c_v of the very high salinities was found to decrease by an order of magnitude over the stress range from 0.3 MPa to 40 MPa .

5.3.2.3 Leached Gulf of Mexico – Eugene Island

Figure 5.9 presents compression data for leached RGOM EI in $e\text{-log}\sigma'_{ac}$ space. The salinities tested include 0 (distilled water), 1, 4, 16, 64, 128, and 256 g/l . Distilled water was used for the leached soil in order to determine how the deflocculated particles would behave when full double layer growth was permitted. All leached RGOM EI specimens were tested to a stress of 40 MPa . The compression behavior of the leached RGOM EI with respect to both stress and salinity follows the same trend as the natural RGOM EI. Initial void ratios decrease with increasing salinity. In contrast to the natural RGOM EI, these low stress values have a narrower range, ranging from 1.23 to 1.38 with an average value less than that of the natural. The compression curves are again strongly non-linear with each curve converging in the normally consolidated region to almost identical behavior at stresses greater than 10 MPa . The void ratios at 40 MPa for the wide range of salinities fall within a much smaller range than the natural,

between 0.24 and 0.27. The final void ratios for the natural and leached are about the same value with no observed trend with salinity. Figure 5.10 presents the compression curves for the same tests in axial strain space. The axial strain required to reach the preconsolidation pressure ranges between 2 and 3 % (compared to 2- 4 % for RGOM EI), indicating that the leached soil is not as prone to swelling as natural RGOM EI. Similar strain behavior is observed to the natural RGOM EI where it undergoes increasing amounts of axial strain for a given stress as the pore fluid salinity of the soil decreases. The axial strain undergone by the specimens at an axial consolidation stress of 40 MPa has a narrower range of between 44.5 and 48.0 %. The fact that each salinity undergoes less straining at the final test stress compared to the natural soil, indicates that the leached soil is a stiffer less compressible soil.

Figure 5.11 shows the permeability-porosity behavior for the range of pore fluid salinities tested. Similar behavior and values are observed to that of the natural RGOM EI – increasing salinity increases the permeability of the soil, and the relationship is log-linear over the porosity range of 0.2 – 0.55. The permeability of the leached soil has about the same range as the natural with less difference with varying salinity at high porosities. The convergence in permeability of all salinities results in very similar values at low porosity.

Figure 5.12 shows the variation in the c_v obtained from the CRS tests. The same general trend is observed in leached RGOM EI as was seen in natural RGOM EI whereby the c_v value increases with increasing salinity. The range of values is similar to the natural over the large range in stress. The only major difference in behavior is the c_v of the leached soil with low salinities decreases with increasing stress. This is in contrast to the constant c_v value observed with stress in the natural soil at similar salinities.

5.3.2.4 Comparison of Natural and Leached GOM EI

Test specimens with a pore fluid salinity of 128 g/L are selected to compare the behavior of the natural RGOM EI to the leached soil. Figure 5.13 shows the compression plots for each soil in e - $\log \sigma'_{ac}$ space. The figure shows that the leached soil has a lower void ratio than the natural at low stress. Note this is opposite to the behavior in the sedimentation experiment, indicating that at very low stress the leached soil undergoes greater compression. It is evident

that the leached soil is less compressible compared to the natural, but once each soil is consolidated to a stress of 10 MPa or greater the behavior is identical.

This can be further explained by comparing the compression index, c_c , values of the two soils. The relationship between c_c and pore fluid salinity for both soils is shown in Figure 5.14. The figure plots the average c_c for three stress ranges, namely; 0.1 – 1 MPa, 1 – 10 MPa, and 10 – 40 MPa. Several observations can be made from this. Firstly, from 0.1 to 1 MPa the c_c of natural RGOM EI decreases with an increase in salinity from a value of 0.8 at 6 g/L to 0.55 at 22 g/L and then remains constant for salinities above 22 g/L. For the same stress range, the c_c of the leached soil shows less sensitivity to salts with values ranging from 0.5 to 0.42. As the axial consolidation stress increases, the impact of salinity on the c_c value decreases, particularly for the natural soil. It is clear that at stresses above 10 MPa, the c_c of both soils are both similar (~ 0.23) and independent of salinity level. Overall, leaching the natural salts from GOM EI and then adding back salts in varying concentrations decreases the compressibility of the soil at low stress, and it also reduces the sensitivity of the soils compression index to changes in salinity.

Another way of comparing the natural to the leached is by looking at the soils stress capacity at a given void ratio. At a void ratio of 1.0, the leached soil has a stress capacity of 0.24 MPa. Whereas the natural soil at the same void ratio has ~ 1.5 times the stress capacity. As described in Section 5.2, the natural soil has pre-existing floccs that are still present post material processing. The author speculates that these “clumps” of pre-existing floccs may have a greater capacity to carry and distribute the axial stress throughout the soil matrix. As the natural soil undergoes increasing consolidation stresses these clumps of natural floccs gradually break down resulting in the soil fabric becoming similar to that of the leached. This point is discussed in further detail in Section 5.4.2.

Figure 5.15 shows the permeability-porosity relationship for both soils at 128 g/L. It is remarkable given the differing compression behavior, that over the porosity range from 0.56 to 0.23 the permeability of both soils is practically identical. Although not presented here, the same observation is made for salinities greater than 64 g/L. The lower salinity leached soil displays increased permeability to that of the natural at high porosity with similar values obtained at low porosity.

5.3.3 Gulf of Mexico – Upper and Lower Interval

5.3.3.1 Introduction

Pore fluid salinities of 4, 70, and 256 g/L (NaCl) were used to investigate the impact of salinity on both soils. Although these soils have similar mineralogy and liquid limit (64.7 % for the Upper and 62.7 % for the Lower), they differ greatly in terms of clay size fraction and degree of expandability of the interlayered illite-smectite mineral. The results of both soils are combined in a set of figures to convey the differences in mechanical behavior. The majority of test specimens were consolidated in the CRS device to 40 MPa with the two 4 g/L specimens tested to 30 MPa.

5.3.3.2 GOM Upper & GOM Lower

Figure 5.16 shows the compression curves in e - $\log \sigma'_{ac}$ space for both soils. The same trend with both salinity and stress observed with RGOM EI is evident in both these soils. For all salinities tested, the RGOM Upper exists at a higher void ratio than that of the RGOM Lower regardless of stress level. Initial void ratios range between 1.37 and 1.67 for RGOM Upper compared to 1.09 and 1.32 for RGOM Lower. It is also evident that the greatest change in compression behavior at low stress occurs from 4 g/L to 70 g/L, where an increase in salinity from 70 to 256 g/L provides very little change in the initial void ratios. The compression behavior of each soil at the same salinity is practically parallel with significant curvature in the normally consolidated region. Although the compression curves converge with stress, the convergence is not as pronounced as that shown by RGOM EI. RGOM Upper shows a reversal in behavior as stress increases with the 256 g/L specimen able to maintain a higher void ratio at 40 MPa stress level than that of the 4 g/L. This behavior illustrates that for RGOM Upper, the higher salinity specimens are denser with lower void ratios at low stress, show stiffer behavior with increasing stress, and above an axial consolidation stress of 1 MPa have greater stress capacity to lower salinities at the same void ratio. The RGOM Lower reaches very low void ratios of between 0.11 and 0.17 at 40 MPa. The author suspects that the differences in void ratio at high stress may be due to specimen variability. Figure 5.17 presents the compression curves

for the same tests in axial strain space. The axial strain undergone by the specimens at an axial consolidation stress of 30 MPa ranges between 44 and 49 % for RGOM Lower and between 42 and 52 % for RGOM Upper. This trend in salinity is in agreement with the observations in void ratio space.

The corresponding permeability plots are shown in Figure 5.18. For each salinity level, RGOM Lower has higher permeability compared to RGOM Upper owing to the greater silt fraction. Both soils display the same trend with salt content of increasing permeability with increasing salinity. The permeability-porosity relationship for both soils is essentially log-linear over the porosity range 0.1 – 0.6. At a porosity of 0.5, the permeability of each soil increases by an order of magnitude with increasing salinity from 4 g/L to 256g/L. The permeability of RGOM Upper for the 3 salinities tested converges as porosity decreases. In contrast to this, the permeability of the RGOM Lower does not have the same degree of convergence with the 256 g/L still having approximately four times the value of the 4 g/L at a porosity of 0.2. The RGOM Upper permeability behaves very similar to RGOM EI. The expandability of the interlayered illite-smectite mineral ranges between 70 and 85 % for the soils displaying convergence in the permeability behavior. The soils with little to no convergence (RGOM Lower, RGOM A, and RGOM B) have lower expandability values of 40 to 60 %. The author hypothesizes that these two differing behaviors may be as a result of the differences in the expandability of the interlayered illite-smectite mineral in each soil.

The coefficient of consolidation data is presented in Figure 5.19. In general, c_v increases with increasing salinity, which is to be expected based on the permeability behavior. The c_v of both soils gradually decreases with increasing stress with very parallel behavior between each salinity.

5.3.4 Gulf of Mexico – Specimens A & B

RGOM A and RGOM B were each resedimented with two different pore fluid salinities of 100 and 200 g/L NaCl. All four specimens were consolidated in the CRS device to 40 MPa.

Figure 5.20 shows the compression curves in e - $\log \sigma'_{ac}$ space for both soils. The same trend with salinity at low stress observed with the other high plasticity soils is evident in both

these soils. Owing to the greater liquid limit and clay sized fraction, RGOM B has a greater void ratio at low stress, ranging between 1.75 and 1.95 compared to 1.64 to 1.74 for RGOM A. However, in the normally consolidated region, both soils behave differently to the other soils. Rather than the compression curves converging with increasing stress, the curves tend to diverge slightly. This results in a relatively large difference in void ratios at 40 MPa, with RGOM A ranging between 0.23 and 0.32, and RGOM B between 0.2 and 0.33. It is merely coincidental that the two different soils at similar salinities have very similar void ratios at 40 MPa. The compression behavior in axial strain space is shown in Figure 5.21. Again, the strain behavior at 40 MPa differs from that observed for the other test soils. Although the axial strain undergone by the specimens stressed to 40 MPa falls within a very small range (52 to 54 % for RGOM A and 55 to 56 % for RGOM B), there is a trend of increasing strain with increasing salinity. This is in contrast to the strain behavior of the four other soils.

Figure 5.22 shows the permeability-porosity relationship for the same four specimens. Similar behaviors are observed to that of the other soils. The permeability-porosity relationship is essentially log-linear, permeability increases with increasing salinity, and for a given salinity RGOM A has a higher permeability than RGOM B due to the greater silt fraction and lower liquid limit. The permeability of each salinity is parallel with little to no convergence observed with decreasing porosity. This behavior is similar to that of RGOM Lower. It is interesting to note that although RGOM Lower, RGOM A and RGOM B differ in terms of liquid limit and clay sized fraction, they both have similarly lower values (compared to RGOM EI and RGOM Upper) of between 40 and 60 % for the degree of expandability of the illite-smectite mixed layer. This further adds to the hypothesis that this parameter may be a controlling factor in determining if the permeability of high plasticity soils with varying salinity converge with decreasing porosity.

The coefficient of consolidation data is presented in Figure 5.23. The trends observed in the figure are similar to the other soils tested, with c_v increasing with increasing salinity and decreasing with increasing stress.

It is worth noting that with the other soils tested, the greatest changes in behavior occurred up to a salinity of say 64 g/L, with much less change occurring with an increase in

salinity to 256 g/L. It is expected that if both RGOM A and RGOM B were resedimented with a low salinity of say, 4 g/L, significant differences in the behavior would be observed compared to that of 100 g/L.

5.3.5 Comparison of Different Soil Types

A similar pore fluid salinity is selected in order to convey the differences in mechanical behavior of all the soils tested due to their varying characteristics such as clay size fraction, liquid limit, mineralogy, and expandability of the mixed layer illite-smectite. RGOM EI, Leached RGOM EI, RGOM Upper, and RGOM Lower were resedimented with similar salinities of 64 g/L and 70 g/L and therefore these test specimens will provide a good comparison. The 100 g/L specimens for RGOM A and RGOM B were selected as they provide the nearest salinity match to the other soils.

Figure 5.24 presents a synthesis plot of the compression results in e - $\log \sigma'_{ac}$ space. The figure shows that in general, there is a trend at low stress of increasing void ratio with increasing liquid limit, ranging from 1.1 to 1.95 over a liquid limit range of 62.7 to 90.4 % (see Table 3-1). Greater curvature is also observed in the normally consolidated range with increasing plasticity. Although there is a wide range in void ratios at low stress, at an axial consolidation stress of 40 MPa the void ratio of each soil falls within a much smaller range from 0.17 to 0.33, with CRS1377 somewhat of an outlier.

The differing behaviors described above are illustrated more clearly in Figure 5.25. This figure plots the c_c of all the soils versus pore fluid salinity. Each data point represents the average c_c value of the soil at that salinity over a stress range from 0.1 – 1 MPa. With the exception of RGOM A, there is a very clear trend of decreasing c_c with increasing salinity. When a comparison is made between c_c and salinity for three different stress ranges (0.1 – 1 MPa, 1 – 10 MPa, and 10 – 40 MPa), taking the data on all the soils into account, there is a clear trend of decreasing c_c with increasing stress. This matches the significant curvature of the virgin compression line (VCL). At the higher stresses of between 10 and 40 MPa the c_c falls within a narrower band of values, between 0.2 and 0.3. Details of this relationship between c_c , salinity and stress are shown in Figure 5.26. For all high plasticity soils tested, increasing the salinity of

the soil decreases the compression index creating a stiffer less compressible soil. At low stress, composition and salinity control the compression behavior, however, at high stresses the influence of salinity and composition reduces with stress level becoming the controlling factor.

Figure 5.27 presents a synthesis plot of the permeability-porosity relationship. The permeability-porosity relationship is essentially log-linear for all soils with each soil follows parallel lines. In general, permeability increases with decreasing liquid limit. For soils ranging in liquid limit from 63 % to 90 %, there is over an order of magnitude difference in permeability at a given porosity.

All high plasticity soils tested display decreasing c_v with increasing stress over the large stress range applied. The largest rate reduction of c_v occurs in the highest plasticity soil – RGOM B. Details of these trends are shown in Figure 5.28.

In addition to the trends identified in the mechanical behavior obtained from CRS testing, further trends with salinity can be determined from the phase relations of the soils tested. Figure 5.29 and Figure 5.30 show both the dry and wet density versus salinity. These values are obtained at the end of resedimentation at which point each soil has been consolidated to an axial stress of 0.1 MPa. There is a clear trend of increasing dry and wet density with increasing pore fluid salinity, and this is the case for all soils tested. Figure 5.31 provides the same data, this time with water content versus salinity. Again, there is a clear trend observed for all soils with the water content decreasing with increasing salinity. Large reductions in water content are observed for RGOM EI, ranging from 68 % to 42 %. This trend with salinity is similar to that of the water contents required to create a workable slurry for resedimenting, as discussed in Chapter 3. Based on this and the findings presented from the CRS results, one can conclude that for high plasticity soils, increasing salinity decreases the water content of the soil and increases the permeability. By determining the relationship between water content and salinity, one can get an early indication of the impact, if any, of changes in salinity on the mechanical behavior of the soil.

5.3.6 Evaluation of CRS Testing Program

The CRS test is relatively simple to perform and a large variety of useful data can be obtained from high quality test results. The author is fortunate that several high plasticity soils

with a wide range of liquid limits, from 63 % to 90 %, were available for testing throughout the course of this research. Observing similar trends with salinity in all the soils strengthens the findings presented here. In addition to this, the CRS testing program generated a substantial bank of reference data. When added to the work by Horan (2012) on the low plasticity RBBC, the findings can now be used for future research in the area of salinity effects as well as to compliment other research ongoing in the MIT Geotechnical Laboratory.

The altering of the fabric of GOM EI by removing the natural salts has produced a great deal of useful data on how the fabric and structure of the soil behaves and evolves with change in stress level.

The testing of several high plasticity soils has brought the limitations of the Wykeham Farrance loading frame into sharp focus. The minimum strain rate in which the frame can be operated is 0.3%/hr. Due to the very low permeability of each soil tested; particularly the soils with the very low pore fluid salinities, the pore pressures developed at the base of the specimen exceeded the capacity of the pore pressure transducer. Once the capacity was reached the frame had to be turned off to allow the pore pressures to dissipate. This point was reached at stresses as low as 15 MPa but in general above 20 MPa. Once the device is turned off, the data for permeability and coefficient of consolidation becomes inaccurate. Although the test is recommenced until an axial consolidation stress of 40 MPa is reached, this limitation prevents the user obtaining permeability and c_v data for the higher stresses. Guidelines in the current ASTM standard on CRS testing (ASTM D8146-12) suggest using a strain rate of 0.1%/hr for high plasticity soils. The author therefore recommends that any future testing on high plasticity soils to axial consolidation stresses greater than 10 MPa be conducted using a load frame with capacity to apply strain rates of 0.1%/hr and less. The lower strain rate reducing the amount of excess pore pressure developing as stress increases, will therefore allow the specimen to be consolidated to far higher stresses without the need to turn off the load frame. The development of the new CRS equipment with an axial consolidation stress capacity of 100 MPa employs the use of a computer controlled hydraulic cylinder to apply the axial loading. Computer control allows the strain rate applied by the hydraulic cylinder to be stepped down in sufficiently small increments as to prevent any transient conditions occurring in the specimen. This system has the ability to apply strain rates ranging from essentially zero up to values greater than those required

for testing high permeability soils. This strain rate flexibility eliminates the two issues associated with the current axial loading arrangement.

ASTM D4186-12 states that a pore pressure ratio ($\Delta u/\Delta\sigma_a$) of between 3 and 15 % is required for the test data to be considered valid. Pore pressure ratios lower than 3 % were generated while testing the higher permeability soils (e.g. RGOM Lower at 256 g/L). The lowest recorded ratio of 0.5 % still produced accurate permeability information. The author recommends that the standard be revised to acknowledge the accuracy of test results obtained from lower pore pressure ratios.

5.4 SEM IMAGE ANALYSIS

5.4.1 Introduction

In order to better explain and understand the observed mechanical behavior of the high plasticity soils with changes in salinity, scanning electron microscope (SEM) images were taken for GOM EI and Leached GOM EI. Concentrated slurry's were prepared with the water contents associated with creating a workable slurry. A small droplet of this slurry was then cryogenically frozen, allowing the soil to be imaged in a slurry state. The frozen surface was then fractured resulting in a broken surface as opposed to a smooth milled surface. The soil was then transferred to the SEM machine to be imaged. The images presented here are provided by Amer Deirich, a colleague at MIT who developed the technique.

5.4.2 Hypothesis for Explaining Mechanical Behavior

Figure 5.32 shows two images at the same magnification of GOM EI in a slurry state with pore fluid salinities of 7 and 64 g/L. A number of points can be made based on a qualitative analysis of the SEM images. Firstly, both salinities create an overall similar flocculated structure with roughly hexagonal shaped pore spaces of similar size, about 2 μ m. Secondly, as the pore fluid salinity increases, the floc wall thickness (domain thickness) increases. With low salinity there is limited charge available to attract particles to each other, resulting in the formation of thin or narrow flocs. Whereas in the high salinity slurry a greater number of particles are attracted to each other in the process of forming each floc due to the greater electrolyte

availability reducing the double layer length. This increased attraction creates flocs with increasing wall thickness. Thirdly, the particles in the floc wall tend to be offset face to face in stacked block configuration. At this ultra-low stress, the increase in salinity creates a denser packing of the soil particles and in turn results in a soil with a lower void ratio than that of soil with a lower salinity. This is in agreement with Figure 5.5 where at low stress, void ratio decreases with increasing salinity. This point is also confirmed by the fact that the dry and bulk densities increase with increasing salinity.

Figure 5.33 shows an image of leached GOM EI. The natural salts have been removed from the soil and the soil powder is mixed with distilled water to form the slurry shown in the image. The image shows that leaching out the salts results in a disaggregation of the flocs, eliminating any pre-existing flocs and creating a disorganized matrix of soil particles. By adding back salts we create a more uniform floc structure, as shown by the 64 g/L salinity slurry in Figure 5.34. The flocculated structure of the natural GOM EI at a similar salinity is presented in Figure 5.35. In contrast to the leached soil, the natural GOM EI soil structure consists of newly formed flocs surrounding clumps of pre-existing flocs that have remained intact from the in-situ state. These natural flocs are denser than the new flocculated structures surrounding them. At super low stresses such as in the sedimentation tubes or in these slurry images, the leached flocculated structure is looser than the natural with its dense clumps. But as stress increases, this uniform structure of the leached soil collapses to a lower void ratio than the natural. Figure 5.13 showed that for a given porosity, the natural soil has a greater stress capacity. The author speculates that as stress increases, the clumps of flocs in the natural soil come into contact with each other and provide greater stress capacity compared to the stress distribution provided by the uniform soil matrix of the leached soil.

Increasing salt concentration in the pore fluid can influence permeability by reducing the thickness of double layers. The data presented in Figure 5.7 confirms this trend in permeability with salinity. A qualitative analysis of the same SEM images can also offer an explanation for this observed permeability behavior. The thicker individual flocs and overall stiffer floc structure of the high salinity soil in Figure 5.32 has a greater capacity to maintain the main pore spaces or flow paths at low stresses. As the stress increases, the main flow paths in the high salinity soil gradually get cut off and reduce the permeability in line with the low salinities. It can also be

stated, based on the SEM images, that lower salinities have thinner floc walls with less particles per floc, and hence for the same soil mass will create more of these “tubes” or hexagonal pore spaces. With an increasing number of “tubes”, an increased resistance to flow is generated, resulting in lower permeability.

5.5 CORRELATIONS WITH PLASTICITY

5.5.1 Introduction

This section proposes correlations between the sensitivity of a soils compressibility and permeability with changes in pore fluid salinity to liquid limit. Data on all six soils tested as well as data from similar research on RBBC from Horan (2012) is combined for the analysis.

5.5.2 Compressibility

The compression behavior of each soil discussed previously, as well as the c_c data presented at three different stress levels, namely: 0.1 MPa, 1 MPa, and 10 MPa showed that at 10 MPa the compression behavior is salinity independent. That is, the behavior is more stress dependent than salinity dependent. The correlation between changes in compressibility with salinity to liquid limit is therefore assessed at the two lower stress levels of 0.1 MPa and 1 MPa.

Figure 5.36 shows the change in void ratio with respect to salinity for RGOM EI at a consolidation stress of 0.1 MPa and 1 MPa. The data for 10 MPa is plotted to illustrate the fact that at this stress level the void ratio is essentially salinity independent. A power-law function is plotted through each data set. The slope of the line, the C parameter, describes the change in void ratio with pore fluid salinity. A negative value of C indicates decreasing void ratio with increasing salinity, and vice versa. Note that the slope of the line should increase at low salinity, but this fit is used as a general index of behavior.

Figure 5.37 plots the C parameter of each soil tested against the corresponding liquid limit. Data on RBBC is also included. Although there is a large amount of scatter in the data, there is a general trend with liquid limit. As liquid limit increases, void ratio sensitivity to changes in salinity increases. Larger negative values indicate a greater change with salinity.

RBBC, with a slightly positive C parameter, displays the opposite behavior of increasing compressibility with increasing salinity, although the impact is almost negligible.

5.5.3 Permeability

Figure 5.38 presents the change in permeability with respect to salinity for RGOM EI at a porosity of 0.5, 0.4, and 0.3. A power-law function is plotted through each data set. The slope of the line, the D parameter, describes the change in permeability with pore fluid salinity. The figure shows that for RGOM EI, the sensitivity of the soils permeability to changes in salinity decreases with decreasing porosity (increasing consolidation stress). Note that a positive value of D indicates increasing permeability with increasing salinity, and vice versa.

Figure 5.39 plots the D parameter of each soil tested against the corresponding liquid limit. By combining the data from all the soils, and although there is large scatter present, there is a definite trend of increasing permeability sensitivity to changes in salinity with increasing liquid limit. Positive D parameter values indicate increasing permeability with increasing salinity, whereas a negative value indicates the opposite behavior. The low stress permeability behavior is in general more sensitive to pore fluid salinity changes.

An explanation for the correlations between liquid limit and the D parameter is offered. Increasing liquid limit is associated with a larger quantity of clay minerals present in a soil as well as a reduction in the size of said minerals. Increasing liquid limit is therefore linked to a decrease in mean pore size, to an increase in the influence of double layers around clay particles, and to a greater likelihood for the smaller platy shaped smectite clay particles to be oriented perpendicular to the direction of axial stress. These factors combined mean that, at a given porosity, permeability in the direction of axial loading decreases with increasing liquid limit (Figure 5.27). They also mean that with decreasing clay mineral size, salinity has greater impact on particle interactions, and varying the salinity will result in greater changes in permeability.

Test No.	Resed. No.	Salinity (g/l)	Initial Conditions					At $\sigma'_{ac} = 10\text{MPa}$			At Maximum Stress			
			w_o (%)	Degree of Saturation (%)	e_o	γ_d (g/cm ³)	γ_w (g/cm ³)	ϵ_a (%)	e	c_v (cm ² /sec)	σ'_{ac} (MPa)	ϵ_a (%)	e	c_v (cm ² /sec)
RGOM EI														
CRS1361	RS332	6	67.67	99.9	1.885	0.960	1.611	53.55	0.339	4.47×10^{-5}	34.40	58.31	0.202	-
CRS1362	RS333	7	65.97	100.0	1.828	0.980	1.627	49.78	0.419	1.04×10^{-4}	38.55	54.75	0.278	3.38×10^{-6}
CRS1363	RS339	10	59.65	99.5	1.672	1.037	1.659	48.06	0.389	6.25×10^{-5}	36.76	53.36	0.248	-
CRS1400	RS342	22	56.12	100.0	1.569	1.081	1.699	43.56	0.411	9.06×10^{-5}	39.04	49.40	0.265	-
CRS1364	RS335	64	53.84	99.4	1.592	1.080	1.704	45.48	0.413	1.10×10^{-4}	36.42	50.58	0.281	-
CRS1366	RS343	128	48.26	97.7	1.531	1.117	1.735	44.77	0.397	9.54×10^{-5}	36.69	49.98	0.266	6.81×10^{-5}
CRS1368	RS336	256	41.42	95.2	1.507	1.151	1.770	44.69	0.385	1.56×10^{-4}	38.97	50.26	0.246	9.05×10^{-5}
Leached RGOM EI														
CRS1373	RS346	0	50.57	100.0	1.406	1.151	1.735	42.62	0.381	5.63×10^{-5}	33.39	47.92	0.253	-
CRS1374	RS373	1	49.97	99.3	1.390	1.155	1.732	42.21	0.387	5.61×10^{-5}	39.06	47.89	0.251	-
CRS1375	RS377	4	47.38	99.6	1.326	1.192	1.759	39.82	0.399	5.60×10^{-5}	39.17	45.76	0.261	-
CRS1372	RS374	16	49.57	99.6	1.400	1.157	1.740	41.72	0.399	9.30×10^{-5}	37.06	47.20	0.267	-
CRS1370	RS352	64	43.75	97.2	1.313	1.209	1.772	40.43	0.377	1.01×10^{-4}	37.36	46.10	0.246	-
CRS1367	RS353	128	40.50	95.5	1.301	1.228	1.789	40.03	0.379	1.03×10^{-4}	38.54	45.70	0.248	-
CRS1369	RS362	256	35.41	96.5	1.246	1.284	1.856	38.63	0.378	1.00×10^{-4}	39.30	44.58	0.245	-

Table 5-1 List of Constant Rate of Strain tests performed (1 of 2)

Test No.	Resed. No.	Salinity (g/l)	Initial Conditions					At $\sigma'_{ac} = 10\text{MPa}$			At Maximum Stress			
			w_o (%)	Degree of Saturation (%)	e_o	Y_d (g/cm^3)	Y_w (g/cm^3)	ϵ_a (%)	e	c_v (cm^2/sec)	σ'_{ac} (MPa)	ϵ_a (%)	e	c_v (cm^2/sec)
RGOM Lower														
CRS1398	RS401	4	48.25	98.3	1.338	1.160	1.722	45.31	0.278	5.39×10^{-5}	28.30	49.53	0.180	-
CRS1377	RS380	70	38.56	99.2	1.111	1.293	1.830	39.24	0.282	9.76×10^{-5}	40.23	45.24	0.156	-
CRS1395	RS399	256	27.93	82.3	1.102	1.325	1.790	41.61	0.228	1.03×10^{-4}	38.04	47.36	0.107	-
RGOM Upper														
CRS1397	RS402	4	59.46	99.5	1.686	1.044	1.668	46.90	0.427	4.61×10^{-5}	31.03	51.97	0.290	-
CRS1376	RS381	70	48.06	97.9	1.460	1.152	1.747	41.54	0.439	8.05×10^{-5}	39.22	47.48	0.292	-
CRS1396	RS400	256	35.51	88.7	1.375	1.228	1.777	36.73	0.501	1.93×10^{-4}	40.95	43.37	0.344	-
RGOM A														
CRS1350	RS252	100	55.67	94.7	1.745	0.998	1.625	47.99	0.428	7.78×10^{-5}	35.72	52.26	0.311	-
CRS1357	RS262	200	51.16	99.9	1.673	1.039	1.715	49.04	0.363	1.20×10^{-4}	39.22	54.11	0.227	-
RGOM B														
CRS1354	RS251	100	62.30	96.9	1.962	0.943	1.613	50.52	0.467	4.60×10^{-5}	39.40	55.14	0.330	-
CRS1360	RS266	200	50.65	96.0	1.757	1.033	1.689	50.96	0.352	8.00×10^{-5}	39.77	56.13	0.209	-

Table 5-2 List of Constant Rate of Strain tests performed (2 of 2)



Figure 5.1 Sedimentation test performed on natural BBC Series IV powder. Salinities from LR: 1, 4, 16, 64, 128 & 256 g/l NaCl. 5 grams of soil used in each tube (Horan, 2012)



Figure 5.2 Sedimentation test performed on leached BBC powder. Salinities from L-R: 0 (distilled water) 1, 4, 16, 64, 128 & 256 g/l NaCl. 5 grams of soil used in each tube (Horan, 2012)



Figure 5.3 Sedimentation test performed on GOM EI powder. Salinities from L-R: 1, 4, 16, 64, 128, 256 g/l. 5g of soil in each tube

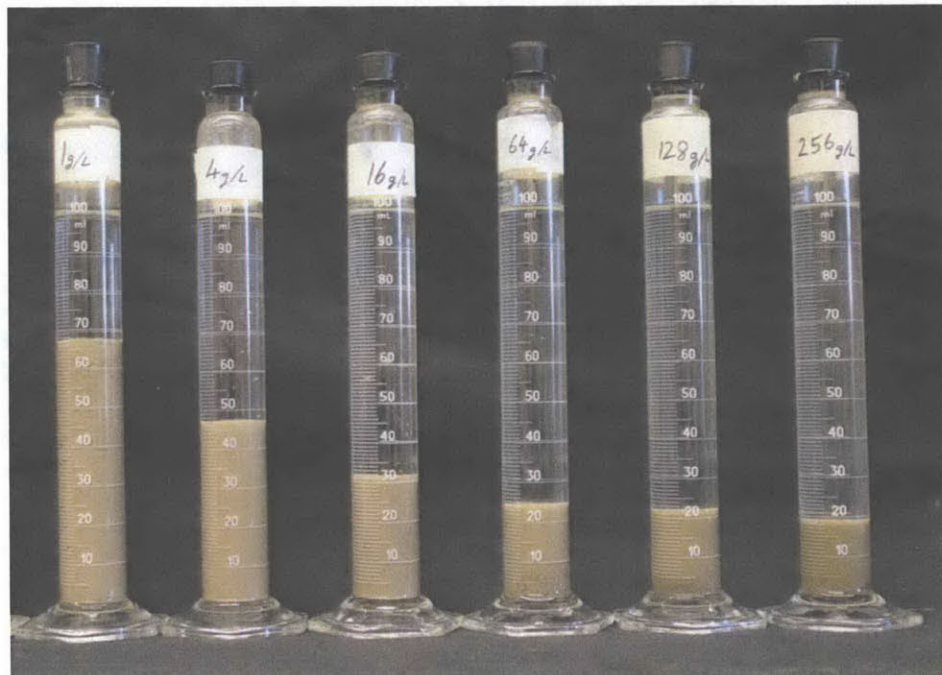


Figure 5.4 Sedimentation test performed on GOM EI powder. Salinities from L-R: 1, 4, 16, 64, 128, 256 g/l. 5g of soil in each tube

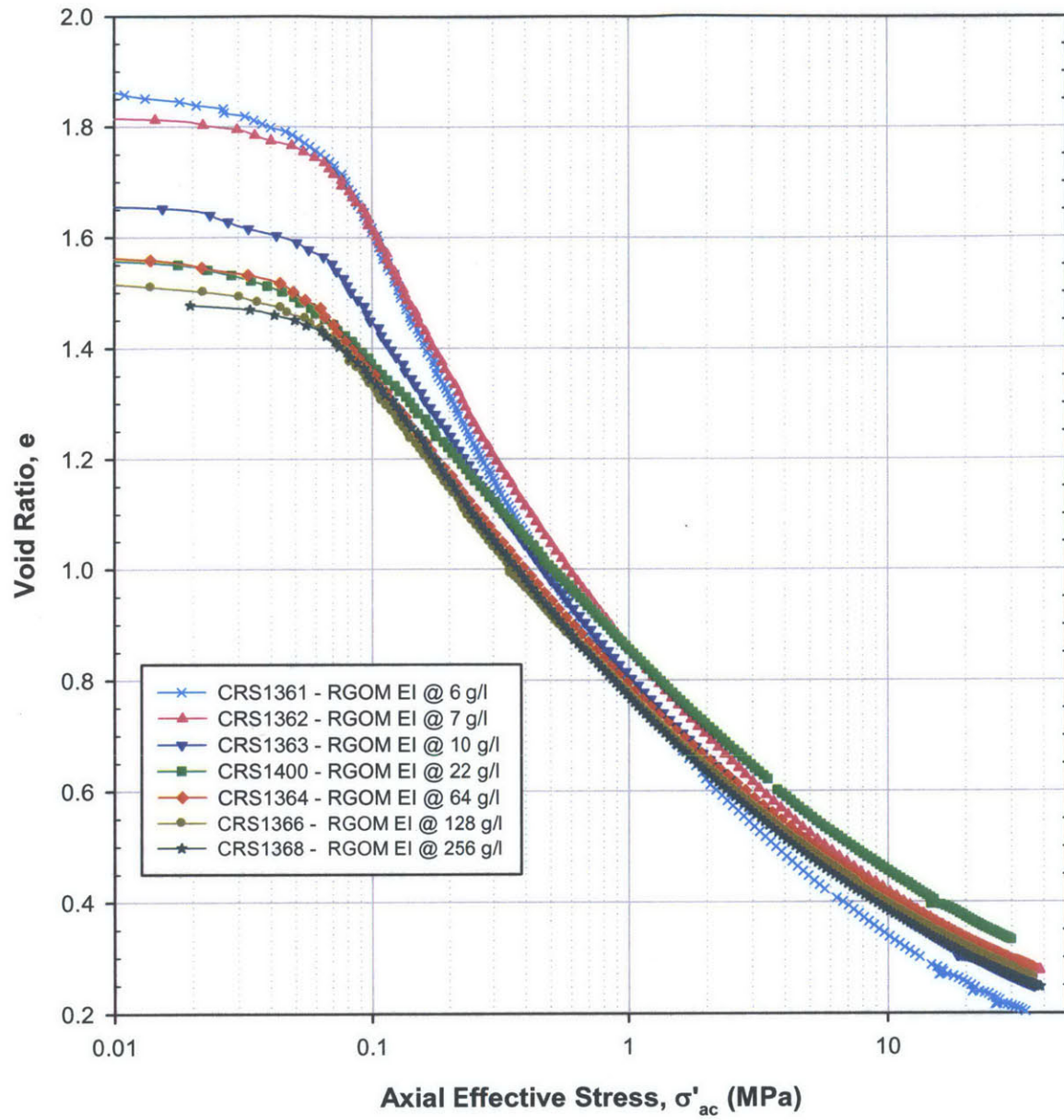


Figure 5.5 Compression behavior in $e - \log \sigma'_{ac}$ space for RGOM EI at various pore fluid salinities

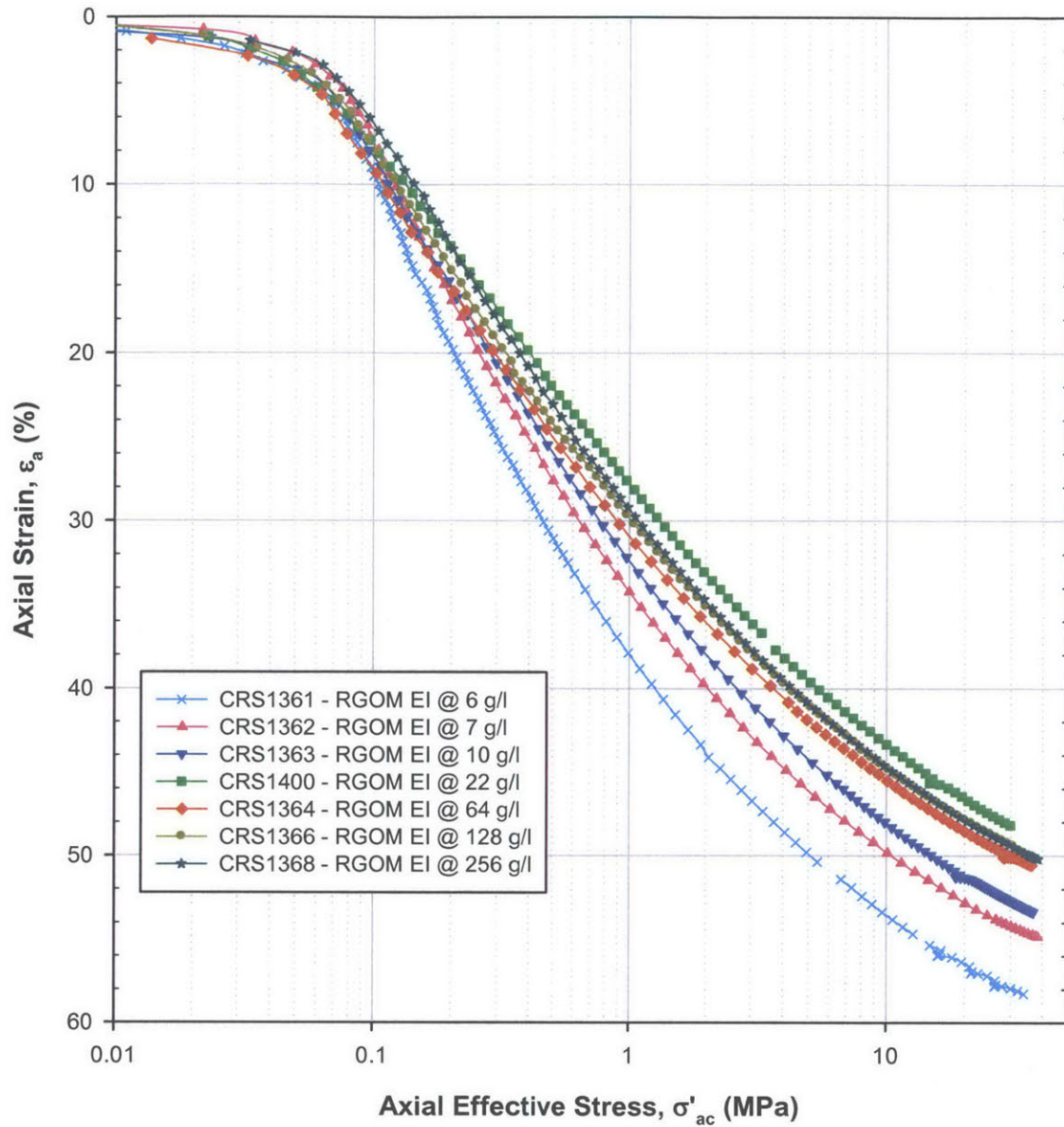


Figure 5.6 Compression behavior in $\epsilon_a - \log \sigma'_{ac}$ space for RGOM EI at various pore fluid salinities

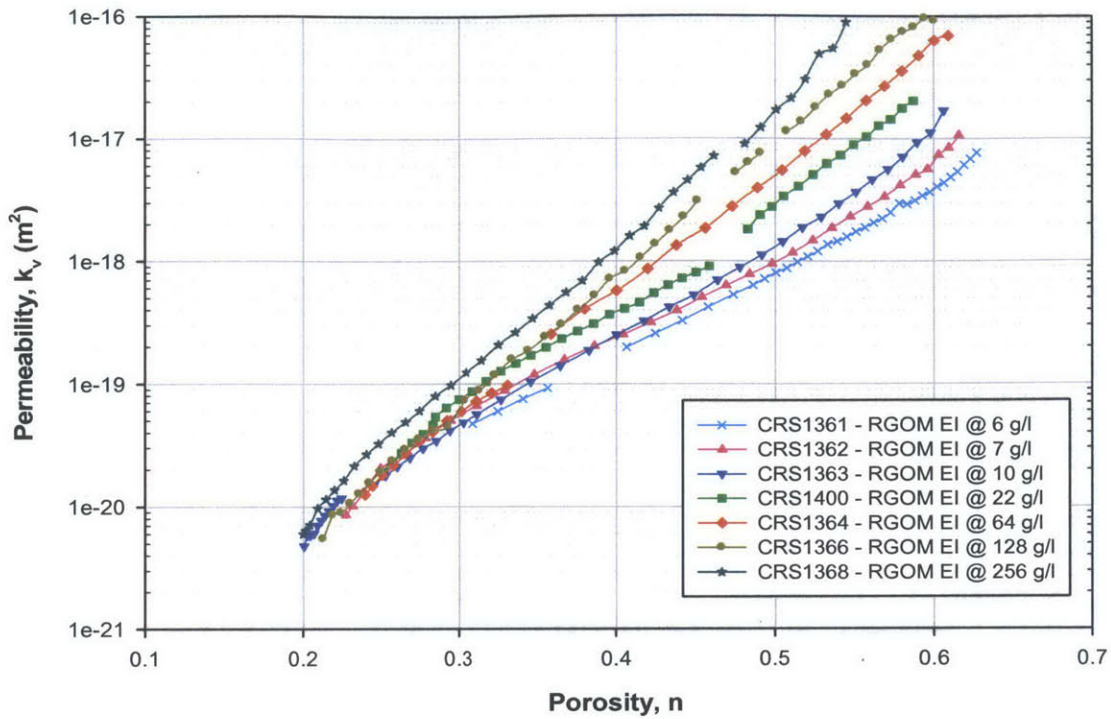


Figure 5.7 Permeability in porosity space for RGOM EI at various pore fluid salinities

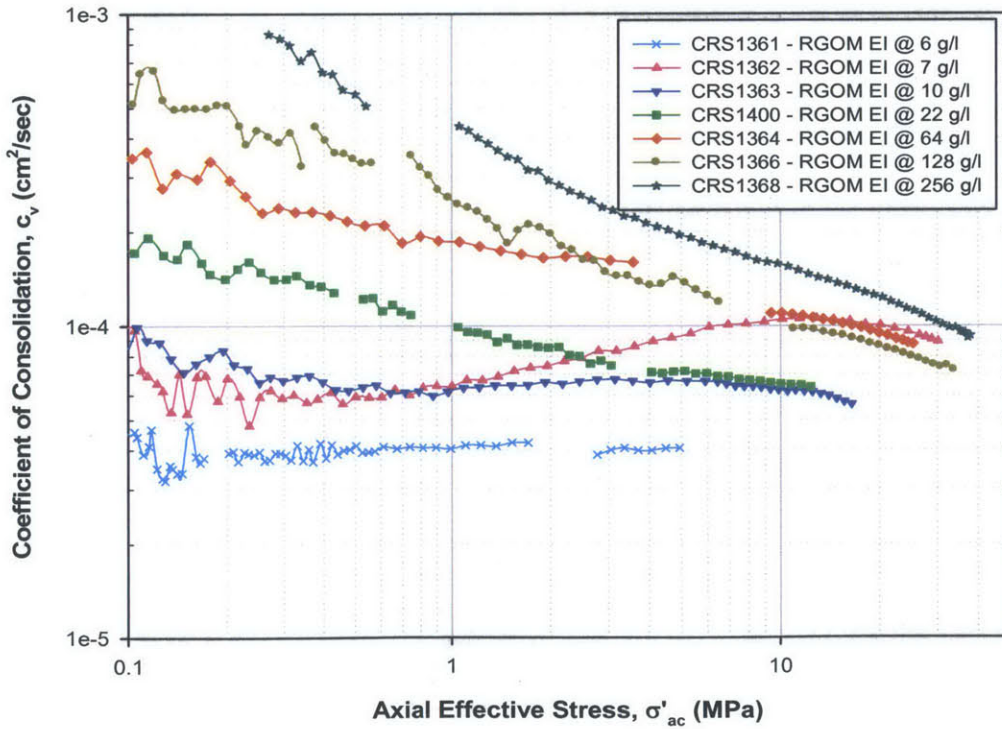


Figure 5.8 Coefficient of consolidation in $\log \sigma'_{ac}$ space for RGOM EI at various pore fluid salinities

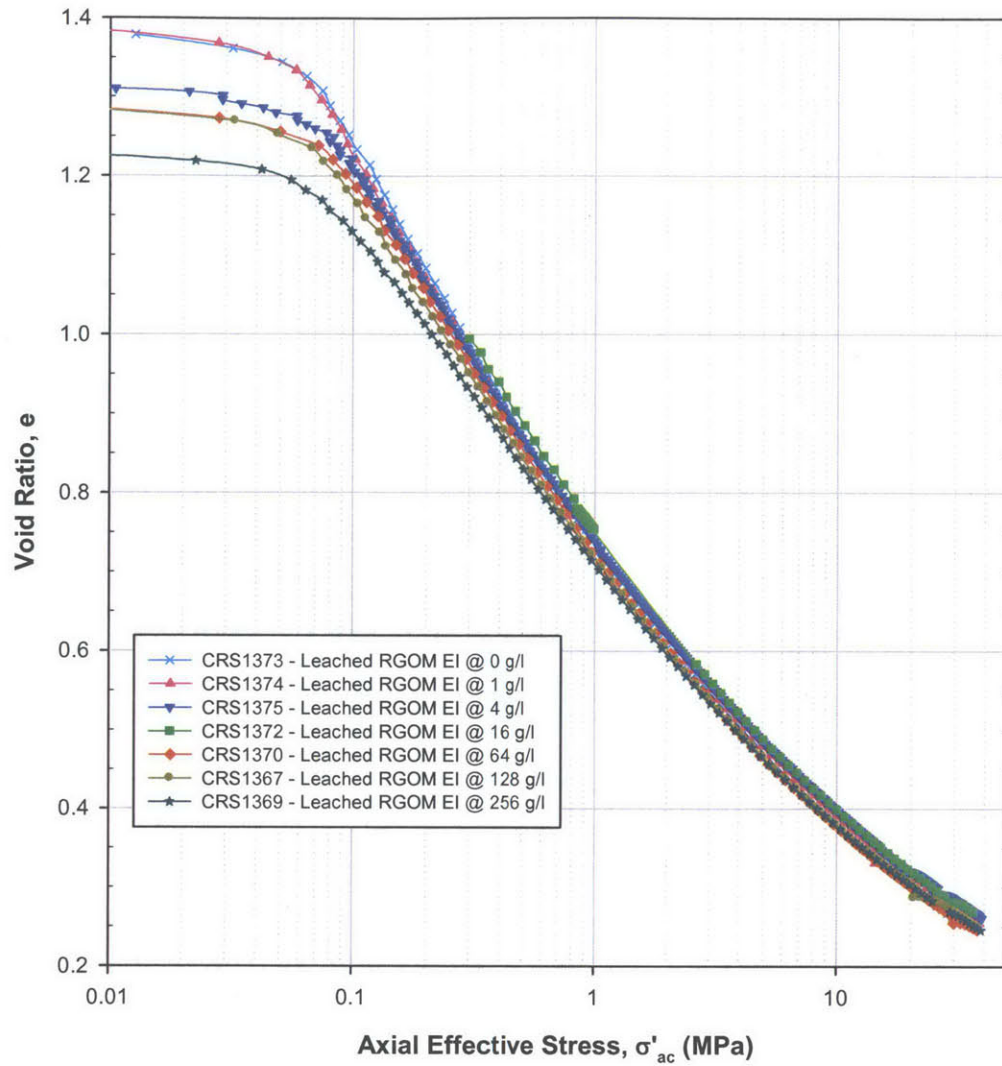


Figure 5.9 Compression behavior in $e - \log \sigma'_{ac}$ space for Leached RGOM EI at various pore fluid salinities

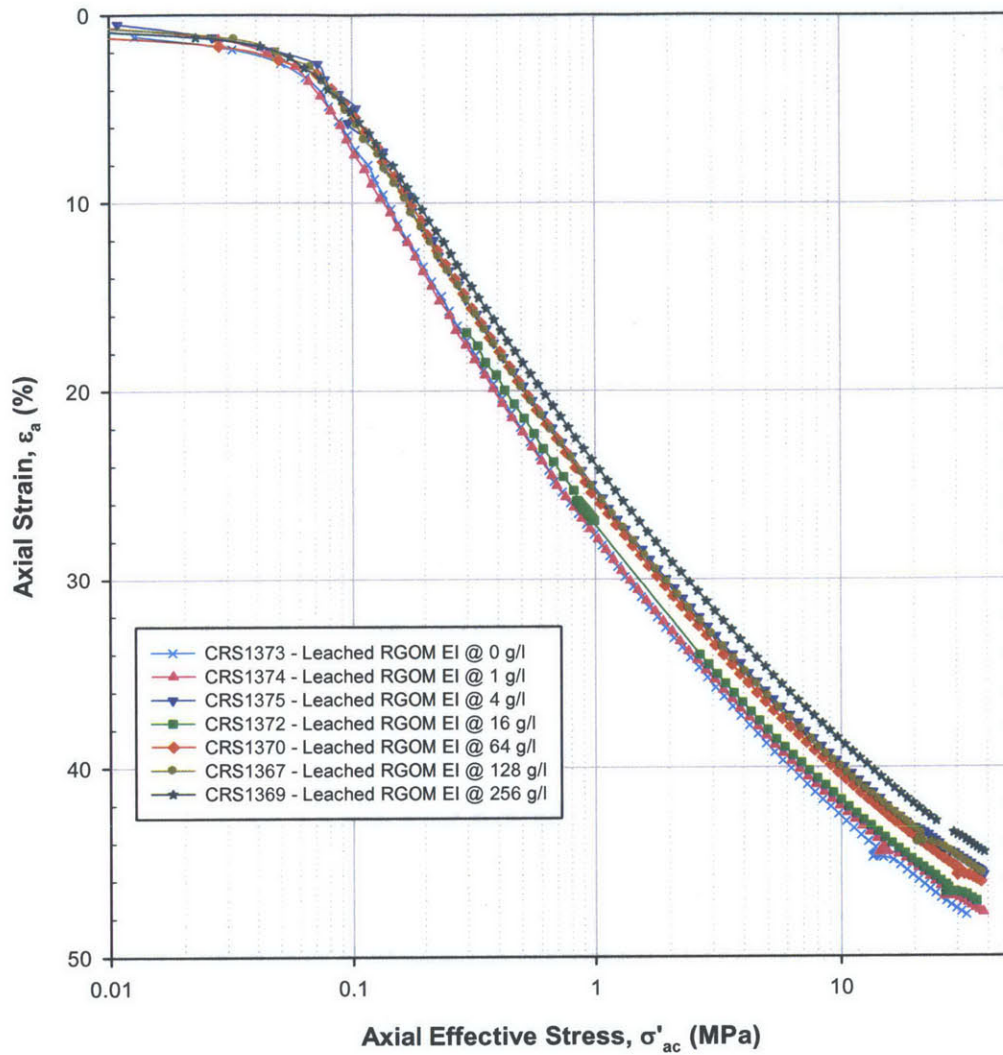


Figure 5.10 Compression behavior in $\epsilon_a - \log \sigma'_{ac}$ space for Leached RGOM EI at various pore fluid salinities

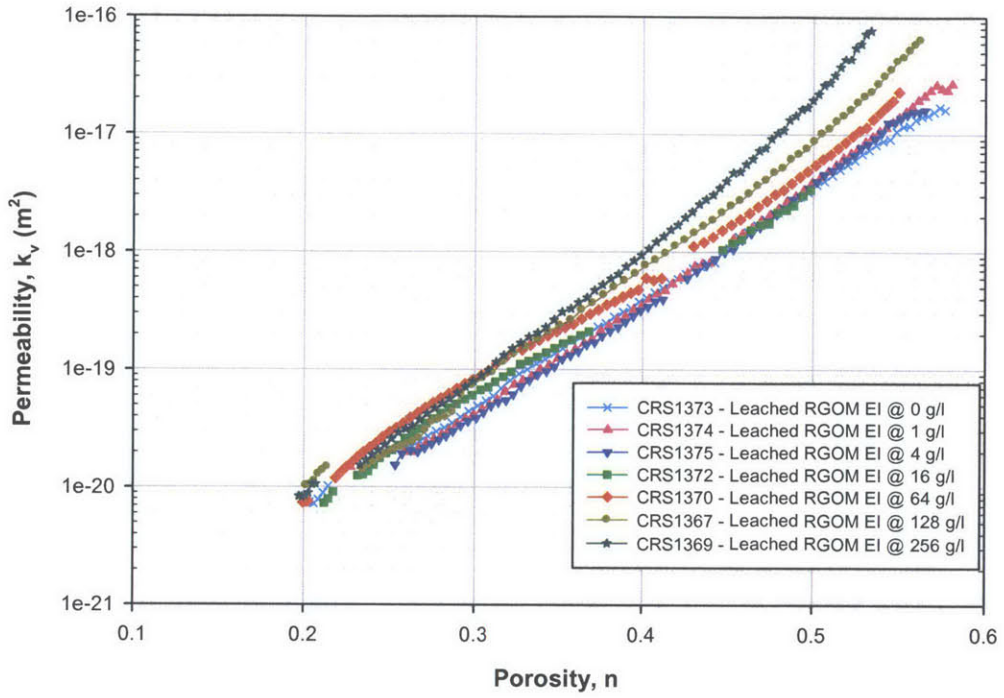


Figure 5.11 Permeability in porosity space for Leached RGOM EI at various pore fluid salinities

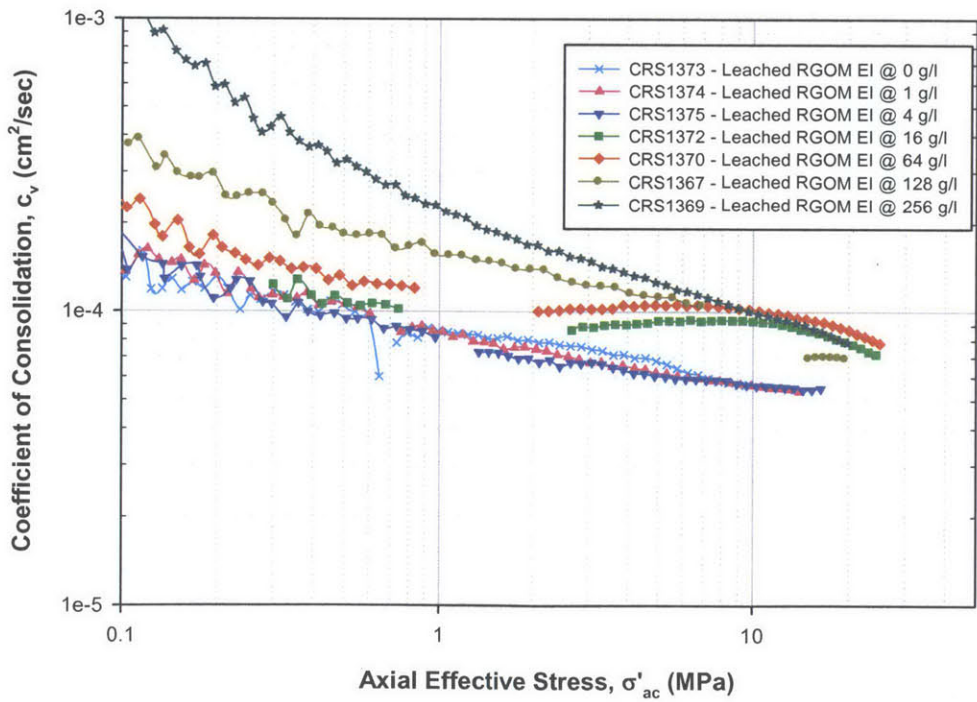


Figure 5.12 Coefficient of consolidation in $\log \sigma'_{ac}$ space for Leached RGOM EI at various pore fluid salinities

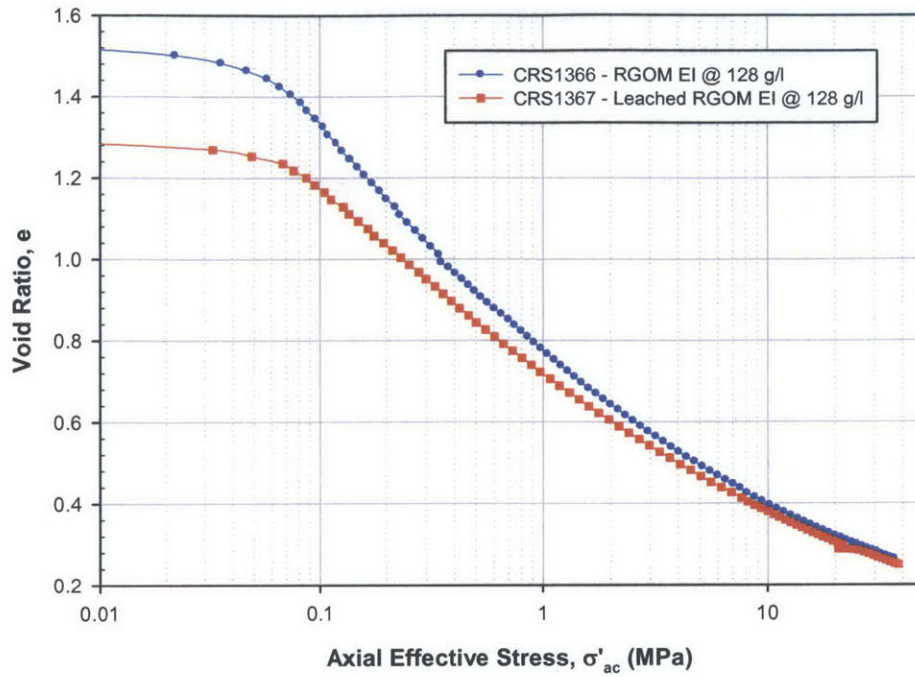


Figure 5.13 Compression behavior comparison for RGOM EI and Leached RGOM EI (in $e - \log \sigma'_{ac}$ space)

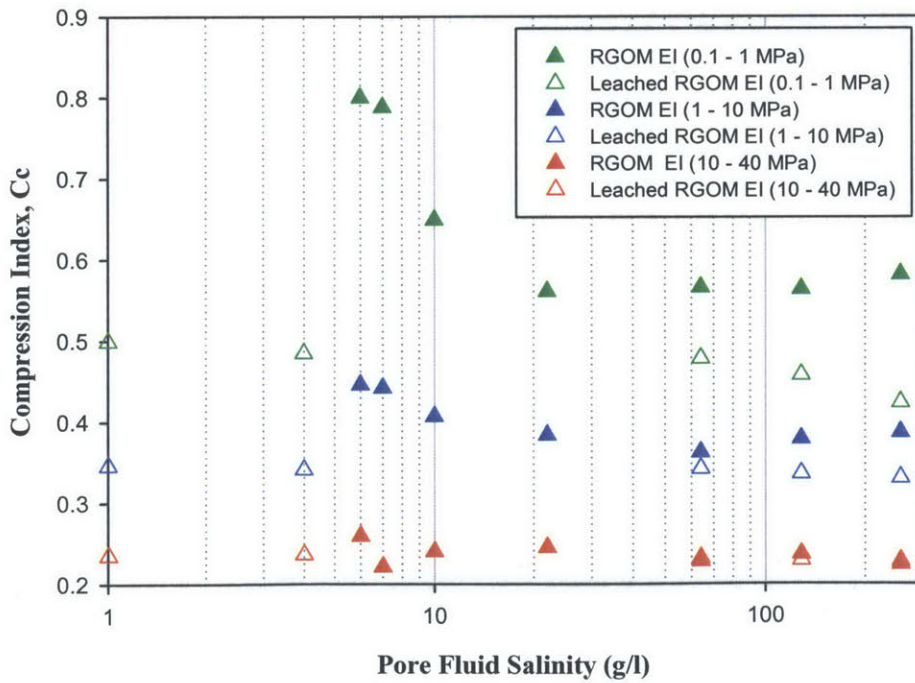


Figure 5.14 Compression Index versus salinity comparison between RGOM EI and Leached RGOM EI over three stress ranges

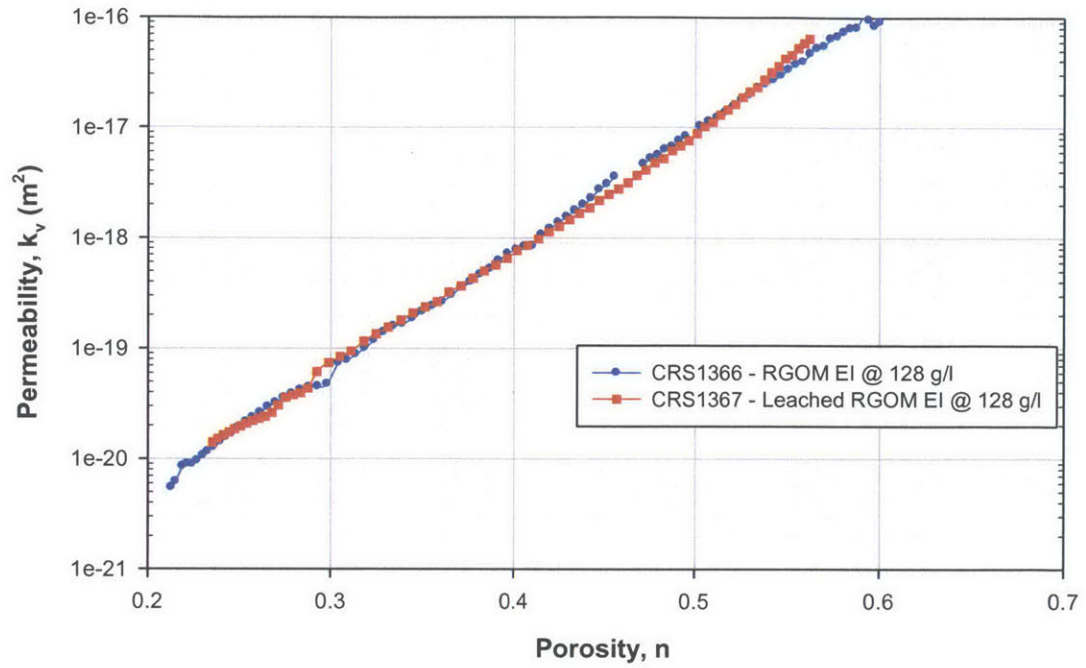


Figure 5.15 Permeability behavior comparison for RGOM EI and Leached RGOM EI (in porosity space)

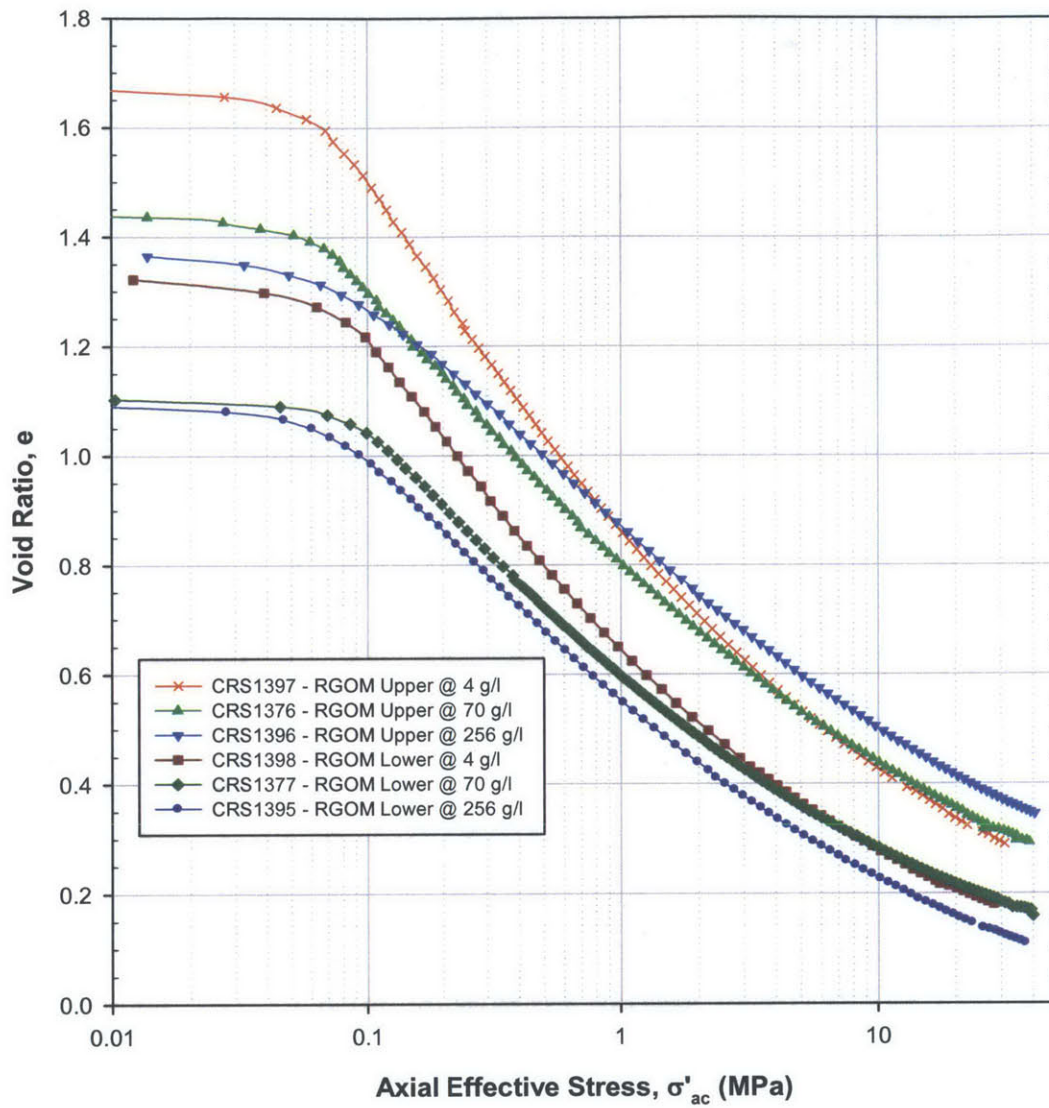


Figure 5.16 Compression behavior in $e - \log \sigma'_{ac}$ space for RGOM Upper and Lower at various pore fluid salinities

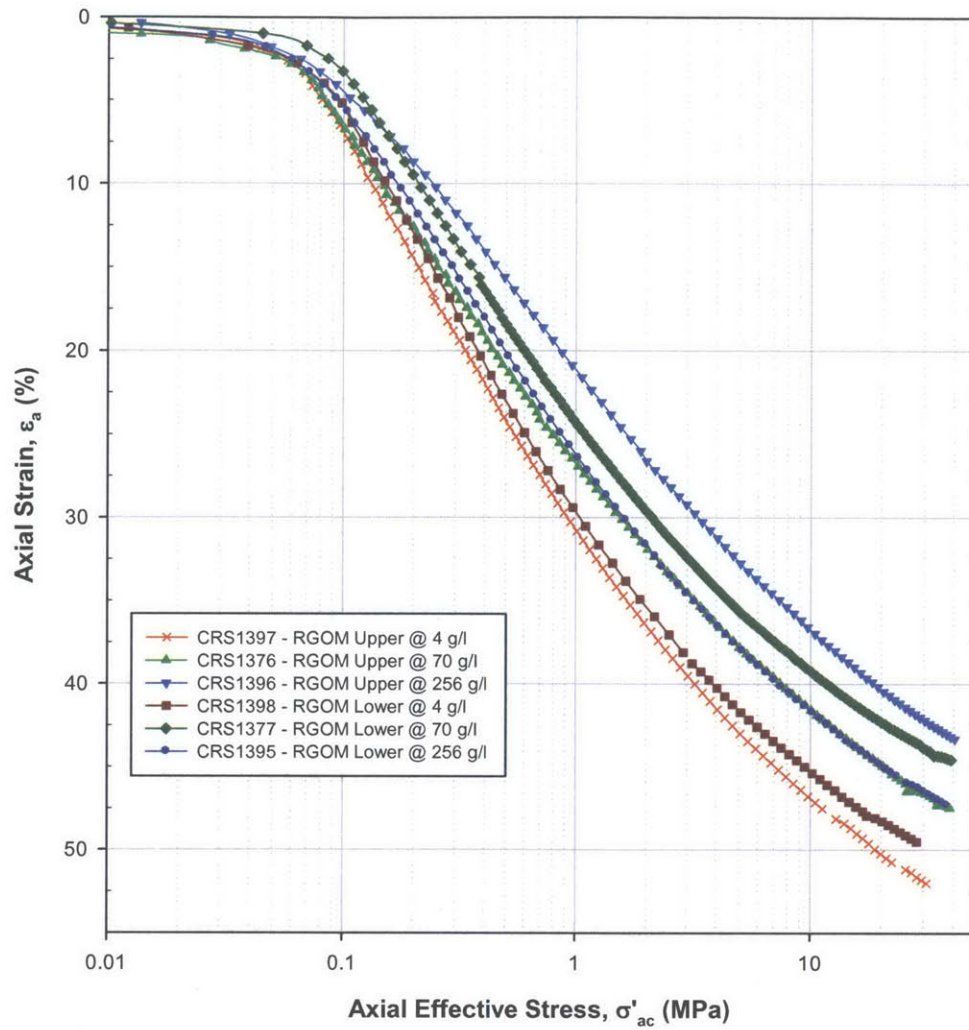


Figure 5.17 Compression behavior in $\epsilon_a - \log \sigma'_{ac}$ space for RGOM Upper and Lower at various pore fluid salinities

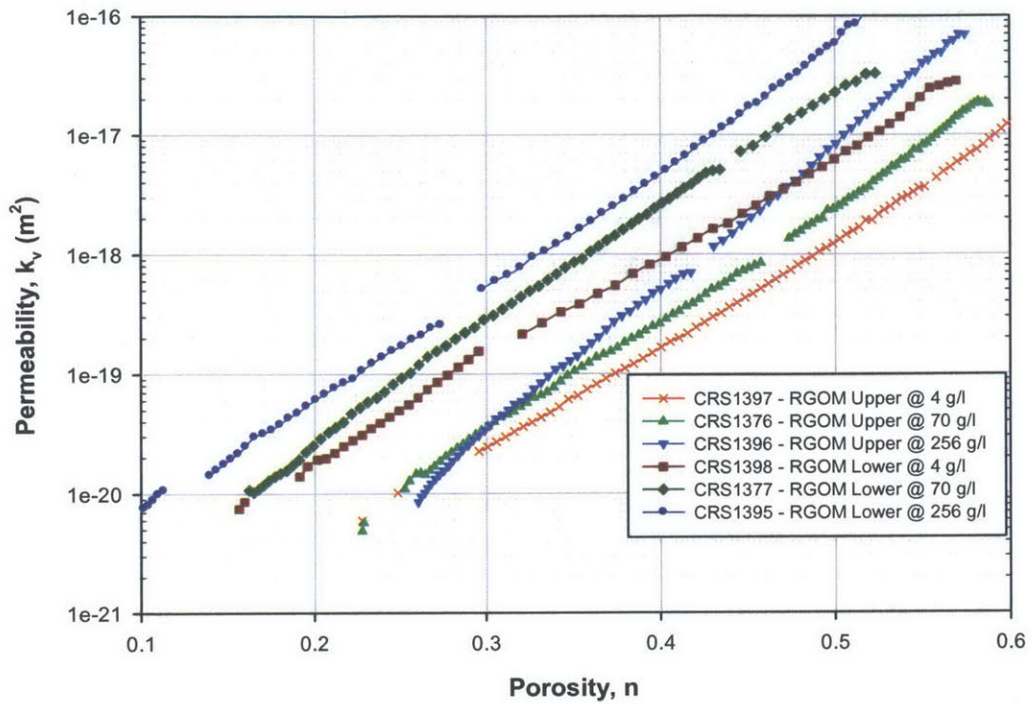


Figure 5.18 Permeability in porosity space for RGOM Upper and Lower at various pore fluid salinities

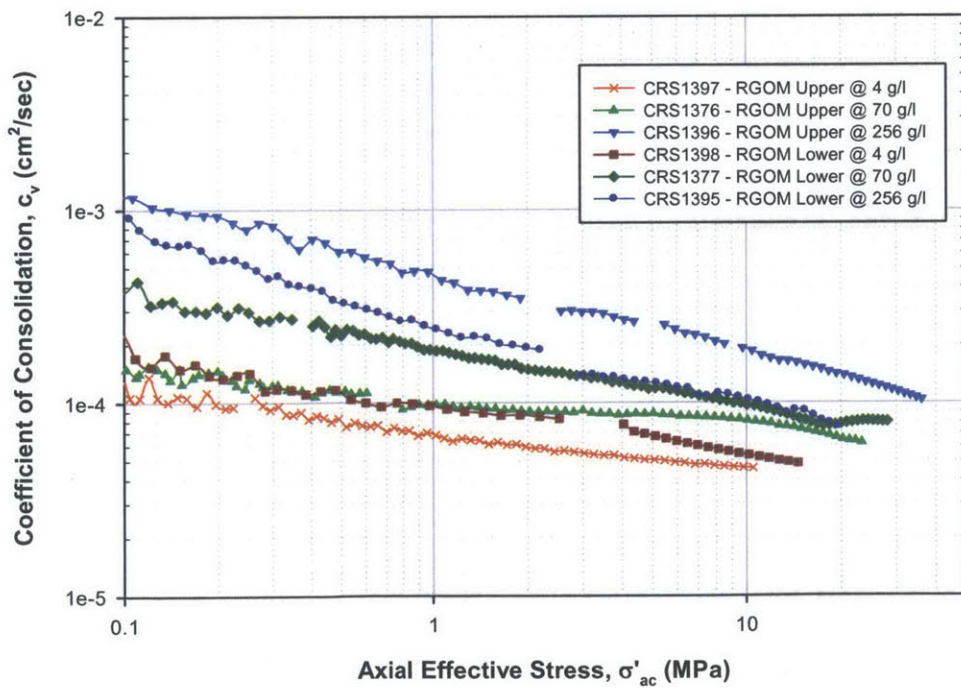


Figure 5.19 Coefficient of consolidation in $\log \sigma'_{ac}$ space for RGOM Upper and Lower at various pore fluid salinities

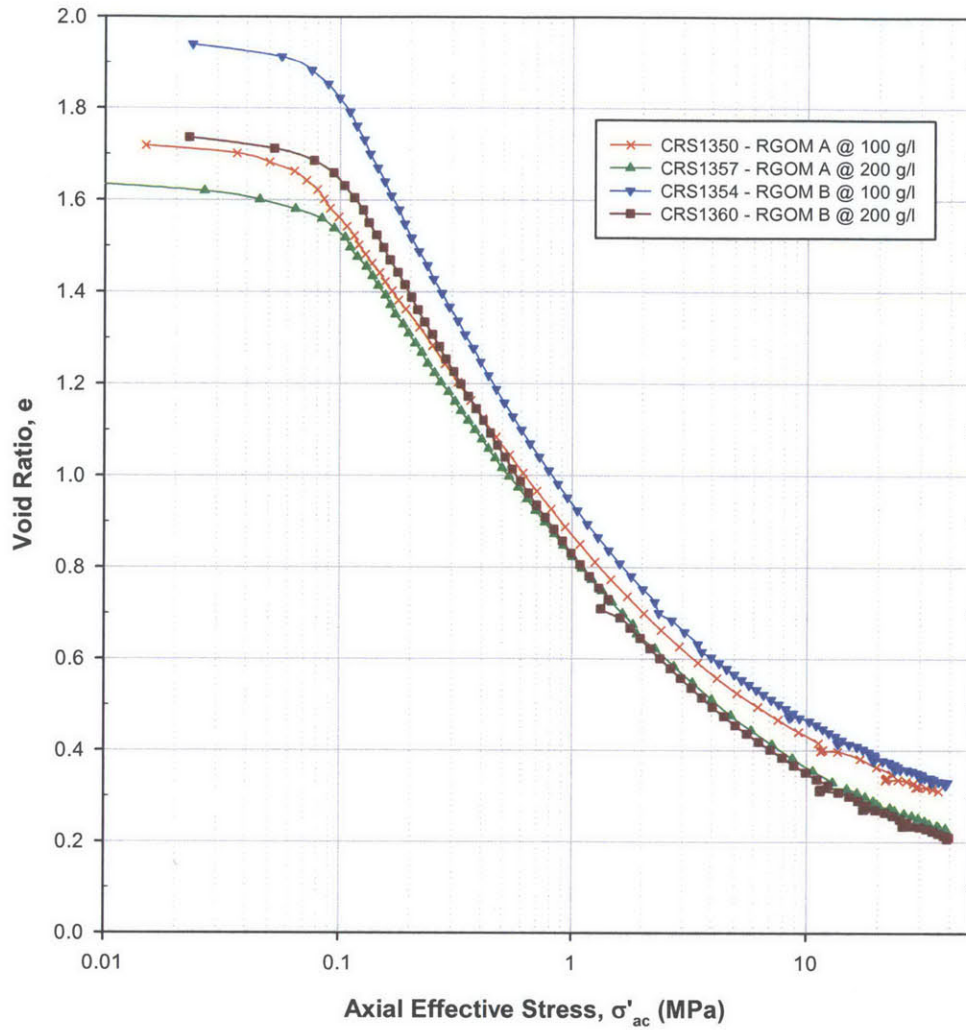


Figure 5.20 Compression behavior in $e - \log \sigma'_{ac}$ space for RGOM A and B at various pore fluid salinities

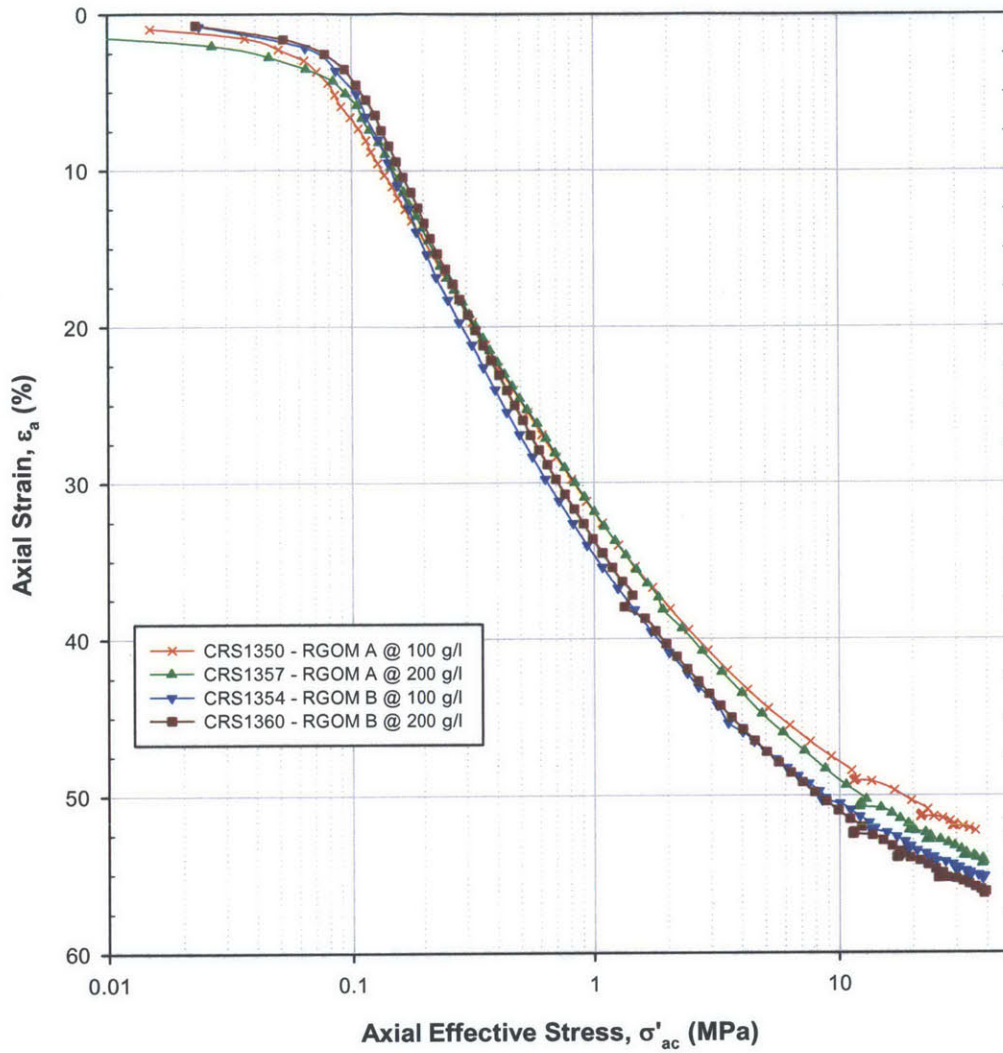


Figure 5.21 Compression behavior in $\epsilon_a - \log \sigma'_{ac}$ space for RGOM A and B at various pore fluid salinities

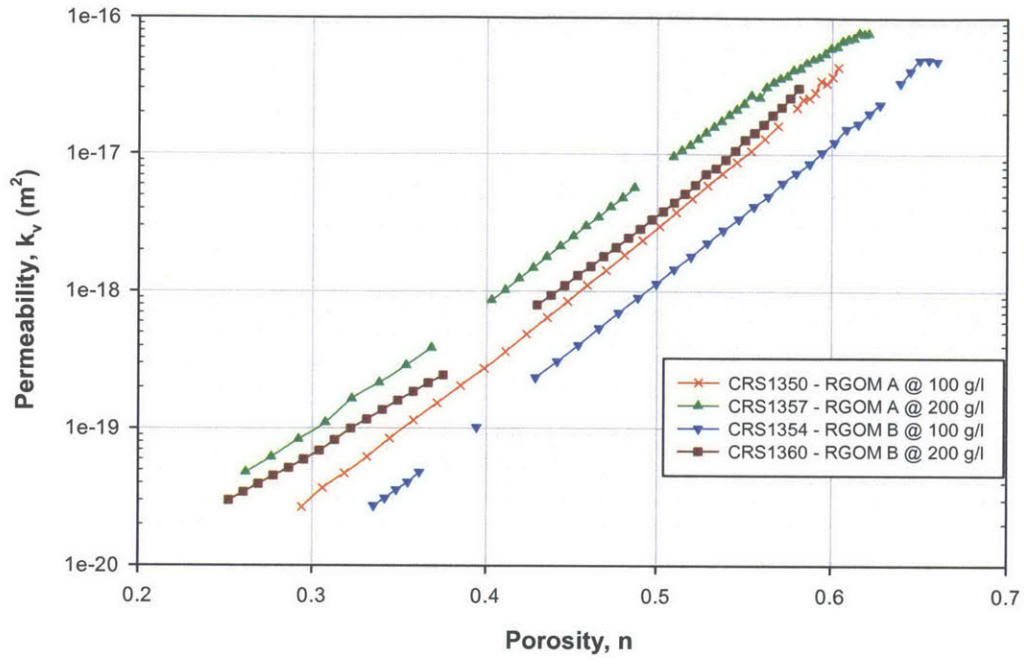


Figure 5.22 Permeability in porosity space for RGOM A and B at various pore fluid salinities

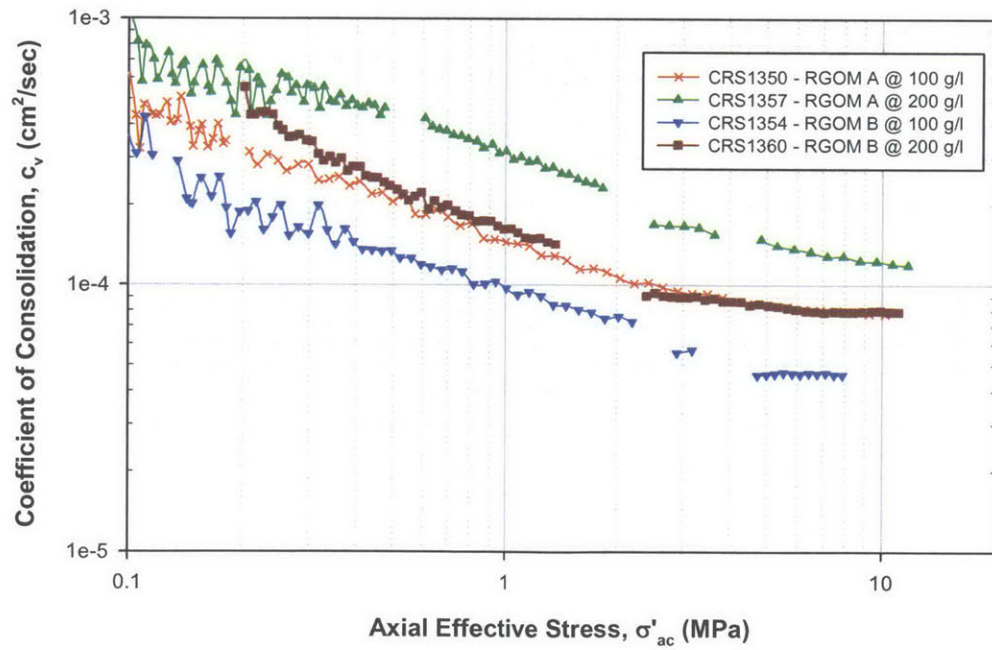


Figure 5.23 Coefficient of consolidation in $\log \sigma'_{ac}$ space for RGOM A and B at various pore fluid salinities

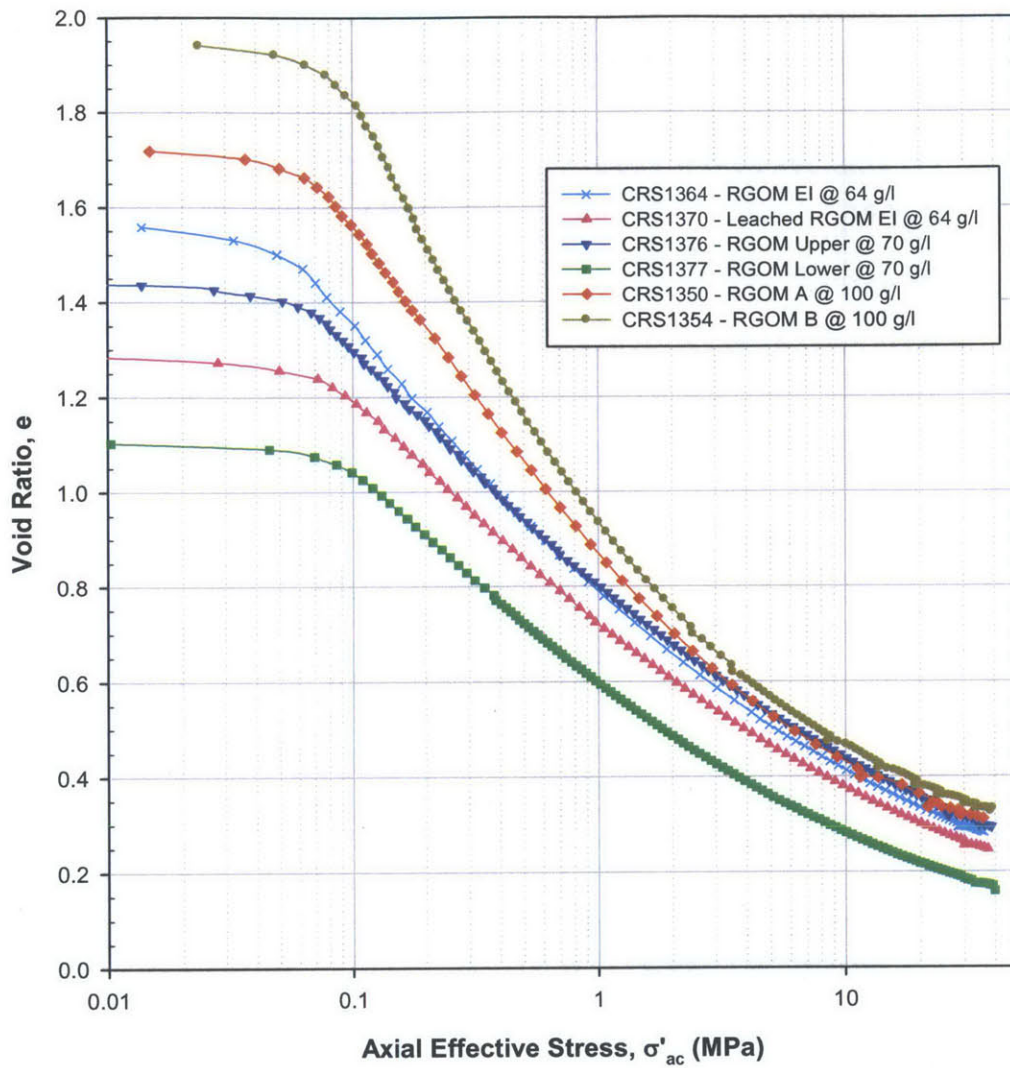


Figure 5.24 Compression behavior synthesis plot in $e - \log \sigma'_{ac}$ space for all soils in testing program

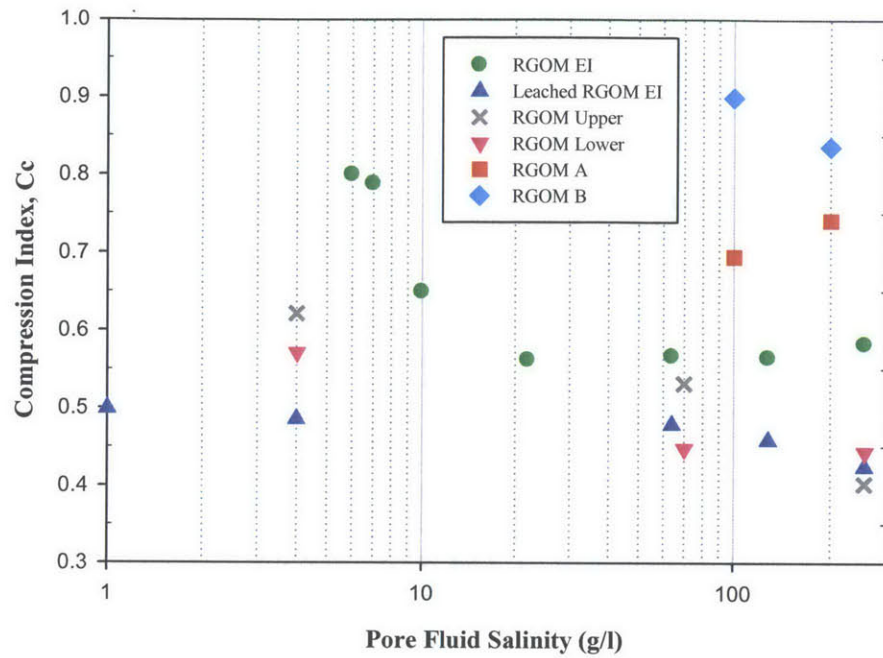


Figure 5.25 Compression Index versus salinity for all soils in test program averaged over a stress range from 0.1 to 1.0 MPa

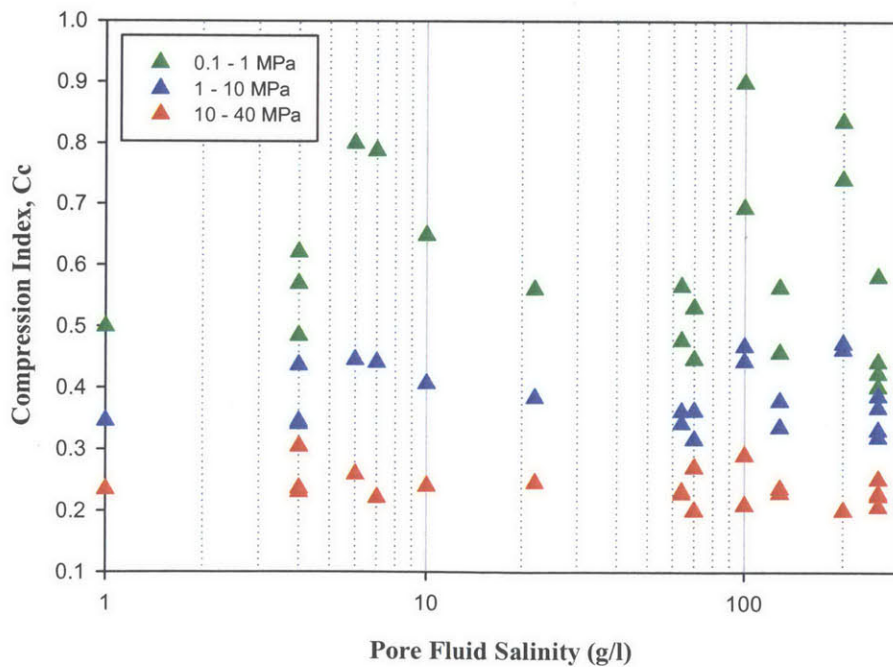


Figure 5.26 Compression Index versus salinity for all soils in test program averaged over three stress ranges (0.1 to 1 MPa data is the same as that shown in Figure 5.25)

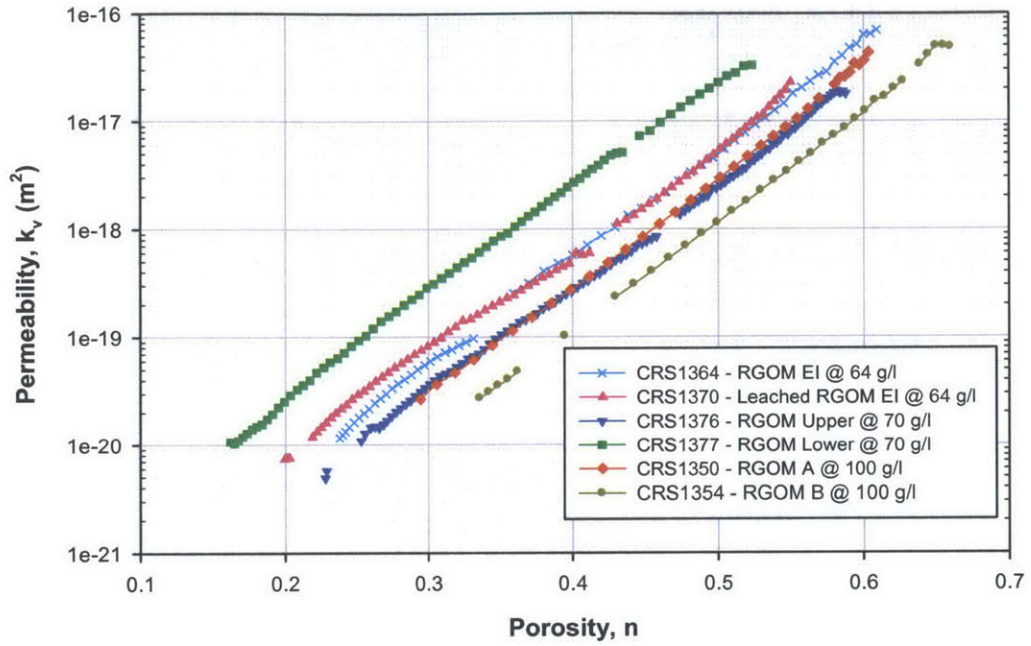


Figure 5.27 Permeability in porosity space synthesis plot for all soils in testing program

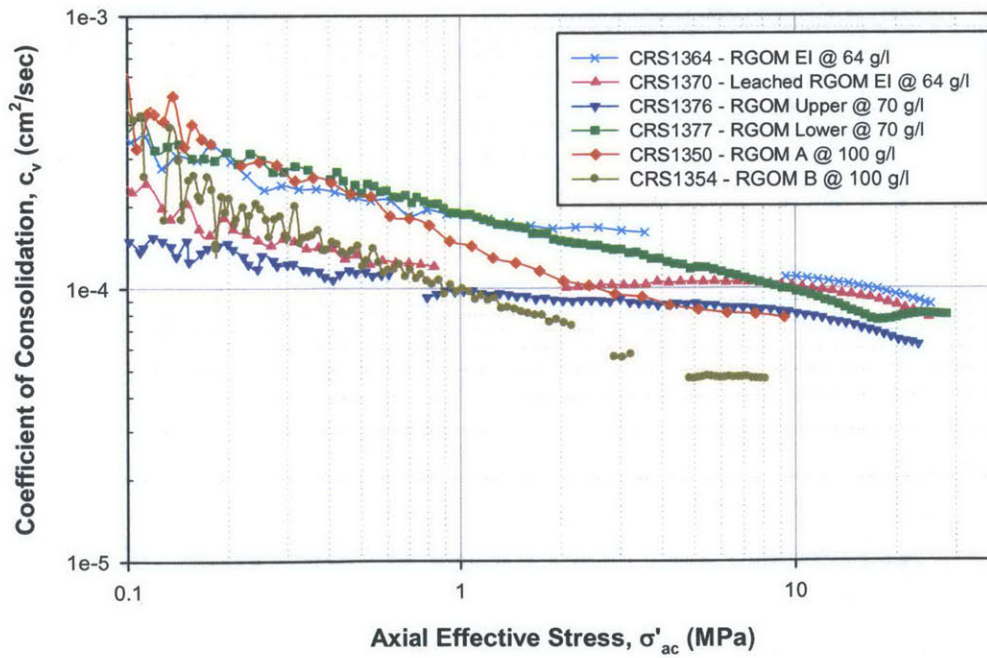


Figure 5.28 Coefficient of consolidation synthesis plot in $\log \sigma'_{ac}$ space for all soils in testing program

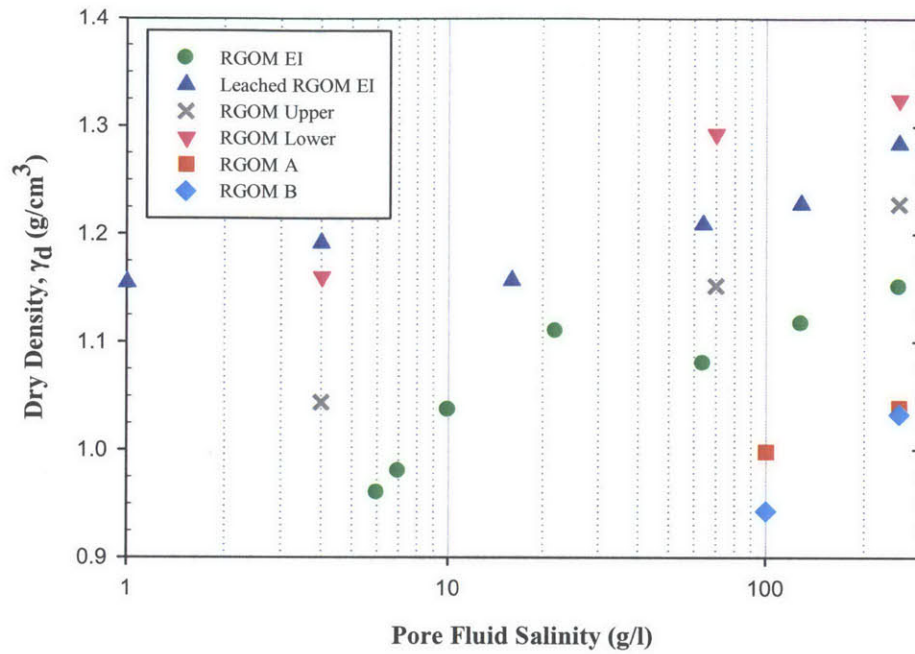


Figure 5.29 Relationship between pore fluid salinity and dry density for all soils in test program after consolidation to 0.1 MPa

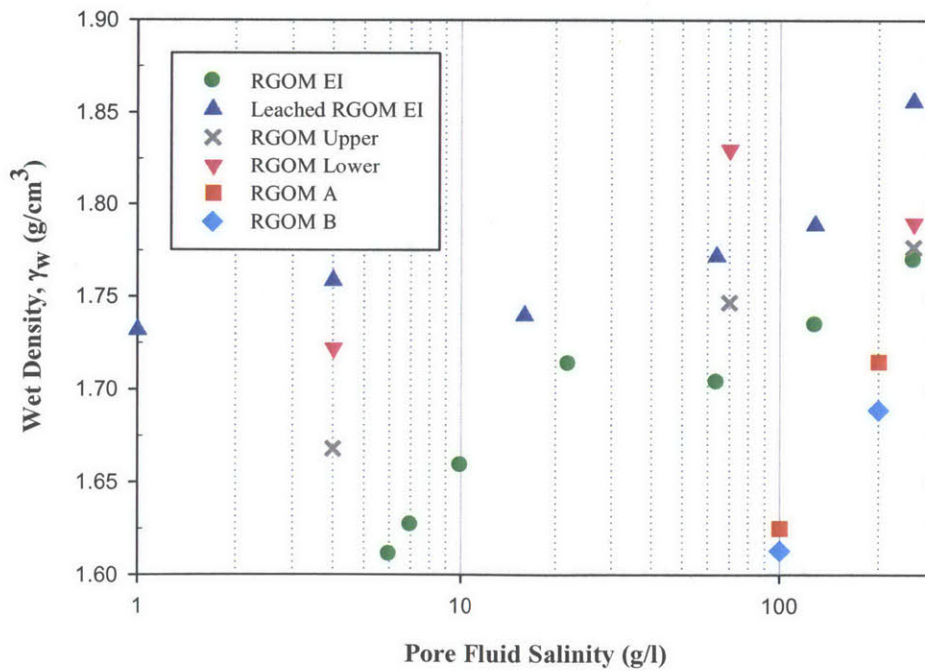


Figure 5.30 Relationship between pore fluid salinity and wet density for all soils in test program after consolidation to 0.1 MPa

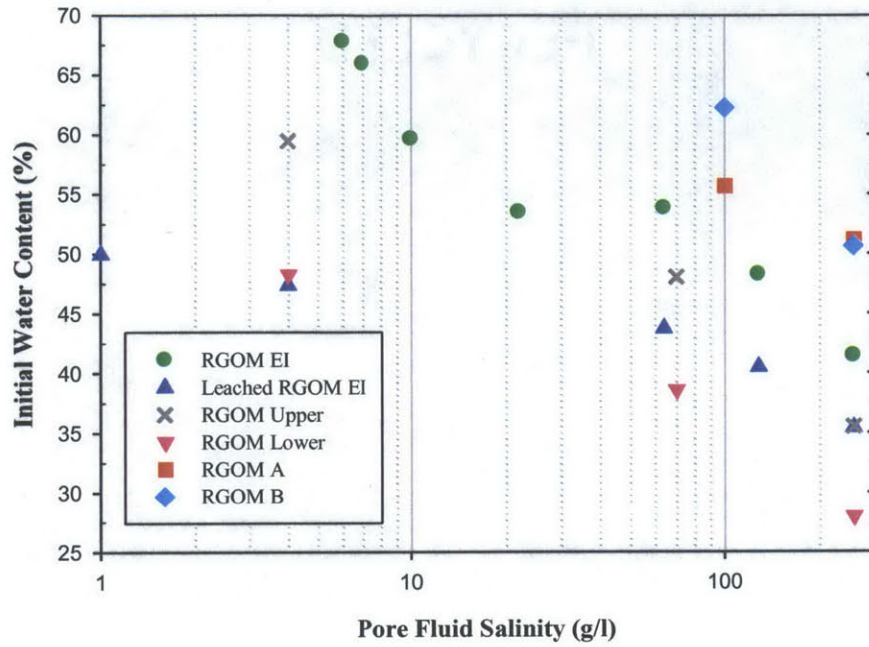


Figure 5.31 Relationship between pore fluid salinity and initial water content for all soils in test program after consolidation to 0.1 MPa

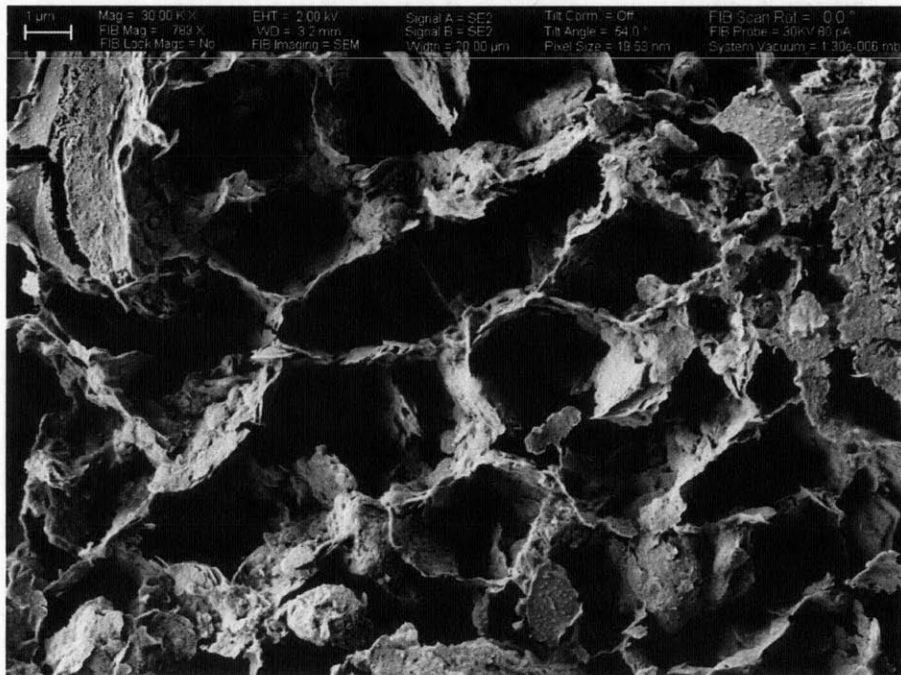
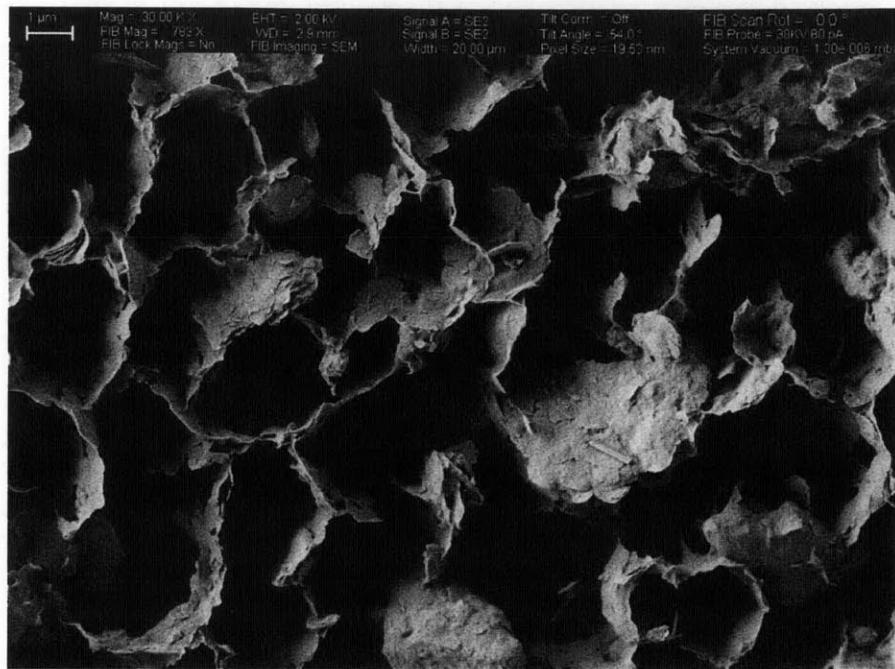


Figure 5.32 Cryo SEM images of GOM EI in a slurry state. Top: pore fluid salinity of 7 g/L, Bottom: pore fluid salinity of 64 g/L



Figure 5.33 Cryo SEM image of Leached GOM EI hydrated with distilled water in a slurry state

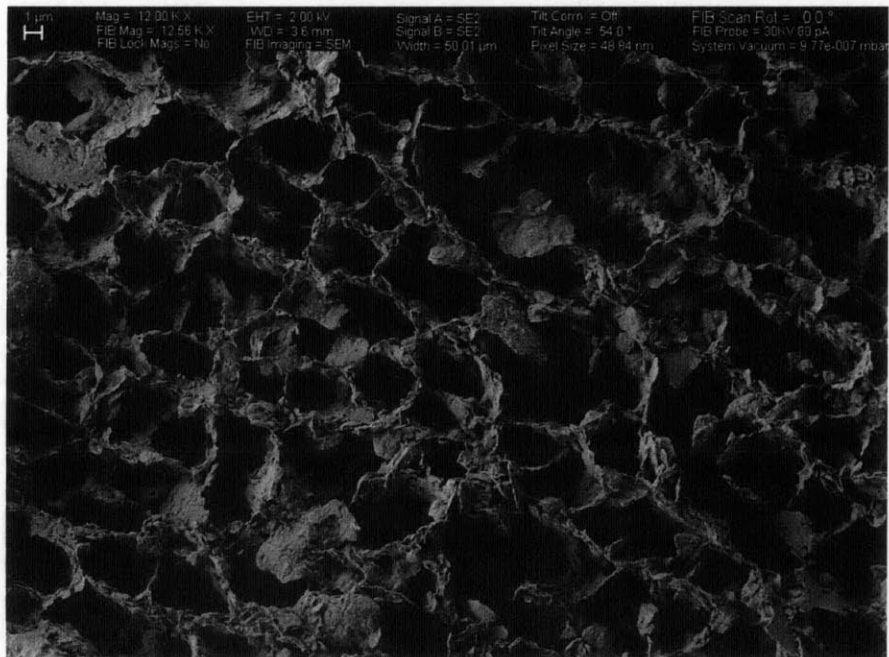


Figure 5.34 Cryo SEM image of Leached GOM EI in a slurry state. Pore fluid salinity is 64 g/L



Figure 5.35 Cryo SEM image of GOM EI in a slurry state. Pore fluid salinity is 64 g/L



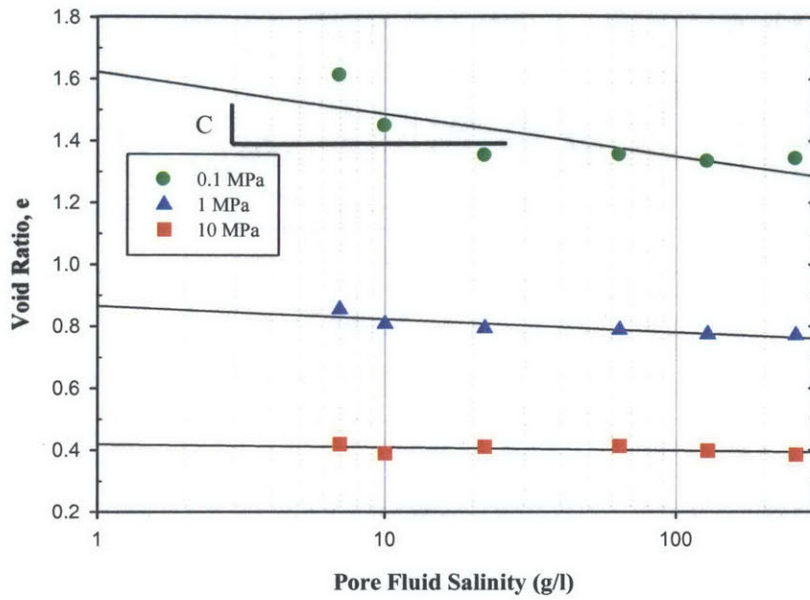


Figure 5.36 Void ratio as a function of pore fluid salinity for RGOM EI at 0.1 MPa, 1 MPa, and 10 MPa axial effective stress

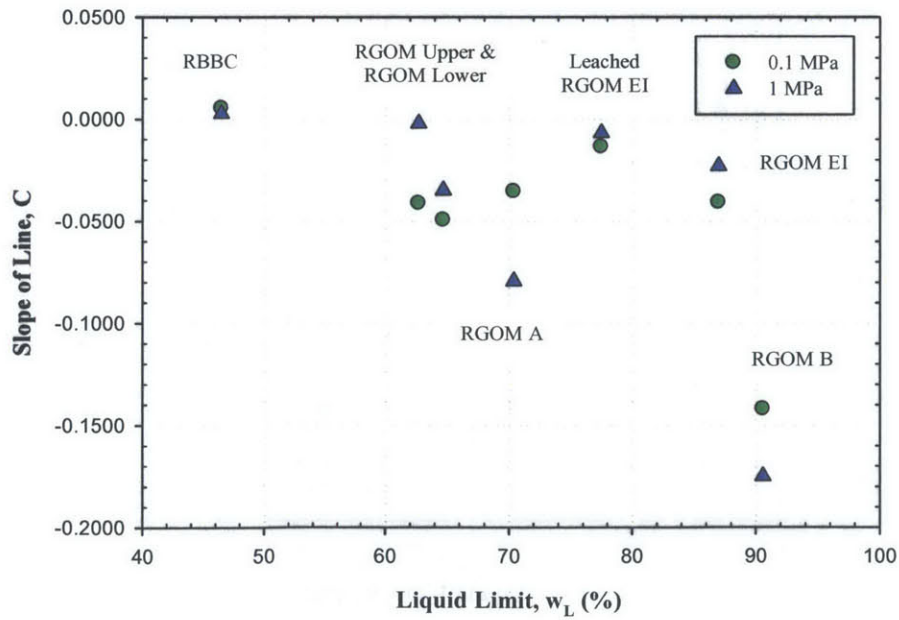


Figure 5.37 Correlation between the parameter C and liquid limit. The value of C generally decreases with liquid limit, indicating that compressibility sensitivity to salinity increases with liquid limit

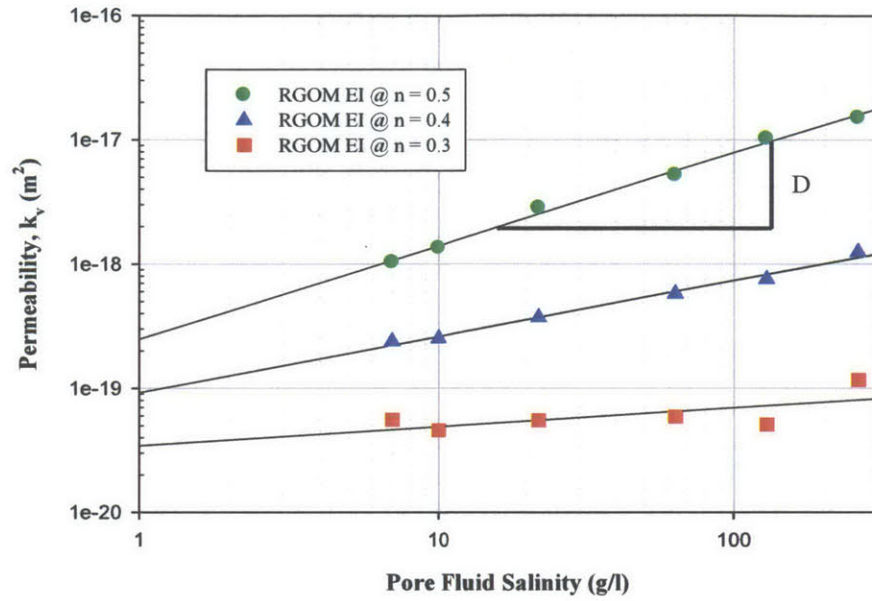


Figure 5.38 Permeability as a function of pore fluid salinity for RGOM EI at porosities of 0.5, 0.4, and 0.3

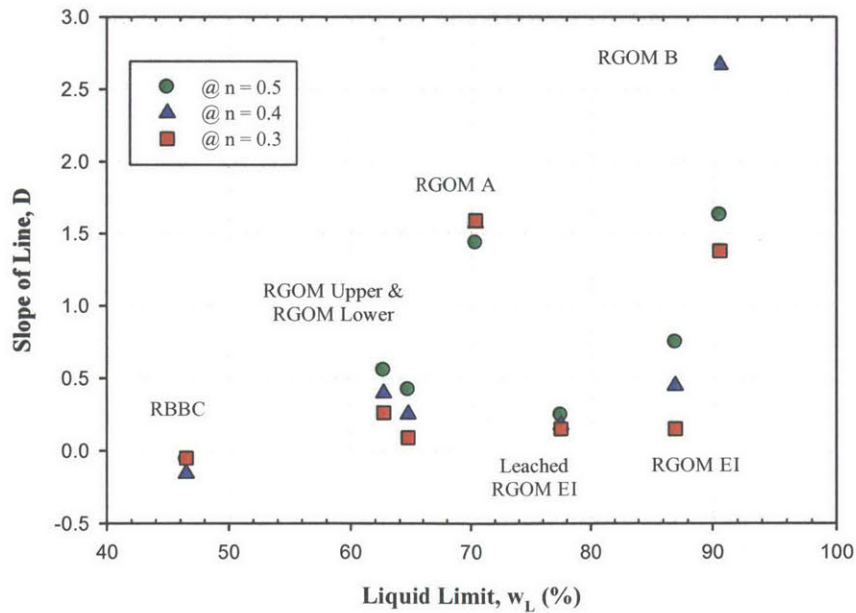


Figure 5.39 Correlation between the parameter D and liquid limit. The value of D generally increases with liquid limit, indicating that permeability sensitivity to salinity increases with liquid limit

6 TRIAXIAL TEST RESULTS

6.1 INTRODUCTION

This chapter presents the results of the experimental triaxial testing program carried out to investigate the stress dependent and salinity dependent behavior of RGOM EI. This is the first systematic triaxial study conducted on this particular soil. Resedimented specimens were sheared undrained in compression at a constant axial strain rate of 0.5 %/hr after K_0 -consolidation to axial consolidation effective stresses, $\sigma'_{ac} = 0.15 - 10$ MPa. One specimen was consolidated to 63 MPa prior to undrained shearing. This specimen was resedimented by the author and tested by Brendan Casey. A minimum period of 24 hours of secondary compression was allowed on the specimen prior to shearing. Behavior is examined at three different pore fluid salinities, namely; 4 g/L, 64 g/L, and 256 g/L. Of the 15 tests carried out, 9 tests were performed on natural RGOM EI and 6 tests were performed on Leached GOM EI. The majority of testing was conducted at 64 g/L. To investigate the behavior with changing salinity, tests at 4 g/L and 256 g/L were conducted at two greatly different consolidation stresses, namely, 0.4 and 10 MPa. For each test, the salinity of the fluid in both the device drainage lines and pore water PVA matched the pore fluid salinity of the specimen. The importance of this is described in Chapter 2. A problem occurred during the shearing phase of 3 tests where an external leak resulted in the specimen being sheared in a partially drained condition. Only relevant consolidation and friction angle data for these tests is therefore reported.

The results obtained from the K_0 consolidation stage of triaxial tests are presented in Section 6.2. In particular, the section summarizes measured compression behavior and the trend in K_0 with stress level and salinity.

Section 6.3 presents results from the undrained shear phase of triaxial tests. Correlations between the undrained strength properties and liquid limit are presented in Section 6.4.

Table 6-1 provides a list of all the triaxial tests performed, including details on the test number, the apparatus, the pre-shear consolidation conditions, and the pertinent stress-strain-strength parameters at peak shear stress and at maximum obliquity.

6.2 ONE DIMENSIONAL CONSOLIDATION BEHAVIOR

6.2.1 Introduction

The triaxial tests involved K_0 consolidation of RGOM EI resedimented specimens in three different triaxial devices (low stress, medium stress, and high stress) to stresses 2 times higher than the applied batch preconsolidation pressure. All triaxial specimens were K_0 consolidated so that the axial strain was greater than 10 % in accordance with SHANSEP recommendations.

6.2.2 Compression behavior during Consolidation

Figure 6.1 shows compression curves obtained during the K_0 consolidation stage of triaxial tests in e -log σ'_{ac} space for five GOM EI specimens with a pore fluid salinity of 64 g/L. The specimens were consolidated to maximum axial effective consolidation stresses, $\sigma'_{ac} = 0.125 - 9.759$ MPa. The 4 tests performed in the low stress triaxial device were first resedimented to nominal maximum vertical stresses of 0.1, 0.2, 0.4, and 1.0 MPa in the consolidometer before being unloaded to an OCR = 4 prior to extrusion; while the test performed in the medium stress triaxial device was resedimented to 2.0 MPa. This was done in order to control the consolidation strains in the triaxial apparatus. The maximum axial strains reached in both devices were about 13% (after one cycle of secondary compression). Both the low and medium stress triaxial devices can accommodate about 30% axial strain due to equipment restrictions (for specimens with standard initial height of 8.1 cm). Since at least 12% axial strain is needed during triaxial compression shearing to reach steady state values, the maximum allowable strain during consolidation is about 18%.

Each compression curve displays log-linearity in the normally consolidated range, however when viewed together, the C_c value changes with increasing stress level. This is similar to that observed in the CRS testing. There is relatively good repeatability observed for the

specimens consolidated to approximate axial effective consolidation stresses of 0.4, 0.9, and 2 MPa. However, both the lowest stress (0.125 MPa) and the highest stress (10 MPa) specimens are outliers as they show a smaller and larger stress capacity for a given void ratio, respectively. It is not clear what causes this difference in trends between the two tests, but the phase relation calculations suggest that this is not a void ratio error.

It can be seen from Figure 6.1 that the yield stresses of the compression curves appear to be lower than the preconsolidation pressures which were supposedly applied during the resedimentation process. The only exception to this is test TX1179. This observation is consistent with previous studies and can reasonably be attributed to friction acting between the soil sample and the sides of the consolidometer during resedimentation. The maximum stress applied to the sample during resedimentation, will be equal to the applied stress at the top and bottom of the sample (since the sample is allowed to consolidate from both ends, as described in Chapter 3) but will be reduced by side-wall friction with increasing distance away from the ends. During reconsolidation in the triaxial device the middle of the specimen therefore yields at stresses lower than the target batch stress, with yielding occurring progressively from the middle of the specimen towards the ends as the applied stress increases. This results in the lower preconsolidation pressures being observed for reconsolidation in the triaxial device (Casey, 2011). A small amount of disturbance caused during the process of extruding the samples from consolidometers may also contribute to reduced preconsolidation pressure. However, following the SHANSEP reconsolidation technique, any impact which these effects would have on undrained shear behavior is eliminated following K_0 consolidation in the triaxial device to stresses much higher than the batch preconsolidation pressure.

Figure 6.2 shows the pre-shear void ratio at the end of the consolidation phase for each triaxial test conducted on both the leached and natural GOM EI. As expected, the figure shows a consistent reduction in void ratio with increasing consolidation stress. At a nominal consolidation stress of 0.4 MPa, there is a clear trend of decreasing void with increasing salinity. There appears to be convergence in the range of void ratios at 10 MPa stress level with the general trend with salinity also evident at this stress. No definite trend is evident between the pre-shear void ratios of the leached and the natural specimens.

6.2.3 Consolidation Stress and Salinity Dependence of K_0

Figure 6.3 shows the change in K_0 during consolidation as measured in the same triaxial tests outlined in Section 6.2.2. The tests show a general trend of K_0 decreasing during the initial loading within the overconsolidated (OC) region until the preconsolidation pressure is reached. However, two different behaviors are observed in the normally consolidated region. TX1180 and TX1178 exhibit a levelling off of K_0 to a constant value in the normally consolidated region, whereas TX1214, TX1175, and TX1179 show an increase in the K_0 value from that of the preconsolidation pressure and continue to increase up to the end of the consolidation phase. Both behaviors have been observed on tests conducted on RBBC by a number of researchers. Casey (2011) and Abdulhadi (2009) reported a K_0 levelling off in the normally consolidated region where as Sheahan (1991) and Santagata (1994) observed the latter behavior. During the initial pressure-up and back-pressure saturation phases of a test, the OC specimen is subjected to almost isotropic stress conditions. The value of K_0 is therefore close to unity at the beginning of the consolidation phase. Note that in tests TX1175 and TX1178 a small deviator force was applied to the specimen at the start of consolidation and as a result K_0 starts at a value significantly less than 1 for these tests.

Figure 6.4 shows the values of K_0 at maximum stress obtained from all triaxial tests conducted. This K_0 value is taken as the average value recorded during secondary compression using the hold stress routine in the computer program. The axial effective stress ranges from 0.125 to 63.5 MPa. K_0 was found to range between a value of 0.547 and 0.9 for this stress range (taking all salinities into account) clearly showing that the value is strongly dependent on the consolidation stress level. This increase is significant, especially given the fact that the pre-shear value of K_0 will dramatically affect the values of undrained strength, as reported by Abdulhadi (2009) and discussed in the following section. The significance of these results can also be highlighted by comparison with RBBC values over a similar stress range. Previous research by Casey (2011) and Abdulhadi (2009) on RBBC found that for a stress range from 0.15 to 10 MPa, K_0 was found to increase from 0.518 to 0.564 only. For the same range in stress, the K_0 for RGOM EI at 64 g/L was observed to increase from 0.619 to 0.844.

The trend of increasing K_0 with increasing stress level is similar regardless of pore fluid salinity. With the only exception being the relatively large value obtained from test TX1180 at a salinity of 64 g/L. Comparisons between K_0 and salinity can be made at axial effective consolidation stresses of 0.4 and 10 MPa. At both stress levels, the Figure shows a clear trend of a reduction in K_0 with increasing salinity.

Tests were conducted on leached RGOM EI at the same 3 salinities and 2 stress levels. As can be seen in Figure 6.4, although there is a bit of scatter in the data making it hard to get trend lines, the leached soil shows a very clear trend with salinity and stress. However, there is no clear trend between the K_0 value of GOM EI and Leached RGOM EI at the same salinity and stress level.

The normally consolidated K_0 values presented here are the largest observed for laboratory testing on a wide variety of normally consolidated soils. These values are in agreement with the high K_0 values observed in the field from in-situ testing conducted in deep petroleum exploratory wells (Stump and Flemings, 2002).

6.3 UNDRAINED SHEAR BEHAVIOR

6.3.1 Introduction

This section presents results from the undrained shear phase of the triaxial tests. Shearing was performed at a constant axial strain rate of 0.5 %/hr in all tests. Prior to shearing, a leak check is performed as described in Section 4.4.4.2. This rate is sufficiently slow to ensure that pore pressures generated during undrained shearing are distributed uniformly across the specimen (Casey, 2011). For each test with a successful undrained shear phase,

Table 6-1 summarizes the test number, pre-shear consolidation conditions, as well as pertinent stress-strain parameters measured during shearing.

Each of the following sections describes the behavior of RGOM EI with respect to changes in stress, salinity, and fabric (Leached RGOM EI). Section 6.3.2 describes the stress-strain behavior and undrained strength results with particular attention given to the trends in undrained shear strength with consolidation stress. Details on the soils friction angle and observed trends with consolidation stress and salinity are discussed in Section 6.3.3. Section

6.3.4 describes the effective stress behavior during undrained compression shearing, while the soils stiffness properties are discussed in Section 6.3.5.

6.3.2 Shear Stress-Strain Behavior

Figure 6.5 shows shear stress-strain behavior ($q = (\sigma_1 - \sigma_3)/2$ vs. ϵ_a) measured during undrained shearing for five triaxial tests performed at different stress levels on RGOM EI at 64 g/L. The maximum axial consolidation stress is stated in the legend. The tests range between a consolidation stress of 0.126 and 9.759 MPa, with a maximum shear stress of 0.035 and 1.347 MPa respectively. As expected, undrained strength increases with increasing consolidation stress.

Figure 6.6 shows the same five tests given in Figure 6.5 but this time the shear stress has been normalized with respect to the pre-shear axial consolidation stress. There is a clear trend of decreasing normalized undrained strength with increasing consolidation stress. By observing the normalized shear stress behavior of the five tests at an axial strain of 5 % we see a greater decrease in the normalized shear stress at higher consolidation stress. The decrease in the normalized shear stress value between 0.126 and approximately 1 MPa consolidation stress is about 0.03 MPa. Whereas with a further ten-fold increase in consolidation stress to 9.759 MPa, the decrease in the value is rises to approximately 0.09 MPa. The stress-strain behavior also becomes more ductile with increasing stress level as the strain to failure (ϵ_f) increases. At a consolidation stress of 0.126 MPa failure occurs at 0.34 % axial strain, whereas at a consolidation stress of 9.759 MPa 5.03 % axial strain is required to reach failure. Figure 6.7 presents the same test results as Figure 6.6 but only up to an axial strain of 3 %. This Figure more clearly shows this observed trend with increasing consolidation stress. For consolidation stresses up to 0.4 MPa the tests show a post peak strain softening. At a consolidation stress of 1 MPa the behavior transitions to perfectly plastic. While at stresses of 2 and 10 MPa, the test specimens display strain stiffening, with the amount of stiffening increasing with increasing consolidation stress. Figure 6.8 shows the strain to failure for all tests conducted. The figure shows a clear trend of increasing strain to failure with increasing consolidation stresses for RGOM EI at 4 g/L and 64 g/L and Leached RGOM EI at 4 g/L. The successful undrained shear tests conducted at the three different salinities (4g/L, 64 g/L, and 256 g/L) at the relatively low

consolidation stress of approximately 0.4 MPa indicate that the strain to failure is independent of salinity. No successful undrained shear results are available for 256 g/L at 10 MPa to determine a trend in failure strain with salinity at this particular stress.

As mentioned above, there is a clear trend of decreasing normalized undrained strength with increasing consolidation stress for RGOM EI at 64 g/L salinity. This trend is also observed in the lower salinity soil of 4 g/L. Figure 6.9 shows the normalized undrained strength for all tests with respect to axial effective consolidation stress. It is observed that at a nominal consolidation stress of 0.4 MPa with an increase in salinity there is an increase in the soils normalized undrained shear strength. Both the leached and the natural GOM EI display this behavior. The behavior with salinity can be explained from the fact that for RGOM EI, at a stress of 0.4 MPa, specimens with higher salinities exist at lower void ratios and in turn have a denser stiffer soil matrix. There is no definitive trend in normalized strength between RGOM EI and Leached RGOM EI at a similar stress level. As with the permeability behavior described in Chapter 5, the influence of salinity may decrease with increasing consolidation stress. The two normalized undrained shear strengths at 10 MPa are insufficient to determine if the values at each salinity converge as stress increases, or if the value for 64 g/L at 10 MPa is an outlier. Further testing is required to confirm the trend with stress. The undrained strength of each test relative to its corresponding axial consolidation stress is presented in Figure 6.10. This figure illustrates the consistency in the test and the fact that the undrained shear strength changes a lot with increasing consolidation stress to 10 MPa. The relationship between the normalized undrained strength of a soil and its corresponding axial consolidation stress can be described by Equation 6.1:

$$s_u/\sigma'_{ac} = S_1 (1,000\sigma'_{P[MPa]})^T \quad (6.1)$$

This equation, developed by Casey (2013), is obtained by fitting a power law function through all the data in Figure 6.9. As shown in the Figure, the two fitting parameters S_1 and T are 0.677 and -0.161 respectively. Note that the values for parameters S_1 and T presented here are different to those presented by Casey and Fahy (2014) and Casey (2014); this is due to additional testing conducted by the author on RGOM EI since the publishing dates. Casey (2014) determined S_1 and T parameters of 0.600 and -0.148 respectively.

As previously stated in Section 6.2.3, a soils K_0 and normalized undrained shear strength are interlinked. Figure 6.11 illustrates the relationship between K_0 and s_u/σ'_{ac} for all the tests performed in this research. The figure shows as the K_0 increases there is a corresponding reduction in the normalized undrained strength, and this is independent of salinity. This relationship can be defined by the Equation 6.2:

$$s_u/\sigma'_{ac} = 0.580 - 0.517K_0 \quad (6.2)$$

A linear regression fit by Casey (2014) through data obtained on a wide variety of soils ranging in liquid limit from 26 to 87 % provided the following relationship:

$$s_u/\sigma'_{ac} = 0.560 - 0.48K_0$$

The relationship between normalized undrained shear strength and K_0 for RGOM EI is in general agreement to that determined by Casey (2014).

In each test a peak strength is reached followed by some degree of strain softening. The degree of post-peak strain softening reduces with increasing consolidation stress, as shown in Figure 6.6. A soils brittleness is defined as the ratio of its undrained shear strength over the shear strain resistance of the soil at $\epsilon_a = 10\%$. In other words, the peak shear strength over the residual shear strength. Figure 6.12 shows the brittleness of RGOM EI and Leached RGOM EI at the three salinities over the range of axial consolidation stresses. The main trend in the data shows that the soils brittleness decreases with increasing consolidation stress, with the only exception being the Leached RGOM EI at 4 g/L showing a very slight ratio increase from 1.026 to 1.038. Additionally, at a consolidation stress of 0.4 MPa there are indications that brittleness increases with increasing salinity for RGOM EI. However, there is no clear trend for the Leached RGOM EI at a similar stress. Due to the small amount of data presented and varying trends with natural and leached soil, further research is required to confirm what impact salinity has on the brittleness of RGOM EI. In general, once a stress of 1 MPa is exceeded, the values are all about 1.

6.3.3 Friction Angle

Figure 6.13 provides details of the friction angle measured during the undrained shearing phase for the same five tests outlined in Section 6.3.2. Similar to the normalized undrained strength, the friction angle at maximum obliquity (ϕ'_{mo}) decreases with increasing consolidation stress, from 27° at 0.125 MPa to 14° at 10 MPa. This observed large reduction results in an effective stress envelope that possesses significant curvature. An axial strain of between 8 and 10 % was required to obtain the maximum obliquity friction angle for the tests shown. Test TX1179 was terminated during the shearing phase prior to reaching the strain required to determine maximum obliquity and therefore the friction angle presented in Table 6-1 for this test has been extrapolated.

The relationship between friction angle at maximum obliquity and consolidation stress for all tests conducted is shown in Figure 6.14. With all salinities considered, the friction angle values decrease significantly from 28.2° to as low as 10.6° . This relationship can be defined by the following:

$$\phi'_{cs} = A(0.001\sigma'_{P[MPa]})^B \quad (6.3)$$

Similarly to the undrained strength, this equation also developed by Casey (2013), is obtained by fitting a power law function through all the data in Figure 6.14. As shown in the figure, the two fitting parameters A and B for RGOM EI are 7.23 and -0.159 respectively.

In terms of salinity, with the exception of RGOM EI at 4 g/L, the results suggest that an increase in friction angle occurs with increasing salinity for the lower consolidation stress of 0.4 MPa. In contrast, there is no clear trend with salinity at the higher stress of 10MPa. Therefore, based on the research, the impact of salinity on the friction angle of this high plasticity soil is small, but more testing is required to confirm the influence of salinity.

6.3.4 Effective Stress Behavior

Figure 6.15 shows the excess pore pressure ($u_e = \Delta u - \Delta\sigma_3$) generated during undrained shear normalized to the axial effective consolidation stress (σ'_{ac}) for the same five tests on RGOM EI at 64 g/L. The results show that the pore pressure response during shearing is similar

for tests consolidated between 0.125 MPa and 2 MPa. Each test shows a continuous rise in excess pore pressure to some axial strain and then taper off to a value of between 0.28 and 0.31. In contrast, test TX1179, with a higher consolidation stress of 10 MPa, develops larger excess pore pressures. As stated previously, this test was terminated prior to reaching steady state, and this is the reason for the observed continued increase in excess pore pressure without any tapering off. The behavior of the Leached RGOM EI is similar with no trend in pore pressures in salinity level.

The corresponding normalized shear induced pore pressures ($u_s = \Delta u - \Delta \sigma_{oct}$, where $\Delta \sigma_{oct} = (\sigma_1 + 2\sigma_2)/3$) are shown in Figure 6.16. The shear induced pore pressure isolates the change due to shear stress alone, removing the effect of the total stress path and starting K_0 value. The results differ from the excess pore pressures presented in Figure 6.15 whereby there is no distinct plateau in pore pressures; they are continually rising throughout the test. This continues for the entire shearing process and the values are still rising when the test is terminated. The magnitude of the shear induced pore pressures are similar to the excess pore pressures towards the end of shearing, ranging between 0.24 and 0.3 for the five tests shown in the figure. As the consolidation stress increases, there is a trend of initially negative shear induced pore pressures. The three tests consolidated to stresses up to 1 MPa have positive pressures generated throughout shearing. This behavior is indicative of the contractive behavior of NC soil. In contrast, tests TX1178 and TX1179 conducted on RGOM EI at 64 g/L with consolidation stresses of 2 MPa and 10 MPa respectively, in addition to TX1209 (4 g/L with $\sigma'_{ac} = 63.5$ MPa) initially develop negative pressure and gradually increase to become positive at low strains. This dilative behavior of NC soil at high consolidation stresses is similar to that observed in OC soils.

Combining stress-strain and pore pressure data, Figure 6.17 plots the effective stress paths for the five tests. The stress paths are drawn in normalized MIT q - p' space, i.e. $(\sigma_1 - \sigma_3)/2\sigma'_{ac}$ versus $(\sigma'_1 + \sigma'_3)/2\sigma'_{ac}$. For tests TX1180, TX 1214, and TX1175, which were sheared at consolidation stresses below 1 MPa, the general shape of the effective stress path measured remains similar. The initially low shear induced pore pressures causes the stress path to rise somewhat vertically. A clear yield point is then reached, after which the generation of large shear induced pore pressures causes the effective stress to decrease and the stress path to move to the left before reaching the large strain Mohr-Coulomb failure envelope. For tests TX1178 ($\sigma'_{ac} =$

1.959 MPa) and TX1179 ($\sigma'_{ac} = 9.759$ MPa), the initially negative shear induced pore pressures cause the effective stress paths for these tests to move progressively more to the right, as consolidation stress increases, prior to yield. Consistent with what was observed in Figure 6.6, the normalized shear strength decreases with increasing stress level. At low stress the yield point of the stress path coincides with peak shear strength. However, as the consolidation stresses increase the point of peak shear strength occurs further along the stress path and does not coincide with the yield point, i.e. peak shear strength occurs at a lower effective stress. This is in agreement with the observation of an increase in the required failure strain with increasing consolidation stress. Note that the different starting point for each of the effective stress paths shown in Figure 6.17 is due to different pre-shear values of K_0 . The shape of the effective stress path, as described above, is similar for all three salinities tested.

The pore pressures expressed here by the Skempton pore pressure parameter A ($A = (\Delta u - \Delta \sigma_3) / (\Delta \sigma_1 - \Delta \sigma_3)$) at peak shear stress (A_f), versus stress level is shown in Figure 6.18. The A_f value essentially indicates the orientation of the average effective stress at peak relative to its pre-shear stress value. The figure shows that A_f starts off from about 0.6 at low stress (0.125 MPa) and increases with stress level to a value of 3.0 at high stress (10 MPa). These larger values at high stress are due to the increased axial strain to failure with increasing stress and hence the generated pore pressures are greater. Additionally, as the peak point moves down (left) along the stress path, the A_f value increases. There is no trend in this parameter with the salinity of the soil.

6.3.5 Stiffness

Figure 6.19 plots the curves of normalized undrained secant Young's modulus (E_u / σ'_{ac}) versus axial strain on log scales for the five tests outlined in Section 6.3.2. The measurement of axial displacement in the tests was performed using an external LVDT and thus the measured stiffnesses are only considered reliable for ϵ_a above about 0.01 %. In general, the figure illustrates that the soil exhibits strong non-linearity and that yielding occurs at small strains. The decrease in stiffness is evident once the soil reaches failure as post-peak strain softening begins to occur. The results show a clear trend of decreasing stiffness with increasing consolidation stress. At a strain of 1 % the soil has a very similar stiffness over the stress range from 0.125

MPa to 2MPa, but a greatly reduced stiffness at a consolidation stress of 10 MPa. No trend in the normalized secant modulus with respect to salinity or changing the fabric of the soil by leaching is observed and therefore the results are not presented here.

6.4 STRENGTH CORRELATIONS WITH PLASTICITY

6.4.1 Introduction

As described in Chapter 2, Casey and Germaine (2013) developed correlations that allowed the undrained strength and friction angle of a fine grained soil, as well as a variation in these properties with stress level, to be estimated from the soils liquid limit. The variations in both properties can be described using a power law function containing two parameters, and it is these parameters that have been correlated to liquid limit. This section describes how the results presented here on RGOM EI fits the correlations.

6.4.2 Undrained Shear Strength Correlation

Figure 6.9 shows the variation of normalized undrained shear strength with axial consolidation stress in log scale for all tests conducted on RGOM EI and Leached RGOM EI. The data are fit with a power law function of the form:

$$s_u/\sigma'_{ac} = S_1 (1,000\sigma'_{p[MPa]})^T$$

The parameter S_1 is an intercept value and corresponds to the undrained strength ratio at an effective stress of 1 kPa. The T parameter describes the change in undrained strength ratio with effective stress level. The parameters $S_1 = 0.677$ and $T = -0.161$ for this particular soil. By plotting these two parameters against the soils liquid limit, it is clear that the results for undrained shear strength versus axial consolidation stress obtained by this research are in excellent agreement with the correlations. The T parameter with a negative value of -0.161, indicating a reduction in shear strength with stress level, is the largest value of all the soils in the data set, indicating that the very high plasticity RGOM EI has the largest strength rate decrease with stress level compared to all the other soils in which triaxial testing has been performed on at the MIT Geotechnical Laboratory. Figure 6.20 shows the correlation between each parameter and liquid limit for the wide range of soils with the values for RGOM EI represented by the red

triangular symbol. These soils range in liquid limit from 26 % in the case of Skibbreen Silt (SS) to the 87 % of RGOM EI. The relationship between each parameter and liquid limit are also shown in the Figure. Note that the values for parameters S_1 and T presented here are slightly different to those presented by Casey and Fahy (2014) and Casey (2014); this is due to additional testing conducted by the author on RGOM EI since the publishing dates.

The correlation between parameters S_1 and T with w_L (shown in the figure), are well approximated with r^2 of 0.97 and 0.95 respectively, by the following log-linear equations:

$$S_1 = 0.95 \log_{10}(w_L[\%]) - 1.18 \quad (6.4)$$

$$T = -0.47 \log_{10}(w_L[\%]) + 0.75 \quad (6.5)$$

Note that due to the additional testing mentioned above, the values in the above equations differ slightly from those presented by Casey (2014).

6.4.3 Friction Angle Correlation

Figure 6.14 shows the variation of friction angle at maximum obliquity with axial consolidation in log scale for all tests conducted in this research. Similar to the undrained strength, the data are fit with a power law function of the form:

$$\phi'_{cs} = A(0.001\sigma'_{P[MPa]})^B$$

Again, two parameters are used to determine the friction angle. The parameter A is an intercept value and corresponds to a friction angle (non-measured) at an effective stress of 1000 MPa. The B parameter describes the change in ϕ'_{cs} with effective stress level. For this soil the parameters are; $A = 7.23$ and $T = -0.159$. Figure 6.21 shows the correlation between each parameter and liquid limit for the same soils with the values for RGOM EI again represented by the red triangular symbol. Similar to the T parameter, the B parameter is the largest negative value in the data set, giving RGOM EI the largest rate of friction angle decrease with stress level among all the soils.

The correlation between parameters A and B with w_L (shown in the figure), are closely approximated with r^2 of 0.89 and 0.95 respectively, by the following log-linear equations:

$$A = -74\log_{10}(w_{L[\%]}) + 146 \quad (6.6)$$

$$B = -0.39\log_{10}(w_{L[\%]}) + 0.58 \quad (6.7)$$

For the same reason outlined above, the A and B parameters in these equations differ very slightly from those presented by Casey (2014).

The agreement of the results presented in this research with the undrained shear strength and friction angle correlations have great practical relevance for engineering practice as they allow for a reasonable estimate of these properties for a soil based on its liquid limit together with the in-situ preconsolidation stress. This reduces the need to perform laboratory tests on intact samples obtained from the field.

Test No.	Resed. Number	Device	Soil Type	Salinity (g/l)	Pre-shear Conditions			At Peak Stress				At Maximum Obliquity		
					σ'_{ac} (Mpa)	Void Ratio, e	K_0	ϵ_a (%)	q/σ'_{ac}	A_f	ϕ'_p	q/σ'_{ac}	p'/σ'_{ac}	ϕ'_{mo}
TX1180	RS348	MIT04	RGOM EI	64	0.126	1.103	0.619	0.34	0.276	0.62	20.7	0.222	0.511	26.9
TX1214	RS407	MIT03	RGOM EI	64	0.380	0.945	0.595	0.48	0.270	0.60	20.3	0.225	0.539	26.1
TX1175	RS354	MIT04	RGOM EI	64	0.878	0.757	0.655	1.91	0.238	1.18	19.4	0.216	0.563	22.8
TX1178	RS355	MIT03	RGOM EI	64	1.959	0.641	0.698	3.24	0.231	1.22	18.3	0.215	0.627	20.2
TX1179	RS351	MIT13	RGOM EI	64	9.759	0.496	0.805	5.02	0.138	3.02	12.5	0.136**	0.581**	13.6**
TX1182	RS364	MIT03	RGOM EI Leached	64	0.379	0.956	0.626	0.39	0.263	0.60	19.2	0.237	0.589	23.9
TX1192*	RS365	MIT13	RGOM EI Leached	64	9.885	0.509	0.828	-	-	-	9.8	-	-	11.5
TX1183	RS349	MIT04	RGOM EI	256	0.387	0.747	0.552	0.28	0.282	1.30	24.9	0.180	0.493	28.3
TX1195*	RS363	MIT13	RGOM EI	256	9.814	0.402	0.725	-	-	-	14.4	-	-	14.4
TX1186	RS375	MIT04	RGOM EI Leached	256	0.386	0.776	0.547	0.32	0.293	0.57	23.0	0.241	0.559	28.2
TX1206*	RS376	MIT13	RGOM EI Leached	256	9.792	0.334	0.779	-	-	-	10.6	-	-	10.6
TX1199	RS378	MIT03	RGOM EI	4	0.333	1.076	0.680	0.45	0.236	1.85	21.9	0.191	0.455	26.7
TX1209***	RS379	MIT09	RGOM EI	4	63.445	0.312	0.900	6.90	0.110	2.65	10.4	0.103	0.500	11.9
TX1201	RS382	MIT03	RGOM EI Leached	4	0.372	0.979	0.649	0.36	0.237	1.53	18.0	0.189	0.565	23.2
TX1213	RS383	MIT13	RGOM EI Leached	4	9.797	0.479	0.844	4.34	0.160	2.05	13.2	0.142	0.558	14.3

Notes: *External leak developed during shear, **Extrapolated data, ***Test carried out by Brendan Casey

Table 6-1 List of CK_0UC triaxial tests performed on Normally Consolidated RGOM EI and Leached RGOM EI

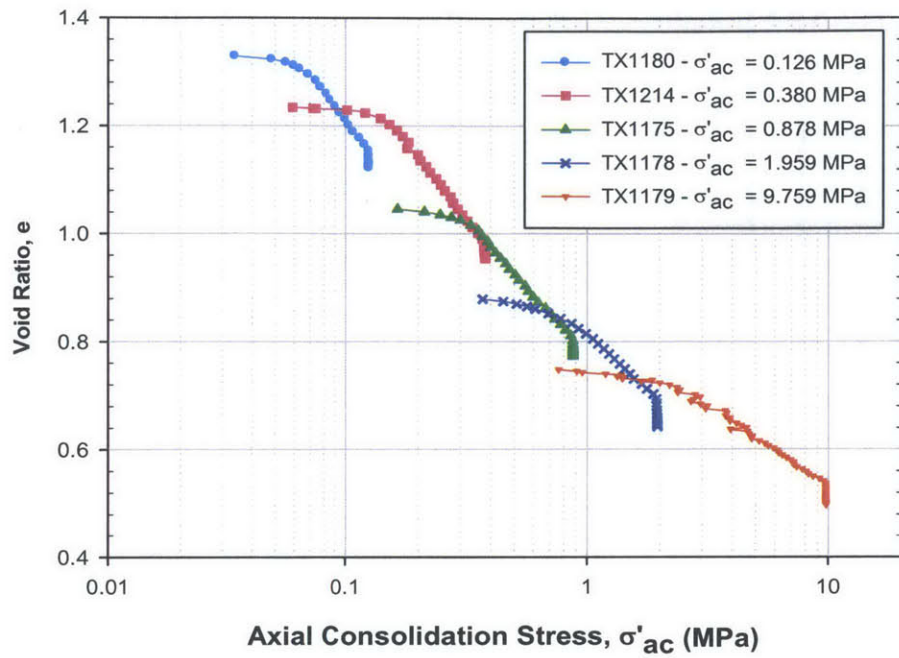


Figure 6.1 1-D compression behavior in e - $\log \sigma'_{ac}$ space for RGOM EI at 64 g/L from triaxial tests

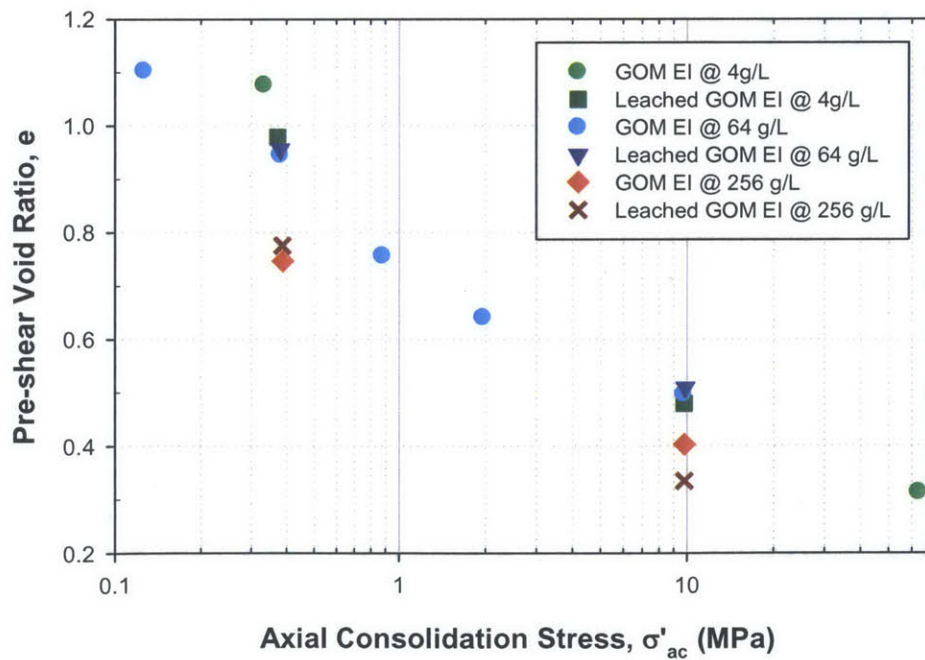


Figure 6.2 Pre-shear void ratio versus axial consolidation stress for RGOM EI and Leached RGOM EI at three salinities from CK₀UC triaxial tests

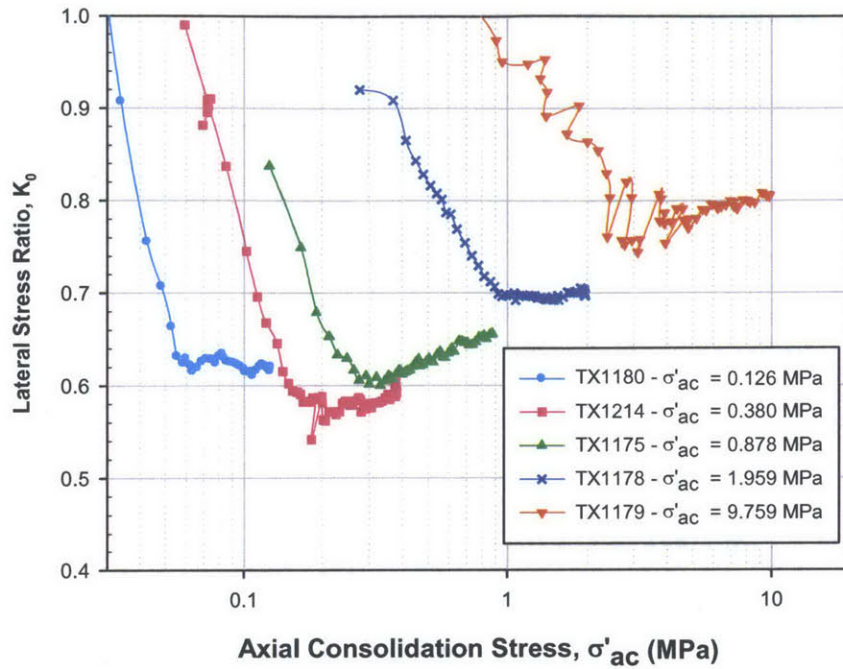


Figure 6.3 The variation in K_0 with stress level as measured during the consolidation stage of triaxial tests for RGOM EI at 64 g/L

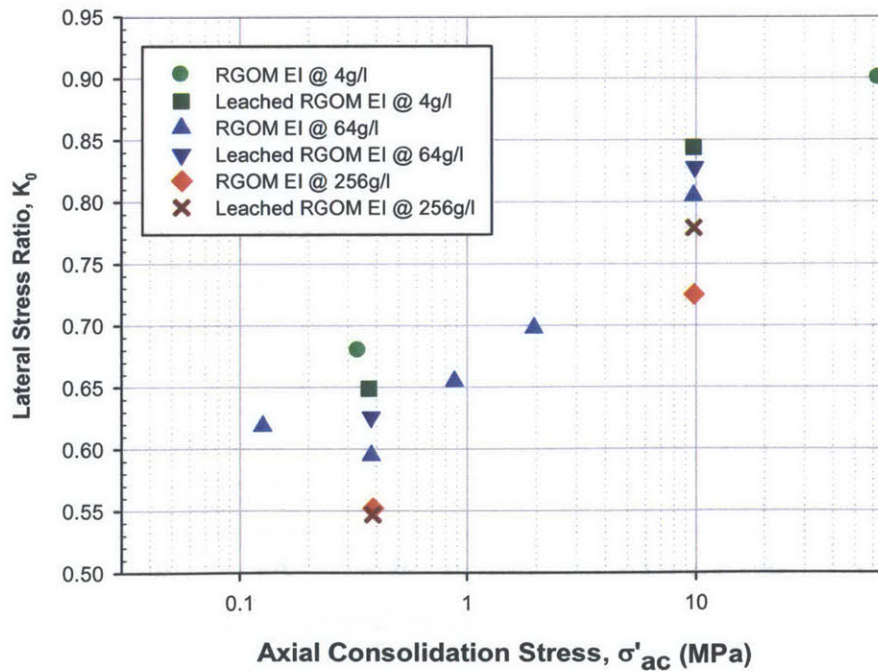


Figure 6.4 Lateral stress ratio at the end of virgin consolidation versus stress level for RGOM EI and Leached RGOM EI at three salinities from NC CK₀UC triaxial tests

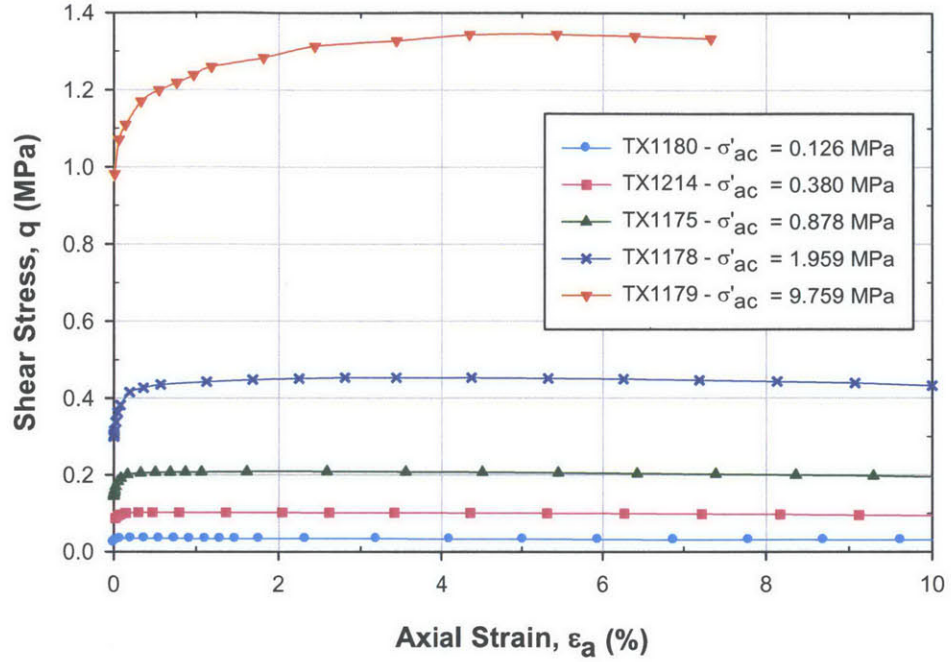


Figure 6.5 Stress-strain curves for RGOM EI at 64g/L salinity

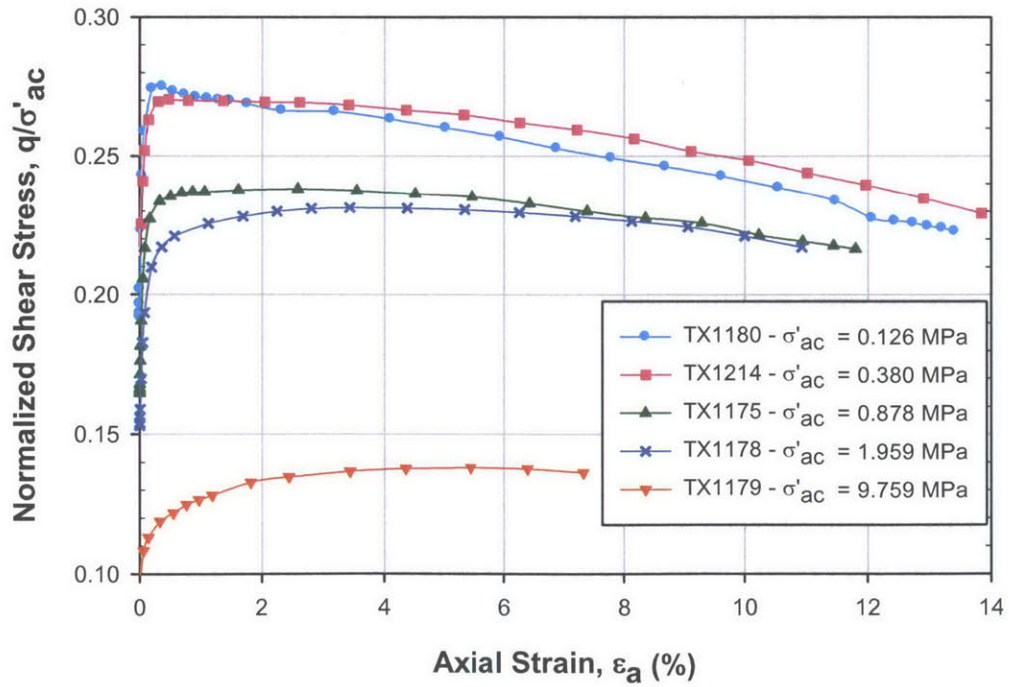


Figure 6.6 Normalized stress-strain curves for RGOM EI at 64g/L salinity

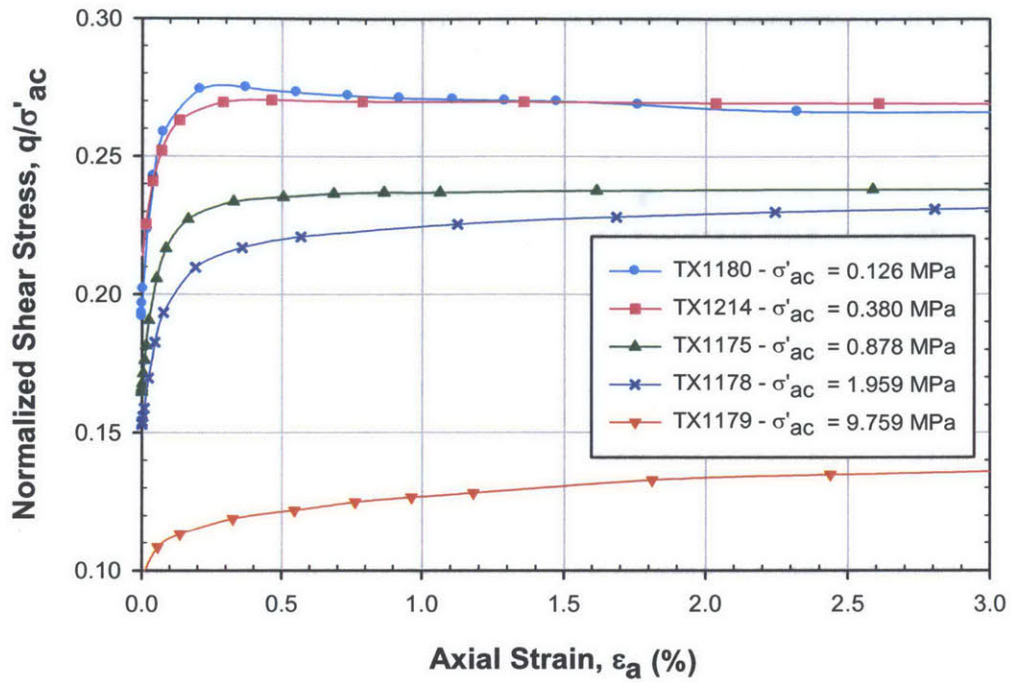


Figure 6.7 Normalized stress-strain curves (small strains) for RGOM EI at 64g/L salinity

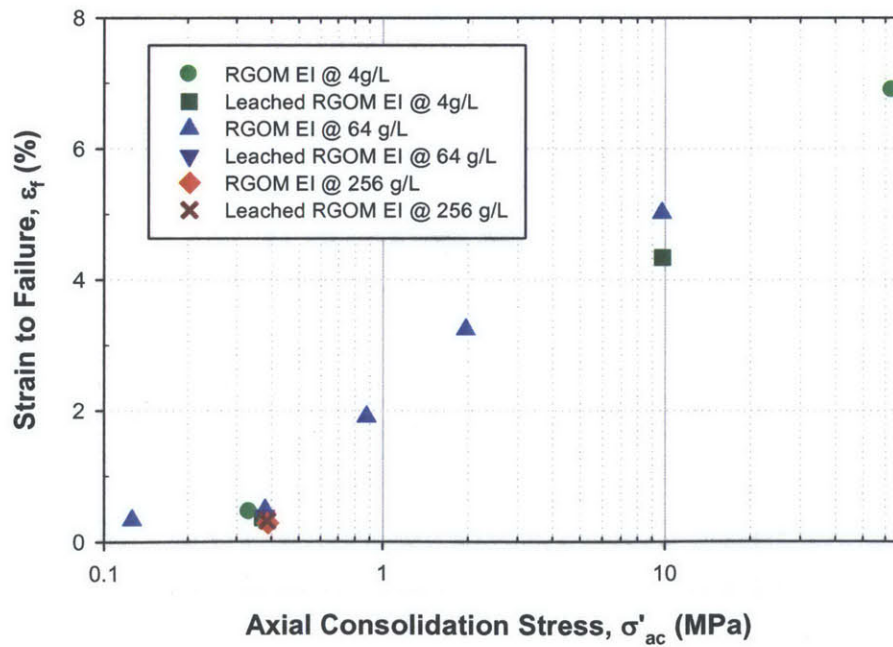


Figure 6.8 Strain at failure versus stress level for RGOM EI & Leached RGOM EI at three salinities

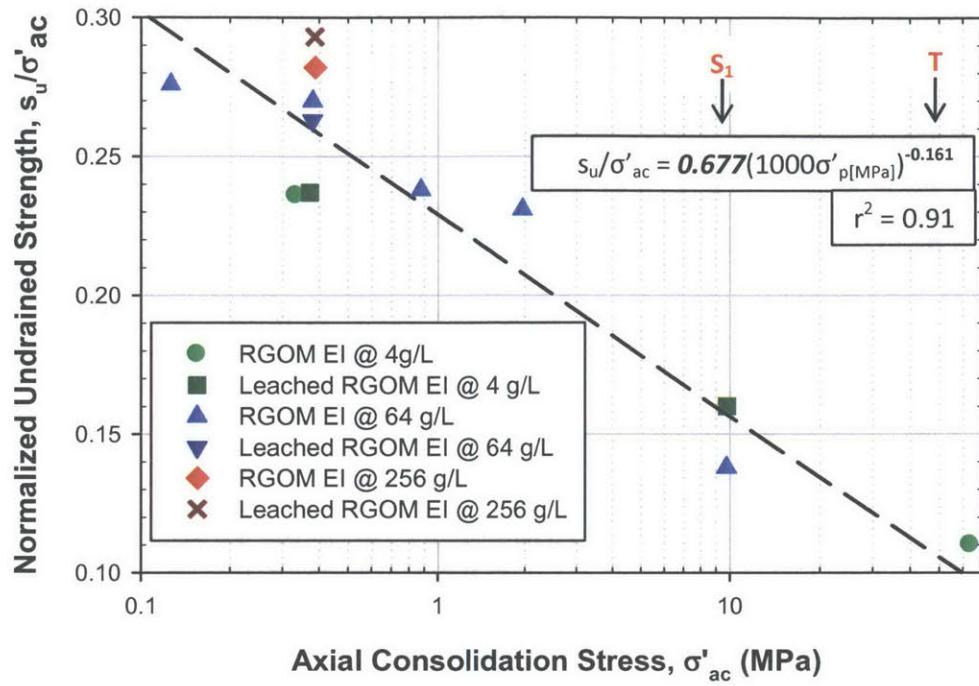


Figure 6.9 Normalized undrained shear strength versus stress level for RGOM EI & Leached RGOM EI at three salinities

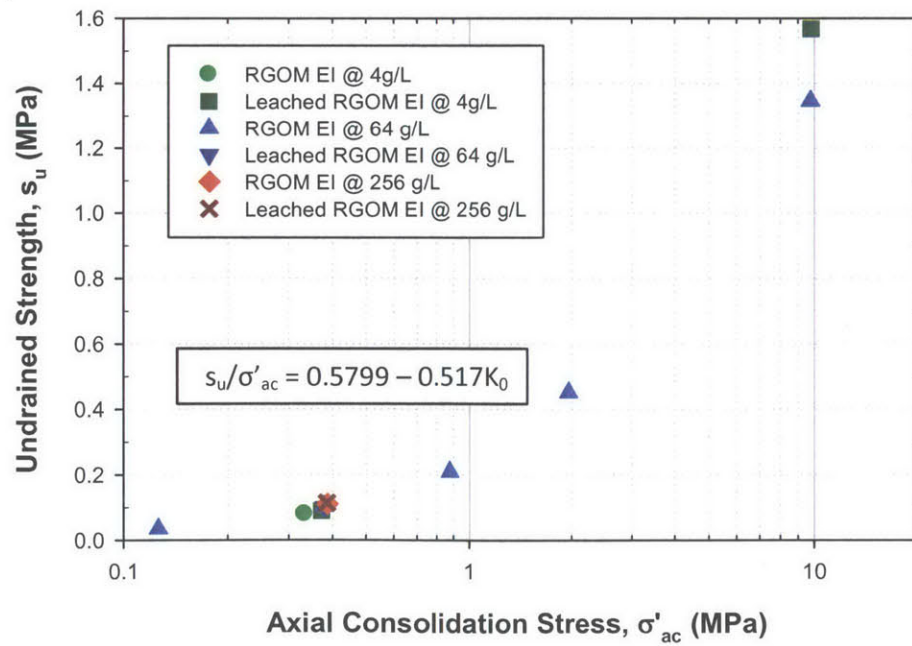


Figure 6.10 Undrained shear strength versus stress level for RGOM EI & Leached RGOM EI at three salinities

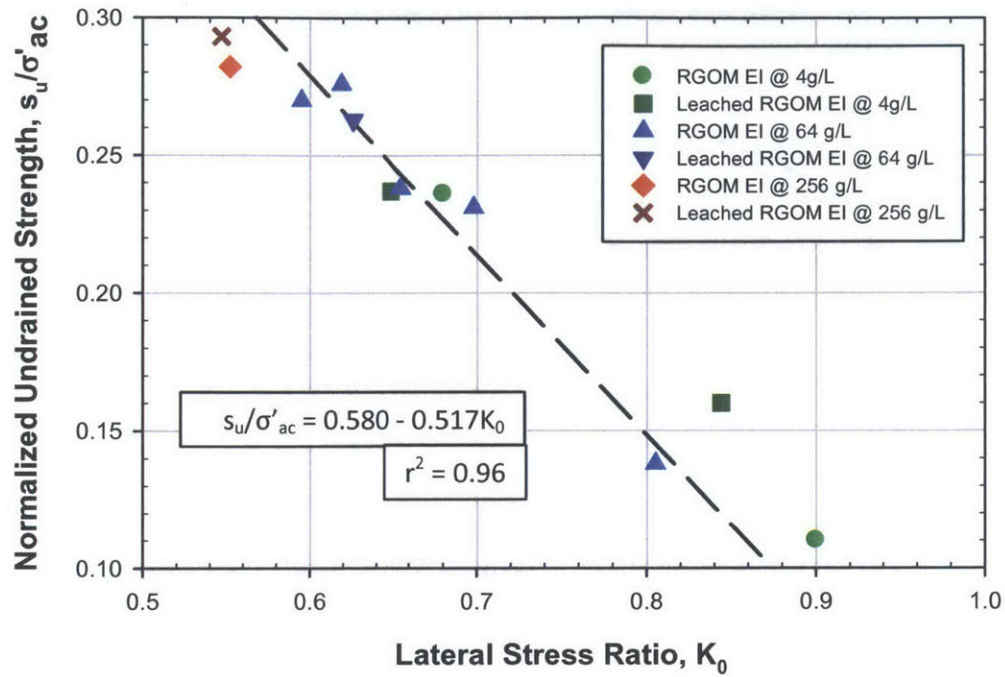


Figure 6.11 Normalized undrained shear strength versus lateral stress ratio for RGOM EI & Leached RGOM EI at three salinities

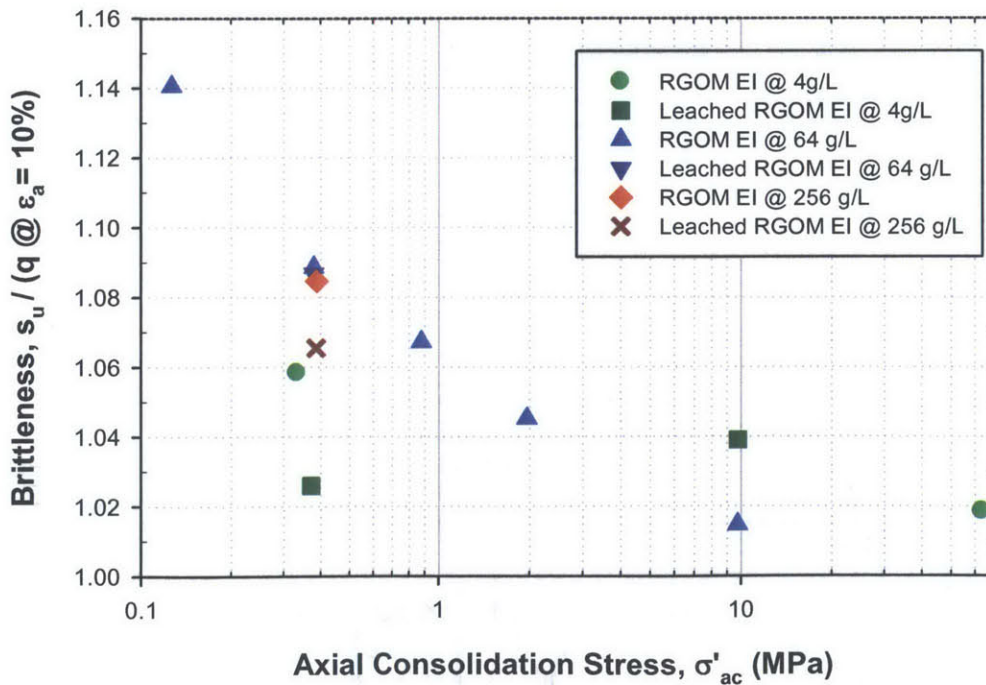


Figure 6.12 Brittleness versus stress level for RGOM EI & Leached RGOM EI at three salinities

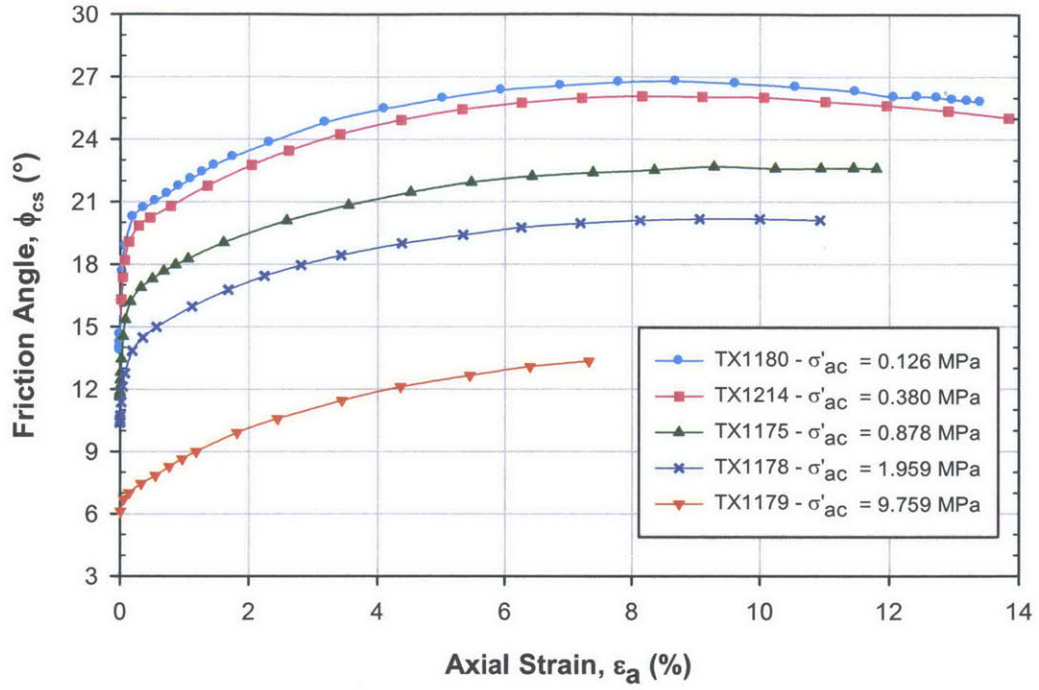


Figure 6.13 Friction angle versus axial strain for RGOM EI at 64 g/L

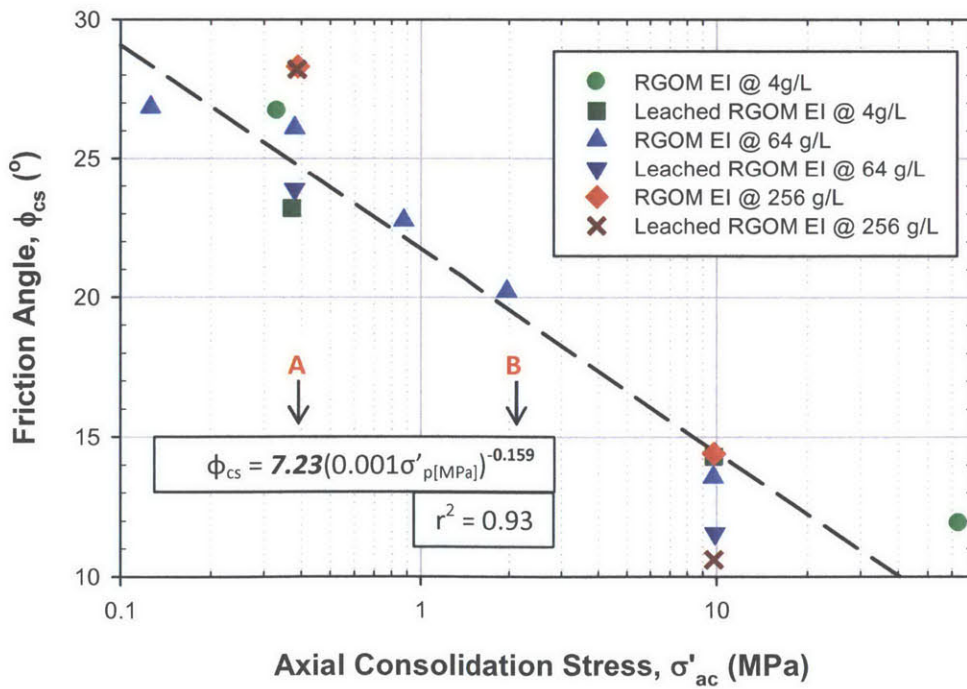


Figure 6.14 Friction angle at maximum obliquity versus stress level for RGOM EI & Leached RGOM EI at three salinities

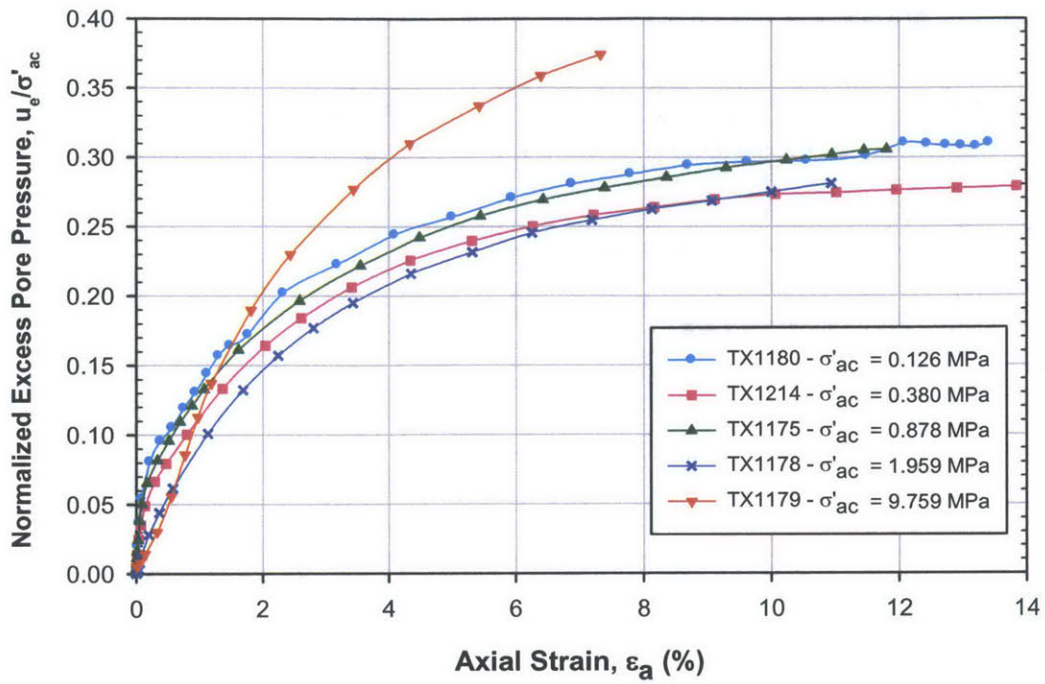


Figure 6.15 Normalized excess pore pressure versus axial strain for RGOM EI at 64 g/L salinity

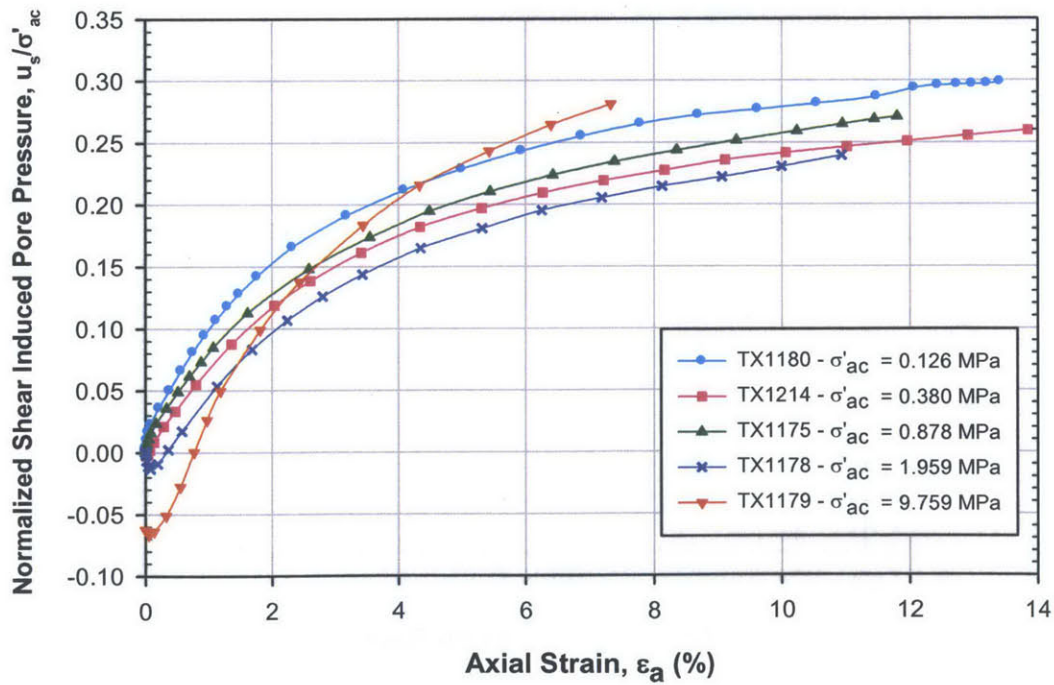


Figure 6.16 Normalized shear induced pore pressure versus axial strain for RGOM EI at 64 g/L salinity

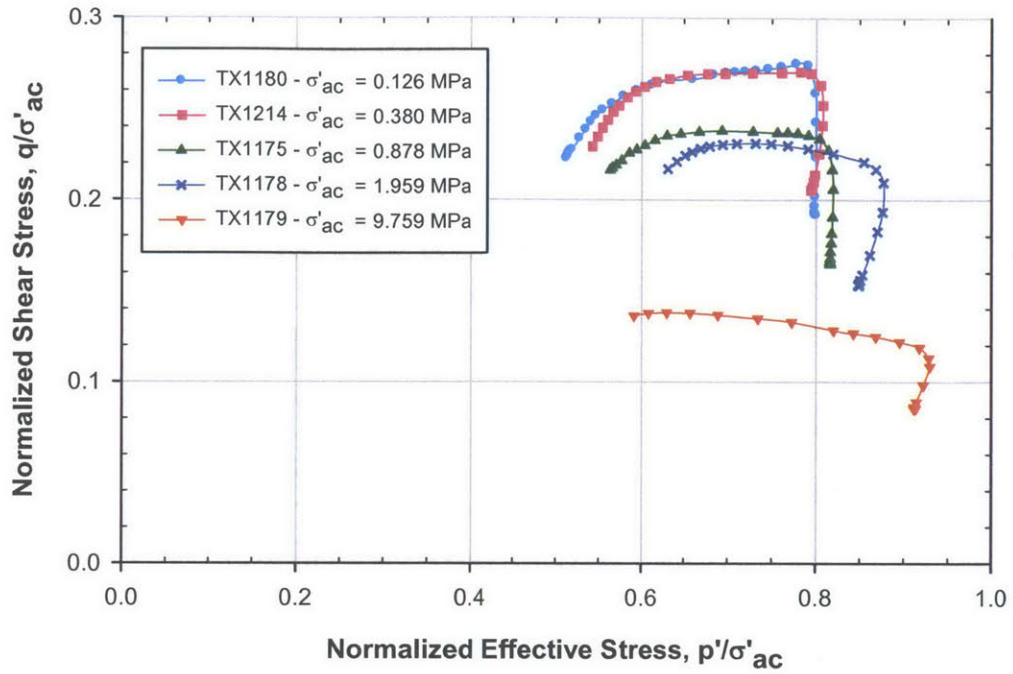


Figure 6.17 Normalized effective stress paths for RGOM EI at 64 g/L salinity

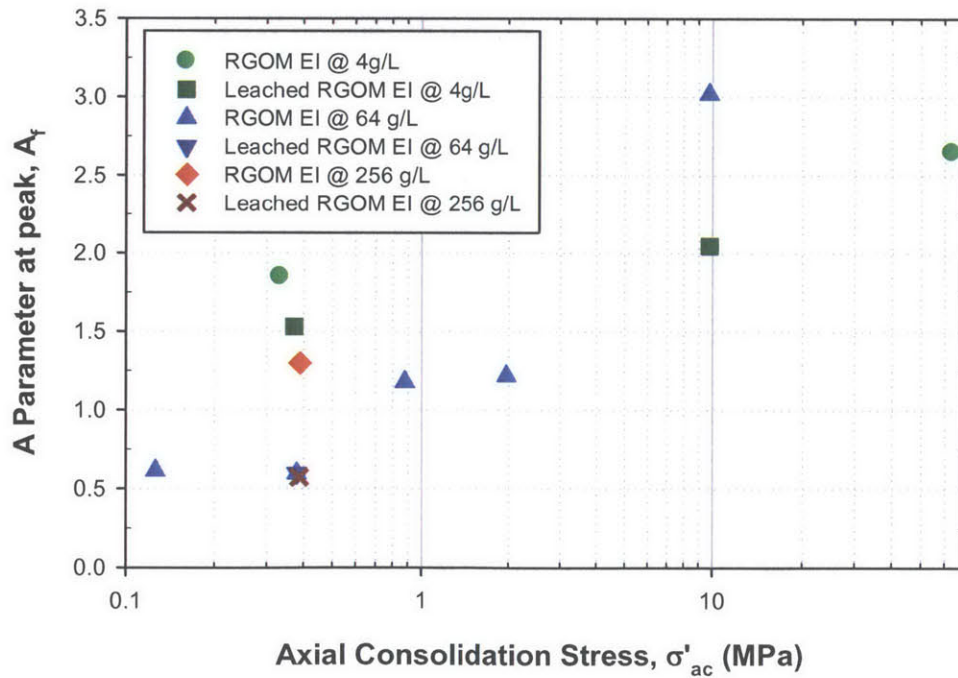


Figure 6.18 Skempton A parameter at peak versus stress level for RGOM EI & Leached RGOM EI at three salinities

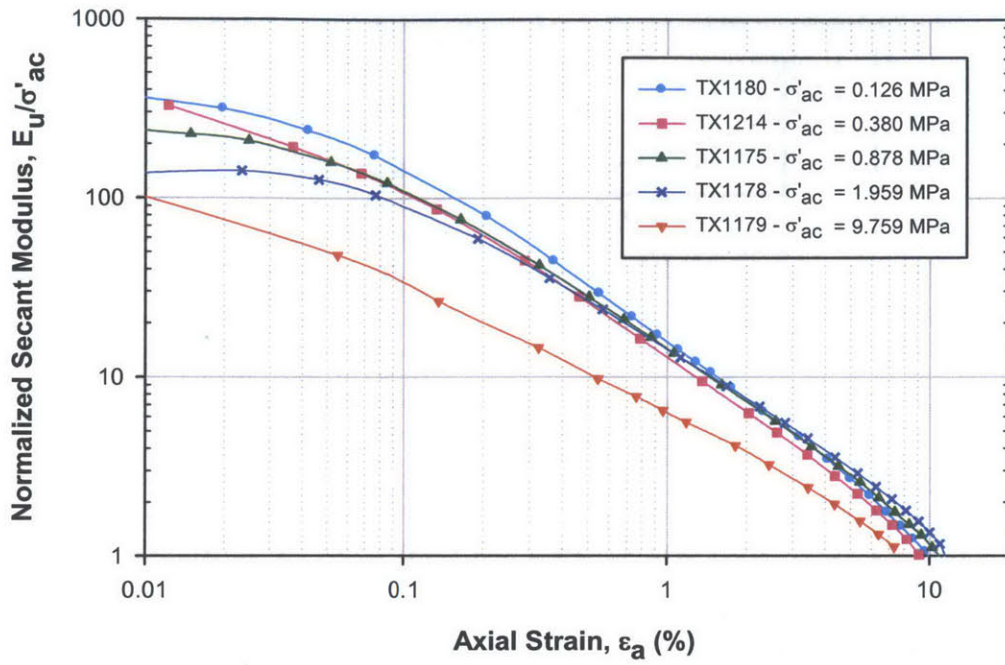


Figure 6.19 Normalized undrained secant modulus versus axial strain for RGOM EI at 64 g/L salinity

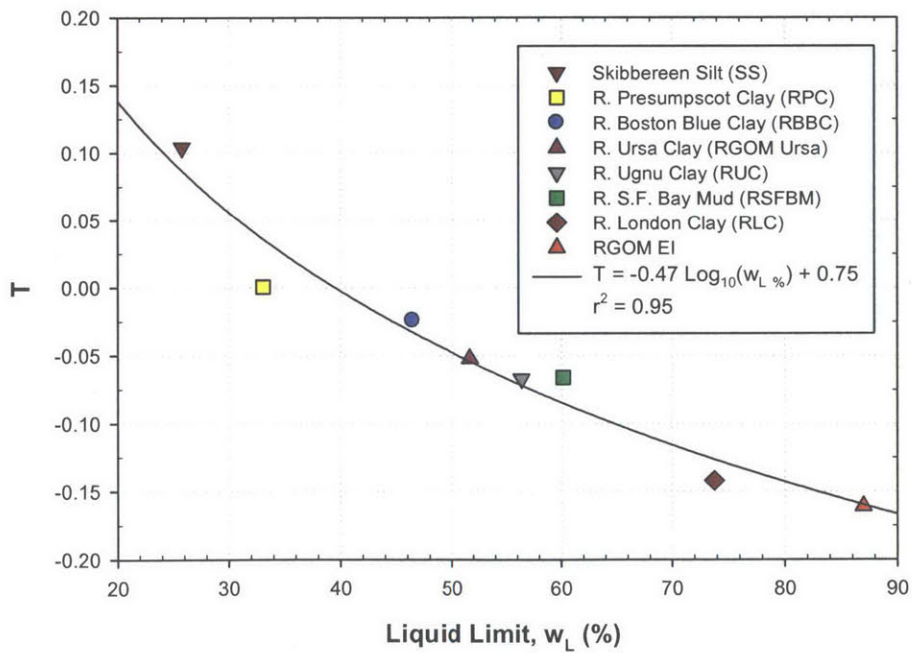
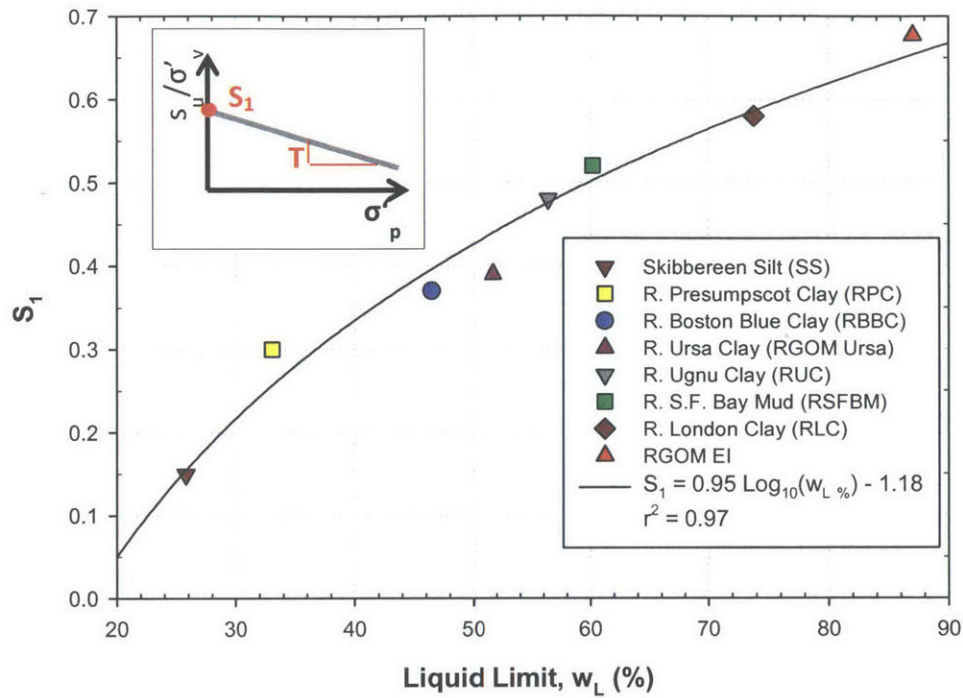


Figure 6.20 Correlation between undrained strength ratio and liquid limit. Top Left: Correlation between S_1 parameter and liquid limit, Top Right: Correlation between T parameter and liquid limit (updated from Casey, 2013)

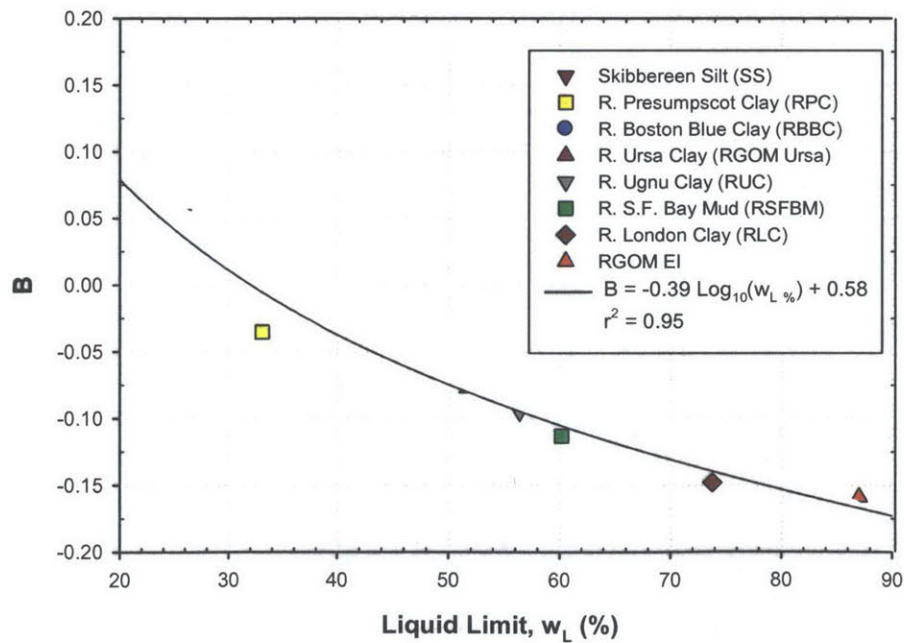
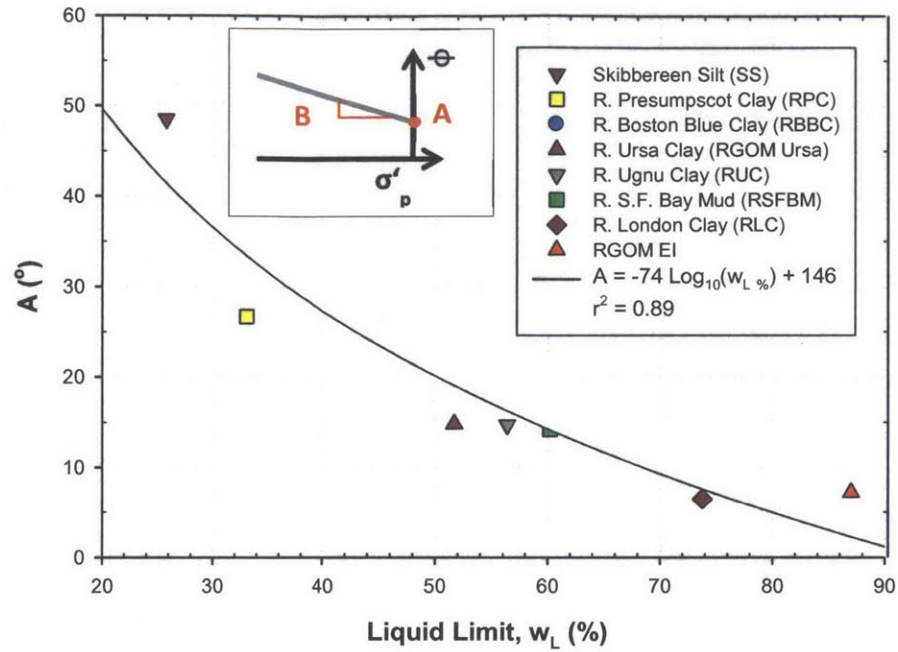


Figure 6.21 Correlation between friction angle and liquid limit. Top Left: Correlation between parameter A and liquid limit, Top Right: Correlation between parameter B and liquid limit (updated from Casey, 2013)

7 CONCLUSIONS AND RECOMMENDATIONS

7.1 INTRODUCTION

This chapter presents a summary of the main results and conclusions which can be drawn from the research, along with recommendations for future work.

The research investigated the mechanical behavior of six different high plasticity smectitic soils, which were resedimented in the laboratory from natural source materials. These source materials, obtained from the Gulf of Mexico region, with similar mineralogy have clay fractions varying between 52 and 70 %, and liquid limits ranging from 62 to 90 %. The varying plasticity allowed for any trends in the one dimensional consolidation and permeability behavior with varying salinity and stress level to be investigated with respect to increasing plasticity. The majority of testing was carried out on natural Gulf of Mexico – Eugene Island (GOM EI). This material was also used to examine the behavior of a soil whose fabric has been changed by the removal of the natural salts via leaching. Both leached and natural GOM EI were tested to investigate the influence of salinity on strength properties. Sea salt purchased from Morton's was used for resedimenting the natural and leached GOM EI. Very limited previous research has investigated the influence of a wide range in salinity (0 – 256 g/L) on the mechanical behavior of high plasticity soils over large consolidation stresses up to 40 MPa.

An extensive laboratory testing program involving Constant Rate of Strain (CRS) and K_0 consolidated undrained shear in compression triaxial testing (CK_0UC) was undertaken. Specimens tested in the modified CRS device reached axial effective stresses between 30 and 40 MPa. Triaxial testing was performed over a very wide range of effective stresses from 0.125 to 10 MPa, with one test consolidated to 63 MPa. Behavior is examined at pore fluid salinities of 4, 64, and 256 g/L. The shear behavior of all specimens was obtained in the normally consolidated region.

Section 7.2 summarizes the results obtained from the CRS tests. In Section 7.3 the main results and conclusions determined from the triaxial testing program are presented. Finally, in Section 7.4 recommendations are made for further research.

7.2 ONE DIMENSIONAL CONSOLIDATION BEHAVIOR

The sedimentation test, whereby a small quantity of soil is placed in test tubes with pore fluids of different salinities, agitated, and then allowed to settle, proved to be a very insightful and quick means of determining the impact that salinity may have on the soils mechanical behavior. In the case of GOM EI, the reduction in sediment height with increasing salinity at this ultra-low stress is in agreement with the observations at low stress from CRS tests. Increasing salinity created a denser floc structure, reducing the sedimentation height, and thereby reducing the void ratio for the same soil mass. The leached soil showed a similar trend with salinity, however, the sedimented height was roughly twice that of the natural of all salinities. This simple test is a very useful means of investigation the influence of salinity on a new soil arriving to a geotechnical laboratory for testing.

When dealing with a new soil, another early observation of the likelihood of pore fluid salinity influencing mechanical behavior can be made by determining the water contents required to create a stable slurry. A study conducted on Boston Blue Clay by Horan (2012) whereby he varied the pore fluid salinity found that for this low plasticity illitic soil the mechanical behavior was independent of pore fluid salinity. As part of that research, Horan determined that over a wide range of pore fluid salinities – from 0 g/L to 128 g/L, the same water content of 100% was sufficient. The research presented here has shown that for high plasticity smectitic soils, mechanical behavior is influenced by pore fluid salinity. It also found that the water content required to create a stable slurry using a wide range of pore fluid salinities ranged from 112 – 140 % in the case of GOM EI, decreasing in quantity with increasing salinity. Therefore, by determining the water contents required to form a stable slurry for a wide range of salinities, observations can be made as to the influence changes in salinity will have on a soils mechanical behavior. Details of the water contents required to form a slurry for each soil is presented in Table 3-4.

During the resedimentation phase of the research program, it was observed that as the pore fluid salinity increased, the time to reach end of primary (EOP) consolidation decreased. In addition to this, the amount of axial deformation undergone by the soil at EOP also decreased with increasing salinity. These two simple observations early in the research, prior to any

extensive CRS testing being conducted, indicated that for smectitic high plasticity soils, an increase in salinity results in both increasing c_v and hence permeability as well as decreasing compressibility.

The compression behavior measured during CRS testing indicated several clear trends with salinity for all soils tested. At low stress behavior is sensitive to pore fluid salinity. An increase in salinity resulted in a decrease in void ratio. Increasing plasticity is also found to increase the void ratio at low stress, as shown in Figure 5.24. It is also evident for all soils tested that the greatest change in compression behavior at low stress occurs up to a salinity of 70 g/L, with a further increase in salinity to 256 g/L providing very little change in the initial void ratios. This is in agreement with the sedimentation test behavior for GOM EI where the greatest change in sedimentation height occurred up to a salinity of 64 g/L. Significant curvature is observed in the normally consolidated range for all soils, with curvature increasing with increasing plasticity. The stress dependent behavior of each soil varied somewhat. GOM EI and Leached GOM EI showed convergence in the compression curves for the wide range of salinities with increasing stress, whereas the four other soils tested showed far less convergence, with GOM A and B diverging slightly with increasing stress. At consolidation stress of 40 MPa, the void ratios of all soils tested fall in a narrower band of values, while still maintaining the same general trend in void ratio with plasticity. Comparing the behavior determined from CRS testing and that observed in the sedimentation test indicates that at ultra-low stress, the leached soil had higher void ratios than the natural for all salinities

A comparison of the compression behavior of natural to leached GOM EI, presented in Figure 5.13, shows that the leached soil exists at a lower void ratio than the natural at low stress (0.1 MPa). This reverses the trend identified in the sedimentation tubes at ultra-low stress. Over the applied stress range from the ultra-low stress state to 0.1 MPa it is clear that the fabric of the leached GOM EI collapses to a greater extent compared to the natural. This indicates that by leaching the natural salts from GOM EI and then adding back salts in varying quantities created a uniform more compressible soil at low stress and a stiffer less compressible soil at stress greater than 0.1 MPa. Figure 5.14 illustrates that for each salinity, the compression index (c_c) of the leached soil is lower than that of the natural, over a stress range from 0.1 to 10 MPa. The leached soil also showed a reduced sensitivity to changes in salinity, with a narrower range in void ratio

at low stress, which can be seen in Figure 5.9. Increasing stress resulted in a convergence in the compression behavior of both soils with similar void ratios and c_c values at consolidation stresses of 40MPa. It was observed that the high stress variation in void ratio is smaller for the leached soil, suggesting a more uniform flocculated structure.

With the significant curvature in the normally consolidated region, the c_c of each soil varied with stress. All soils display a clear trend of decreasing c_c with increasing salinity and increasing consolidation stress. There is large scatter in the value of each soil in the low stress range of between 0.1 and 1 MPa, however, at the higher stress range of 10 to 40 MPa the c_c falls within a narrower band of values, between 0.2 and 0.3. At low stress, composition and salinity control the compression behavior, however, at high stresses the influence of salinity and composition reduces with stress level becoming the controlling factor. Details of the change in c_c with salinity and stress level are presented in Figure 5.26.

The compression curves obtained from CRS testing found that the yield stresses are considerably lower than the supposed batch preconsolidation pressures. This is due to friction acting between the soil sample and the sides of the consolidometer during resedimentation. This issue is of no concern in CRS testing as only the data obtained after the preconsolidation pressure in the normally consolidated region is analyzed. In the case of triaxial testing, following the SHANSEP reconsolidation technique, any impact which this issue would have on undrained shear behavior is eliminated following K_0 consolidation in the triaxial device to stresses much higher than the batch preconsolidation stress.

The permeability behavior obtained from CRS testing indicated several clear trends with salinity for all soils. For each salinity, the permeability-porosity relationship is essentially log-linear over a porosity range from 0.1 to 0.6. An increase in salinity was found to increase the permeability, with significant differences in permeability between 6 g/L and 256 g/L salinity. For instance, at a porosity of 0.5, the permeability of GOM EI with 256 g/L salinity is over an order of magnitude greater than that of the 6 g/L. This behavior is shown in Figure 5.7. In general, permeability was found to decrease with increasing plasticity, as illustrated in Figure 5.27. A comparison of the behavior between the natural GOM EI and that of the leached soil, presented in Figure 5.15, shows that both soils display the same trends with increasing salinity and

decreasing porosity. The higher salinity specimens (64, 128, and 256 g/L) display remarkably similar permeability over a porosity range from 0.2 to 0.6. However, the lower salinities show an increase the permeability at the higher porosities when the soil is leached. Two differing trends with decreasing porosity were observed in the soils tested. The permeability of GOM EI and GOM Upper for all salinities tested converge as porosity decreases. In contrast to this, the permeability of the GOM Lower, GOM A, and GOM B does not have the same degree of convergence. The expandability of the interlayered illite-smectite mineral ranges between 70 and 85 % for the soils displaying convergence in the permeability behavior. The soils with little to no convergence have lower expandability values of 40 to 60 %. The author hypothesizes that these two differing behaviors may be as a result of the differences in the expandability of the interlayered illite-smectite mineral in each soil.

The coefficient of consolidation in the vertical direction, c_v , increases with increasing salinity, which is to be expected based on the permeability behavior. All soils showed a decrease in c_v with increasing stress. The only exception to this being GOM EI at 6 and 10 g/L, which showed a fairly constant value over the wide stress range. The rate at which c_v decreased with increasing stress was found to increase with plasticity.

A qualitative analysis of SEM images of GOM EI and Leached GOM EI obtained on cryogenically frozen concentrated slurries aided in both providing an explanation for and gaining a better understanding of the observed mechanical behavior. Images of slurry with increasing pore fluid salinities showed an overall similar flocculated structure. Secondly, the floc wall thickness is observed to increase with increasing salinity. A greater number of particles are attracted to each other as salinity increases, creating a denser packing of the soil particles, and in turn resulting in lower void ratios. This observation from the SEM images is in agreement with both the behavior in the sedimentation test and the mechanical behavior at low stress. The images also confirmed that the leaching process disaggregated the flocs to individual soil particles, and the addition of salt created a more uniform flocculated structure to that of the natural. The natural soil was seen to consist of “clumps” of pre-existing flocs surrounded by newly formed flocs, with the clumps visibly denser. Figure 5.13 showed that for a given porosity, the natural soil has a greater stress capacity. The author speculates that as stress increases, the clumps of flocs in the natural soil come into contact with each other and provide

greater stress capacity compared to the stress distribution provided by the uniform soil matrix of the leached soil. An explanation for the permeability behavior with salinity is also postulated from the image. The lower salinities have thinner floc walls with less particles per floc, and hence for the same soil mass will create more of these “tubes” or hexagonal pore spaces. With an increasing number of “tubes”, an increased resistance to flow is generated, resulted in lower permeability.

Correlations between the sensitivity of a soils compressibility and permeability with changes in pore fluid salinity to liquid limit are proposed. For each soil, the change in void ratio with respect to salinity is plotted at consolidation stresses of 0.1 and 1 MPa. By fitting a power law function through the data at each stress, the slope of this line – the C parameter is determined. This parameter describes the rate at which void ratio changes with salinity. Plotting this parameter against liquid limit indicates a general trend, all be it with a large amount of scatter in the data. The correlation indicates that as liquid limit increases, void ratio sensitivity to changes in salinity increase. A similar procedure is applied to the permeability sensitivity, with the permeability of each soil at porosities of 0.5, 0.4, and 0.3 plotted against salinity. The parameter D describes the rate at which permeability changes with salinity. Plotting the D parameter against liquid limit shows a definite trend of increasing permeability sensitivity to changes in salinity with increasing liquid limit. These correlations are presented in Figure 5.37 and Figure 5.39.

7.3 STRENGTH BEHAVIOR

Values of K_0 measured during consolidation in the triaxial device on GOM EI show strong dependence on both stress level and salinity. K_0 starts off at a relatively high value of 0.6 at 0.125 MPa and increases with increasing consolidation stress to 0.9 at 63 MPa. The normally consolidated K_0 values determined from this research are the largest observed for laboratory testing on a wide variety of normally consolidated soils. These high values are in agreement with values measured in the field as well as those determined on one other high plasticity clay, resedimented London Clay, reported by Casey (2014). There is also a clear trend of a reduction in K_0 with increasing salinity; salinity ranging from 4 to 256 g/L for strength testing. This trend with salinity is observed at a stress of 0.4 and 10 MPa. Tests carried out on leached GOM EI

resedimented with the same three salinities and consolidated to 0.4 and 10 MPa prior to undrained shearing show similar trends of increasing K_0 with stress as well as reducing K_0 values with increasing salinity. No clear trend is evident between the K_0 value of GOM EI and leached GOM EI at the same salinity and stress level. Details of the K_0 behavior are shown in Figure 6.4.

Significant and consistent decreases in both normalized undrained shear strength and critical state friction angle of GOM EI with increasing stress level is observed, corresponding with an increase in the value of K_0 . Figure 6.9, Figure 6.11 and Figure 6.14 illustrate this behavior. The strength behavior of GOM EI is consistent with that observed for other materials from a wide variety of geologic backgrounds.

The shear stress-strain behavior displayed increased ductility with increasing stress. The post peak shear stress behavior is seen to vary depending on the consolidation stress. Specimens consolidated to a low stress of 0.125 MPa displayed post peak strain softening. An increase in consolidation stresses to 1 MPa resulted in specimens behaving perfectly plastic, while at the higher consolidation stress of 10 MPa, the post peak behavior changed to strain stiffening. This behavior is shown in Figure 6.7. An increase in the axial strain to failure is also observed with increasing consolidation stress. The strain to failure is independent of salinity at a consolidation stress of 0.4 MPa. Unfortunately, the lack of a successful undrained shear at 10 MPa for 256 g/L prevents any trend in failure strain with salinity being identified at this particular stress. A decrease in the soils brittleness is also evident with increasing consolidations stress, with values of about one obtained at consolidation stresses exceeding 1 MPa.

Increasing salinity showed a clear trend of increasing the normalized undrained shear strength of both the leached and natural GOM EI at 0.4 MPa consolidation stress. At the same stress level, the influence of salinity on friction angle is not as clearly defined, but in general, increasing salinity is seen to increase the friction angle of the natural and leached soil. Due to a leak occurring during the shear phase of several tests at a consolidation stress of 10 MPa, no trends in shear stress-strain and undrained strength behavior with respect to salinity could be determined. Further testing is required to determine if the salinity dependence of the normalized undrained shear strength at a low stress of 0.4 MPa remains constant with stress, or if increasing

consolidation stress resulting in the influence of salinity on strength behavior becoming negligible.

Casey & Germaine (2013) developed correlations that allowed the undrained strength and critical state friction angle of a fine grained soil, as well as a variation in these properties with stress level, to be estimated from the soils liquid limit. The variations in both properties can be described using a power law function containing two parameters. These parameters have been correlated to liquid limit. Details of these correlations are presented in Section 6.4. Fitting power law functions to the data presented here obtained the parameters required for both the undrained shear strength and friction angle correlations. The parameters associated with the undrained shear strength and friction angle of GOM EI determined in this research are in excellent agreement with the correlations, as shown in Figure 6.20 and Figure 6.21. The correlations also show that GOM EI has the largest stress rate decrease in both undrained shear strength and friction angle of all the soils tested from a wide range of geological backgrounds.

The liquid limit correlations, when combined with Equation 6.1 and 6.3, have great practical relevance for engineering practice. They allow for a reasonable estimate of the critical state friction angle and normalized undrained shear strength of a soil based on its liquid limit together with the in-situ preconsolidation stress. This reduces the need to perform laboratory tests on intact samples obtained from the field, which is frequently infeasible in the case of deep sediments or sediments from the deep ocean.

7.4 RECOMMENDATIONS FOR FUTURE WORK

The extensive laboratory testing program conducted for this research provided valuable insight into the influence of salinity on the mechanical behavior of high plasticity soils. However, several areas have been identified where further experimental studies would be beneficial.

The one dimensional compression and particularly the permeability behavior of the six soils tested showed differing behavior at a consolidation stress of 40 MPa. Continuing the research using the newly developed CRS device with capacity to 100 MPa axial consolidation stress will determine if the compression behavior of some high plasticity soils converges to

similar values at a particular stress. Secondly, testing to 100 MPa will identify if the differing permeability behavior with respect to salinity will continue, in the case of some soils without convergence, or decrease to become insignificant at a particular porosity.

The leaching of the natural salts from a smectite rich high plasticity soil, then adding back varying amounts of salts, and CRS testing to high stress provided an excellent comparison to the observed behavior of the natural soil. Similar research should be carried out to investigate what impact leaching the natural salts out of other high plasticity soils such as GOM Upper, GOM Lower, GOM A, and GOM B has on mechanical behavior. It would be interesting to determine if this leaching process creates similar trends in behavior, in particular the very similar compression behavior at consolidation stresses of up to 40 MPa observed in leached GOM EI.

The stress dependent permeability behavior of the soils tested showed two distinct trends, either a convergence or lack of convergence in the permeability of all salinities with decreasing porosity. As each soil had a similar mineralogy and very similar quantities of the illite-smectite mineral, the author hypothesizes that these two differing behaviors may be as a result of the differences in the expandability of the interlayered illite-smectite mineral in each soil. Testing should be carried out on a manufactured soil with identical clay fraction and mineralogy but differing degrees of expandability to confirm if the varying expandability is the cause of this differing permeability behavior.

The proposed correlations between the sensitivity of a soils compressibility and permeability with changes in pore fluid salinity to liquid limit are specific for soils ranging in liquid limit from 46 to 90 %. It would be worthwhile to carry out similar research on the influence of salinity on mechanical behavior of soils with liquid limits both above and below this range. This testing would expand the correlations, and help to confirm the observed trends. Large changes in the behavior was observed up to a salinity of 64g/L. The sedimentation test showed that with the addition of just 1 g/L of pore fluid the sedimentation height decreased significantly from that with distilled water. The author recommends investigating the changes in mechanical behavioral using several salinities between 0 and 1 g/L.

Due to the limitations of the CRS load frame and the low c_v values of high plasticity soils, the author recommends that when carrying out CRS testing on soils with c_v in the range of

0.0001 and lower, the axial rate should be computer controlled similar to the newly developed high stress CRS. This computer controlled axial motor will allow the rate to be gradually reduced as the excess pore pressure builds up, in addition to applying strain rates significant less than the current system.

With the recent development of triaxial testing capacity to 100 MPa at the MIT geotechnical laboratory, and given that the results presented here on high plasticity soils showing the largest stress dependent behavior, testing of Gulf of Mexico soils should be conducted to 100 MPa to investigate the strength behavior at this stress.

The limited strength data obtained at 10 MPa on GOM EI should be expanded so that the shear strength trends with salinity observed at 0.4 MPa can be compared and contrasted. The author recommends that another high plasticity soil be tested with three similar salinities over a stress range from 0.1 to 10 MPa to investigate the salinity dependent strength behavior, and facilitate a comparison to be made with this research.

Lastly, a qualitative analysis of SEM images of GOM EI and Leached GOM EI in a slurry state provided an excellent insight into the influence of salinity at the micro-scale on the flocculated structure. Clear trends with increasing salinity were observed, with thicker individual flocs forming in higher pore fluid salinities. In addition to this, an explanation for and a greater understanding of the observed mechanical behavior could be advanced. The author recommends that further research be conducted involving a qualitative and quantitative analysis of changes observed in SEM images of high plasticity soils over a wide range of stresses, starting from the ultra-low stress state of the slurry. A greater understanding of the stress and salinity dependent mechanical behavior can be obtained by analysis of said images.

REFERENCES

- Abdulhadi, N.O. (2009). "An Experimental Investigation into the Stress-Dependent Mechanical Behavior of Cohesive Soil with Application to Wellbore Instability", Ph.D. Thesis, MIT, Cambridge, MA
- Adams, A.L. (2011) "Laboratory Evaluation of the Constant Rate of Strain and Constant Head Permeability Techniques for Measurement of the Hydraulic Conductivity of Fine Grained Soil", SM Thesis, MIT, Cambridge, MA
- Adams, A.L. (2014) "Permeability Anisotropy and Resistivity Anisotropy of Mechanically Compressed Mudrocks", Ph.D. Thesis, MIT, Cambridge, MA
- Ajmera, B. & Tiwari, B., (2012) "Consolidation Characteristics of Soft Clays with Saline Water as a Pore Fluid", GeoCongress, ASCE, 1223-1232
- Allen, L.S. & Matijevic, E. (1974) "Surface and Colloid Chemistry of Clays", Chemical Reviews, ACS, 74 (3), 385-400
- ASTM D4186 - 12 Standard Test Method for One-Dimensional Consolidation Properties of Saturated Cohesive Soils using Controlled Strain Loading.
- ASTM D422 Standard Test Method for Particle-size Analysis of Soils, in ASTM 04.08 Soil and Rock (1), 2007
- ASTM D4318 - 10 Standard Test Methods for Liquid Limit, Plastic Limit, and Plasticity Index of Soils.
- Betts, W.S. (2014) "Compression and Permeability Behavior of Gulf of Mexico Mudrocks, Resedimented and In-situ", M.S. Thesis, University of Texas at Austin
- Bolt, G.H. (1956) "Physio-Chemical Analysis of the Compressibility of Pure Clays", Geotechnique, 6(2), 86-93
- Burland, J.B. (1990) "On the Compressibility and Shear Strength of Natural Soils". Geotechnique, 40, 329-378

Calvello, M., Lasco, M., Vassallo, R., and Di Maio, C. (2005) "Compressibility and Residual Shear Strength of Smectitic Clays: Influence of pore aqueous solutions and organic solvents", *Rivista Italiana Di Geotecnica*

Casey, B. (2011) "The Significance of Specimen End Restraint in High Pressure Triaxial Testing of Cohesive Soil", SM Thesis, MIT, Cambridge, MA

Casey, B. (2014) "The Consolidation and Strength Behavior of Mechanically Compressed Fine-Grained Sediment", Ph.D. Thesis, MIT, Cambridge, MA

Casey, B. and Germaine, J.T. (2013) "The Stress Dependence of Shear Strength in Fine-Grained Soils and Correlations with Liquid Limit", *Journal of Geotechnical and Geoenvironmental Engineering*, 139 (10), 1709-1717.

Casey, B., Fahy, B.P., Flemings, P.B., & Germaine, J.T. (2014) "Shear Strength of Two Gulf of Mexico Mudrocks and a Comparison with Other Sediments", *Fourth EAGE Shale Workshop*

Casey, B., Germaine, J.T., Flemings, P.B., Reece, J.S., Gao, B., and Betts, W. (2013) "Liquid Limit as a Predictor of Mudrock Permeability", *Journal of Marine and Petroleum Geology*, 44, 256-263

Engelhardt, W. & Gaida, K.H. (1963) "Concentration Changes of Pore Solutions during the Compaction of Clay Sediments", *Journal of Sedimentary Petrology*, 33(4), 919-930

Germaine, J.T. & Germaine, A.V. (2009) "Geotechnical Laboratory Measurements for Engineers", John Wiley and Sons, Inc.

Germaine, J.T. (1982) "Development of the Directional Shear Cell for Measuring Cross Anisotropic Clay Properties", Sc.D., MIT, Cambridge, MA

Gonzalez, J.H. (2000) "Experimental and Theoretical Investigation of Constant Rate of Strain Consolidation", SM Thesis, MIT, Cambridge, MA

Horan, A.J. (2012) "The Mechanical Behavior of Normally Consolidated Soils as a Function of Pore Fluid Salinity", SM Thesis, MIT, Cambridge, MA

Jones, C.A. (2010) "Engineering Properties of Resedimented Ugnu Clay from the Alaskan North Slope", SM Thesis, MIT, Cambridge, MA

Ladd, C.C. & Varallyay, J. (1965) "The Influence of Stress System on the Behavior of Saturated Clays during Undrained Shear", Research Report R65-11, Soil Publication No. 177, Department of Civil Engineering, MIT, Cambridge, MA

Ladd, C.C. & Foott, R. (1974) "New Design Procedures for Stability of Soft Clays", Journal of the Geotechnical Engineering Division, ASCE, 100 (7), 763-786

Ladd, C.C. & Kinner, E. (1967) "The Strength of Clays at Low Effective Stress," Research in Earth Physics, Research Report R67-4, Phase Report 8

Ladd, C.C. (1960) "Stress-Strain Behavior of Saturated Clay and Basic Strength Principles", Research Report R64-17, Research on Earth Physics, Department of Civil Engineering, MIT, Cambridge, MA

Lambe, T.W. & Whitman, R.V. (1969) "Soil Mechanics", John Wiley and Sons, New York

Man, A. & Graham, J. (2010) "Pore Fluid Chemistry, stress-strain behavior, and yielding in reconstituted highly plastic clay", Journal of Engineering Geology, Vol. 116, 296-310

Mazzei, D. (2008) "Normalized Mechanical Properties of Resedimented Gulf of Mexico Clay from Integrated Ocean Drilling Program Expedition Leg 308", SM Thesis, MIT, Cambridge, MA

Mesri, G. & Olsen, R.E. (1971) "Mechanisms Controlling the Permeability of Clays", Clays and Clay Minerals, Vol. 19 (3), 151-158

Nguyen, X. C., Nguyen, X.P., Cui, Y.J., Tang, A.M., Deng, Y.F., Li, X.L., & Wouters, L. (2013) "Effects of pore water chemical composition on the hydro-mechanical behavior of natural stiff clays", Journal of Engineering Geology, 166, 52-64

Pineda, J.A., Kelly, R., Bates, L., Sheng, D., & Sloan, S. (2013) "Effects of pore fluid salinity on the shear strength of a soft clay", Poromechanics V, ASCE, 1460-1469

Robinson, R. & Allam, M.M. (1998) "Effect of Clay Mineralogy on Coefficient of Consolidation", *Clays and Clay Minerals*, 46(5), 596-600

Santagata, M.C. (1994) "Investigation of Sample Disturbance in Soft Clays Using Triaxial Element Tests", SM Thesis, MIT, Cambridge, MA

Sheahan, T.C. (1991) "An Experimental Study of the Time-Dependent Undrained Shear Behavior of Resedimented Clay using Automated Stress-Path Triaxial Equipment", ScD Thesis, MIT, Cambridge, MA

Stump, B. & Flemings, P.B. (2002) "Consolidation State, Permeability, and Stress Ratio as Determined from Uniaxial Strain Experiments on Mudstone Samples from the Eugene Island 330 Area, Offshore Louisiana", *American Association of Petroleum Geologists*, 76, 131-144

Terzaghi, K., Peck, R.B. & Mesri, G. (1996) "Soil Mechanics in Engineering Practice", Third Edition, John Wiley and Sons, Inc.

Tiwari, B., Tuladhar, G.R., & Marui, H. (2005) "Variation in Residual Shear Strength of the Soil with the Salinity of Pore Fluid", *Journal of Geotechnical and Geoenvironmental Engineering*, ASCE, 131 (12), 1445-1456

Van Olphen, H. (1977) "An Introduction to Clay Colloid Chemistry", Krieger Publishing Company

van Paassen, L.A. & Gareau, L.F. (2004) "Effect of Pore Fluid Salinity on Compressibility and Shear Strength Development of Clayey Soils", *Engineering Geology for Infrastructure Planning*, 104, 327-340

Wissa, A.E.Z. (1961) "A Study of the Effects of Environmental Changes on the Stress-Strain Properties of Kaolinite", SM Thesis, MIT, Cambridge, MA

Witteveen, P., Ferrari, A., & Laloui, L (2013) "An Experimental and Constitutive Investigation on the Chemo-Mechanical behavior of a clay", *Géotechnique*, 63(3), 244-255

APPENDIX A

Procedure for Conducting a Constant Rate of Strain (CRS) Test to 40MPa

Stage 1 – Prepare Apparatus

1. Ensure the valve to the CRS cell is in the closed position. Open the reservoir valve at the top of the cell pressure PVA. Manually adjust the PVA piston so that it is raised to the fully upward position.
2. Insert a tube into the top of the PVA via the reservoir and apply a vacuum to remove the water from the PVA and reservoir. During this process, pour the appropriate salt water concentration for the test into the reservoir.
3. Using manual control gradually lower the PVA piston to draw the selected test pore fluid salinity into the PVA. Steadily lower the tube into the PVA as the piston moves.
4. Once the PVA is lowered to the lowest position, continue vacuuming the fluid until the volume of the PVA and reservoir have been exchanged at least 3 times.
5. Gradually remove the tube from the PVA ensuring no air pockets form in the process. Once removed, manually raise the PVA to check if any air is in the system. If no air bubbles appear in the reservoir then the flushing of the PVA is complete.
6. Flush the line from the reservoir to the cell with the test salt water and then close the valve at the reservoir.
7. Place the disassembled CRS cell on a tray in front of the loading frame.
8. Clean the square O-ring seal and apply vacuum grease to it.
9. Obtain the mass of the cutting ring and one filter paper. Also obtain the mass of two oven tares for trimmings
10. Put the large base porous stone, top and bottom porous stone and both filter papers into a jar filled with the fluid matching the pore fluid salinity of the test specimen. Place the jar into the ultra-sonic bath for 10 minutes.
11. Apply a thin film of silicone grease to inside of cutting ring to reduce friction between it and the soil.
12. Obtain the CRS test number from the data acquisition room.

Stage 2 - Trim Specimen

1. Extrude a sufficient amount of soil from the consolidometer and place soil sample on a perspex plate with wax paper between soil and plate.
2. Insert the cutting ring upside down into the recessed mold. Then place the soil on to the base of the trimming device, positioned concentric with the cutting ring.
3. Apply a small downward force from the cutting ring via the piston while gradually trimming the soil around the perimeter.

4. Continue trimming until a sufficient amount of soil has entered the ring.
5. Remove the trimming ring from the device and place right side up. Remove Perspex plate and wax paper.
6. Place just the Perspex plate on the soil extruding from the top of the cutting ring. Trim off this extruded soil with wire saw and finish with straight edge.
7. Place filter paper on the top surface followed by the recess tool. Insert the recess tool a slight amount into the cutting ring, then turn the ring upside down.
8. The weight of the soil and cutting ring should provide sufficient downward force for the recess tool to be fully inserted into the cutting ring.
9. Trim off the extruded end with wire saw and finish with straight edge.
10. Determine mass of specimen, cutting ring, filter paper, and recess tool.

Stage 3 - Setup Specimen

1. Place the large porous stone into the base, ensuring it is saturated surface dry.
2. Place filter paper to bottom surface followed by bottom porous stone.
3. Apply a small force to the porous stone inserted it half way into the ring.
4. Place cutting ring in the base of the CRS cell.
5. Fit the square O-ring seal around the ring.
6. Remove the recess tool and insert top porous stone.
7. Open the air vent at the top of the cell by unthreading the nut.
8. Place the CRS cell over the base, ensuring that the piston is in the fully retracted position, and then tighten the 3 nuts. Once fully tight, lower the piston onto the top porous stone gently and lock in place.
9. Next fill the cell by opening the valve at the PVA reservoir and the valve entering the cell. Once the cell is filled, close the air vent.
10. Connect the pore pressure transducer once the water has filled the transducer housing.
11. Place the cell in the load frame, mount the LVDTs and moment break.
12. Adjust the strain rate to an appropriate value for the soil being tested.
13. Take the load cell zero value.
14. Manually raise the frame so that the moment break makes contact with the load cell. Monitor the voltmeter to ensure that a small load is applied to the specimen.
15. Record the zero values (from both the voltmeter and the computer) for the two LVDT's, the cell pressure transducer, and the pore pressure transducer. Ensure that both transducers are open to atmosphere when doing so.
16. Release the piston lock and set the frame to be controlled by the motor. Ensure the valve to the pore pressure transducer is open.
17. Turn on the temperature control and close the door to the temperature enclosure.

Stage 4 - Back Pressure Saturate

1. Run the CRS setup program and fill in all the data.

2. When complete, continue to the computer control option.
3. Check that all the computed values are reasonable.
4. Start data acquisition on 10 min. increments.
5. Close the valve at the top of the PVA.
6. Increment the pore pressure and cell pressure by 0.5 ksc using the hydrostatic option. Set the pore pressure value slightly less than that of the cell, otherwise the program will not run.
7. Turn on the motor to control the PVA.
8. Allow time for equilibration.
9. Continue the increments until the back pressure reaches 3 ksc.

Stage 5 - Consolidate the Specimen

1. Once the specimen is back pressure saturated, close the valve to the cell. Ensure that the piston lock is released and that the clutch is in place for the frame to be controlled by the motor.
2. Check to make sure there are no leaks in the cell or the drainage lines.
3. Set the data acquisition to record at a particular rate. A rule of thumb for the rate selection is: for a strain rate of 2%, record data every 2 minutes. 1% = every 4 minutes, 0.5 % = every 8 minutes, etc.
4. Turn on the motor to begin consolidation.
5. Periodically check the test to ensure there are no issues. In particular, monitor the pore pressure to ensure that it does not exceed the capacity of the pressure transducer. If it reaches the capacity, then the frame must be turned off to allow the pore pressure to dissipate.

Stage 6 – Disassemble

1. Once the predetermined consolidation stress is reached, turn off the motor and allow the pore pressure to dissipate
2. Exit from the computer control program and turn off the motor controlling the cell PVA.
3. Disassemble the cell, removing the cutting ring and specimen as swiftly as possible, and thoroughly dry off any excess water around the specimen that may cause swelling.
4. Mass an oven tare and mass the dried cutting ring immediately after the test.
5. Extrude the specimen from the cutting ring, remove the porous stones and filter papers.
6. Mass the final specimen and place in oven for 24 hours, then obtain the dry mass.
7. Wash any extruded soil from the cutting shoe, filter paper, and porous stones into another tare, place in oven for 24 hours and record its dry mass. This is critically important for the phase relation calculations.
8. Place the three porous stones and filter paper in distilled water and put in the ultra-sonic bath for ten minutes. Afterwards, store in sealed container.
9. Thoroughly clean the CRS cell, base and O-ring seal.
10. Remove the fluid in the PVA and drainage lines by flushing with distilled water and repeating the process outlined in Stage 1.

APPENDIX B

Procedure for Conducting a K0 Consolidated Sheared Undrained Compression Test in a Low Stress Triaxial Device

The following procedure is a modified version of that developed by Dr. John Germaine for the Graduate Laboratory course at MIT (course number 1.37)

Stage 1 - Prepare Cell

1. Ensure both drainage valves are in the closed position. Open the reservoir valve at the top of the pore pressure PVA. Manually adjust the PVA piston so that it is raised to the fully upward position.
2. Insert a tube into the top of the PVA via the reservoir and apply a vacuum to remove the water from the PVA and reservoir. During this process, pour the appropriate salt water concentration for the test into the reservoir.
3. Using manual control gradually lower the PVA piston to draw the selected test pore fluid salinity into the PVA. Steadily lower the tube into the PVA as the piston moves.
4. Once the PVA is lowered to the lowest position, continue vacuuming the fluid until the volume of the PVA and reservoir have been exchanged at least 3 times.
5. Gradually remove the tube from the PVA ensuring no air pockets form in the process. Once removed, manually raise the PVA to check if any air is in the system. If no air bubbles appear in the reservoir then the flushing of the PVA is complete.
6. Flush both the top and bottom drainage lines with the test salt water.
7. Retract piston (gently) and lock in position with split collar. (Note: if piston is hard to move, apply a vacuum to the top of the bearing with the shop vac or air pressure to the chamber to expand the rolling diaphragm).
8. Place a dummy specimen on the pedestal and adjust the position of the piston for the type of test. Pull the piston to the upper most position. For a compression test, there should be just enough clearance to fit the specimen and filter stones. For an extension test, there should be about 1 cm of gap.
9. Flush water through the bottom line from the pressure controller filling the container formed by the plastic bottle on the base pedestal.
10. Allow water to flow down the bore hole to the transducer block.
11. Connect the pressure transducer and record the zero reading.
12. Check the response of the pressure transducer by pressing on the bore hole (you should get an increment of several mv).
13. Close the bottom valve to the pressure controller.
14. Flush water through the top drainage line.
15. Close the top valve to the pressure controller.

16. Close the supply valve on top of the pressure controller.
17. Measure compressibility of volume change system.
18. Check for internal leakage by, opening the top drainage valve, plugging the top cap hole with your finger and applying pressure with the controller.
19. Close the top valve to the pressure controller.
20. If using an internal load cell then record the zero value and unplug the transducer from the triaxial base.
21. Clean and grease the sides of the top cap and bottom pedestal.
22. Set rubber sleeves around pedestal and top cap such that the stone thickness will be covered.
23. Locate the first thin membrane around the pedestal with the roll close to the top edge.
24. Fix with two O-rings.
25. Place the second membrane over the O-rings with the roll between the top O-ring and first membrane roll.
26. Fix with one O-ring between the first two O-rings.
27. Place four O-rings on the stretcher and set this over the pedestal.
28. Boil or ultrasound the stones for ten minutes. (note: the stones should always be stored in a sealed container of water.)
29. Place filter paper on stone underwater.
30. Pick up stone and place on pedestal with filter paper.
31. For *compression* tests, tuck eight 1/4" wide by 3-1/2" long filter strips between the rubber sleeves and the stone.
32. For *extension* tests, cut five 1/4" wide by 8" long filter strips and cut half way across the width of the strip every cm from alternating sides.

Stage 2 - Trim Specimen

1. Rough trim the specimen with a wire saw and obtain several water contents.
2. Place specimen in miter box.
3. Rough cut cylinder with miter box.
4. Final cut specimen with miter box.
5. Wrap specimen in one layer of wax paper which is 3 mm shorter than final specimen height. Use split mold to size the wax paper.
6. Place specimen in split mold and gently tighten.
7. Trim off specimen ends to height of mold with wire saw and finish with straight edge.
8. Determine mass of specimen and mold. Remember to get mold mass after setup.
9. Measure the diameter of the specimen at several locations with the caliper of the optical caliper.
10. Measure the specimen height (normally equal to the mold height).

Stage 3 - Setup Specimen

1. Remove excess water from around pedestal.

2. Place second filter paper on specimen.
3. Locate specimen on base pedestal.
4. Slide top filter stone on specimen.
5. Lower piston to contact specimen and lock in place.
6. Cover top stone with rubber sleeve.
7. Locate filter drains along sides of specimen and tuck ends under top rubber sleeve. For extension tests, wrap the filter drains around the specimen at an angle of 35-40 degrees to the horizontal.
8. Roll membrane over specimen.
9. Fix with two O-rings.
10. Roll second membrane over specimen.
11. Fix with third O-ring.
12. If last O-ring is not necessary, release it on the pedestal.
13. Plug in internal load cell.
14. Assemble cell, cylinder, and top plate.
15. Fill with silicone oil.
16. Place displacement gauge bar on piston (above groove).
17. Lock piston retaining clamp in place.
18. Record zero for external force transducer if used.
19. Raise triaxial cell into contact with force transducer and lock together with screw clamps.
20. Connect LVDT and record zero value.
21. Remove retaining clamp (split ring) from piston.
22. Engage axial motor drive system. (On WF load frames put lever to FINE and pull out the clutch. On the Oslo frame, release the clutch.)
23. Run the triaxial setup program and fill in all the data.
24. When complete, continue to the computer control option.
25. Check that all the computed values are reasonable.
26. Turn the axial and cell motors to computer control.
27. Select the pressure up option and apply about 25% of the in situ vertical effective stress or enough chamber pressure to cause positive pore pressure.

Stage 4 - Back Pressure Saturate

10. Allow the specimen to equilibrate overnight with drainage lines closed.
11. Measure pore pressure and cell pressure to obtain sampling effective stress the next day.
12. Manually set the back pressure to the pore pressure value (maintain at least 0.1 kg/cm² effective stress), record zero volume and open drainage lines.
13. Allow volume change to stabilize if necessary.
14. Start data acquisition on 10 min. increments.
15. Measure pore pressure coefficient, B, using an increment of 0.25 ksc.
16. Increment the pore pressure and cell pressure by 0.25 ksc using the hydrostatic option.

17. Allow time for equilibration.
18. Continue steps f through h until the back pressure reaches 3 ksc or the B value equals unity.

Stage 5 - Consolidate the Specimen

1. If final B value is 1.00 ± 0.02 , the specimen may be consolidated immediately; if not, allow the specimen to sit overnight.
2. Record final volume change and displacement due to "saturation" of system.
3. Reset the back pressure controller to be at the upper limit of the LVDT. Do this by recording the pore pressure, closing the drainage valves, releasing the pressure in the controller, using manual control to raise the piston until the LVDT reads about 2.5 volts (maybe positive or negative), close the controller valve, manually increase the pressure to the back pressure value, opening the drainage valves, and returning to computer control.
4. Compute and record a new volume change zero to have equal axial and volumetric strain. This requires you to return to the setup program and change the volume zero.
5. Select the hold stress option and be sure the numbers look reasonable. This is a very important step because it loads target values in the computer memory that are required for the consolidation process.
6. Start data acquisition (5 to 10 min increments).
7. Select the Ko option on the control computer.
8. Use an effective stress limit of 6 ksc and a strain rate of 0.15 %/hr.
9. Stop consolidation (by selecting the hold stress option) any time after 10% axial strain.
10. Allow the final stress to remain on the specimen for one cycle of secondary compression or at least 24 hrs.

Stage 6 - Shear Undrained

1. Close off drainage lines and verify that pore pressure is constant (about 30 min.).
2. Record PP change during this period.
3. Record preshear specimen dimensions and conditions.
4. Obtain zero readings on data acquisition system.
5. Select the undrained shear option.
6. Turn off the axial and pore pressure controllers.
7. Select the appropriate strain rate based on an estimate of the coefficient of consolidation (for $BBC = 0.5\%/hr$).
8. Start the data acquisition system (2 sec. time interval. This must be increased several times during shear by factors to 2 to 3 up to 5 minutes.)
9. Shear the specimen by turning the axial controller to computer.
10. Continue to shear until a failure plane has developed or 20% strain.

Stage 7 - Disassemble

1. Turn off control program.

2. Open both pressure controller fill valves.
3. Drain oil back into the storage container.
4. Disconnect the piston clamp.
5. Remove Plexiglas cylinder.
6. Dry off specimen.
7. Roll down membranes and remove specimen.
8. Measure total mass, dimensions and failure plane information.
9. Cut specimen into three pieces and measure water contents.
10. Place plastic sleeve over pedestal and fill with water.
11. Put stones and filter fabric in container with water and close.

APPENDIX C

Procedure for the Removal of In-Situ salts from soils using Dialysis Tubing

1. Obtain 1 – 1.2 kg of dry soil powder
2. Add sufficient amount of distilled water (approximately twice the soils Liquid Limit) to the soil and mechanically mix to form a pourable slurry
3. Set up the plastic bath and peristaltic pump
4. Obtain a 50 foot roll of 1 5/16” dialysis tubing and cut into 15 lengths approximately the length of the bath
5. Place each length of tubing into distilled water to soak and soften
6. Obtain bowl with soil, spoon, spatula, funnel, and plenty paper towels ready for filling the tubes
7. Obtain one length of tube and attach clip to one end
8. Place the other end of the tube over the opening in the funnel and hold in place
9. Fill the funnel with soil until the tube is filled to within 3 inches of the top
10. Remove the funnel and attach a clip to the end of the tube, sealing the soil in place. Ensure that no air is entrapped
11. Place this filled tube or ‘sausage’ into the bath
12. Repeat steps 7-11 until all the soil has been placed in tubes
13. Place a known quantity of distilled water in the bath, ensuring that the water level is above all of the tubes
14. Take an initial reading using the conductivity meter just after the bath has been filled.
15. Change the water every 12 or 24 hours and measure the salinity of the water each time. Remove the water to a bucket via a syphon.
16. For every measurement, also measure the salinity of a 1 g/L control solution to control for temperature changes
17. Rotate the tubes every 6 days
18. If necessary replace the tubes after 15 days as the material is known to disintegrate after this period
19. Once the required level of salinity has been reached, remove the soil from the tubes to a bowl
20. Thoroughly wash the tubing to extract as the valuable leached soil
21. Dry the soil using the assistance of a desk fan
22. Spread the soil out on several large glass plates until a uniform layer depth of roughly 10mm is achieved. This will reduce the drying time required as well as providing thin plates of dry soil (~5mm thick) which is easier to break down compared to large nuggets of soil
23. Once dry, grind the soil using a mortar and pestle until all the soil passes through the US#100 sieve.
24. Store the leached soil in the humid room in a sealed contained until it is required for resedimentation